

Investigating the contribution of protein dynamics to catalysis in protochlorophyllide oxidoreductase

A thesis submitted to the University of Manchester for the degree of Doctor of Philosophy (PhD) in the Faculty of Life Sciences

2015

Robin Hoeven

Table of contents

Abbreviations	6
List of Figures	10
List of tables	13
Abstract	14
Declaration	15
Copyright statement	15
Acknowledgement	16
Preface to the alternative format	17
<i>Chapter 1 - Introduction</i>	<i>18</i>
1.1. The role of dynamics in enzyme catalysis	19
1.1.1. Hydrogen tunneling	21
1.1.1.1. The concept of wave-particle duality and tunneling	21
1.1.1.2. Marcus-like model	24
1.1.2. Promoting motions	28
1.1.2.1. Pressure dependence of the kinetic isotope effect (KIE)	29
1.2. A light-activated enzyme	33
1.2.1. Overview of chlorophyll synthesis	33
1.2.2. Reduction of Pchl _{ide}	36
1.2.2.1. Light-independent POR	36
1.2.2.2. Light-dependent POR	39
1.2.2.3. The biological role of POR	41
1.3. Structural studies on POR	43
1.4. The reaction mechanism of POR	46
1.4.1. Substrate binding	46
1.4.2. Pchl _{ide} analogues	47
1.4.3. Excited state processes	48
1.4.3.1. Ultrafast dynamics of free Pchl _{ide}	48
1.4.3.2. Ultrafast reactions during catalysis in POR	51
1.4.4. Hydride transfer	53
1.4.5. Proton transfer	56
1.4.6. Product release	57
1.5. The evolution of dynamically-coupled tunneling in POR	59
1.6. Aims and objectives	61
1.6.1. Pressure dependence of POR	61
1.6.2. Evolution of dynamics in POR	61

Chapter 2 - Experimental set-up	62
2.1. Cloning	63
2.1.1. Plasmid preparation	63
2.1.2. Gene synthesis	63
2.1.3. Restriction digest	63
2.1.4. Ligation	63
2.2. Expression and purification of POR from <i>Thermosynechococcus elongatus</i>	64
2.2.1. Transformation and expression	64
2.2.2. Purification	64
2.2.2.1. Nickel-column	64
2.2.2.2. Blue Sepharose column	65
2.2.3. Determining the concentration of protein	66
2.3. Phylogeny	66
2.4. Substrates and other chemicals	66
2.4.1. Pchl _a synthesis and extraction	66
2.4.2. Other chemicals	67
2.5. Spectroscopy	67
2.5.1. Absorption spectroscopy	67
2.5.2. Pressure spectroscopy	68
2.5.3. Fluorescence	69
2.5.4. Laser flash photolysis	69
2.5.5. Ultrafast transient absorption spectroscopy	71
2.5.6. Global analysis.	72
<i>Chapter 3 - Does the pressure dependence of kinetic isotope effects report usefully on dynamics in enzyme H-transfer reactions?</i>	74
3.1. Abstract	75
3.2. Isotope effects and dynamics in enzyme catalysed reactions	76
3.3. Pressure–temperature dependence of KIEs	79
3.4. <i>p-T</i> dependence of KIEs in flavoproteins	81
3.5. <i>p-T</i> dependence of KIEs for aromatic amine dehydrogenase	84
3.6. Model chemistry (ascorbate and ferricyanide)	85
3.7. Light-activated POR	87
3.8. Correlating the pressure and temperature of KIEs	94
3.9. Trends/outlooks/unifying concepts	96
3.10. Materials and methods	97
<i>Chapter 4 - Expression, purification and kinetic characterisation of POR homologues from different evolutionary origins.</i>	99

4.1.	Abstract	100
4.2.	Introduction	101
4.3.	Materials and methods	104
4.3.1.	Construction of expression vector	104
4.3.2.	Protein overexpression and purification	104
4.3.3.	Substrates and other chemicals	105
4.3.4.	Laser flash photolysis	106
4.3.5.	Steady-state measurements and binding titrations	106
4.3.6.	Phylogeny	106
4.4.	Results	107
4.4.1.	Vector design	107
4.4.2.	Expression and purification of His-tagged POR homologues	107
4.4.3.	Kinetic parameters	117
4.4.4.	NADPH binding constant	126
4.5.	Discussion	134
<i>Chapter 5 - An evolutionary analysis of protein dynamics in the catalytic cycle of the light-driven enzyme protochlorophyllide oxidoreductase (POR).</i>		137
5.1.	Abstract	138
5.2.	Introduction	139
5.3.	Materials and methods	141
5.3.1.	Expression and purification of POR homologues	141
5.3.2.	Laser flash photolysis	142
5.3.3.	Ultrafast transient pump-probe spectroscopy	143
5.3.4.	Global analysis	143
5.3.5.	Phylogeny	144
5.4.	Results	144
5.4.1.	Steady-state characterisation of PORs from different evolutionary origins	144
5.4.2.	Excited state hydride transfer step	146
5.4.3.	Proton transfer step:	151
5.4.4.	Thermodynamic analysis of the proton transfer step	153
5.5.	Discussion	155
Supplementary information - Chapter 5		159
<i>Chapter 6 - Discussion</i>		167
6.1.	Discussion	168
References		171

Abbreviations

A

a	An intermediate to a ‘tunneling-ready conformation’
A	Eyring prefactor
A_{\max}	Maximum change in absorbance upon binding
AADH	Aromatic amine dehydrogenase
Abs	Absorbance
AFM	Atomic force microscopy
ALA	5-aminolevulinic acid
Asc	Ascorbate
ATP	Adenosine Triphosphate

B

b	Almost degenerate product and acceptor states
BSA	Bovine serum albumin

C

Chlide	Chlorophyllide
cP	centipoise
cv	Column volume
Cys	Cysteine

D

Da	Dalton
DAD	Donor-acceptor distance
$\Delta\beta^\ddagger$	Activation isothermal compressibility
ΔV^\ddagger	Apparent activation volume
ΔG^\ddagger	Gibbs free energy
ΔH^\ddagger	Standard enthalpy
ΔS^\ddagger	Standard entropy
DHA	Dehydroascorbic acid
DPOR	‘dark’ Protochlorophyllide oxidoreductase

E

ENDOR	Electron nuclear double resonance
EPR	Electron paramagnetic resonance
ESA	Excited state absorption
F	
F.C.	Franck-Condon
FMN	Flavin mononucleotide
FRET	Förster resonance energy transfer
FTIR	Fourier transform infrared spectroscopy
FWHM	Full width at half maximum
G	
GSB	Ground state bleach
H	
h	Planck constant
\hbar	Planck constant over 2π
HC	Hydrogen coordinate
I	
ICT	Intramolecular charge transfer
IPTG	Isopropyl β -D-1-thiogalactopyranoside
J	
K	
k	Rate
k_b	Boltzmann constant
k_{cat}	Apparent unimolecular rate constant
K_d	Dissociation constant
K_i	Inhibition constant
K_m	Michaelis constant
KIE	Kinetic isotope effect
L	
λ	Wavelength
LB	Lysogeny broth
LED	Light-emitting diode
Lys	Lysine
M	

MOPS	3-(N-morpholino)propanesulfonic acid
MR	Morphinone reductase
MUSCLE	Multiple sequence comparison by log-expectation
MWCO	Molecular weight cut-off
N	
η	Absolute viscosity
NAD(H)	Nicotinamide adenine dinucleotide (reduced form)
NADP(H)	Nicotinamide adenine dinucleotide phosphate (reduced form)
Nd:YAG	Neodymium-doped Yttrium Aluminium Garnet
NMR	Nuclear magnetic resonance
O	
OD	Optical density
ω	Harmonic
OPA	Optical parametric amplifier
OPO	Optical parametric oscillator
P	
p	Pressure
p - T	Pressure-temperature
Pchl _{ide}	Protochlorophyllide
PCET	Proton-coupled electron transfer
PETNR	Pentaerythritol Tetranitrate Reductase
PLB	Prolamellar bodies
POR	Protochlorophyllide oxidoreductase
ψ	Probability density
Q	
q	Environmental coordinate
q^*	Pseudo-transition state
R	
R	Universal gas constant
r_0	Equilibrium barrier width
RED	Reductases, Epimerases, Dehydrogenases
RHR	Reductive half reaction
ROS	Reactive oxygen species

rpm	Rotations per minute
S	
S	Singlet
S ₀	Singlet ground state
S ₁	Singlet first electronically excited state
S ₂	Singlet second electronically excited state
σ	Protein's friction contribution
SADS	Species associated difference spectra
SDR	Short-chain dehydrogenase
SDS-PAGE	Sodium dodecyl sulphate polyacrylamide gel electrophoresis
SKIE	Solvent kinetic isotope effect
T	
τ	Lifetime
T	Temperature
TEA	Tetraethylammonum chloride
TEM	Transmission electron microscope
Tris	Tris(hydroxymethyl)aminomethane
TS	Transition state
TST	Transition state theory
TRS	Tunneling-ready state
Tyr	Tyrosine
U	
UV	Ultraviolet
UV/Vis	Ultraviolet/visible
V	
V	Electronic coupling
W	
X	
X	Any amino acid
Y	
Z	

List of Figures

Chapter 1

Figure 1.1. H-tunneling based on a static barrier (TST-derived) model and the definition of the different tunneling regimes	23
Figure 1.2. Environmentally coupled H-tunneling model.	25
Figure 1.3. Representation of how promoting vibrations improve probabilities of ground-state H-tunneling	27
Figure 1.4. The chlorophyll biosynthesis pathway starting from 5-aminolevulinic acid (ALA).	34
Figure 1.5. Proposed mechanism of DPOR.	38
Figure 1.6. The protochlorophyllide oxidoreductase (POR) reaction	40
Figure 1.7. Phylogeny of the POR protein family	42
Figure 1.8. homology model of <i>Synechocystis</i> POR	45
Figure 1.9. Kinetic scheme of the substrate binding events in POR	47
Figure 1.10. Pchlde molecule with important modification sites highlighted	48
Figure 1.11. Pchlde light-induced excited state branched relaxation process	49
Figure 1.12. Sequential model for light-induced excited Pchlde relaxation	51
Figure 1.13. Proposed mechanism for excited state reactivity of Pchlde in the POR active site	53
Figure 1.14. Energy diagram of the H-transfer reactions in POR, calculated by DFT	57
Figure 1.15. An overall scheme for the catalytic cycle of <i>T. elongatus</i> POR	58
Figure 1.16. Evolution of hydride and proton transfer dynamics catalysed by POR	60

Chapter 2

Figure 2.1. Expression and purification of POR from <i>T. elongatus</i> .	65
Figure 2.2. The Pchlde absorption spectrum and a representation of the corresponding Jablonski diagram	68
Figure 2.3. The set-up for pressure spectroscopy for steady-state measurements	69
Figure 2.4. Laser flash photolysis set-up	71
Figure 2.5. Ultrafast transient absorption set-up	72

Chapter 3

Figure 3.1. Overlay of the FMN and nicotinamide coenzyme within the active sites of NADH ₄ -bound MR (2R14.pdb, green carbons) and PETNR (3KFT.pdb, teal carbons)	82
Figure 3.2. Ascorbate (L-Asc ⁻) oxidation by ferricyanide ([Fe(CN) ₆] ³⁻) in aqueous solution	86
Figure 3.3. Pressure dependence of the ternary enzyme–substrate formation for POR.	89
Figure 3.4. Representative POR photolysis transients	92
Figure 3.5. (A) Pressure dependencies of the observed rate constants for the sequential hydride and proton transfers catalysed by POR at 25 °C	93
Figure 3.6. Linear correlations of $\Delta\Delta H^\ddagger$ with $\Delta\Delta\beta^\ddagger$, $\Delta\Delta V^\ddagger$, $\Delta\Delta S^\ddagger$ and KIE_0	95

Chapter 4

Figure 4.1. Proposed reaction mechanism of POR	102
Figure 4.2. Phylogenetic tree of the POR genes	103

Figure 4.3. Expression and purification of PORs from cyanobacteria	108
Figure 4.4. Expression and purification of PORs from algae	110
Figure 4.5. Soluble fractions of <i>C. merolae</i> from an expression trial using different IPTG concentrations	111
Figure 4.6. Total and soluble fractions of <i>M. paleacea</i> POR from an expression trial	112
Figure 4.7. Expression and purification of PORs from non-angiosperm land plants	113
Figure 4.8. Expression and purification of PORs from angiosperms	115
Figure 4.9. Mass spectrometry of indicated bands of <i>N. tabacum</i> purification	116
Figure 4.10. Spectral changes associated with POR catalysis	117
Figure 4.11. The dependence of the initial rate of Chlide formation on the concentration of NADPH for PORs from cyanobacteria	118
Figure 4.12. The dependence of the initial rate of Chlide formation on the concentration of NADPH for PORs from algae	119
Figure 4.13. The dependence of the initial rate of Chlide formation on the concentration of NADPH for PORs from non-angiosperm land plants	119
Figure 4.14. The dependence of the initial rate of Chlide formation on the concentration of NADPH for PORs from angiosperms	120
Figure 4.15. The dependence of the initial rate of Chlide formation on the concentration of Pchlide for PORs from cyanobacteria	122
Figure 4.16. The dependence of the initial rate of Chlide formation on the concentration of Pchlide for PORs from algae	122
Figure 4.17. The dependence of the initial rate of Chlide formation on the concentration of Pchlide for PORs from non-angiosperm land plants	123
Figure 4.18. The dependence of the initial rate of Chlide formation on the concentration of Pchlide for PORs from angiosperms	124
Figure 4.19. Representation of the inner-filter effects observed at high Pchlide concentrations.	125
Figure 4.20. Fluorescence spectra associated with NADPH binding for POR from <i>C. merolae</i> upon excitation at 295 nm	127
Figure 4.21. Binding titration of NADPH to <i>C. merolae</i> and <i>N. tabacum</i> POR measured by FRET	128
Figure 4.22. Fluorescence spectra associated with NADPH binding for POR from <i>Z. mays</i> upon excitation at 295 nm	129
Figure 4.23. The dependence of the POR-Pchlide-NADPH ternary complex formation on the concentration of NADPH for PORs from cyanobacteria	131
Figure 4.24. The dependence of the POR-Pchlide-NADPH ternary complex formation on the concentration of NADPH for PORs from algae	131
Figure 4.25. The dependence of the POR-Pchlide-NADPH ternary complex formation on the concentration of NADPH for PORs from non-angiosperm land plants	132
Figure 4.26. The dependence of the POR-Pchlide-NADPH ternary complex formation on the concentration of NADPH for PORs from angiosperms	133

Chapter 5

Figure 5.1. The reaction mechanism of protochlorophyllide oxidoreductase (POR).	140
Figure 5.2. Phylogenetic tree of the POR genes	145
Figure 5.3. Kinetic transients at 696 nm showing rates of hydride and proton transfer for <i>N. punctiforme</i> (red) and <i>N. tabacum</i> (blue) POR	148
Figure 5.4. Species associated difference spectra (SADS) resulting from a global analysis of time-resolved ‘fast’ absorption data for different POR homologues	149

Figure 5.5. Species associated difference spectra (SADS) resulting from a global analysis of time-resolved ‘slow’ absorption data (5 ns to 0.5 μ s or 2 μ s) for different POR homologues	150
Figure 5.6. Proton transfer rate as a function of solvent viscosity for all POR homologues	153
Figure 5.7. Temperature dependence of the rate constants for the proton transfer step for three POR homologues	155
Figure S5.1. Alignment of the protein sequence of POR homologues using Clustal W 2.0	161
Figure S5.2. Representative transients showing the absorbance changes at 696 nm for the hydride and proton transfer steps on a log scale	162
Figure S5.3. Transients for hydride transfer for all POR homologues at 4°C	163
Figure S5.4. Time-resolved spectroscopy data for three representative POR homologues after photoexcitation with a laser pulse centred at ~450 nm	164
Figure S5.5. Transients for proton transfer for all POR homologues at 25°C	165
Figure S5.6. Comparison of the proton transfer transients for a viscosity-dependent and viscosity-independent POR homologue	166

List of tables

Chapter 3

Table 3.1. Tabulated rate constants for the POR-catalysed hydride and proton transfer data.....	91
Table 3.2. Pressure dependencies of the rate of hydride and proton transfer catalysed by POR.....	96
Table 3.3. Pressure and temperature dependencies of selected 1° KIEs on biological H-transfers.....	97

Chapter 4

Table 4.1. The average protein yield after purification for the POR homologues.....	116
Table 4.2. Summary of K_m , K_i , V_{max} and k_{cat} values for each of the POR homologues	125
Table 4.3. Comparison of K_d values for NADPH binding from fluorescence and absorbance experiments for the different POR enzymes.....	134

Chapter 5

Table 5.1. The rates of hydride transfer of the POR homologues at 4°C	147
Table 5.2. Rates and solvent viscosity-dependence of the proton transfer step for the POR homologues	152
Table 5.3. The thermodynamic parameters derived from fitting the data in figure 5.6	155
Table S5.1. The rates of hydride transfer for the cyanobacterial POR homologues at 4°C obtained by fitting to a double exponential equation.....	164
Table S5.2. Rates of proton transfer at different solvent viscosities for all POR homologues.....	166

Abstract

Investigating the contribution of protein dynamics to catalysis in Protochlorophyllide oxidoreductase.

A thesis submitted to The University of Manchester for the degree of Doctor of Philosophy (PhD) in the Faculty of Life Sciences by Robin Hoeven, 2015.

Enzyme dynamics has been established to play a crucial role in catalysis, and it has therefore become an important area of research to better understand enzymatic rate enhancements. The light-activated enzyme protochlorophyllide oxidoreductase (POR) is a well-studied model system where dynamics are known to be important for catalysis. The catalytic reaction involves a sequential hydride and proton transfer to reduce the C17-C18 double bond in the protochlorophyllide (Pchlde) substrate with NADPH as a cofactor to yield the chlorophyllide (Chlide) product. Both H-transfer steps are established to undergo quantum tunneling, as derived from the temperature-dependence of the kinetic isotope effects (KIEs). Furthermore, a role for ‘promoting motions/vibrations’ has been presumed from the temperature-dependence KIE data, which will be investigated further in this thesis by the study of the KIE response to pressure. A general overview of the pressure-dependence as a new experimental probe is presented and compared with temperature-dependencies of KIEs, to establish whether pressure is suitable as an alternative technique for studying the role of enzyme dynamics in catalysis. This involves a comparison of pressure data from other enzyme systems to newly collected data for POR. However, no clear trend between temperature and pressure data is observed and hence, it can be concluded that pressure effects can be difficult to interpret. A case by case analysis is required and needs to be combined with computational simulations based on structural evidence (*e.g.* X-ray crystallographic), which is not yet available for POR.

Solvent-viscosity has been successfully used to probe enzyme dynamics in POR and provides information on the extent of any protein networks that are involved along the reaction coordinate. Here I investigate the solvent-viscosity dependence of both H-transfer reactions in POR for a range of homologous POR enzymes to obtain an evolutionary perspective of the protein dynamics required for catalysis. This has been successfully used in the past on a limited number of POR homologues and has led to the formulation of a hypothesis supporting a twin-track evolution of the two catalytic steps in POR. I observed a lack of solvent-viscosity dependence in case of the hydride transfer across all the investigated lineages, while the proton transfer was shown to be more strongly affected by viscosity in prokaryotic enzymes than in their eukaryotic counterparts. This supports the proposed theory, suggesting an early optimisation of the dynamics involved in the light-activated hydride transfer with a strong reliance on localised motion. Conversely, the proton transfer experienced selective pressure to reduce its dependence on complex solvent-slaved motion and that has led to localised dynamics in eukaryotic POR homologues. Additionally, I found that the enzymes from eukaryotic species have a higher rate of both H-transfer steps, suggesting that an optimisation of the active site architecture occurred upon endosymbiosis. Enzyme dynamics clearly have a pivotal role to play in catalysis of this unique light-activated enzyme and detection of these will only be possible by detailed structural information.

Declaration

No portion of the work referred to in the thesis has been submitted in support of an application for another degree or qualification of this or any other university or other institute of learning.

Copyright statement

- i. The author of this thesis (including any appendices and/or schedules to this thesis) owns certain copyright or related rights in it (the “Copyright”) and s/he has given The University of Manchester certain rights to use such Copyright, including for administrative purposes.
- ii. Copies of this thesis, either in full or in extracts and whether in hard or electronic copy, may be made only in accordance with the Copyright, Designs and Patents Act 1988 (as amended) and regulations issued under it or, where appropriate, in accordance with licensing agreements which the University has from time to time. This page must form part of any such copies made.
- iii. The ownership of certain Copyright, patents, designs, trademarks and other intellectual property (the “Intellectual Property”) and any reproductions of copyright works in the thesis, for example graphs and tables (“Reproductions”), which may be described in this thesis, may not be owned by the author and may be owned by third parties. Such Intellectual Property and Reproductions cannot and must not be made available for use without the prior written permission of the owner(s) of the relevant Intellectual Property and/or Reproductions.
- iv. Further information on the conditions under which disclosure, publication and commercialisation of this thesis, the Copyright and any Intellectual Property and/or Reproductions described in it may take place is available in the University IP Policy (see <http://www.campus.manchester.ac.uk/medialibrary/policies/intellectual-property.pdf>), in any relevant Thesis restriction declarations deposited in the University Library, The University Library’s regulations (see <http://www.manchester.ac.uk/library/aboutus/regulations>) and in The University’s policy on presentation of Theses

Acknowledgement

First and foremost I would like to thank Derren Heyes for all his help and guidance during my time in the lab, as well as his patience during the writing of this thesis. I will miss our lively and sometimes odd discussions while working in the lab. Most of my understanding of laser flash photolysis, and enzyme kinetics in general, I owe to you, which I am very grateful for. Also, teaching me some of the more obscure expressions and words in the English language is something I need to thank you for!

I need to express my gratitude to Nigel Scrutton for accepting me to his lab and giving me the freedom and trust to pursue my PhD. I couldn't have asked for a better place to work. Especially your experience and guidance, together with the access to state of the art equipment have made this an unforgettable time. I should not forget to thank you, Sam Hay and Derren for getting my first paper published!

A massive thanks goes to the people in the Scutton group for making my work so enjoyable both in and outside of the lab. With Michi in particular for your patience in dealing with my stupid questions and the occasional chat that made working so much more pleasant. Also a thank you to the other people in and around the lab (*e.g.* Munro group, Linus, Binu. *etc.*) past and present that have made me feel welcome and were always available for providing help or a chat.

I will especially cherish my friendship with Manca, George and John, who have helped me feel welcome and at home in a new city. Thank you for the great memories of our road trip and other extracurricular activities, like running from zombies.

Ten slotte wil ik mijn familie bedanken om mij de mogelijkheid en vrijheid te geven om verder te studeren, ook als dat niet zo kort bij huis is als ge zou willen. Zonder u hulp had ik het niet gekund!

Preface to the alternative format

This thesis is presented in the alternative format with permission from the University of Manchester. In contrast to the traditional format, results chapters are here included as manuscripts for publication in peer-reviewed journals. Some elements have been formatted to ensure consistency throughout this work.

Results chapters and contributions are as follows:

Chapter 3: Does the pressure dependence of kinetic isotope effects report usefully on dynamics in enzyme H-transfer reactions?

Authors: Robin Hoeven, Derren J. Heyes, Sam Hay and Nigel S. Scrutton

Published in: The FEBS journal, 29 January 2015

Contributions: The experiments were carried out by RH with guidance from DH and NS. RH, DH, SH and NS prepared the manuscript.

Chapter 4: Expression, purification and kinetic characterisation of POR homologues from different evolutionary origins.

Authors: Robin Hoeven, Derren J. Heyes and Nigel S. Scrutton

Published in: manuscript in preparation

Contributions: All experiments and manuscript preparation was carried out by RH with the guidance of DH and NS.

Chapter 5: An evolutionary analysis of protein dynamics in the catalytic cycle of the light-driven enzyme protochlorophyllide oxidoreductase (POR).

Authors: Robin Hoeven, Samantha O. J. Hardman, Nigel S. Scrutton and Derren J. Heyes

Published in: manuscript in preparation

Contributions: Laser flash photolysis experiments were carried out and analysed by RH with guidance of DH. Samples for ultrafast transient absorption were prepared by RH, and ran by SH. Global analysis of the data was performed by SH. The manuscript was prepared by RH with the guidance of DH and NS.

Chapter 1

Introduction

1.1. The role of dynamics in enzyme catalysis	19
1.1.1. Hydrogen tunneling	21
1.1.1.1. The concept of wave-particle duality and tunneling	21
1.1.1.2. Marcus-like model	24
1.1.2. Promoting motions	28
1.1.2.1. Pressure dependence of the kinetic isotope effect (KIE)	29
1.2. A light-activated enzyme	33
1.2.1. Overview of chlorophyll synthesis	33
1.2.2. Reduction of Pchl _{id}	36
1.2.2.1. Light-independent POR	36
1.2.2.2. Light-dependent POR	39
1.2.2.3. The biological role of POR	41
1.3. Structural studies on POR	43
1.4. The reaction mechanism of POR	46
1.4.1. Substrate binding	46
1.4.2. Pchl _{id} analogues	47
1.4.3. Excited state processes	48
1.4.3.1. Ultrafast dynamics of free Pchl _{id}	48
1.4.3.2. Ultrafast reactions during catalysis in POR	51
1.4.4. Hydride transfer	53
1.4.5. Proton transfer	56
1.4.6. Product release	57
1.5. The evolution of dynamically-coupled tunneling in POR	59
1.6 Aims and objectives	61
1.6.1. Pressure dependence of POR	61
1.6.2. Evolution of dynamics in POR	61

1.1. The role of dynamics in enzyme catalysis

Enzymes have the potential to perform chemistry with incredible efficiency and specificity. Experimental rate enhancements of 10^{25} -fold have been measured for enzyme catalysed reactions compared to the same reaction in solution, although the actual value might be even higher (Wolfenden 2006). Understanding how enzymes manage to perform these extraordinary enhancements has been the subject of intense research and debate since the dawn of enzymology as a science. Early studies suggested that enzyme-substrate interactions were thought to proceed via a “lock and key” mechanism, which provides a clear and simple explanation for the specificity of enzymes but fails to address the mechanisms by which they work (Fisher 1894). One of the first working models was the “induced fit” mechanism, where the binding of the substrate leads to changes in the active site to allow for the correct orientation and geometry of the substrate for catalysis (Koshland 1958, Koshland 1995). This model coincides with a change in view of what an enzyme is, in that it is now seen as a flexible and dynamic structure, as opposed to a static “lock and key” system. In terms of the way enzymes are capable of “guiding” the chemistry, an important model is the transition state theory (TST), where the lowering of the activation energy of the reaction drives the rate enhancement (Pauling 1948, Lienhard 1973, Kraut 1988). The lower activation energy is proposed to be achieved by having an active site that is energetically more favourable to the transition state (TS) than to the reactants. Even though this model is a closer approximation to reality, it is still lacking some of the complexities that make enzymes such great catalysts. The limitations of the “transition state stabilisation” model can be demonstrated by the lack of success of catalytic antibodies to achieve significant rate enhancements, which rely on forming an “active site” that favours the binding of the transition-state (Hilvert 2000). These antibodies have very small rate enhancements compared to the ‘in solution’ reaction. There are a number of reasons the rates never measured up to the natural enzymes, such as the lack of active-site functional groups, the use of imperfect transition-state analogues, but importantly the lack of a mobile ‘active site’ architecture (Hilvert 2000). This lack of flexibility is probably crucial as we now know that the involvement of protein dynamics plays an essential role in achieving high catalytic efficiencies. We can distinguish two major features by looking at the way enzymes function, one is to have substrates from solution moved into the active site and the eventual removal of

product back into solution (Klinman & Kohen 2013). Second is the actual catalysis that involves the chemistry for conversion of the reactants to form product. In order for the first feature to occur the enzyme needs to be able to accommodate an array of bound species (reactants, TSs, intermediates, product), while the second demands conformational changes that move functional groups in the active site (for example, domain movement to bring in electron donor groups located on a different subunit) (Klinman & Kohen 2013, Miller & Agard 1999). These two types of flexibility have been part of extensive discussion as to whether upon substrate binding conformational selection takes place (Fraser *et al.* 2009, Henzler-Wildman & Kern 2007). The ‘induced fit’ model relies on selection of active site conformations after binding of substrate, while conformational selection depends on the existence of a landscape of conformational states of the enzyme, and upon substrate binding the landscape equilibrium shifts (Koshland 1958, Koshland 1994). Furthermore, it is not enough to just form the enzyme-substrate complex; the enzyme needs to find itself in the correct sub-state in order to be able to perform the bond making or breaking steps in catalysis (Henzler-Wildman & Kern 2007). The most accurate understanding of the contribution of dynamics to enzyme catalysis would be achieved if it were possible to experimentally monitor individual atomic movement within the protein. Unfortunately this is not feasible with current technology, and therefore the contribution of protein dynamics to catalysis has mainly been inferred from physical properties that can be measured by using sophisticated biophysical methods. The majority of these studies have focussed on H-transfer enzymes, including oxidoreductases and dehydrogenases, and the role of quantum mechanical tunneling in these reactions (Kohen & Klinman 2000, Heyes *et al.* 2009, Pudney *et al.* 2010, Johannissen *et al.* 2007, Sutcliffe *et al.* 2006, Alhambra *et al.* 2000, Parker *et al.* 1998, Olsson *et al.* 2004). Dynamics in hydrogen transfer enzymes has proven particularly important, as tunneling by nature demands short internuclear distances between the H-donor and acceptor. The advantage of short distances is that the reliance on localised movement and the relatively simple nature of the H-transfer chemistry makes for a good model system (Saen-Oon *et al.* 2008, Antoniou & Schwartz 2011, Davarifar *et al.* 2011). Furthermore, quantum mechanical effects have the strongest influence on small particles (like hydrogen) and have only started being included in enzyme mechanism models in the last couple of decades. Hence, modern interpretations of the catalytic functioning of enzymes relies on a mixture of classical and quantum processes, with

an array of active-site interactions between substrate and enzyme, driven by a dynamic sampling of transient protein reactant states (Devault 1980, Marcus & Sutin 1985, Moser *et al.* 2006).

1.1.1. Hydrogen tunneling

1.1.1.1. The concept of wave-particle duality and tunneling

One of the limitations of TST is that it only takes the particle-like properties of the reactants into consideration. However, due to the wave-particle duality of matter, one should also consider the wave-like properties of matter (especially for small masses). This wave-like behaviour of mass allows it to pass through regions that otherwise would be inaccessible if it were a particle. In the context of enzymatic reactions this means that under the right conditions it might not be necessary for it to pass over the barrier (as is assumed for TST), but it could go straight through. Therefore, this principle is called quantum tunneling, as it would seem that instead of climbing over the energy barrier (pictured as a mountain), it reaches the other side by going through a tunnel. Especially in enzymatic electron transfer and enzyme catalysed H-transfer reactions it is important to consider these quantum effects as they can significantly affect the reaction chemistry. Enzymes that catalyse electron transfer reactions have been known for some time to employ quantum tunneling, due to the large positional uncertainty of the electron (de Vault & Chance 1966, Marcus & Sutin 1985). The uncertainty of a mass is given by the de Broglie wavelength, which can be calculated from the equation: $\lambda = \frac{h}{\sqrt{2mE}}$, where h is Planck's constant, m is the mass of the particle, and E is its energy. If an energy of 20 kJ·mol⁻¹ is assumed a deBroglie wavelength (λ) of 0.63 Å for protium (H, or ¹H) and 0.45 Å for deuterium (D, or ²H) is obtained. The average distance hydrogen is typically transferred over is similar to these values (< Å) (Cha *et al.* 1989, Kohen & Klinman 1998). Consequently, this overlap in the deBroglie wavelength and average H-transfer distance leads to the use of non-classical hydrogen transfer equations. The representation of a particle's motion and location are contained within the wave function and when this quantity is squared gives a probability for the particle being found in a given region of space. This means that there is a finite probability to find a particle if a non-zero wave function exists for that space (Sutcliffe & Scrutton 2000). Consequently, while classical reactions are strongly determined by barrier height, quantum tunneling reactions are governed by

barrier shape to a much greater extent (Gray & Winkler 1996, Hammes-Schiffer & Soudackov 2008). The established experimental method to investigate H-tunneling in a reaction is to measure the kinetic isotope effect (KIE), with KIE defined as the difference in rate between two isotopes (e.g. protium and deuterium). It is still not trivial to determine whether a reaction makes use of tunneling, as in the past with semi-classical models the only way to say this with any kind of certainty was if the primary KIE was higher than the semi-classical upper limit. The way to calculate this limit is a first order approximation of the difference between the zero-point energies of the two isotopes, which for C-H cleavage at 25°C is 6.9 and 15.8 for k_H/k_D and k_H/k_T , respectively (Melander & Saunders 1987). Even though large KIEs are still evidence of H-tunneling, reactions with more conservative KIE values can still be partly or completely driven by tunneling. It is established within the experimental enzymology community that the temperature-dependence of the KIE and application of quantum tunneling models can be used to deduce a role for tunneling and possible dynamics involved in the reaction (Fraser *et al.* 2009, Henzler-Wildman & Kern 2007, Koshland 1958). In Figure 1.1 A. the representation of the reaction rate ($\ln k/T$) versus temperature ($1/T$) is shown based on a static (TST-like) barrier model for H-tunneling (Jonsson *et al.* 1996). Four regimes can be identified from Figure 1.1: regime I as a classical TST description with large ΔH^\ddagger values and extrapolated values for the Arrhenius prefactor with a ratio of $A^H:A^D \sim 1$. The part of the graph represented with II-IV have increasing H-tunneling contributions going from II through to IV, which are accompanied by inflated isotope effects and extrapolated Arrhenius prefactor ratios moving away from unity. The protium tunnels more than deuterium for regime II, which translates into a larger KIE value and extrapolated $A^H:A^D$ ratios less than one. An inflated KIE is still part of regime III, but the distinction is due to the harder to predict Arrhenius prefactor ratios. Finally, in case of solely ground-state tunneling as in regime IV, it is expected that the reaction rate and KIE are completely temperature-independent and an extrapolated A^H/A^D ratio equal to the KIE value (Jonsson *et al.* 1996). As a direct consequence, reactions with a primary KIE that is temperature-independent can be considered to work by a quantum tunneling mechanism. Experimental data show this model to hold true for certain enzyme systems (Basran *et al.* 1999), but there is a discrepancy between prediction and observation, especially for enzymes catalysing the breaking of C-H bonds (Glasstone *et al.* 1941, Basran *et al.* 1999). The limitations of this static model are that it does not take into account the

dynamic motions of the rather fluid enzyme molecule, which would allow for more complex temperature dependencies.

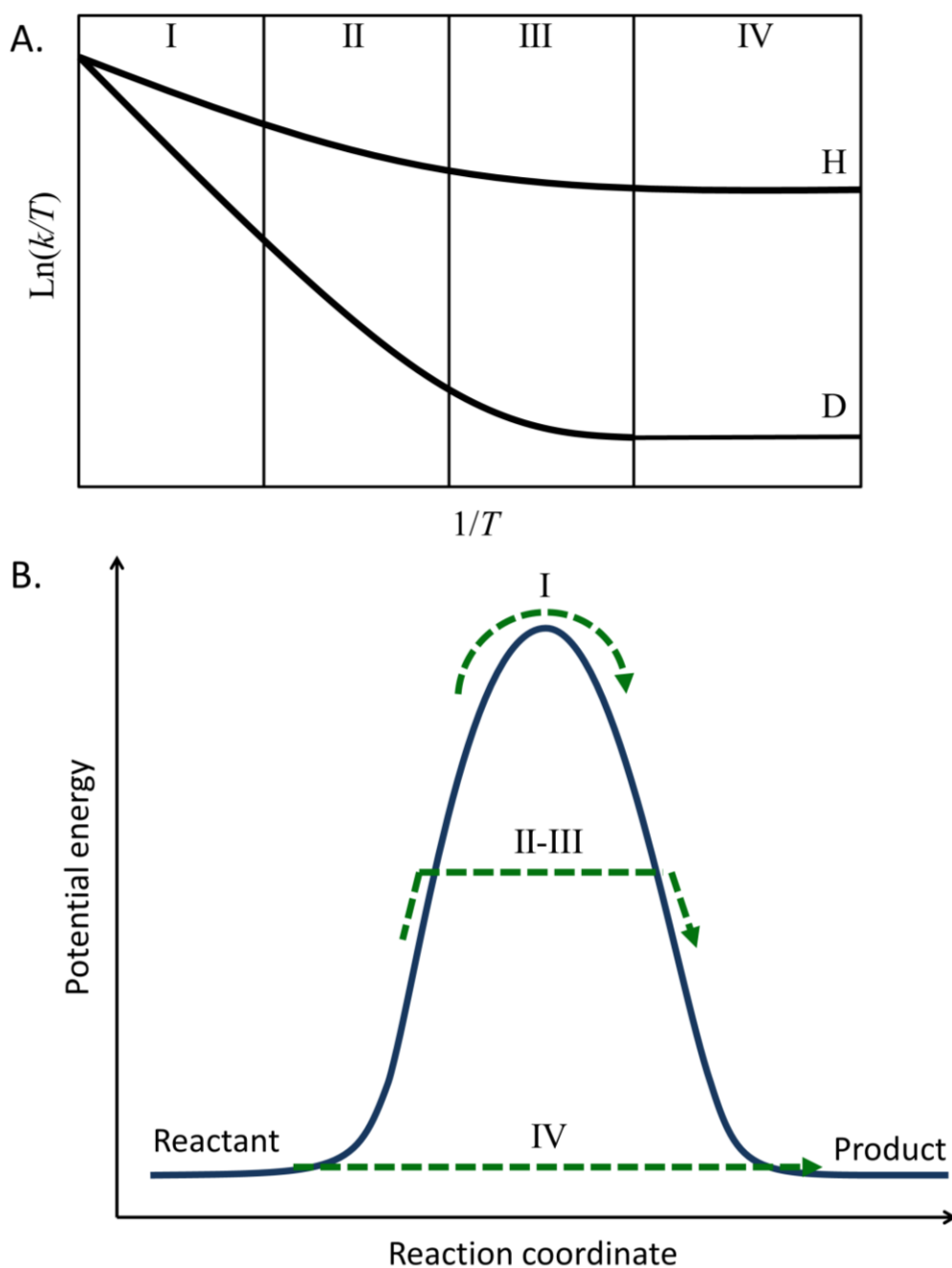


Figure 1.1. H-tunneling based on a static barrier (TST-derived) model and the definition of the different tunneling regimes. A. Diagram of the predicted rates (k/T) in function of temperature ($1/T$) for the protium (top curve) and deuterium (bottom curve) isotopes. Regimes II and III might be thermally dependent as higher vibrational energy states might have to be reached. B. Illustration of the four different regimes and how they traverse to the product side in a static barrier model, representing the transfer with different degrees of quantum-tunneling involvement (Sutcliffe & Scrutton 2000).

One example of a theory that incorporates the quantum nature of the hydrogen transfer, is the Bell correction model, which takes transition state theory (TST) as a base and extends it with a correction to incorporate a contribution from H-tunneling (Bell 1980). The validity of this model however is limited and increasingly breaks down for more tunneling-heavy reactions. In particular, these semi-classical models struggle to explain temperature-independent KIEs even when the step sensitive to isotopic labelling has significant activation energy. The reason for this is that the sole focus of TS-based models is on the H-transfer coordinate, and there is an oversight of dynamics from the heavy-atom environment. Consequently, an increasing number of models have been proposed in which the hydrogen transfer reactions are treated fully quantum-mechanically. A commonly used theory to model quantum mechanical H-tunneling reactions is Marcus theory, which considers the heavy-atom coordinates associated with electron transfer as an environmental energy term ($k_{\text{ET}} \sim e^{-\Delta G^*/RT}$). Here R is the gas constant, ΔG^* is the free energy barrier to the reaction, and T is absolute temperature (Marcus & Sutin 1985). The assumption made in this theory is that the reaction coordinates are mainly determined by the heavy atom coordinates and not the electron. In order to understand hydrogen transfer the Marcus model has been taken as a base on which to build a full quantum tunneling theory for enzyme catalysed H-transfer reactions. It is possible to apply a model built for electron transfer reactions and apply it to hydrogen transfer reactions, because hydrogen is also a light particle with a large uncertainty in its position. One important limitation that has to be noted is that the Marcus model was designed for non-adiabatic (weak coupling) electron transfer reactions, while H-transfer reactions are mostly adiabatic.

1.1.1.2. Marcus-like model

It is important to note that in the literature the Marcus-like model is referenced under different names, for example: “environmentally coupled tunneling” (Nagel & Klinman 2006, 2010), “Marcus-like models” (Sen & Kohen 2010, Dutta *et al.* 2012), “Vibrationally enhanced tunneling” (Bruno & Bialek 1992). These fully quantum tunneling models are still based on the Marcus theory of electron tunneling (Marcus & Sutin 1985), where the electron is substituted by the hydrogen atom. The assumption in these models is that heavy atom reorganisation leads to the formation of a tunneling-ready state (TRS), which causes a transient degeneracy of the potential

energy surfaces of reactants and products allowing a donor-acceptor wave function overlap (see equation 1.1; see Figure 1.2; Knapp & Klinman 2002, Hammes-Schiffer 2006, Pudney *et al.* 2010, Klinman & Kohen 2013).

$$k = C(T) \frac{[V]^2}{\hbar} \sqrt{\frac{\pi}{\lambda k_B T}} e^{\frac{-(\Delta G^\circ + \lambda)^2}{4\lambda k_B T}} \times \int_0^\infty F.C.term_{0,0} e^{\frac{-E(r_x)}{k_B T}} dr_x \quad (1.1)$$

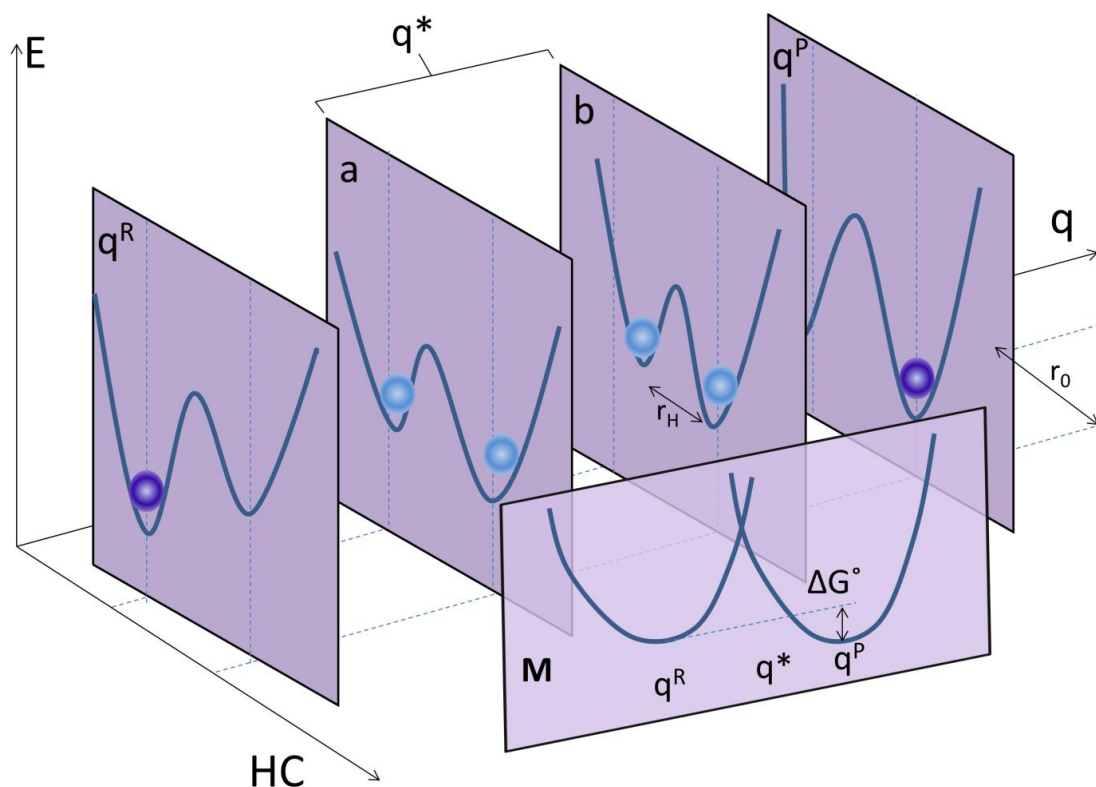


Figure 1.2. Environmentally coupled H-tunneling model. The three axes are: E , energy; q , environmental coordinate; HC , the hydrogen coordinate. The grey spheres represent the ground-state vibrational wavefunction of the H nucleus. The four vertical panels, q^R , a , b , q^P , show the double-well potential energy surface during the reaction progress: from the reactant state, q^R ; to a state where the reactant and product states potential energy are approximately degenerate, but r_0 , the equilibrium barrier width, is too large to have tunneling to occur, a ; intermediate to a ‘tunneling-ready conformation’, b , almost degenerate product and acceptor states and tunneling can occur with reasonable probability, because the tunneling distance, r_H , is small enough; eventually to the product state, q^P . Both, a and b can be imagined of as a pseudo-transition state, q^* . Panel M shows the free-energy parabolas as functions of this environmental coordinate (Hay *et al.* 2008, Hay & Scrutton 2012).

The part of the equation before the integral is similar to the Marcus theory for the rate to reach a TRS, with λ being the reorganisation energy, $C(T)$ is the fraction of reactive enzyme complexes that are able to proceed to product, V the electronic coupling, T the absolute temperature and the reaction-driving force ΔG° and the constants used are the

Boltzmann constant (k_B) and the Plank constant over 2π (\hbar). It can be noted that the term can explain the temperature dependence of the rate, but not the isotopically divergent temperature dependence required to explain the effects of temperature on KIE (Kuznetsov & Ulstrup 1999, Knapp & Klinman 2002, Pudney *et al.* 2010, Hammes-Schiffer 2006, Knapp *et al.* 2002).

$$F.C.term_{0,0} = e^{\frac{-m_H \omega_H r^2}{2\hbar}} \quad (1.2)$$

This is where the term within the integral sign becomes important, as the Franck-Condon (F.C.) term is determined by the mass (m_H), frequency (ω_H), and transfer distance (r) of the tunneling particle from a ground-state vibrational mode (as indicated by 0,0) (equation 1.2). The other term within the integral sign is influenced by the energetic barrier for donor-acceptor distance (DAD) fluctuation $E(r_x)$; which in turn is determined by collective mass (m_x) and frequency (ω_x) of the heavy atoms controlling distance sampling. This is therefore the part within the integral sign that is entirely responsible for the isotope effects, as it is a calculation of the tunneling probability over all possible DADs at the TRS (see Figure 1.3). The fact that the TRS thermal activation energy is uncoupled from the tunneling probability makes Marcus-like models so effective in rationalising kinetic data both for non-enzymatic as well as enzymatic reactions. As mentioned previously, the semi-classical models cannot account for temperature-independent KIEs with temperature-dependent rates (Bell 1980), as opposed to the Marcus-like models that can.

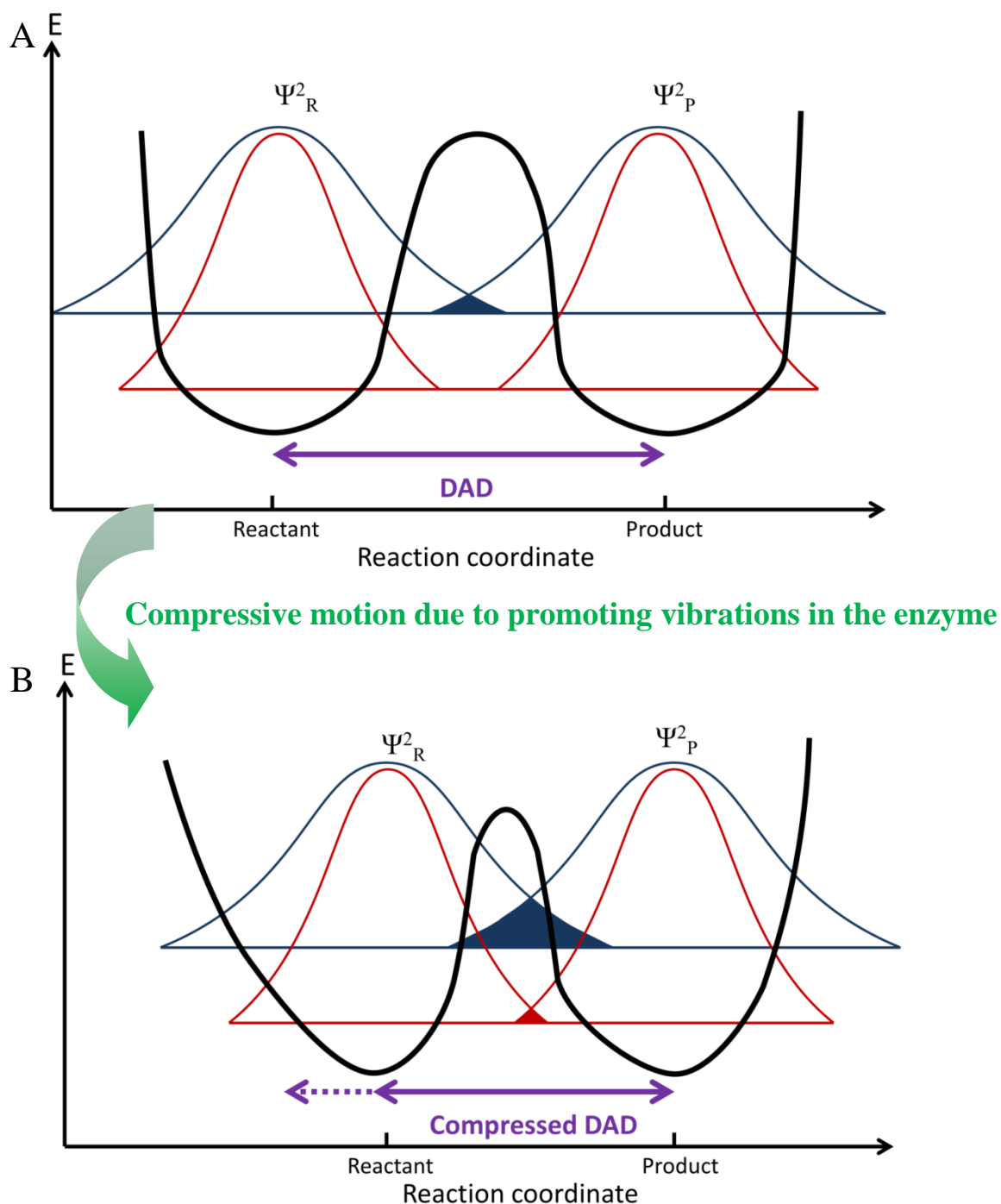


Figure 1.3. Representation of how promoting vibrations improve probabilities of ground-state H-tunneling, where Ψ_R^2 and Ψ_P^2 are the probability densities of the reactant and product, respectively. The blue and red bell curves represent the protium and deuterium probability distribution, respectively. Panel A shows the situation after the TRS is reached and before the action of any promoting motions. Compressive motion allows for a narrowing of barrier shape, by lowering the donor-acceptor distance (DAD) as shown in panel B. The area of overlap for reactant and product differs between isotopes and between panel A and B, where panel B has a larger probability of tunneling for both isotopes. This area can be calculated mathematically from the integral in the Marcus-like model (equation 1.1), which is basically determined by the Franck-Condon term giving a probability of tunneling (Klinman & Kohen 2013).

For certain (enzymatic) reactions a temperature-dependent KIE can be observed (Knapp *et al.* 2002), which can be explained by looking at the second exponential term within the integral of equation 1.1, because it is temperature and mass dependent. According to this model, the different response to temperature for hydrogen and deuterium can be explained by further adjustments to the DAD (i.e. larger $E(r_x)$) values at the TRS that are required for the heavier isotope, in order to achieve a better overlap of the wave functions (see Figure 1.3; Kohen & Klinman 1998, Hay *et al.* 2007, Klinman & Kohen 2013). Consequently, in a full tunneling model, the temperature dependence of the KIE can be considered evidence of a quantum mechanical tunneling reaction (Sutcliffe & Scrutton 2000, Klinman & Kohen 2013, Pudney *et al.* 2013).

1.1.2. Promoting motions

The above mentioned Marcus-like model (equation 1.1) is informative on quantum tunneling, but it also points to a crucial role for protein dynamics in catalysis (at least for H-transfer reactions). The second exponential term within the integral highlights the involvement of the heavy atoms in catalysis, namely by its pivotal role in controlling the DAD. It is important to note that the heavy-atom motions are in a thermal equilibrium with their environment on a timescale that is equal or faster than the experimentally measured rate constant of the chemistry. However, this remains a constantly evolving model so the role for these dynamics in enzyme-catalysed reactions is still a hotly debated topic among scientists. Protein structure plays a fundamental role in enzymology, but in solution proteins are very dynamic molecules with a range of motions from slow-domain movements (ms to sec) through to the fast bond stretches (fs-ps). The significance of all of these vibrations within proteins for catalysis is still a highly controversial topic, especially whether vibrations/motions faster than turnover can influence catalysis (Hay & Scrutton 2012). NMR has been a particularly useful technique in studying loop opening/closing motions (ns-ms) and their function in catalysis, by providing direct observations of how these vibrations affect enzyme function (Boehr *et al.* 2006, Henzler-Wildman *et al.* 2007). However, analysis of the coupling of faster dynamics (<ns) to enzyme turnover with empirical methods still remains very challenging, and mostly depend on indirect measurements, such as the observation of anomalous KIE temperature-dependency data (Kohen *et al.* 1999, Maglia & Allemann 2003, Hay *et al.* 2007, Heyes *et al.* 2009). Understanding

fast protein motions (ps-fs) and their influence on the chemistry happening on the same timescales (like transition-state crossing) is of crucial importance to control enzyme catalysis (Thomas *et al.* 2008, Hay & Scrutton 2012, Hong & Tantillo 2014). By assigning the type of motion to a certain timescale allows us to derive a degree of locality to these motions. Large-scale conformational changes tend to occur on a microsecond to millisecond timescale, while local protein configurational changes occur within the picosecond to nanosecond range, and barrier crossing being the fastest on the femtosecond to picosecond range. In the case of the tunneling model we can consider quantum mechanical wave function overlap as an instantaneous event, while barrier crossing is dependent on the slower heavy-atom motions (Klinman & Kohen 2013). Consequently, if tunneling can be considered instantaneous, and is therefore faster than the fast protein dynamics (ps-fs), it means that the KIE (if rate-limiting) will report on these promoting vibrations. Another advantage of making use of KIE data is that there is a high degree of spatial resolution by only reporting on the local motions directly involved in catalysis, as opposed to global isotope-independent conformational changes. There is a large degree of flexibility in the way the KIE is affected by temperature, and mostly depends on the average DAD and its fluctuations (Roston *et al.* 2012). It is however required that the DAD is shorter than van der Waals distances in order to attain the TRS, either through ground-state effects or the mentioned DAD sampling process. The very short (compressed) DAD distances can be achieved by a protein conformational sampling process that creates transient substates with a short enough DAD to allow for an effective wave function overlap (Nagel *et al.* 2012, Klinman & Kohen 2013). It is this protein conformational sampling that is hypothesised to be the promoting motions in the Marcus-like model called “Environmentally coupled tunneling model”.

1.1.2.1. *Pressure dependence of the kinetic isotope effect (KIE)*

Temperature-dependent KIEs are now well established as a probe for quantum tunneling in enzymatic H-transfer reactions. The use of hydrostatic pressure on KIE has been suggested as a complementary method to temperature dependence as a technique to study environmentally coupled H-transfer reactions (Northrop 2006, Hay & Scrutton 2008). Pressure is expected to affect the activation volume of the isotope effect because according to equation 1.1 it is the H-transfer distance (r) and the force constant for DAD sampling (through the $E(r_x)$) that are the main contributions to the

pressure response (Hay & Scrutton 2008). As experimental observations mostly depend on KIE data, equation 1.3 gives a theoretical understanding of the KIE response to pressure (Klinman & Kohen 2013). It should be noted that the DAD (r_x) response to pressure has to be perturbed along the reaction coordinates in order to be picked up by the observed KIE (Hay *et al.* 2012). Equation 1.3 is in effect equation 1.1 for the protium divided by equation 1.1 for deuterium, where the first term (before the integral) drops out as it is virtually isotope independent.

$$KIE(p, T) = KIE_0 \times \frac{\int_0^\infty (e^{-\omega_H m_H r(p)^2 / 2\hbar}) e^{\beta[-E(r_x(p))_H] / k_B T} dr_x}{\int_0^\infty (e^{-\omega_D m_D r(p)^2 / 2\hbar}) e^{\beta[-E(r_x(p))_D] / k_B T} dr_x} \quad (1.3)$$

An interesting case is that of the flavoprotein pentaerythritol tetranitrate reductase (PETNR), which performs a reductive half reaction by transferring a hydride from either the NADH or NADPH coenzyme to the flavin cofactor. Interestingly, a different KIE temperature dependence is observed for each coenzyme, with NADH having a temperature-independent response while the NADPH reaction has a KIE that is thermally sensitive. These data allowed the authors to present a model with the involvement of promoting motions in the case of NADPH as coenzyme, while the NADH reaction has a very small level of or even no promoting motions to help drive the reaction (Pudney, Hay, *et al.* 2009). Furthermore, the authors have looked at what influence pressure has on the system and the KIE in particular. The presence of a curvature in the plot of KIE as a function of pressure for the NADPH reaction and no such curvature for the NADH reaction led to the hypothesis that a curvature in the KIE pressure dependence graph indicates the presence of promoting motions (Pudney *et al.* 2009). Caution is nonetheless advised with trying to generalise these PETNR observations, as it took an array of techniques and manipulations to get to these conclusions. Therefore, it is likely that the effects of pressure on a protein system are not always straightforward and tend to have a highly system dependent response. These differential responses are likely the cause of an anisotropic propagation of pressure across the protein structure, which is different from the, experimentally measureable, directional change along the reaction coordinate (Hay *et al.* 2012). Pressure is generally assumed to perturb pre-existing equilibria in favour of species with smaller volumes (Northrop 1999, Masson & Balny 2005). Therefore, pressure is suggested to disturb rate constants and/or KIEs in a heterogeneous system with

multiple conformational states, by affecting the relative concentrations of reactive states (Hay *et al.* 2012, Pudney *et al.* 2009).

Pressure can perturb both large conformational changes as well as local active site geometry and single side-chain vibrations. The use of ‘heavy’ proteins is an example of an experimental technique to selectively alter the frequency of enzyme vibrational modes, but not to affect the electrostatic environment or protein geometry. ‘Heavy’ proteins have their non-exchangeable atoms replaced by heavier isotopes, such as ^{13}C , ^{15}N and ^2H , which have the same electrostatic properties according to the Born-Oppenheimer theory (Silva *et al.* 2011, Kipp *et al.* 2011). Consequently, if the ‘heavy’ enzyme is reactively different from the natural ‘light’ enzyme it is reasonable to assume that this is due to the coupling between protein motion and enzyme catalysis, and indeed this has been observed for a number of enzyme systems (Rod *et al.* 2003, Stojković *et al.* 2010, Silva *et al.* 2011, Ruiz-Pernia *et al.* 2013, Pudney *et al.* 2013). The temperature-dependence of the KIE in PETNR is affected by isotopically labelling the protein (Pudney *et al.* 2013). Interestingly, the temperature-dependence of the KIE for both the reactions with NADH and NADPH as coenzymes are perturbed. Even though, the KIE for NADH is temperature-independent for the ‘light’ enzyme, a slight temperature-dependence is observed for the ‘heavy’ form. A temperature-independent KIE does not therefore necessarily exclude the involvement of promoting motions (Pudney *et al.* 2013). These observations do show that ‘heavy’ enzyme labelling is a powerful tool in relating enzyme dynamics to catalysis.

An *in silico* study by Johannissen *et al.* 2011 of the pressure-temperature (p - T) data of morphinone reductase (MR) has suggested an explanation for the observed increase of KIE and rate. The experimental data showed a decreasing KIE at higher pressures with a more compressed DAD, which is seemingly counter intuitive as DAD compression should affect deuterium more than protium (Hay *et al.* 2007). Modelling of the data with the Marcus like equation (equation 1.1) highlights the importance of the force constant (k_x), hidden within the $E(r_x)$ variable (equation 1.4).

$$E_x = \frac{1}{2} r_x^2 k_x \quad (1.4)$$

Pressure decreases the DAD within MR due to an increasing force constant (and consequent increase in free energy), which in turn is caused by a significant increase in the frequency of the promoting vibration (Johannissen *et al.* 2011). These results show the importance of pressure dependency studies to probe barrier compression and promoting motions, which exhibits the complex nature of donor-acceptor compression and the KIE.

The advent of more advanced gene synthesising technology has allowed for a comparison of the different ‘evolutionary ages’ of an enzyme, which can help in elucidating how these dynamic vibrations have come to play a role in catalysis over time. Knowledge of the origin of these promoting motions, in turn can aid understanding of how they are important and can help in designing better inhibitors and improve yields of bio-catalytic processes. Research into the evolutionary origins of dynamics and its role in catalysis has shown that in some cases enzymes have actively optimised their reaction coordinate for tunneling (Basran *et al.* 1999, Antoniou *et al.* 2002, Sutcliffe & Scrutton 2002, Knapp & Klinman 2002, Yahashiri *et al.* 2008, Klinman 2010). The concept of promoting vibrations actively been selected for during evolution in order to improve catalysis, is still highly controversial. A better understanding of the actual molecular motions would aid the argument for dynamic coupling greatly.

In conclusion, the effects of a temperature dependent KIE are relatively well understood, but the response to pressure does not appear to be straightforward, and seem to vary strongly from one system to the next. The limited understanding of the pressure dependence is in part due to the small number of actual experimental data available and in part because of the anisotropic response of pressure on different enzyme systems. One of the objectives of this work is to further our understanding of pressure on H-transfer enzymes by contributing to the body of data with a pressure dependence of a hydride and proton transfer step for a unique light activated enzyme.

1.2. A light-activated enzyme

Due to the small size of the hydrogen atom the rate of transfer of hydrogen has the potential to be quite fast, which can make these reactions difficult to follow directly. Hence, understanding how motions within the enzyme contribute to H-tunneling remains a challenging objective, especially the inability to simultaneously trigger catalysis and measure chemical steps on the nano- to microsecond timescales. In the case of thermally-activated enzymes rapid mixing techniques are often used to follow these reactions on a millisecond timescale, but this might not always be fast enough to directly study the chemical steps in a reaction or to analyse the formation of intermediates in real time. A much better solution is to utilise a trigger that is faster than the fastest dynamics involved in the reaction and light-activated enzymes, such as DNA photolyase (Aubert *et al.* 2000), protochlorophyllide oxidoreductase (Masuda & Takamiya 2004, Heyes & Hunter 2005) and photosynthetic reaction centres (Okamura *et al.* 2000, Paddock *et al.* 2003), provide the possibility to investigate such catalytic processes. Within this thesis the focus is on the light-driven enzyme, protochlorophyllide oxidoreductase (POR), which has proven to be an excellent model system to study reaction dynamics in enzyme catalysis.

1.2.1. Overview of chlorophyll synthesis

Production of chlorophyll is essential for phototrophic organisms as it is the main pigment to capture light energy, which can in turn be transferred by resonance energy transfer to a specific chlorophyll pair in the reaction centre of one of the photosystems. Furthermore, in the case of eukaryotic phototrophs, production of chlorophyll is also a prerequisite for the correct development of chloroplasts (Yuan *et al.* 2012). Chlorophyll belongs to the tetrapyrrole class of molecules, which also includes other important biological molecules, such as haem, coenzyme B₁₂ and bilins. The tetrapyrrole biosynthesis pathway starts with the universal precursor, 5-aminolevulinic acid (ALA), which is a 5 carbon compound and for this reason this pathway is sometimes also called the C5-pathway (Von Wettstein *et al.* 1995, Tanaka & Tanaka 2007). There are a series of steps that are common for the production of all tetrapyrroles starting from ALA (see Figure 1.4). The chlorophyll branch starts with the insertion of Mg²⁺ into protoporphyrin IX, catalysed by the ATP-dependent magnesium chelatase. The following steps consist of changes to the ring's conjugation

system and to side groups, with the addition of a long carbon chain as the final step to form chlorophyll.

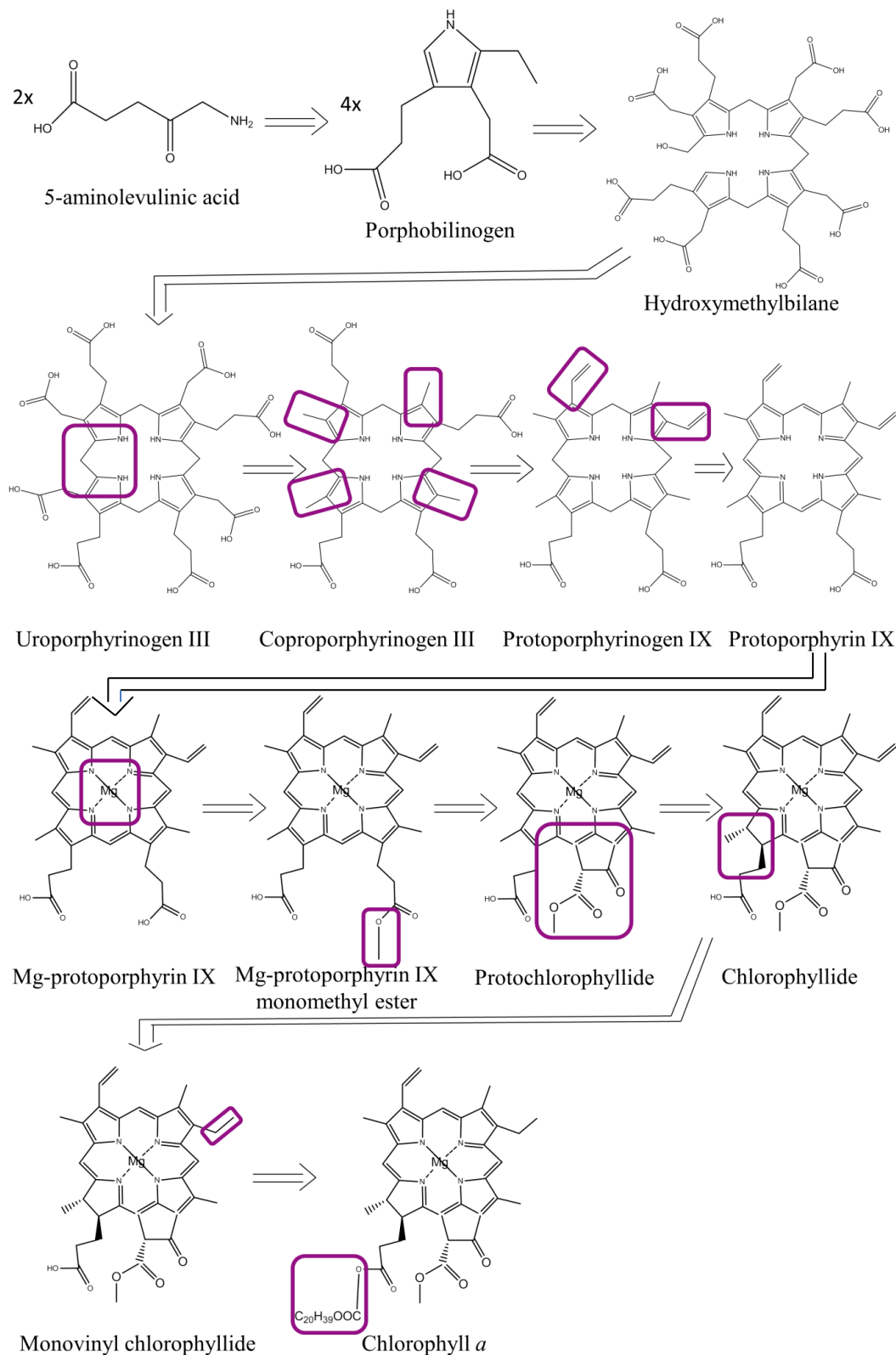


Figure 1.4. The chlorophyll biosynthesis pathway starting from 5-aminolevulinic acid (ALA). Each step beginning from uroporphyrinogen III has the change from the previous structure marked with a purple box. In the case of protoporphyrin IX the conjugation system of the entire tetrapyrrole system is altered so no purple box is used.

It is important to tightly control the tetrapyrrole pathway as the demand for each branch can change in time, which requires a response in the regulation of the enzymes involved (Tanaka & Tanaka 2007). If more haem is required, it is obvious that the haem producing branch needs to be up regulated. At the same time an increase of the general tetrapyrrole pathway is necessary if loss of substrate flow to the other branches needs to be prevented. Consequently, ALA plays a very important role in the cellular regulation of the biosynthetic pathway, especially because the downstream intermediates have the potential to form reactive singlet oxygen under illumination. The cell has mechanisms available to minimise the potential damage from reactive oxygen species (ROS). One of the tight regulations of the pathway is to keep the intermediate concentrations low. Alternatively, the cellular levels of chlorophyll free in solution are kept low by keeping it bound to proteins of the photosynthetic apparatus. Finally, the chlorophyll branch of the pathway is located in relatively anaerobic conditions of the lipid bilayer of the thylakoid membranes, to minimise exposure to oxygen (Von Wettstein *et al.* 1995, Reinbothe *et al.* 1996, Blankenship 2001). Within the chlorophyll pathway one of the key steps is the conversion of protochlorophyllide (Pchl_{id}) into chlorophyllide (Chl_{id}) (see Figure 1.4), as this step is regulated in a unique fashion (at least in angiosperms). Under dark conditions the pathway will stop at this step of the reaction, because light is required for the reaction chemistry. This will lead to the accumulation of the Pchl_{id} intermediate, which is bound to POR in a ternary complex with the NADPH coenzyme. Upon illumination Pchl_{id} is converted into Chl_{id} leading to the rapid formation of chlorophyll. There are at least two advantages of binding Pchl_{id} to POR, one is that Pchl_{id} photodestruction is limited; secondly POR is insensitive to oxygen and therefore prevents ROS formation. Overexpression studies in *A. thaliana* have clearly demonstrated the protective properties of POR against photooxidative damage (Sperling *et al.* 1997). Therefore, POR plays a pivotal role for the proper functioning of the cells of phototrophs.

It should be noted that the conversion of Pchl_{id} into Chl_{id} can be catalysed by two genetically and structurally different enzymes. The two enzymes show differences in their dependence on light for catalytic activity and hence, the light-independent enzyme is known as 'dark' Protochlorophyllide oxidoreductase (DPOR).

1.2.2. Reduction of Pchlide

The conversion of Pchlide into Chlide can be catalysed by two genetically and structurally different enzymes. The two enzymes show differences in their dependence on light for catalytic activity and hence, the light-independent enzyme is known as ‘dark’ Protochlorophyllide oxidoreductase (DPOR). Both enzymes are widely dispersed and present in the majority of photosynthetic organisms. In both cases the reaction involves the reduction of the double bond at the C17-C18 position of Pchlide to a single bond in the Chlide product. However, completely different reaction mechanisms are used by the 2 enzymes to catalyse the same reaction.

1.2.2.1. Light-independent POR

A light-independent DPOR enzyme is found in some photosynthetic bacteria and cyanobacteria that can catalyse the reduction of the double bond in ring D of Pchlide, but is completely different to the light-driven POR enzyme in terms of subunit composition, DNA sequence, catalytic mechanism and molecular structure (Masuda & Takamiya 2004). Until recently very little was known about DPOR, but progress has been facilitated by studies on *Rhodobacter* mutants, such as *Rhodobacter sphaeroides* and *R. capsulatus*. Mutants of these facultative anoxygenic phototrophs that were impaired in some steps of bacteriochlorophyll synthesis (Bauer *et al.* 1993), helped to identify three loci, *bchL*, *bchB* and *bchN*. After closer investigation of the open reading frame (ORF) of these three genes and numerous mutagenesis experiments (Ohyama *et al.* 1986, Kohchi *et al.* 1988, Fujita *et al.* 1992, Suzuki & Bauer 1992) it was revealed that the mutant phototrophs lost the ability to synthesize chlorophyll in the dark. The proteins that are encoded by these three genes were shown to be the three subunits that form the active DPOR enzyme. This led to the surprising conclusion that these proteins, with significant sequence similarity to the nitrogenase enzyme that is involved in the reduction of dinitrogen, seemed to be a light-independent POR enzyme (Suzuki & Bauer 1992, Fujita 1996, Lidholm & Gustafsson 1991, Richard *et al.* 1994, Choquet *et al.* 1992). Moreover, DPOR appears to be an ancient enzyme that is widespread among a large group of phototrophs, but seems to have been lost in angiosperms (Burke *et al.* 1993, Suzuki & Bauer 1995). If DPOR has an evolutionary nitrogenase origin it would be reasonable to expect some nitrogenase-like characteristics, such as thiol reductant and ATP requirement for activity, as well as a strong sensitivity to molecular oxygen. These features have been confirmed *in*

vitro with recombinant BchL, BchB and BchN subunits from *R. capsulatus* (Fujita & Bauer 2000). In particular, the molecular oxygen sensitivity is an unusual characteristic for an enzyme of the chlorophyll biosynthetic pathway in oxygenic phototrophs and it is possible that DPOR has some tolerance towards oxygen and/or has some mechanisms in place that help protect it against the oxygen produced by photosynthesis. Evidence for oxygen sensitivity can be found in the inverse proportionality of light intensity and DPOR activity, because more light corresponds with more oxygen production (Fujita *et al.* 1998). It is likely that chlorophyll production is controlled by an interplay of light-dependent and –independent POR, so that light-dependent POR is less functional when DPOR is more abundant (Shui *et al.* 2009).

The overall DPOR structure consists of two components, the NB-protein (BchN-BchB heterotetramer) and the L-protein (BchL dimer), which show structural similarity to nitrogenase MoFe protein and Fe protein, respectively (Fujita & Bauer 2000). The crystal structure of the NB-protein has recently been resolved at 2.3Å resolution for *Rhodobacter capsulatus* (Muraki *et al.* 2010). This showed that each BchN-BchB unit contains one iron-sulphur cluster and one Pchlide (NB-cluster) that is organized uniquely by the interaction with three cysteines and one aspartate. Cluster assembly does not require aspartate ligation necessarily, but it does play a crucial role for catalysis. The binding of the Pchlide substrate induces a partial unwinding in an α -helix in the neighbouring catalytic BchN-BchB unit. The reaction mechanism in DPOR is therefore thought to involve a *trans*-specific reduction mechanism, in which the protons for the C17 and C18 positions of Pchlide are donated by an aspartate from BchB and the distorted C17-propionate of Pchlide, respectively (Muraki *et al.* 2010). The expected similarity with MoFe protein is clearly represented by the almost identical arrangement of Pchlide and the NB-cluster, compared with the respective arrangement of the FeMo-cofactor and the P-cluster in nitrogenase MoFe-protein. The existence of a common architecture between the two enzymes can be explained by their function in reducing the stable chemical bonds in their respective substrates, porphyrin and dinitrogen (Muraki *et al.* 2010). For the reaction mechanism it is important to understand the coupling of proton- and electron-transfers, as the NB-cluster is assumed to be a single-electron mediator, while the reduction of Pchlide requires two electrons and two protons. One recently suggested mechanism by Nomata *et al.* (2014), starts with the transfer of an electron from the NB-cluster to reduce

Pchlide and form an anion radical intermediate (see Figure 1.5). The next step involves donation of a proton from the C17-propionate to the C18 position of the same Pchlide molecule. In turn, the propionate is suggested to be reprotonated by the BchB-His378 residue, which is only located 6.5 Å away from this group. This second step results in the loss of charge on the Pchlide molecule to form a neutral radical intermediate. During the third step the radical is converted to a non-radical anion intermediate by the transfer of an electron from the NB-cluster. Finally, an aspartate in the active site (Asp274) provides a final proton to complete the reaction and yield Chlide (Nomata *et al.* 2014). The catalytic mechanism described here for DPOR is completely different from light-triggered POR, which depends on a consecutive hydride and proton transfer during the light-dependent step and at least two subsequent dark-reactions (Heyes & Hunter 2005) (see below).

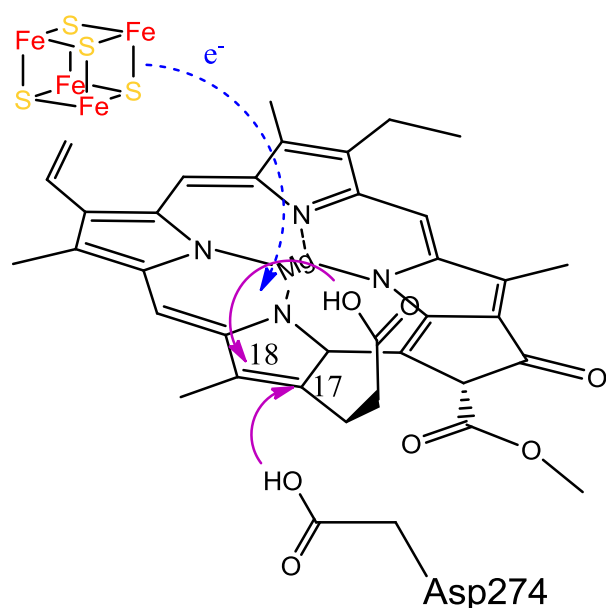


Figure 1.5. Proposed mechanism of DPOR. An initial electron transfer (blue dashed arrow) from the [4Fe-4S]-cluster generates a Pchlide anion radical (not shown). The ensuing proton transfer to C18 from the C17 propionate group and a second proton transfer from the Asp274 (purple arrows) together with another electron transfer result in the formation of Chlide product (Nomata *et al.* 2014).

1.2.2.2. *Light-dependent POR*

The focus of this thesis is on the light-dependent POR and hence, the acronym 'POR' will refer specifically to the light activated enzyme. POR can be found in almost all oxygenic phototrophs and is responsible for the conversion of protochlorophyllide (Pchl_{id}) into chlorophyllide (Chl_{id}), which is the precursor for chlorophyll. The reduction of Pchl_{id} by POR occurs using NADPH as a coenzyme for the conversion of the double bond at the C17-C18 position of Pchl_{id} to a single bond in the Chl_{id} product (see Figure 1.5).

The genes for light-dependent POR are widely distributed among many photosynthetic organisms, with the apparent exception of the non-oxygen evolving photosynthetic bacteria (Fujita 1996, Armstrong 1998). As these non-oxygen evolving phototrophic bacteria make use of the most ancient photosystems, this seems to indicate a link between the evolution of POR and the evolution of oxygenic photosynthesis (Reinbothe *et al.* 1996).

With the increasing amount of genomic data available a better overview of the phylogeny of the POR gene family is now possible. Cyanobacteria appear to only have one POR gene, according to the whole genome sequences available for cyanobacteria (Kaneko *et al.* 1996, Nakamura *et al.* 2003, Dufresne *et al.* 2003). However, the case is different in angiosperms, where the expression of POR has caused a certain amount of confusion, because the expression featured a rapid and significant negative regulation after illumination of seedlings grown in the dark. This effect was shown to vary significantly between different plant species, ranging from a negative response, with the expression of POR reduced upon increased illumination, to no effect at all. Closer investigation led to the discovery of two POR isoforms, called PORA and PORB, in barley (Holtorf *et al.* 1995) and *Arabidopsis thaliana* (Armstrong *et al.* 1995). These variant isoforms show prominent differences in gene expression, as both are expressed in the dark but during growth in light, PORA expression rapidly drops while PORB mRNA levels increase. This phenomenon of two distinctly regulated POR genes is thought to be widespread among angiosperms, with different ratios of PORA and PORB expression caused by variations in their response to light (Armstrong *et al.* 1995, Holtorf *et al.* 1995). A search for POR genes in gymnosperms, such as loblolly pine (*Pinus taeda* L.), revealed two separate subfamilies, containing genes similar to the PORA and PORB genes of angiosperms, where the PORA family

has two members and the PORB family has at least 11 members (Skinner & Timko 1998). Within angiosperms a third isoform of POR was discovered in *Arabidopsis thaliana*, PORC (Oosawa *et al.* 2000). Analysis of genes in other angiosperm species unravelled a great diversity of POR gene expression and combination of isoforms, with POR isoforms of the same plant species being closely related, so that the POR protein family can phylogenetically be divided into groups, which are cyanobacteria, green algae, moss, monocotyledons, gymnosperms and dicotyledons (Masuda & Takamiya 2004, see Figure 1.6). Comparison of the PORA and PORB isoform sequences of *Arabidopsis* and barley showed no significant phylogenetic relationship between the two, suggesting that the isoforms arose from an independent gene duplication in each of the plant species individually (Oosawa *et al.* 2000, Masuda *et al.* 2002).

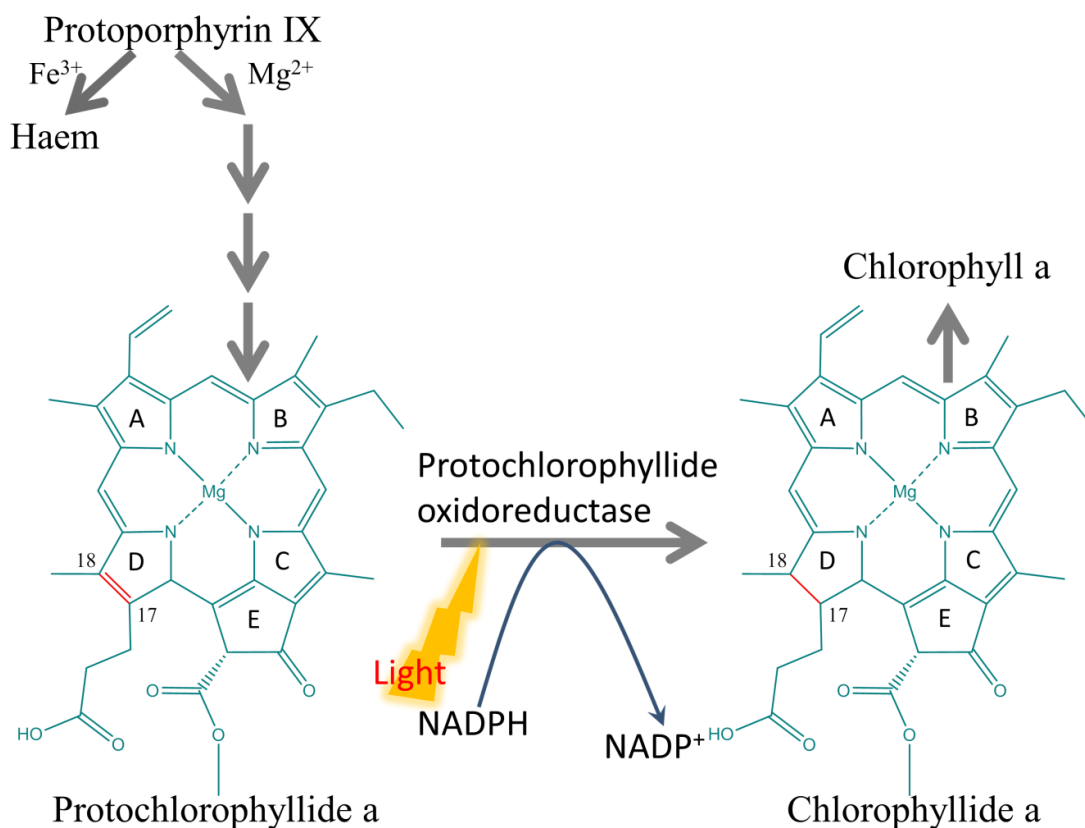


Figure 1.6. The protochlorophyllide oxidoreductase (POR) reaction, *trans* addition of hydrogen from NADPH to the C17-C18 double bond (red) in Pchl_{ide}, resulting in formation of Chlide. Insertion of Mg^{2+} or Fe^{2+} into the protoporphyrin IX porphyrin ring is the branchpoint of chlorophyll and haem biosynthesis (Lebedev & Timko 1999, Masuda & Takamiya 2004, Heyes & Hunter 2004, Heyes *et al.* 2006).

1.2.2.3. *The biological role of POR*

Most phototrophs, including cyanobacteria, algae and gymnosperms, have both light-dependent POR and the DPOR enzymes, whereas angiosperms only have the light-dependent version (Masuda & Takamiya 2004). This is the reason why developing angiosperms remain yellow when grown in the dark and greening only occurs after illumination (Masuda & Takamiya 2004). Chlorophyll is synthesised and chloroplasts are formed, which is accompanied by morphological changes in the plant, such as greening and the start of leaf expansion (Virgin 1963). Furthermore, this light-driven reaction causes profound changes in the morphological development of the plant, which results in the modification and reorganisation of the plastid membranes (Lebedev & Timko 1998, Masuda & Takamiya 2004). A possible explanation for these morphological effects is that in etiolated plants POR is found as a ternary complex of POR-NADPH-Pchlide and is organised in a network of tubular membranes called prolamellar bodies (PLB) (Virgin *et al.* 1963). The regular and three-dimensional network of PLBs is thought to be caused by the attachment of the ternary POR complex to the membranes and absence of POR can cause the membrane integrity to be distorted (Sundqvist & Dahlin 1997, Franck *et al.* 2000). The combination of transmission electron microscopy (TEM), and atomic force microscopy (AFM) have identified PLBs as spherical structures with a diameter of 1-2 μm (Grzyb *et al.* 2013). When the plant has been illuminated, the ternary complex disintegrates as Chlide is formed, leading to the dispersion of the prolamellar bodies and the subsequent formation of the chloroplast (Zhong *et al.* 1996). The process of PLB dispersion has recently been unravelled with the use of TEM and AFM, where the PLBs first increase in size after Pchlide reduction, immediately followed by dispersion into small spherical entities. These described changes to the PLBs have been attributed to the degradation of the POR ternary complex, because artificially induced degradation of the complex in the dark yields the same results in PLB rearrangement (Grzyb *et al.* 2013).

Various spectral forms of Pchlide can be found in these membranes isolated from etioplasts. The variation in spectral features is believed to be due to the interactions of Pchlide with POR and the membranes, along with structural arrangement and pigment aggregation (Ryberg & Sundqvist 1982). Disintegration of the POR-Pchlide aggregates and the following PLB dispersion, caused by illumination and the

formation of Chlide, is accompanied by a short shift in wavelength of the fluorescence maximum and absorption of Chlide, termed the Shibata shift (Heyes & Hunter 2009).

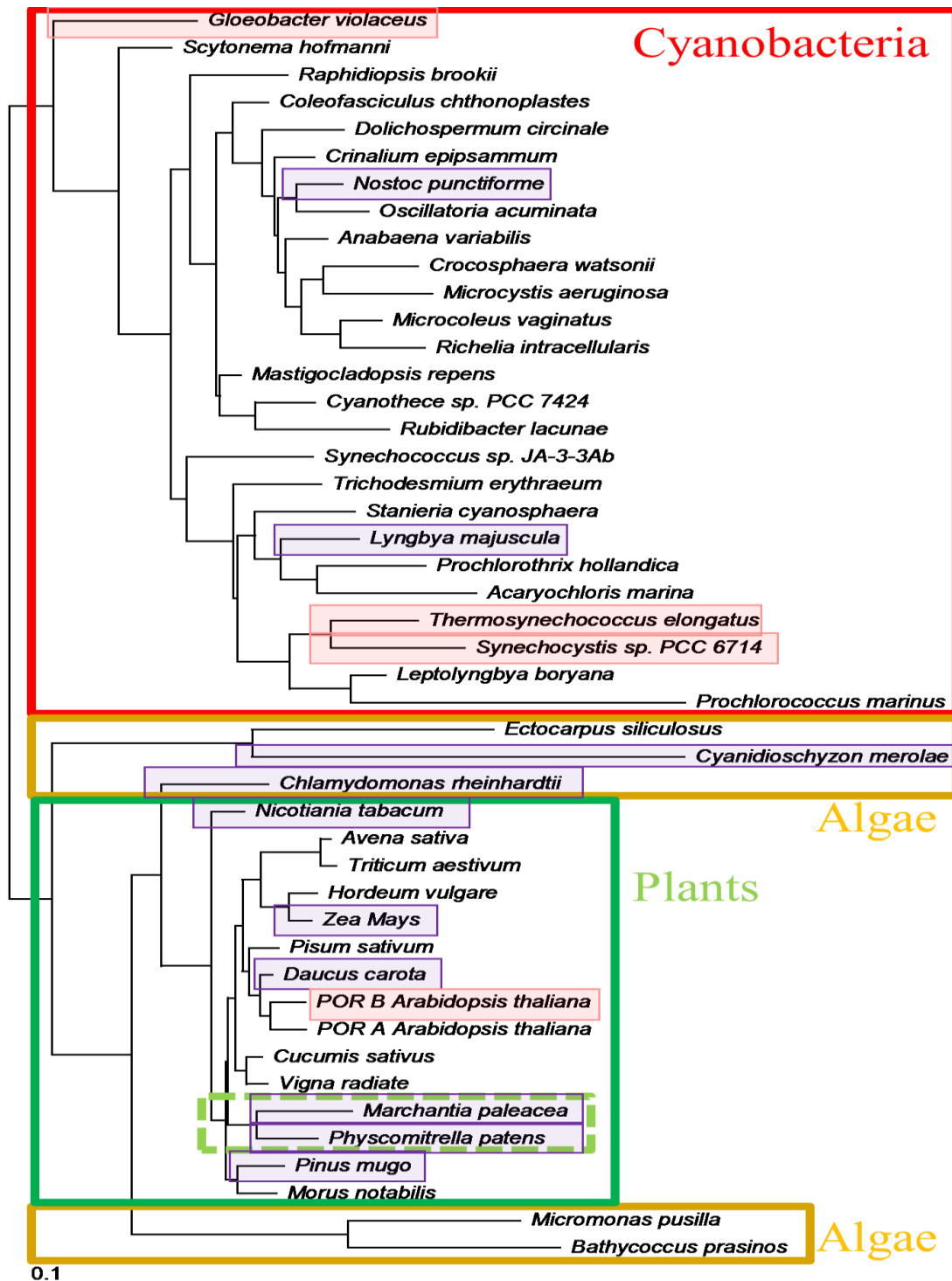


Figure 1.7. Phylogeny of the POR protein family. There is a clear distinction between cyanobacterial (red window), algae (orange window) and eukaryotic PORs (dark green window). The bryophyte species are highlighted by a light green dashed window. The scale bar represents the evolutionary distance. Species highlighted with a purple box are investigated in this thesis, while pink boxes mark species analysed in previous work (Heyes *et al.* 2011).

1.3. Structural studies on POR

Despite extensive studies there is currently still no crystal structure available for POR. However, POR has been classified as a member of the short-chain dehydrogenase family or 'SDR', previously known as the 'RED' (Reductases, Epimerases, Dehydrogenases) superfamily of enzymes (Baker 1994, Wilks & Timko 1995, Kallberg *et al.* 2002). This large family of proteins are all oxidoreductases that use either NAD(P)H or NAD(P)⁺ as a cofactor and typically occur as dimers or tetramers. Furthermore, most proteins in this family have two domains, one for binding of the cofactor and another for binding the substrate (Benyajati *et al.* 1981). Hence, the molecular structures (at atomic resolution) of some of the members of the SDR family of oxidoreductases have been used to produce a homology model of light-dependent POR from *Synechocystis* (Townley *et al.* 2001; see Figure 1.8). It was suggested that POR has a secondary structure with a central parallel β sheet consisting of seven β strands and surrounded by nine α helices (Dahlin *et al.* 1999, Townley *et al.* 2001). A unique feature for POR within this group is a large extra loop region of 33 residues in between the 5th and 6th β -sheets. The role of this hydrophobic loop-region is unclear but roles in protein complex formation, membrane anchoring or Pchlide binding have been suggested (Birve *et al.* 1996, Reinbothe *et al.* 2003). The amino-terminal region of POR is proposed to be the NADPH cofactor binding site, and is characterised by the presence of a GxxxGxG nucleotide-binding motif, containing a tight $\beta\alpha\beta$ fold called the Rossmann fold (Townley *et al.* 2001). Charged-to-alanine scanning mutagenesis provided more experimental evidence regarding which regions are important for POR-Pchlide interactions and which are essential for the catalytic activity of POR. Mutations to α helical regions of the protein had the least effect on enzyme activity, while the β sheet regions showed consistent negative effects in function (Dahlin *et al.* 1999). Moreover, amino acid sequence comparison of POR with other members of the SDR family highlighted conserved sequences and individually conserved amino acids, such as a tyrosine and a lysine residue located in the proposed catalytic side of the enzyme, which are important for POR activity (Wilks & Timko 1995, Heyes & Hunter 2002). It is known that several members of the 'SDR' family, such as alcohol dehydrogenase, dihydrofolate reductases and carbonyl reductases, have proven to be valuable model systems for studying reaction dynamics and theoretical thermodynamics calculations (Benkovic & Hammes-Schiffer 2003, Cui & Karplus

2002, Hammes 2002, Hammes-Schiffer 2002). In terms of kinetic isotope effects this enzyme family was demonstrated to be very useful, especially with the increased awareness of the significance of proton and hydride tunneling, as shown by a number of experimental reports (Kohen *et al.* 1999, Scrutton *et al.* 1999, Kohen & Klinman 2000, Sutcliffe & Scrutton 2000, Hammes-Schiffer 2004). Consequently, in terms of elucidating the mechanisms by which conformational changes and protein dynamics shape catalysis, the ‘light-dependence’ of POR offers a unique experimental advantage compared to other enzymes in the SDR family. Hence, POR is an excellent model system for studying the ‘SDR’ family of proteins and proton and hydride transfer enzymes in general.

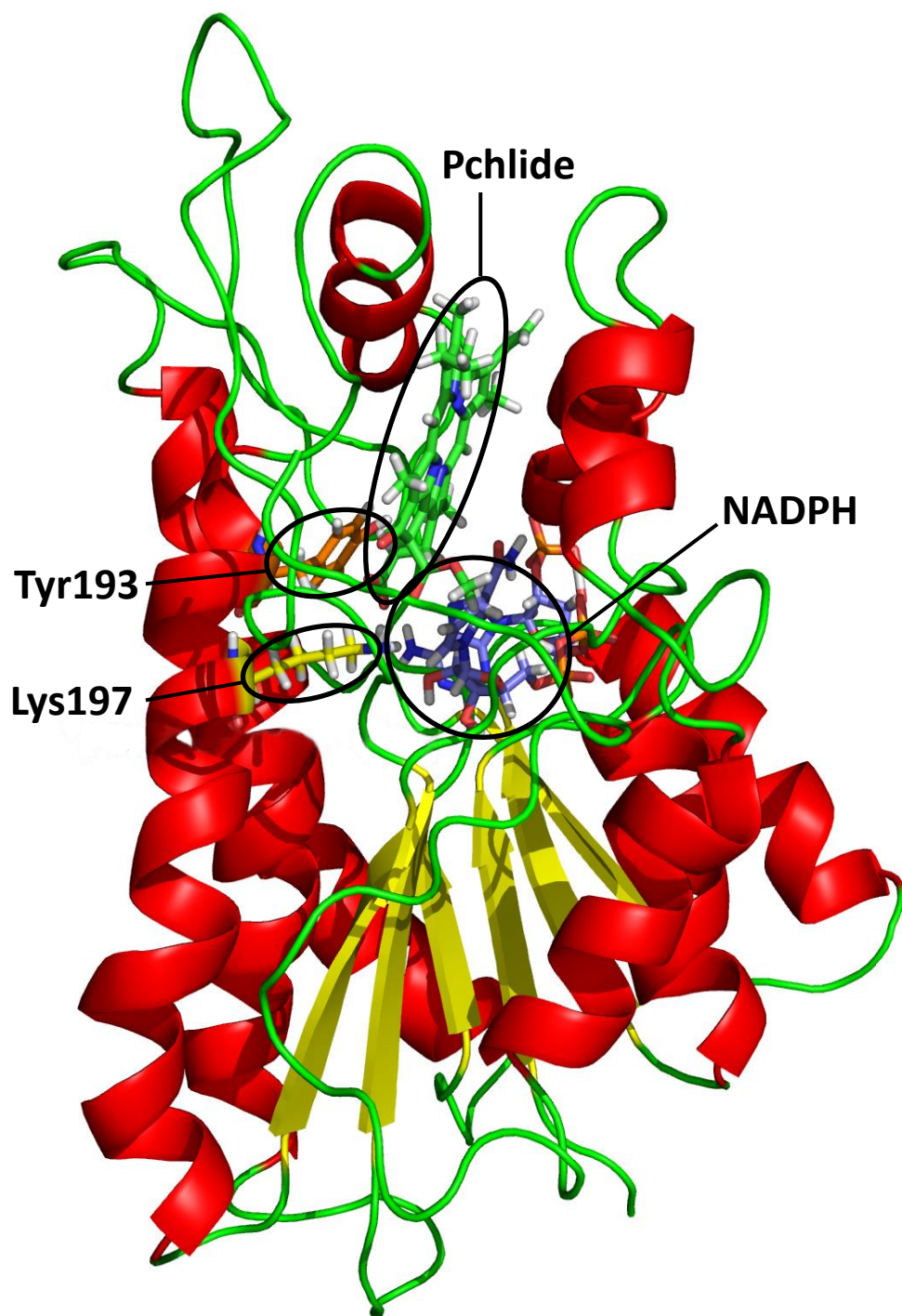


Figure 1.8. homology model of *Synechocystis* POR. α -helices shown in red and β -strands as yellow arrows using the ribbon representation, while Pchlride substrate (green) and the NADPH cofactor (blue) are shown in ball and stick representation. The catalytically important amino acids Tyr193 and Lys197 are highlighted (Townley *et al.* 2001). Image generated with the PyMOL Molecular Graphics System, Version 1.2r3pre, Schrödinger, LLC.

1.4. The reaction mechanism of POR

1.4.1. Substrate binding

The different spectroscopic signals of Pchlide and Chlide that are caused by association with membranes and POR makes it hard to interpret the results from experiments on PLBs isolated from etioplasts. However, the use of heterologous expression systems have helped to overcome these problems by providing *in vitro* purified POR proteins (Fujita *et al.* 1998). This has facilitated studies on the formation of the enzyme-substrate (ternary) complex and the analysis of various reaction steps by spectroscopic assays, resulting in the complete elucidation of the catalytic POR cycle (Heyes & Hunter 2004). These spectroscopic assays showed that there is a significant red-shift in the absorbance and fluorescence emission maximum of Pchlide when it is bound to the enzyme in the presence of either of the two cofactors, NADPH (shift to 644 nm) or NADP⁺ (641 nm). The level of red shift depends on the cofactor bound to POR and indicates that interactions between the pigment and the cofactor are important for the binding of substrate. Fluorescence line narrowing experiments indicated that there is a downshift of 50 cm⁻¹ for the keto carbonyl group in Pchlide (in the cyclopentanone ring) upon binding to POR, suggestive of strong H-bonding between amino acid residues in the enzyme and Pchlide (Sytina *et al.* 2010). Additional stopped-flow and FTIR experiments to study the rate of ternary complex formation showed that Pchlide binding is rate limiting in the overall reaction and is coupled to slow conformational changes in the enzyme (Heyes *et al.* 2008). Furthermore, Pchlide has limited affinity for the 'free' enzyme, and evidence seems to suggest that it only binds in the correct orientation when NADPH is present (Hanf *et al.* 2011). This confirms the finding that the initial step in the catalytic cycle is the binding of NADPH, followed by the formation of the ternary complex upon binding of the Pchlide substrate. These results are in accordance with the reaction mechanism for other SDR family members, such as dihydrofolate reductases, in which the cofactor (NAD) is also bound before the second substrate can be attached (Cameron & Benkovic 1997, Fierke *et al.* 1987, Schnell *et al.* 2004). A more complete overview of the ternary complex formation is given in Figure 1.9 which has been based on the analyses of stopped-flow measurements combined with a mixture of spectroscopic probes (Heyes *et al.* 2008).

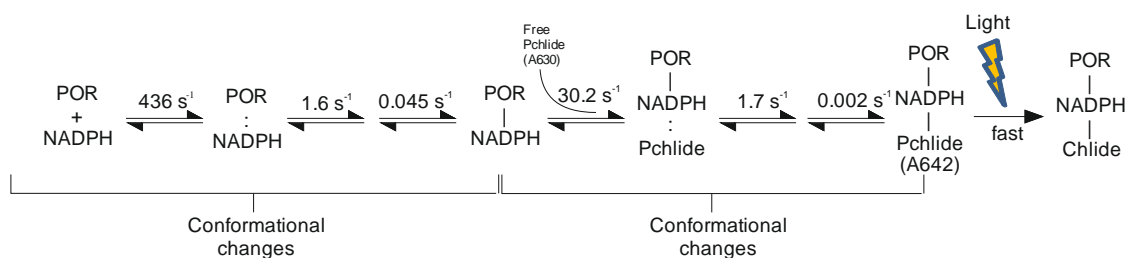


Figure 1.9. Kinetic scheme of the substrate binding events in POR. The calculated apparent rates of all of the binding steps are the sum of the forward and reverse rate constants and these initial steps provide a kinetic description of the reaction mechanism of POR. The binding of both substrates is controlled by conformational changes in the enzyme (Heyes *et al.* 2008).

1.4.2. Pchlide analogues

In the POR reaction the Pchlide molecule acts as the chromophore and captures the light to drive the reaction chemistry. Therefore, a more detailed knowledge of the sites of the substrate that are important for catalysis improves our understanding about how Pchlide is oriented in the (putative) active site and which amino acids of POR are functionally important. One way of extracting such information is by use of substrate analogues, which has revealed three sites in the Pchlide molecule that appear to be important for reactivity (Townley *et al.* 2001, Rüdiger *et al.* 2005). These are the complete structure of ring E, the central metal ion, and the propionic acid side chain of the D ring (see Figure 1.10). Pigments lacking the central metal (Mg) were not suitable as an active POR substrate and replacement of the physiological Mg with Cu, Co or Ni did not restore activity (see Figure 1.10). However, replacement with Zn did yield an active substrate (Griffiths 1980, Klement *et al.* 1999). Additionally, it has been shown that the structure of the isocyclic ring of the Pchlide substrate is important for the reaction. Only the substrate that has the natural $13^2(R)$ -Pchlide a structure can bind the enzyme and will become hydrogenated, as the $13^2(S)$ -Pchlide enantiomer was not accepted as a substrate by the enzyme (Helfrich *et al.* 1996). It was proposed that modifications to the $C13^1=O$ group led to a loss of activity as the Pchlide molecule was unable to form tautomers, and thus a protonation of the $C13^1=O$ was suggested to be required for photoreduction (Klement *et al.* 1999). Also, modifications to the ring D, where substitution of the propionate group by an acrylate or a propionic acid methylester group, are not tolerated by the enzyme, which confirms the postulated rigidity around ring D (Wilks & Timko 1995). Furthermore, enzyme activity is not significantly affected by the presence of either ethyl or vinyl groups at the C8 position

of ring B (see Figure 1.10), as the divinyl and monovinyl Pchlride molecules will both be converted into their respective Chlide products (Klement *et al.* 1999).

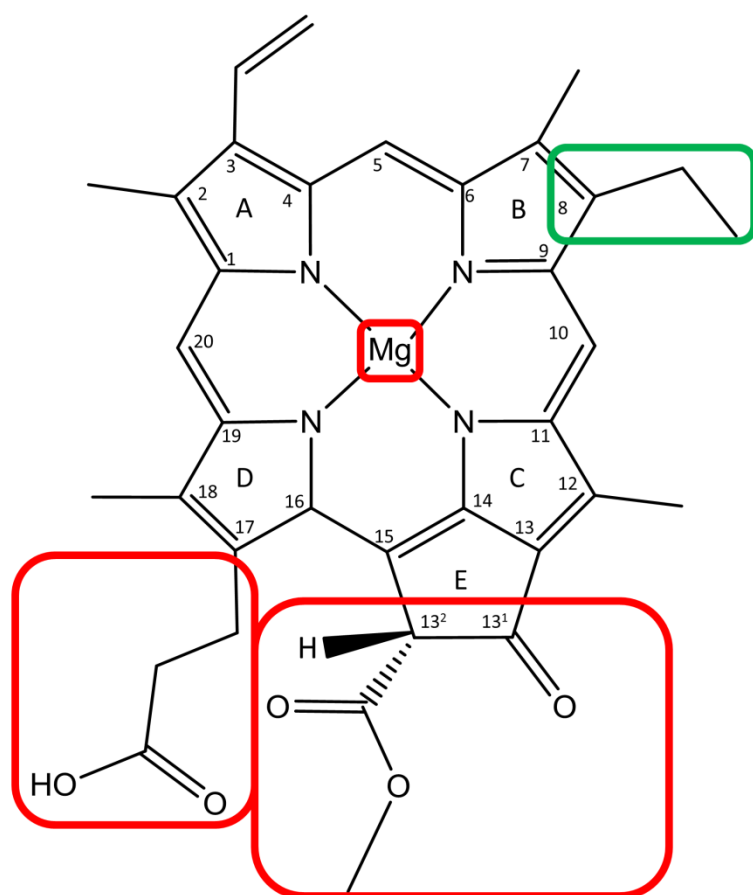


Figure 1.10. Pchlride molecule with important modification sites highlighted. The green box indicates a site where certain modifications do not significantly affect enzyme activity and the red boxes indicate parts of the molecule where chemical alterations result in loss of function. (Klement *et al.* 1999).

1.4.3. Excited state processes

1.4.3.1. Ultrafast dynamics of free Pchlride

As POR is a light-driven enzyme the chemical steps in the reaction are completely dependent on excited state processes in the Pchlride molecule, which occur on an ultrafast timescale. Studies on the excited-state dynamics of the isolated substrate Pchlride in solution have been important in extending our understanding of the more complex processes within the ternary enzyme-substrate complex. Dietzek *et al.* (2004) developed a branched model where the decay of excited-state Pchlride can proceed through two distinct channels (Figure 1.11). The photoexcited Pchlride population can branch into a reactive and a non-reactive channel. On the reactive side of the channel

an ultrafast excited-state motion out of the Franck-Condon (FC) region generates a secondary excited state species (S_X) that can further yield a intramolecular charge transfer state (S_{ICT}) with a time constant of 27 ps. In turn, this S_{ICT} intermediate decays with a 200 ps time constant back to the ground state. In the non-reactive channel the long-lived S_1 state population, formed by vibrational cooling of the photoexcited FC state, decays back to the ground state with a fluorescence lifetime of 3.5 ns (Dietzek *et al.* 2009). Additional experiments showed that the 3.5 ns decay of the S_1 population does not yield a considerable repopulation of the electronic ground state but suggests a non-radiative relaxation towards a photointermediate. This newly discovered long-lived photointermediate has been attributed to a triplet state of Pchl_{ide} and is consistent with the existence of a triplet state in other porphyrin systems (Rodríguez & González-Velasco 1990, Reed *et al.* 1991, Angiolillo *et al.* 1995, Shediach *et al.* 2000). As a negligible fraction of the S_1 state falls back to the ground state an estimate for the triplet yield was suggested to be approximately 85%, a value typical for metalloporphyrins (Spikes & Bommer 1991). The relatively high yield of the triplet state in free Pchl_{ide} is remarkable, considering that in the POR enzyme the triplet state population of the Pchl_{ide} molecule could lead to photodestruction and photosensitised side reactions (Schoefs *et al.* 2003, Yang & Cheng 2004).

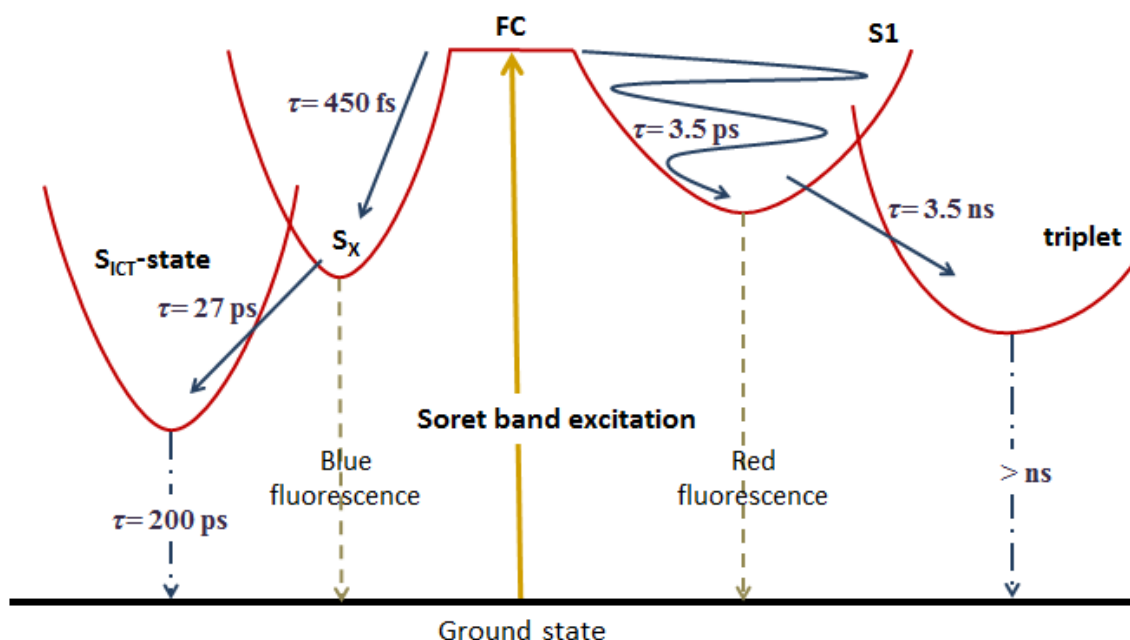


Figure 1.11. Pchl_{ide} light-induced excited state branched relaxation process. The branch on the left side of the Q-band excitation is the ‘reactive’ side of the pathway that forms an intermediate photoproduct (ICT) in 27 ps and consecutively decays back to the ground state in 200 ps (τ = lifetime). The ‘non-reactive’ branch on the right results in the formation of a long-lived triplet state (Dietzek *et al.* 2009).

In a separate study the effect of different solvents on the way excitation energy is channelled through the two different deactivation channels was investigated (Dietzek *et al.* 2006, 2009). The ‘reactive’ pathway of Pchlride was only operational in polar solvents, which suggested that a polar environment is a prerequisite to form the intermediate S_{ICT} state. This indicates that a large dipole moment is formed in the S_{ICT} , which forms the basis of the assignment of this intermediate as an intramolecular charge transfer state. It is likely that the charge transfer character of this intermediate results from the electron withdrawing effect of the carbonyl group in the cyclopentanone ring that is directly attached to the π -electron conjugation system of the porphyrin ring. Non-polar solvents most likely raise the energy of the charge transfer state, preventing the excited-state population from transferring to the S_{ICT} state (Dietzek *et al.* 2004, 2006, 2009, 2010, Sytina *et al.* 2010, 2011).

Separate time-resolved fluorescence and absorption measurements confirmed the formation of the S_{ICT} state in Pchlride and showed that it was not dependent on the H-donating properties of the solvent, but rather that the ICT is an intrinsic characteristic of Pchlride (Sytina *et al.* 2010). This new evidence led to the development of a multiphasic sequential model, which has an additional solvation step of the ICT before it forms the triplet state (Figure 1.12). Solvation of the Pchlride molecule is suggested to be due to the strengthening of the H-bonding between specific sites on the Pchlride molecule and the solvent, yielding a more optimally coordinated H-bonded intermediate (Zhao & Han 2008). It is thought that hydrogen bonding with the keto group of ring E (on C13²) exerts an electron-withdrawing effect that creates an intramolecular charge separation across the Pchlride molecule, leading to other changes in C=C and C=N modes of the tetrapyrrole ring (Sytina *et al.* 2010, Colindres-Rojas *et al.* 2011, Sytina *et al.* 2011, Scrutton *et al.* 2012). Although there are discrepancies between these two proposed models it is clear that the excited state dynamics of Pchlride involve the formation of an ICT and a triplet state. An understanding of the excited state chemistry of Pchlride in solution has the potential to suggest how the enzyme can harness the light energy to drive the chemistry. It is likely that the ICT complex plays an important role, possibly lowering the electron density at the C17 position to aid the transfer of a negatively charged hydride.

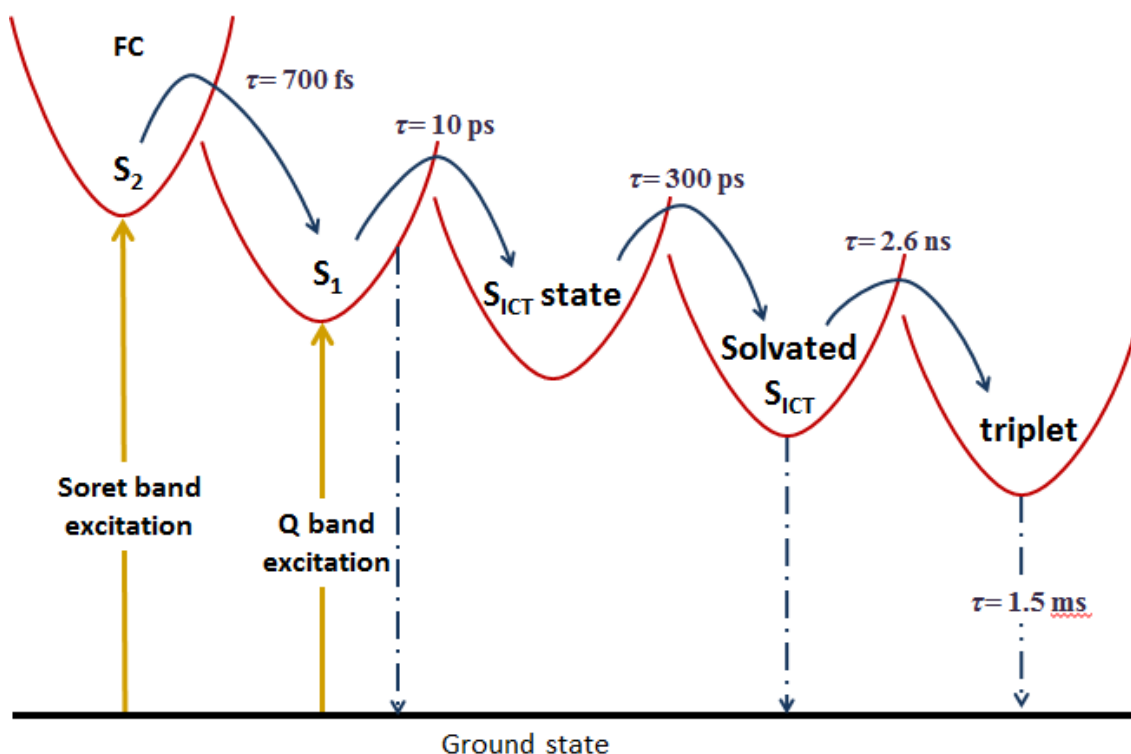


Figure 1.12. Sequential model for light-induced excited Pchlide relaxation. The model is based on observations that solvation of the ICT strengthens the H-bonding network around the Pchlide molecule, leading to formation of the long-lived triplet state (Sytina *et al.* 2010).

1.4.3.2. Ultrafast reactions during catalysis in POR

The catalytic process in POR can be divided into three important sections, an initial excitation by light of the bound Pchlide that leads to a series of excited state processes, followed by a hydride transfer step and a light-independent proton transfer step. This is then followed by a series of further distinguishable ‘dark’ reactions as the products are released from the enzyme and new substrate can rebind to start a new catalytic cycle. By comparing the excited state dynamics of the Pchlide molecule in solution and to a ternary POR-Pchlide-NADPH complex it is possible to gain a more detailed understanding of the photochemistry and the involvement of stabilisation interactions within the enzyme. In pump-probe experiments on the ternary enzyme complex ultrafast absorption changes in the 600-750 nm range revealed a bleaching of the Pchlide ground state together with stimulated emission from Pchlide, indicated by a negative peak around 640 nm (Heyes *et al.* 2002b, Sytina *et al.* 2009). In addition, the formation of a negative signal at approximately 675 nm was also observed after a few picoseconds, corresponding to stimulated emission. This species (termed I675*) formed with time constants of 3 and 400 ps and was believed to be a catalytic product because of its absence in measurements of Pchlide in solution and for the catalytically

inactive Y193F mutant, which lacks the Tyr193 proton donor (Heyes *et al.* 2002, Sytina *et al.* 2008, 2012). However, in a more recent study by Heyes *et al.* (2012), it was shown that the I675* spectral feature is not a catalytic intermediate but is the result of excited-state energy transfer between two pigment molecules in Pchl_a-Chl_a dimers. This is a direct consequence of the build-up of the Chl_a product during the course of the measurements and shows how complicated it is to accurately determine the excited state processes associated with POR catalysis (Heyes *et al.* 2012).

A more detailed understanding of Pchl_a excited-state interactions has now been achieved by the use of time-resolved UV/Vis and IR spectroscopy over a picosecond-microsecond timescale after excitation by a 450 nm laser. It was hypothesised that H-bonding interactions between the OH group of Tyr193 and the carbonyl group at the C17 position occur in the Pchl_a excited state, which exerts an additional electron-withdrawing effect on the C17-C18 double bond in Pchl_a. The double bond in turn becomes an electron-deficient site that is highly polarised and is therefore optimised for a nucleophilic attack by the hydride from NADPH to the C17 position. A thorough comparison was made of the excited state processes for Pchl_a in solution and bound to wild-type POR as well as a Y193F POR mutant (Heyes *et al.* 2015). It was found that removal of the OH group of tyrosine in the mutant prevented the formation of this so-called ‘reactive’ ICT state (see Figure 1.13; Heyes *et al.* 2015). Hence, a mechanism was proposed where the chemistry of the reaction is facilitated by specific H-bonding interactions of residues (*e.g.* Tyr193) in the active site with the C17 carboxyl group of Pchl_a to create an ICT state with an electron-deficient C17 site, allowing nucleophilic attack of the hydride.

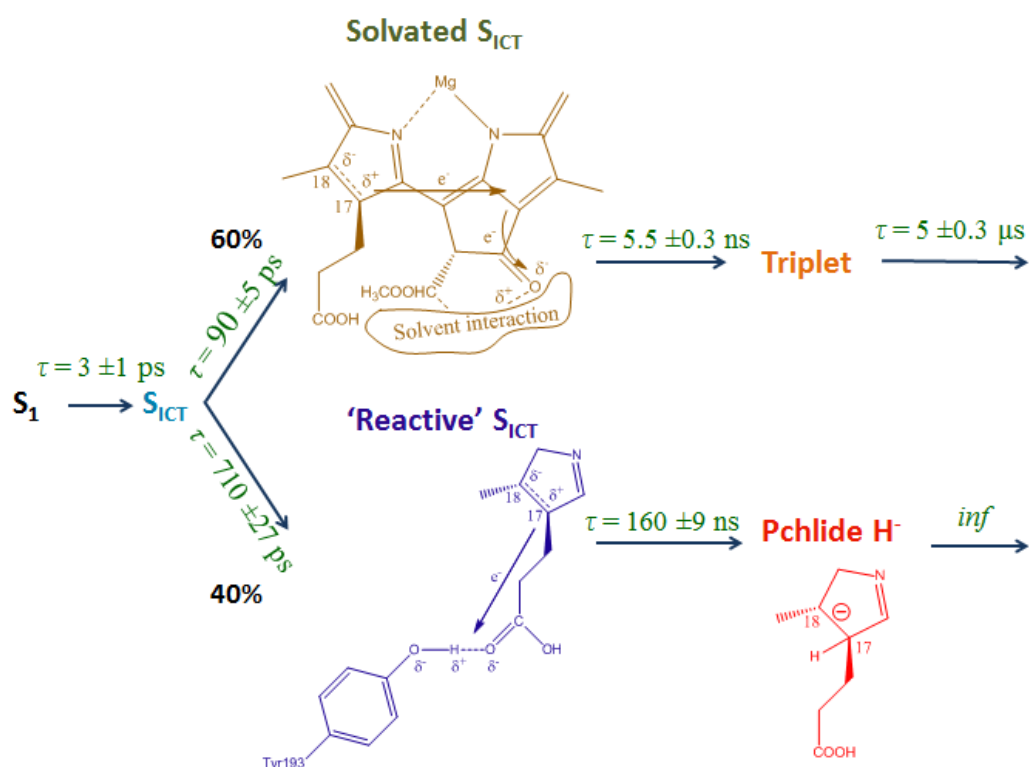


Figure 1.13. Proposed mechanism for excited state reactivity of Pchlide in the POR active site. 40% of the ICT proceeds along the ‘catalytic’ pathway, while 60% becomes solvated and forms a triplet state. τ is a measure of the lifetime of each species, and “inf” in the ‘catalytic’ pathway refers to the proton transfer that happens at a much slower timescale and hence appears unchanged in comparison (Heyes *et al.* 2015).

1.4.4. Hydride transfer

Upon excited state activation the chemical reduction of Pchlide starts with a hydride transfer from the pro-*S* face of NADPH to the C17 atom of Pchlide. The stereochemistry of this step was resolved by studies using ^3H -labeling of the 4*R* and 4*S* positions of NADPH (Begley & Young 1989). Density functional theory (DFT) calculations confirmed that the energy of the Pchlide excited state at the lowest Franck-Condon state transition (210 kJ/mol) is sufficient to cross the barrier (TS1) for hydride transfer ($\Delta G = 169 \text{ kJ/mol}$) (see Figure 1.14; Heyes *et al.* 2009). As the catalytic cycle of POR is initiated by light it means that the ternary enzyme-substrate complex can be cooled down to cryogenic temperatures and a light-driven hydride transfer step can still be triggered at a temperature of 120 K (Heyes, Ruban, *et al.* 2002). It has been suggested that a ‘near attack’ conformation (Lightstone & Bruice 1996) is formed prior to freezing that is thought to involve a combination of electrostatic and steric interactions for the optimal alignment of substrate and cofactor

in the active site of the enzyme, (Benkovic & Hammes-Schiffer 2003, Lightstone & Bruice 1996, Durin *et al.* 2009).

The first intermediate identified upon illumination at low temperatures was a non-fluorescent intermediate with a broad absorbance band at 696 nm (Heyes *et al.* 2002). The intermediate does not form when NADPH is substituted by NADP^+ , which confirms that the ternary complex with NADPH and POR must be formed before this photochemical step can proceed. Initially, due to the significant red-shift in absorbance from 642 nm to 696 nm it was suggested that this intermediate might be a Pchl_a radical. Previous electron paramagnetic resonance spectroscopy (EPR) studies on etioplasts membranes and heterologous POR protein have indicated the involvement of a radical in the reaction mechanism of POR (Belyaeva *et al.* 1988, Lebedev & Timko 1999). However, other experiments suggest that there are no radical species in the reaction chemistry (Townley *et al.* 1998), and it was proposed that the 696 nm intermediate is a charge-transfer state between Pchl_a and NADPH (Raskin & Schwartz 2002). Further analyses of the intermediate by EPR (electron paramagnetic resonance), ENDOR (electron nuclear double resonance), Stark and low temperature absorbance spectroscopy confirmed it to be a charge-transfer complex that is formed upon hydride transfer from NADPH (Heyes *et al.* 2006). Subsequent laser flash photolysis studies revealed that this species was formed with a rate constant of $2.02 \pm 0.21 \times 10^6 \text{ s}^{-1}$ at 25 °C with a KIE of approximately 2 when the deuterated form of the cofactor was used. Investigation of the temperature dependence of the hydride transfer rate revealed a clear breakpoint at -27 °C in the Eyring plot. A weak temperature dependence can be observed above -27 °C ($\Delta H^\ddagger = 9.3 \text{ kJ mol}^{-1}$) with a temperature-dependent KIE. In contrast, below the breakpoint the reaction is considerably more temperature-dependent ($\Delta H^\ddagger = 27.2 \text{ kJ mol}^{-1}$) while the KIE becomes temperature-independent. It was proposed that fast dynamic searches within the Pchl_a excited state lifetime in the enzyme complex are required to form degenerate “tunneling-ready” configurations. The presence of a breakpoint at -27 °C in the Eyring plot for the hydride transfer was hypothesised to reflect the involvement of a promoting motion/vibration that becomes ‘frozen out’ below -27 °C in accordance with the Marcus-like model. These features, in addition to the Eyring prefactor ratios ($A'_\text{H}/A'_\text{D} = 3.59$), indicate that the hydride transfer occurs by quantum tunneling (Heyes *et al.* 2009a). As H-tunneling requires a very short DAD and because hydride transfer in POR continues even at temperatures much lower than 200 K (typically the glass

transition temperature of proteins) it suggests that the hydride transfer relies only on localised motions within the active site (Heyes *et al.* 2009a). This is supported by data showing that the POR hydride transfer is not significantly affected by dielectric or viscosity changes in the solvent, and therefore not dependent on long-range solvent-slaved protein motions for this step (Heyes *et al.* 2009a, 2009b).

Further site-directed mutagenesis studies have been used to understand the impact of certain residues on the active site chemistry. POR contains a conserved Tyr-X-X-X-Lys motif and mutation of the conserved active site Tyr and Lys residues result in a dramatic decrease in reaction rate (Menon *et al.* 2009a). These residues were presumed to serve multiple roles, including ground state ternary POR-NADPH-Pchlide complex formation, stabilisation of the excited state Pchlide to ensure a high quantum yield (around 40%) for the hydride transfer reaction and a role in providing a proton for the proton-transfer step (Heyes *et al.* 2002, 2015, Sytina *et al.* 2008). Previous studies have reported that phenol groups can be involved in the charge transfer stabilisation and other excited state processes (Henneke & Wedding 1975, McFarlane *et al.* 2005) and this was subsequently confirmed in POR (see section 1.4.3.2.), where stabilisation of the Pchlide excited state is thought to happen by H-bonding of the Tyr OH group with the carboxyl group on the C17 position (Dietzek *et al.* 2009, Menon *et al.* 2009, Scrutton *et al.* 2012, Heyes *et al.* 2015). These studies indicate the reliance on local interactions of the enzyme with the substrate in order to stabilise the excited state. Another amino acid residue that plays a significant role in the hydride transfer chemistry in POR is a conserved cysteine at location 226 (in *T. elongatus* POR). Mutation of this Cys residue result in major alterations to the catalytic mechanism as no charge-transfer complex (696 nm absorbance band) is formed. The data suggests that both hydrogens (hydride and proton) are transferred in a single kinetic step within the investigated timeframe for this variant. An alternative catalytic mechanism was proposed, involving an initial fast electron transfer from NADPH upon excitation of Pchlide, followed by a rate-limiting proton transfer (presumably from Tyr193) and finally transfer of the remaining proton and electron from NADPH (Menon *et al.* 2010). This alternative mechanism depends to a much smaller degree than the wild-type on long-range solvent-slaved motions of the enzyme, as there is only a limited influence of solvent viscosity on the proton transfer rate and the KIE is temperature-independent (no promoting motions) (Menon *et al.* 2010, Heyes *et al.* 2009). In the absence of any structural data it is difficult to explain

the exact molecular active site dynamics that influence this dramatic shift in catalytic chemistry, but based on existing homology models it was proposed that Cys-226 interacts with ring A of Pchlide to ensure a short DAD for hydride transfer (Menon *et al.* 2010). It is possible that the loss of this interaction in the mutant increases the DAD for the hydride transfer but simultaneously this may have shortened the DAD for the proton transfer and thereby removed the need for promoting motions and/or domain movements (Menon *et al.* 2010).

1.4.5. Proton transfer

While the hydride transfer step can occur at temperatures below 200 K (Heyes *et al.* 2002), the subsequent thermally-activated proton transfer step can only occur at much higher temperature ranges and results in a new intermediate with an absorbance band at 681 nm. The restriction of this step to a temperature close to or above the glass transition temperature of proteins, suggests a reliance on domain movements and/or reorganisations of the protein (Durin *et al.* 2009; Heyes *et al.* 2009, 2011). Cryogenic spectroscopy measurements confirmed that when the illuminated sample is warmed up to temperatures above 200 K the 681 nm absorbance band (fluorescence peak at 684 nm) appears and is characteristic of a POR-NADP⁺-Chlide product complex. Hence, this was proposed to be formed by proton transfer from a conserved Tyr residue in the active site (Heyes & Hunter 2004, Heyes *et al.* 2009a). A conserved Lys residue is thought to lower the pK_a of this Tyr, thereby facilitating the proton transfer reaction. Both of these residues have been shown to be important for catalysis by site-directed mutagenesis studies (Wilks & Timko 1995, Menon *et al.* 2009).

The rate of proton transfer in *T. elongatus* POR has been determined to be $25.3 \pm 1.5 \times 10^3 \text{ s}^{-1}$ at 25 °C with a SKIE (solvent kinetic isotope effect) of approximately 2 when measurements were performed in D₂O. Further analysis of the rate showed a strong temperature-dependence ($\Delta H^\ddagger = 74.8 \text{ kJ mol}^{-1}$) with a temperature-dependent SKIE and an inverse extrapolated Eyring prefactor ratio ($A'_H/A'_D=0.041$). These results are consistent with a proton-tunneling reaction and are supported by DFT calculations that show a TS2 barrier ($\Delta G^\ddagger = 67.7 \text{ kJ/mol}$ at 25°C) for proton transfer (see Figure 1.14; Heyes *et al.* 2009a). In contrast to the hydride-tunneling reaction, no breakpoints were observed in the Eyring plots, suggesting a reliance on different promoting modes for this part of catalysis (Heyes *et al.* 2009a). This was confirmed by a strong dependence on solvent viscosity, suggesting that the proton transfer is controlled by solvent-slaved

dynamics (Heyes *et al.* 2009b). Although viscosity influences the rate of the proton transfer, no significant dependence of SKIE on solvent viscosity was observed (Heyes *et al.* 2009b). According to the Marcus-like model, this means that the promoting motions along the reaction coordinate are not significantly solvent-slaved, and viscosity is thought to only affect thermally equilibrated motions that cause a degeneracy of reactant and product wells, priming the system for H-tunneling (Heyes *et al.* 2009b).

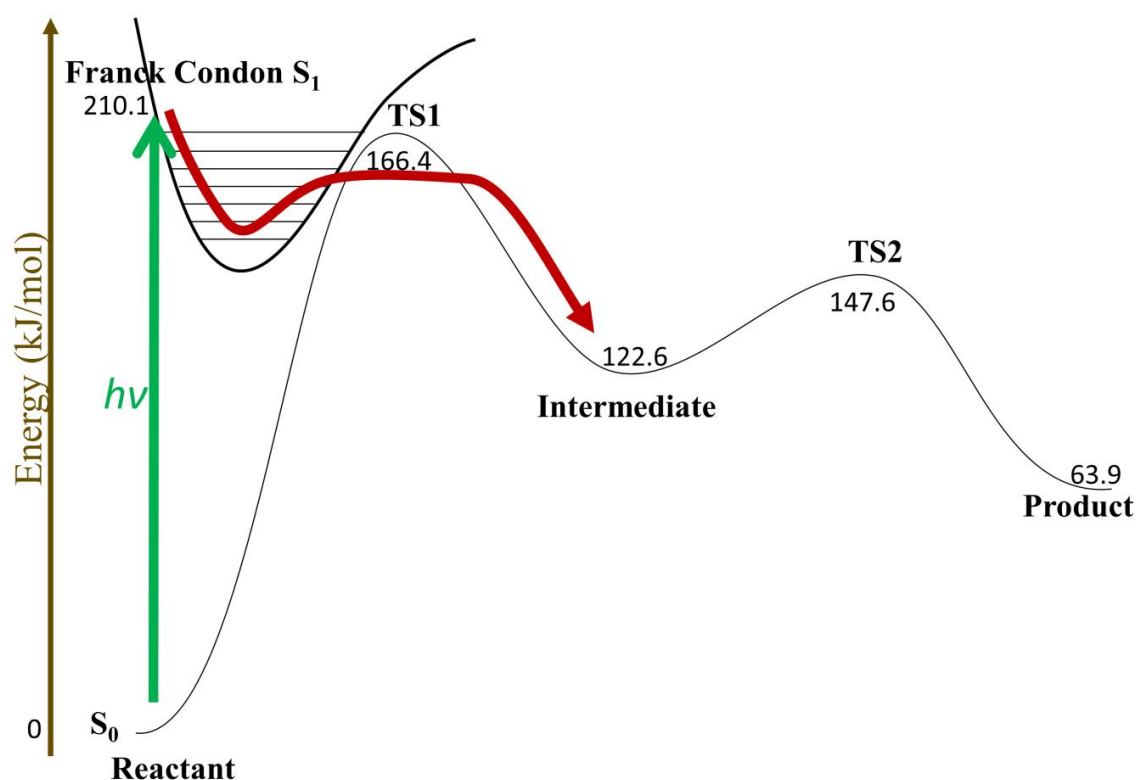


Figure 1.14. Energy diagram of the H-transfer reactions in POR, calculated by DFT. The excited Pchlide molecule (Franck-Condon S_1 state) has enough energy to overcome the barrier for hydride transfer (TS1). Proton transfer is an endergonic process with the TS2 barrier to yield the Chlide product. The overall endothermic reaction has a 63.9 kJ/mol free energy of activation. These values are comparable to experimental data (Heyes *et al.* 2009a).

1.4.6. Product release

Further ‘dark’ steps, observed for *Synechocystis* and *T. elongatus* POR, have been shown to represent a series of ordered product release and substrate rebinding events (Heyes *et al.* 2003, 2007). These only occur at much higher temperatures and the intermediates that were identified were shown to represent various bound and unbound forms of the Chlide product (Heyes & Hunter 2004, Heyes *et al.* 2007). Consequently, a reaction scheme for the entire catalytic cycle was proposed (Figure 1.15; Heyes *et al.*

2008, 2007, 2015). Upon photoexcitation there is a rapid hydride transfer reaction, immediately followed by another rapid proton transfer step to yield the ternary enzyme-product complex (see sections 1.4.4 and 1.4.5). This is then followed by the release of the NADP^+ product and replacement with the NADPH substrate. This in turn is followed by a slower release of Chlide to yield the free product. Finally, the cycle is completed by the re-binding of the Pchlde substrate to form a ternary POR-NADPH-Pchlde complex, which allows the catalytic cycle to be repeated upon further photoexcitation. From this reaction mechanism it can be concluded that the NADP^+ release step has a lower energy barrier than the Chlide release step (see Figure 1.15; Heyes & Hunter 2004). Furthermore, as these processes can only proceed at temperatures well above the ‘glass transition’ phase of proteins it suggests that conformational changes in the protein play an important role in the substrate binding and product release steps (Heyes *et al.* 2003, Heyes & Hunter 2004, Heyes & Scrutton 2009).

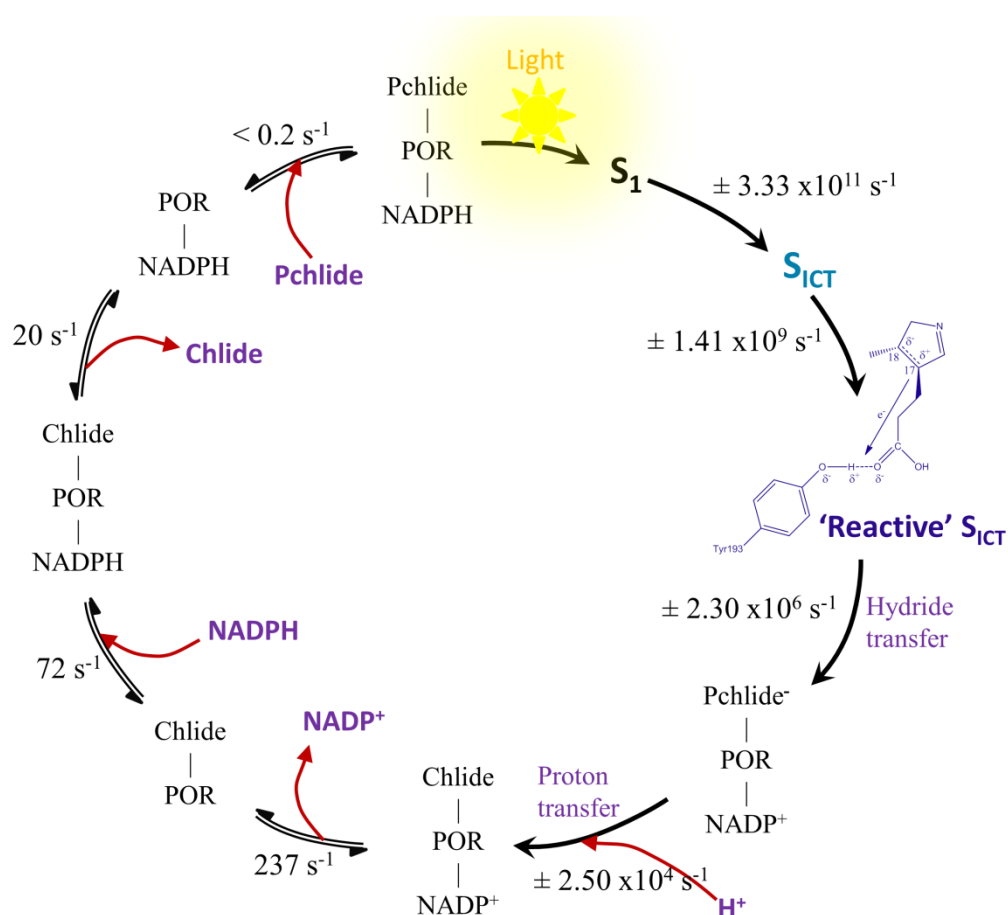


Figure 1.15. An overall scheme for the catalytic cycle of *T. elongatus* POR showing the stepwise formation of the reaction intermediates together with the rate constants that have been calculated previously (Heyes *et al.* 2007, Heyes & Scrutton 2009). Starting with the light dependent excitation of Pchlde into an excited S_1 state, followed by a series of ultrafast steps and the Hydride transfer (Heyes *et al.* 2015).

1.5. The evolution of dynamically-coupled tunneling in POR

The question of whether protein dynamics have evolved to play a role in catalysis is still poorly understood (Benkovic *et al.* 2003; Henzler-Wildman & Kern 2007; Yahashiri *et al.* 2008; Bandaria *et al.* 2009). Ideally, protein dynamics would be studied by comparing the current versions with ‘ancient’ forms of an enzyme, but unfortunately there is no easy way to obtain such ‘ancient’ enzyme forms. Perhaps, the closest way to approximate this evolutionary analysis is by studying homologous enzymes of extant organisms whose ancestors branched off from each other at different evolutionary times. It is fortunate that POR is ubiquitous and is present in most phototrophs, making it possible to do a comparative analysis made between PORs of cyanobacterial, algae and higher plant origin. Sequence comparison shows the variable patterns of structural conservation among different PORs. Heyes *et al.* (2011) investigated enzyme dynamics by comparing three cyanobacterial and one higher plant POR homologue, including the basal cyanobacterial species (*Gloeobacter violaceus*), which has features in common with cyanobacteria as well as plant PORs. In these experiments the viscosity-dependence of the rate and the temperature-dependence of the KIE for hydride and proton transfer were investigated (Heyes *et al.* 2008, Heyes *et al.* 2011). From this comparison it was shown that two distinct approaches for the evolution of dynamics in POR could be identified. Firstly, the dynamics required for the light-driven hydride transfer were found to be conserved across all of the POR enzymes and it appears as though evolutionary pressure has minimised any complex and extensive networks of solvent dynamics and protein motions that are required for this step. In contrast, the dynamics required for the thermally-activated proton transfer are much more variable. Hence, it was concluded that when chemistry stringently depends on the structure, as is the case for the light-driven hydride transfer step, the configuration of the enzyme active site has been optimised early on in evolution. When stringency is less, as is the case for the thermally-activated proton transfer step, multiple dynamical and structural possibilities exist for the reaction to proceed and hence, optimisation is less important and it can take longer for selective pressure to minimise the reliance on solvent dynamics and complex dynamical networks (Figure 1.16).

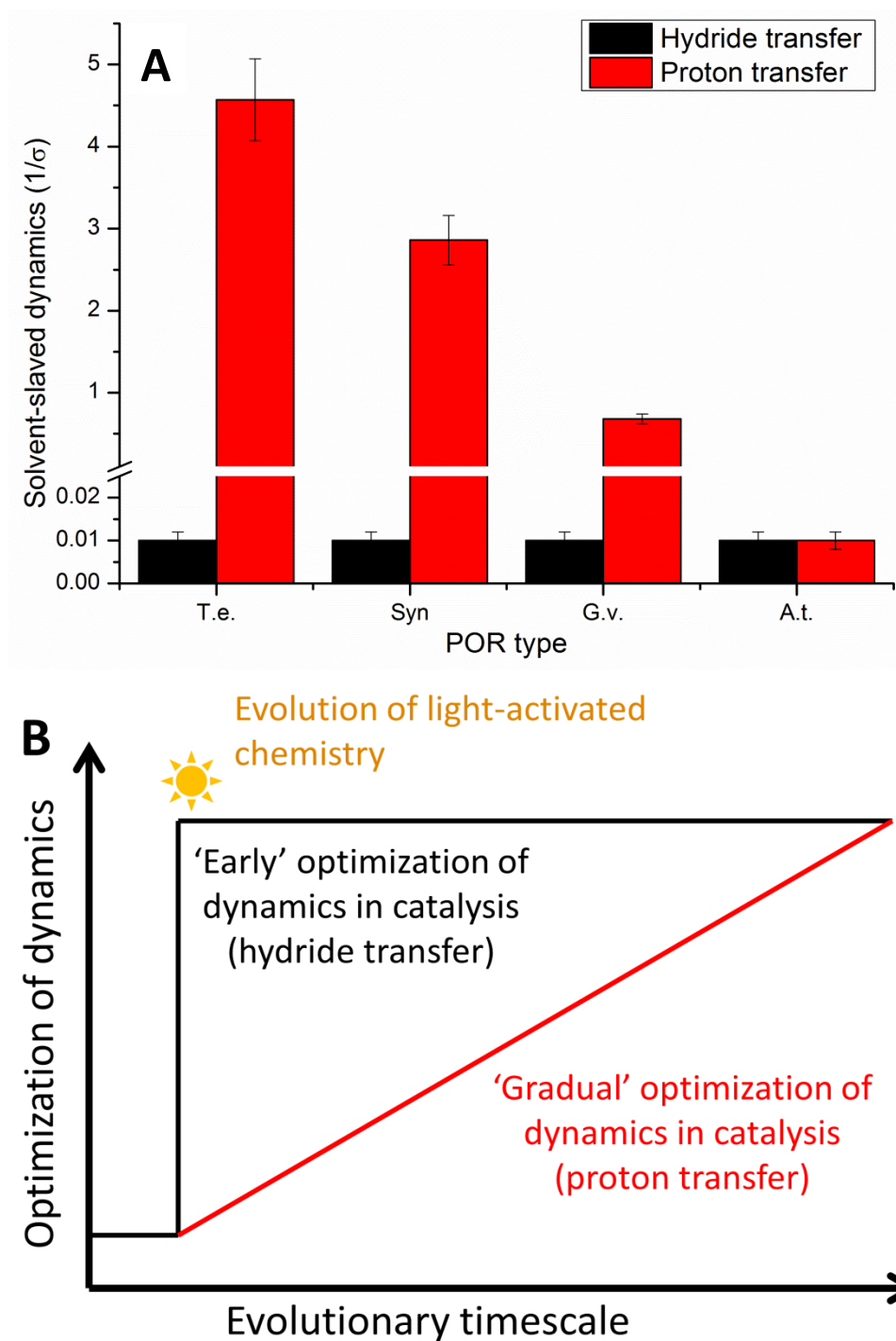


Figure 1.16. Evolution of Hydride and proton transfer dynamics catalysed by POR. A. A comparison of the solvent-coupled dynamics for the hydride and proton transfer steps was made across the evolutionary spectrum. The levels of solvent-slaved dynamics were obtained by measuring the viscosity dependence of the rates of hydride and proton transfer (Heyes *et al.* 2011). The used abbreviations correspond to POR from the following organisms: *A. t.*, *A. thaliana* POR B; *G. v.*, *G. violaceus*; *Syn.*, *Synechocystis* sp.PCC6803; and *T. e.*, *T. elongatus* BP-1. B. The scheme illustrates the hypothesised twin-track evolution of dynamics in POR. The light-driven hydride transfer step depends on localised dynamics and is strongly conserved across all PORs studied, due to strong structural conservation across evolutionary history. Evolution of the dynamics of the proton transfer step on the other hand, is thought of as a more gradual process that evolved towards a smaller reliance on complex dynamic networks for plant PORs (Heyes *et al.* 2011).

1.6 Aims and objectives

1.6.1. Pressure dependence of POR

The effect of pressure on enzyme chemistry is hard to predict as the effects vary greatly between enzymes (Hay *et al.* 2007, 2012). The influence of pressure on catalysis and dynamics is dependent on the enzyme structure and, with only a limited amount of pressure data available, there is still no general model for the effects of pressure. The objectives of this project therefore were to investigate how pressure affects the reaction chemistry in a relatively well understood enzyme model system, such as POR, where the temperature dependent and solvent viscosity experiments have clearly indicated the roles of local and solvent-slaved dynamics for the two H-tunneling steps. Laser flash photolysis experiments have been used to follow the rate of hydride and proton transfer, for both hydrogen as well as deuterium in order to calculate the KIE and SKIE respectively. Measurements of the influence of pressure on the isotope effects reports directly on the changes along the reaction coordinate. These experiments have been conducted within a certain temperature range to yield more information, but it was not possible to go to cryogenic temperatures for pressure dependence studies due to experimental limitations.

1.6.2 Evolution of dynamics in POR

Heyes *et al.* (2011) have shown that evolutionary pressures have brought about variable arrangements in the structural conservation within different POR homologues. As only four homologues were analysed with a limited evolutionary sampling (three cyanobacteria and one plant enzyme), this analysis has now been extended to an additional ten new POR homologues. The analysis involved two cyanobacteria, two algae, one liverwort, one moss, and four higher plants. The expression and purification of the newly synthesised POR homologues was optimised and the purified enzymes were characterised in terms of steady-state and substrate binding properties.

The twin-track evolutionary hypothesis has been investigated further by analysing the rates and viscosity-dependence of the two H-transfer reactions.

Chapter 2

Experimental set-up

2.1. Cloning	63
2.1.1. Plasmid preparation	63
2.1.2. Gene synthesis	63
2.1.3. Restriction digest	63
2.1.4. Ligation	63
2.2. Expression and purification of POR from <i>Thermosynechococcus elongatus</i>	64
2.2.1. Transformation and expression	64
2.2.2. Purification	64
2.2.2.1. Nickel-column	64
2.2.2.2. Blue Sepharose column	65
2.2.3. Determining the concentration of protein	66
2.3. Phylogeny	66
2.4. Substrates and other chemicals	66
2.4.1. Pchl _a synthesis and extraction	66
2.4.2. Other chemicals	67
2.5. Spectroscopy	67
2.5.1. Absorption spectroscopy	67
2.5.2. Pressure spectroscopy	68
2.5.3. Fluorescence	69
2.5.4. Laser flash photolysis	69
2.5.5. Ultrafast transient absorption spectroscopy	71
2.5.6. Global analysis.	72

2.1. Cloning

2.1.1. Plasmid preparation

The pET9-His + POR plasmid (gift from Derren Heyes) was transformed and overexpressed in XL1-blue (Agilent technologies) supercompetent *E. coli* cells and grown overnight in 5 ml LB (lysogeny broth) growth medium. The plasmid was extracted by following the QIAprep Spin Miniprep Kit protocol (Qiagen).

2.1.2. Gene synthesis

The genes and their NCBI, GenBank or UniProtKB reference code for POR from *Chlamydomonas reinhardtii* (XP_001689464.1), *Cyanidioschyzon merolae* (XP_005537439.1), *Daucus carota* (Q9SDT1.1), *Lyngbya majuscula* (WP_008188115.1), *Marchantia paleacea* (O80333.1), *Nicotiana tabacum* (BAB93004.1), *Nostoc punctiforme* (WP_012409292.1), *Pinus mugo* (AAC60560.2), *Physcomitrella patens* (XP_0011772136.1) and *Zea mays* (NP_001167680.1) were synthesised by Genscript.

2.1.3. Restriction digest

To transfer the genes to the pET9-His vector the synthesised genes and plasmid were digested with *Bam*HI and *Nde*I restriction enzymes (New England Biolabs Inc.). A 10 µl reaction mix was prepared, consisting of ± 1 µg DNA (genes or pET9-His vector), 10 units *Bam*HI-HF, 10 units *Nde*I, made up in buffer 4 (New England Biolabs Inc.). This mix was incubated at 37°C overnight before the mix was run on a 1 % agarose gel to separate the DNA fragments. The desired fragments were cut from the gel and extracted by following the protocol for the QIAquick gel extraction kit (Qiagen).

2.1.4. Ligation

The POR genes were inserted into the pET9-His vector by mixing ± 0.5 µg *Nde*I / *Bam*HI POR insert, ± 1 µg *Nde*I / *Bam*HI pET9-His vector, 400 units ligase (New England Biolabs, Inc.) made up in ligase buffer (New England Biolabs, Inc.). The mix was left for 5 min at room temperature to complete the reaction before transformation into XL1-Blue cells (Agilent technologies).

2.2. Expression and purification of POR from *Thermosynechococcus elongatus*

2.2.1. Transformation and expression

The pET9-His+POR plasmid was transformed (heat shock) into *Escherichia coli* BL21(DE3) pLysS competent Cells (Stratagene) and grown in Luria-Bertani (LB) medium containing 30 µg/ml of kanamycin and chloramphenicol at 30°C. When an optical density (OD) of 0.1 at 600 nm was reached the temperature was lowered to 25°C. Once an OD of 0.6 was reached, indicative of log phase growth, expression was induced using 0.1 mM IPTG and cells were grown at 25°C overnight. Cells were then harvested using centrifugation (6000 rpm, 10 min, JLA 8.1000; Beckman Coulter, Inc.).

2.2.2. Purification

Harvested cells (usually from a 6 l culture volume) were re-suspended in a volume of approximately 150 ml cold Nickel-Binding buffer (50 mM Tris-HCl pH 7.5; 500 mM NaCl; 5 mM imidazole) containing 1 protease inhibitor tablet (complete mini EDTA free Protease cocktail inhibitors, Roche Applied Science) and 200 µl DNase (2500 Kunitz units/mL). Cells were then sonicated for 22 cycles of 20 second pulses at 40% amplitude, with 1 min rest in between pulses to keep cells cool (Bandelin, Sonopuls probe VT70T/N494). After sonication the cell debris was removed using centrifugation (30 mins, 14000 rpm JA16.25 rotor; Beckman Coulter, Inc.) and the resulting pellet, containing the cell debris, was discarded. The supernatant was subjected to 20% ammonium sulphate precipitation and centrifuged (30 min, 14000 rpm, JLA16.25; Beckman Coulter, Inc.) again to remove any impurities. All remaining proteins, including POR, were precipitated by a 50% ammonium sulphate solution and centrifuged (30 min, 14000 rpm, JLA16.25; Beckman Coulter, Inc.).

2.2.2.1. Nickel-column

The pellet was dissolved in 100-150 ml of Nickel-binding buffer and loaded onto nickel-IDA column (25 ml) equilibrated with Ni-binding buffer (at least 3 column volumes (cv)). Following this, a wash stage involving 5 cv of Ni-wash buffer (50 mM Tris-HCl pH 7.5, 500 mM NaCl, 50 mM imidazole) was used to remove the majority of impurities. His-tagged POR was subsequently eluted with 5 cv Ni-elute buffer (50 mM Tris-HCl, pH 7.5, 500 mM NaCl, 250 mM imidazole). The eluted protein was

precipitated using 50% ammonium sulphate and centrifuged (20 minutes, 14000 rpm, JLA16.25; Beckman Coulter, Inc.) to generate a protein pellet.

2.2.2.2. *Blue Sepharose column*

The pellet from the the Ni^{2+} column was re-suspended in 100-150 ml of cold Blue-start buffer (50 mM Tris-HCl pH 7.5, 25 mM NaCl, 1 mM DTT) and loaded onto a 20 ml Blue Sepharose column, which had been equilibrated with Blue-start buffer. The Blue Sepharose column was washed with >10 cv of 20% Blue-start buffer (50 mM Tris-HCl pH 7.5, 500 mM NaCl, 1 mM DTT) and finally the purified protein was eluted with 15 cv of 100% Blue-elute buffer (50 mM Tris-HCl pH 7.5, 2.5 M NaCl, 1 mM DTT).

The eluted protein was then subjected to a 50% ammonium sulphate precipitation and centrifuged (30 minutes, 14000 rpm, JLA 16.25; Beckman Coulter, Inc.) to give a pellet of 'purified' Thermophilic POR. This pellet was re-suspended in 100 ml of activity buffer (50 mM Tris-HCl pH 7.5, 500 mM NaCl, 1 mM DTT) and concentrated using a Vivaspin 20 (10kDa MWCO; Sartorius). Figure 2.1 shows the purification process for POR from *T. elongatus* that was used to produce pure protein for the experiments in *e.g.* chapter 3.

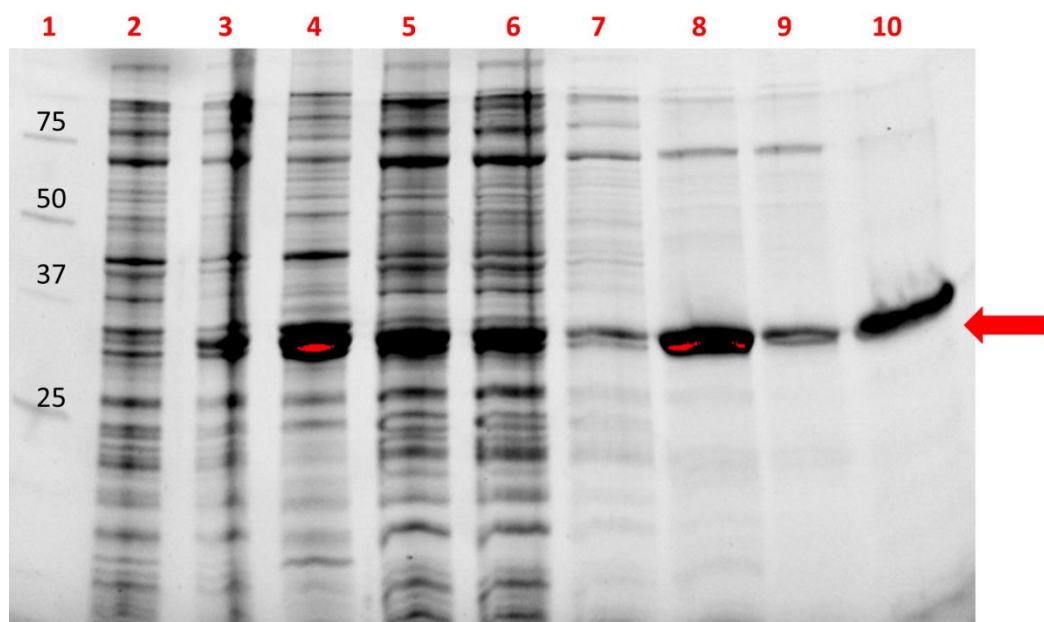


Figure 2.1. Expression and purification of POR from *T. elongatus*. The desired protein is indicated with a red arrow. 1. Precision plus ladder unstained (BioRad) 2. Uninduced cell extract 3. Induced cell extract 4. Insoluble fraction 5. Sonicated cell extract 6. Ni column run-through 7. Ni column wash (20% elution buffer) 8. Ni column elution 9. Blue sepharose run-through 10. Blue sepharose elution.

2.2.3. Determining the concentration of protein

Protein concentration was measured using BioRad DC assay kit with bovine serum albumin (BSA) as a standard. Expression levels in *E. coli* and purification steps were checked by SDS-PAGE on a 12% precast gels (BioRad) and visualised using a Criterion Stain Free™ Gel Imaging System (BioRad).

2.3. Phylogeny

The phylogenetic tree was generated using the phylogeny.fr website (Dereeper *et al.* 2008), with a full MUSCLE setting for alignment and one-hundred maximum likelihood bootstrap replicates.

2.4. Substrates and other chemicals

2.4.1. Pchlride synthesis and extraction

The *R. capsulatus* ZY5 strain was streaked out (Yang & Bauer 1990, Martin *et al.* 1997) on VN (10 g yeast extract, 1 g K₂HPO₄, 0.5 g MgSO₄ at pH 7 in 1 litre) agar with rifampicin (25 µg/ml) and grown at 34 °C for about 48 hours. Several ZY5 colonies were picked and grown in 100 ml VN rifampicin at 34 °C for at least 24 hours. Afterwards, the ZY5 culture were added to 1 litre VN medium with rifampicin and grow at 34 °C for approx. 72 hours with 4 polyurethane foam bungs (foam bungs absorb Pchlride). The foam bungs were replaced when they turned dark green due to absorption of pigment and throughout the whole process Pchlride was protected from light if possible. Once the foam bungs did not appear to absorb anymore pigment, which can be observed by them no longer changing colour (to green), they were dried in the fume hood. In order to dissolve Pchlride in solution, the dry bungs were submerged in (~ 1 litre) methanol. Once most of the Pchlride was removed from the bungs the methanol solution was left to evaporate in the fume hood. The remaining Pchlride residue with at most 2 % (v/v) methanol was resuspended in 100 % acetone. During the evaporation of methanol, the 50 ml CM Sepharose column (Sigma) was set up in a Buchner funnel and equilibrated. In a first step Pchlride was recovered by washing with distilled water under suction, followed by resuspending of the resin with 100 % acetone, stirring and drying repeatedly. The acetone treatment was repeated at least twice (until all water was removed). The resuspended resin (in ~ 100 ml acetone) was then poured down a column (about 5 cm wide) by gravity flow and

left to let the resin settle. Once the column was set up Pchl_{ide} could be passed down the column. Binding of Pchl_{ide} should turn the resin dark green where it binds. The column was washed with several column volumes of 100 % acetone until all carotenoids (orange) were washed off. Another wash with several column volumes of 5 % methanol in acetone was conducted to remove phytol/pheophorbide. Pchl_{ide} was eluted from the column with 25% methanol in acetone. The eluate was evaporated down to approx. 50 ml in the fume hood. Finally, 1 – 1.5 ml aliquots were made in black Eppendorf tubes, which were left, with the Eppendorf tubes open, in the fume hood to let all the acetone and methanol evaporate off. The dry Pchl_{ide} was then stored at -20 °C.

2.4.2. Other chemicals

All chemicals were obtained from Sigma-Aldrich, except for NADPH (Melford Laboratories Ltd.).

2.5. Spectroscopy

2.5.1. Absorption spectroscopy

A Cary 50 spectrophotometer (Varian) was used for all UV/vis absorbance measurements. For steady-state measurements the absorbance increase at 670 nm (Chl_{ide} absorbance maximum) was followed upon illumination with a LED light-source (Thorlabs, Inc.) at 455 nm wavelength (Soret band of Pchl_{ide}; Figure 2.2).

The concentrations of the substrates and products were calculated using the following extinction coefficients in aqueous solution: NADPH, 6.22 mM⁻¹cm⁻¹ at 340 nm (Cameron & Benkovic 1997); NADP⁺, 17.8 mM⁻¹cm⁻¹ at 260 nm (Cameron & Benkovic 1997); Pchl_{ide}, 23.95 mM⁻¹cm⁻¹ at 630 nm (Brouers & Michel-Wolwertz 1983, Klement *et al.* 1999) and Chl_{ide}, 69.96 mM⁻¹cm⁻¹ at 670 nm (Klement *et al.* 1999, Griffiths 1975). Typical steady state buffer conditions were 0.1 μM of each POR homologue, in activity buffer (0.5 M NaCl, 50 mM MOPS, 100 mM ammonium acetate pH 7) with 0.1 % Triton X-100 and 0.1 % 2-mercaptoethanol. Substrate concentrations are as stated per experiment.

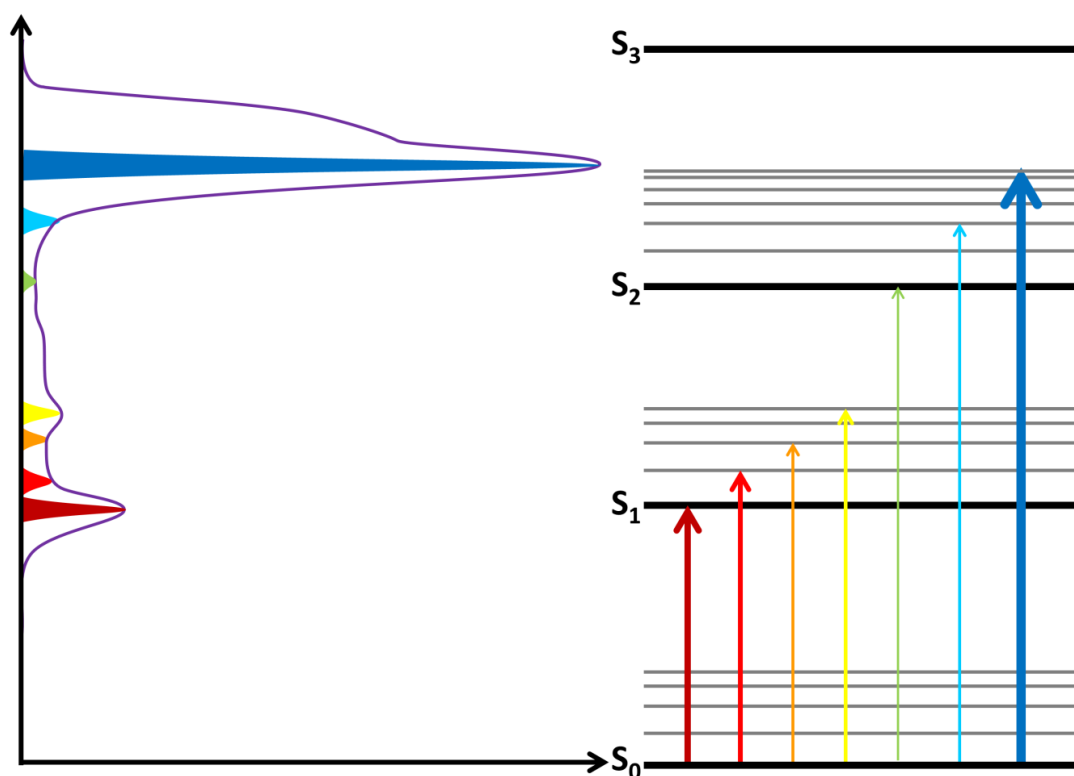


Figure 2.2. The Pchlride absorption spectrum and a representation of the corresponding Jablonski diagram. The left shows the absorption spectrum of Pchlride in the visible region, with a representation of the excitation energies on the right. When the energy gap between the ground and electronically excited states of Pchlride match that of the photon, they get absorbed, resulting in the shown absorption spectrum.

2.5.2. Pressure spectroscopy

The set-up for spectroscopy at high pressures is shown in Figure 2.3. The cuvettes used are made of quartz and are designed to withstand high pressures. The volume of the cells is approximately 1 ml and can be covered with a custom made cap with a ~0.15 ml volume. The temperature can be controlled by connecting the cell to a water bath that can keep the water temperature inside the cell constant. A high-pressure cell system (ISS) was mounted into a Cary 50 (Varian) spectrophotometer, and pressure was generated by pumping water (Figure 2.3 A.) into the pressure cell (Figure 2.3 C.). To determine the NADPH K_d in function of pressure, samples contained 10 μ M Pchlride, 200 μ M NADPH and 0–200 μ M POR in 50 mM Tris-HCl pH 7.5, 150 mM NaCl, 0.1% 2-mercaptoethanol, 0.1% Triton X-100.

For steady-state measurements a Schott KL1500 cold light source (Figure 2.3 B.), containing a 450 nm band-pass filter was used to illuminate samples with a flexible fibre optic cable aimed through the window of the pressure cell. For standard steady

state assays samples contained 100 μ M NADPH, 10 μ M Pchl_a, 0.1% Triton X-100, 0.1% (v/v) 2-mercaptoethanol and a volume of activity buffer required to make 1 ml.

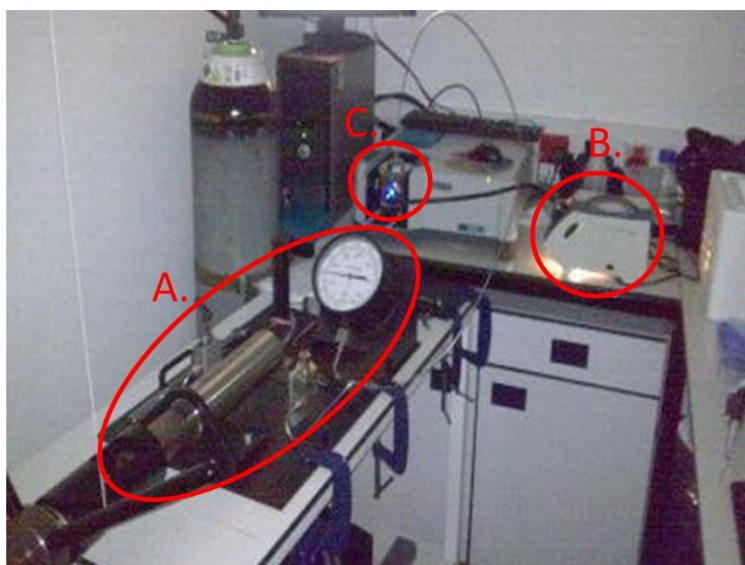


Figure 2.3. The set-up for pressure spectroscopy for steady-state measurements. Pressure is generated by pumping water from a reservoir (A) into a pressure cell (C) containing the sample. The pressure cell can be mounted into a Cary 50 (Varian) spectrophotometer to conduct steady-state measurements as described. The light source for these experiments is a Schott KL1500 cold light source (C), containing a 450 nm band-pass filter, with a flexible optical fibre to guide the light into the pressure cell.

2.5.3. Fluorescence

A Cary Eclipse fluorescence spectrophotometer (Agilent technologies) was used to perform fluorescence measurements. To reduce dilution effects, a 3 ml quartz cuvette was used, 1 cm in length and width. Samples contained 0.1% 2-mercaptoethanol in activity buffer (0.5 M NaCl, 50 mM MOPS, 100 mM ammonium acetate pH 7) containing 0.5 μ M POR, with NADPH titrated in 1 μ l steps up to a maximum of 1% of the total sample volume (30 μ l).

2.5.4. Laser flash photolysis

Laser flash photolysis is a pump-probe technique, which in this case uses a laser pulse at 450 nm to trigger the reaction, as depicted in figure 2.4. A neodymium-doped yttrium aluminium garnet (Nd:YAG) laser (Brilliant B, Quantel) generates a 1064 nm pulse (~8 ns), which is guided through two harmonics to triple the frequency (to 355 nm) and finally tuned by an optical parametric oscillator (OPO) to achieve a 450 nm pulse. Upon excitation of the sample, spectral changes can be followed by measuring

the absorption at a single wavelength using an Applied Photophysics LKS spectrometer. A pulsed 150 W Xenon Arc flash lamp produces white light that passes through a monochromator to generate a single wavelength probe beam. The scattered laser light is cut out by a second monochromator after the sample. Absorbance changes are detected by a photomultiplier tube that transfers the information to a digital oscilloscope, which in turn is linked to a computer.

Laser photoexcitation experiments were conducted as outlined previously (Heyes *et al.*, 2009). Each data point was the average of at least four measurements. The cuvette used had a 2 mm pathlength in the pump direction and 1 cm in the probe direction. Samples contained 50 μ M enzyme, 250 μ M NADPH (except *C. reinhardtii*, *C. merolae*, *L. majuscula*, *D. carota* which had a 2 mM concentration due to the reduced affinity for NADPH) and 12 μ M Pchl_a in activity buffer (0.5 M NaCl, 50 mM MOPS, 100 mM ammonium acetate, 0.1 % Genapol X-080, 0.1% 2-mercaptoethanol). Samples for solvent viscosity measurements were prepared using glycerol as the viscosogen by weight and the solution viscosity was calculated as previously described (Hay *et al.* 2008). The observed rate was plotted as a function of solvent viscosity and fitted to Equation 2.1 (Heyes *et al.* 2009, Ansari *et al.* 1992) to explain the protein friction contribution to the system friction.

$$k_{obs} = \frac{k_B T}{h} \left(\frac{1+\sigma}{\eta+\sigma} \right) e^{\frac{-\Delta G}{RT}} \quad 2.1$$

The absolute viscosity is shown as η , and the protein's friction contribution is represented by σ , in centipoise (cP).

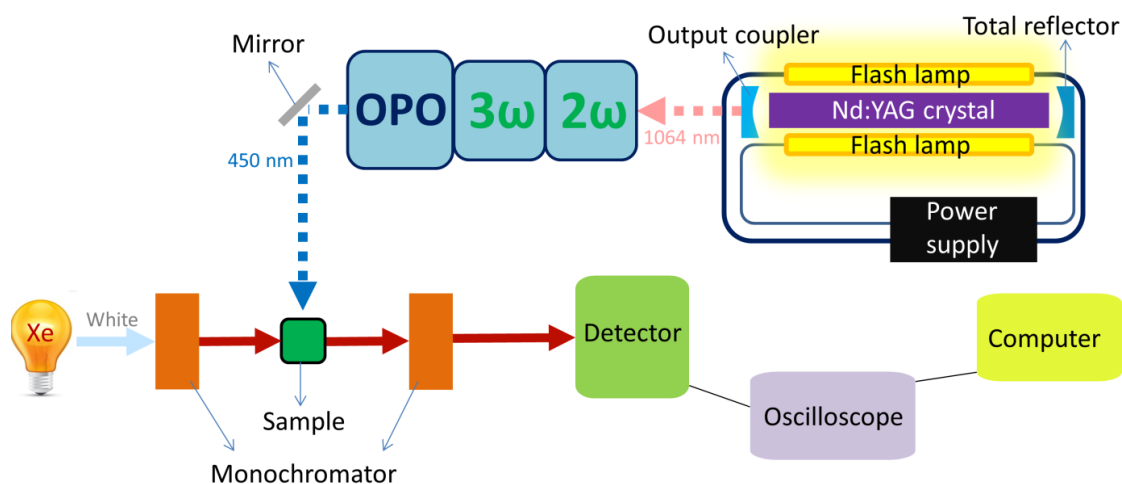


Figure 2.4. Laser flash photolysis set-up. A Nd:YAG laser generates a 1064 nm pulse that passes through two harmonics (2ω , 3ω) and an optical parametric oscillator (OPO), generating a 450 nm pump beam to excite the sample. A 150W Xenon Arc flash lamp produces white light that gets converted to a single wavelength by a monochromator and absorbance changes are detected by a photomultiplier tube (detector).

2.5.5. Ultrafast transient absorption spectroscopy

Transient absorption (Figure 2.5) relies on the same pump-probe principle as the laser flash photolysis method. A Ti:sapphire amplifier system (Spectra Physics Solstice Ace) produced 6 mJ of 800 nm pulses at 1 kHz with 100 fs pulse duration. A portion of the output of the amplifier was used to pump a Topas Prime OPA with associated NirUVis unit which was used to generate the pump beam centred at 450 nm, with FWHM (full width at half maximum) of ca. 10 nm. A broad band ultrafast pump-probe transient absorbance spectrometer ‘Helios’ (Ultrafast systems LLC) was used to collect data (at random timepoints) from ~1 ps to 2.6 ns with a time resolution of around 0.2 ps. The probe beam consisted of a white light continuum generated in a sapphire crystal and absorbance changes were monitored between 500 and 750 nm. Data from this setup are referred to as the ‘fast’ data. A broad band sub-nanosecond pump-probe transient absorbance spectrometer ‘Eos’ (Ultrafast systems LLC) was used to collect data (at random timepoints) up to either 0.5 or 2 μ s. A 2 kHz white-light continuum fibre laser was used to generate the probe pulses. The delay between pump and probe was controlled electronically. Data from this set-up are referred to as the ‘slow’ data. For both sets of measurements samples were excited at 450 nm with 0.5 μ J power and a beam diameter of ~ 200 μ m. Samples were flowed at a rate of approximately 30 ml/min through a 0.2 mm pathlength quartz cell (at room temperature) to ensure that a different area of the sample is excited with each pump

laser pulse. Samples were prepared in the dark containing 500 μM POR, 200 μM Pchlide and 4 mM NADPH in activity buffer with 10 % glycerol, 0.1 % 2-mercaptoethanol, and 0.5 % Triton X-100.

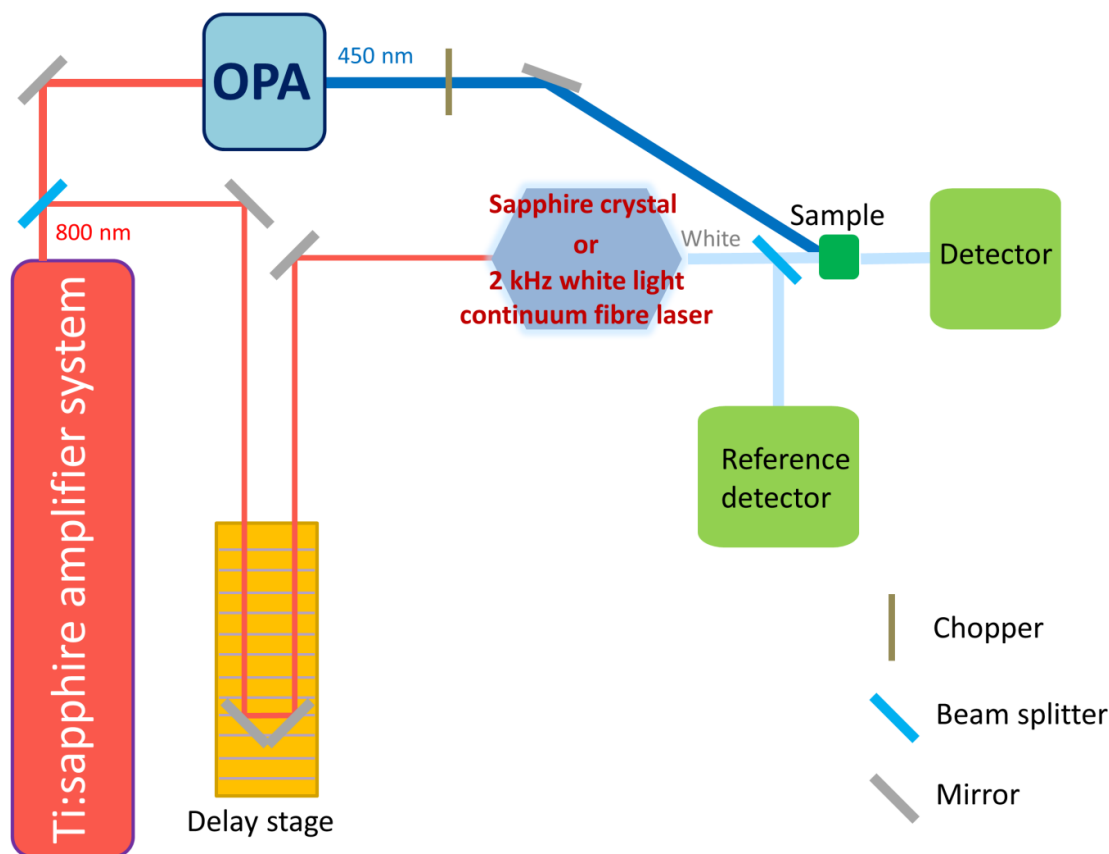


Figure 2.5. Ultrafast transient absorption set-up. A Ti:sapphire amplifier system produces a 800 nm laser pulse that is split to generate pump and probe beams. The pump pulse gets converted to 450 nm by an optical parametric amplifier (OPA) and a chopper ensures the right pulse frequency is achieved before exciting the sample. The probe beam can be set to two different modes dependent on the desired time frame, with a ‘fast’ setting using the ‘Helios’ set-up and ‘slow’ the ‘Eos’ setting. For the ‘fast’ set-up an optical delay stage is used and a sapphire crystal to produce white light, while an electronic delay stage and a 2 kHz white laser continuum fibre laser gets seeded to generate the white light.

2.5.6. Global analysis.

The datasets were analysed globally using the open-source software Glotaran (Snellenburg *et al.* 2012). This procedure reduces the matrix of change in absorbance as a function of time and wavelength, to a model of one or more exponentially decaying time components, as described in results section 5.4.2, each with a corresponding difference spectrum (species associated difference spectra (SADS)). Errors quoted with the lifetime values are the standard errors calculated during the global analysis. For the analysis, the pre-excitation background was subtracted and

both the 'fast' and 'slow' datasets were fitted to a simple sequential model where one species converts to another, which then persists for the lifetime of the experiment. The 'fast' datasets were the result of one scan of <3 minute duration with data analysed from 1 ps to 2.6 ns. The 'slow' datasets were selected after a collection time such that the ratio of the ground state bleach intensity of Pchl_a:Chl_a was similar in all cases (ca. 4) with data analysed from 5 ns to 500 (or 2000) ns.

Chapter 3

Does the pressure dependence of kinetic isotope effects report usefully on dynamics in enzyme H-transfer reactions?

Authors:

Robin Hoeven, Derren J. Heyes, Sam Hay and Nigel S. Scrutton

Affiliation:

Manchester Institute of Biotechnology, Faculty of Life Sciences, The University of Manchester, Manchester M13 9PL, United Kingdom

Published in:

The FEBS Journal, Volume 282, Issue 16, pages 3243–3255, August 2015

First published online: 29 January 2015

doi:10.1111/febs.13193.

3.1. Abstract

The temperature dependence of kinetic isotope effects (KIEs) has emerged as the main experimental probe of enzymatic H-transfer by quantum tunneling. Implicit in the interpretation is a presumed role for dynamic coupling of H-transfer chemistry to the protein environment, the so-called ‘promoting motions/vibrations hypothesis’. This idea remains contentious, and others have questioned the importance and/or existence of promoting motions/vibrations. New experimental methods of addressing this problem are emerging, including use of mass-modulated enzymes and time-resolved spectroscopy. The pressure dependence of KIEs has been considered as a potential probe of quantum tunneling reactions, because semi-classical KIEs, which are defined by differences in zero-point vibrational energy, are relatively insensitive to kbar changes in pressure. Reported combined pressure and temperature (p - T) dependence studies of H-transfer reactions are, however, limited. Here, we extend and review the available p - T studies that have utilized well-defined experimental systems in which quantum mechanical tunneling is established. These include flavoproteins, quinoproteins, light-activated enzymes and chemical model systems. We show that there is no clear general trend between the p - T dependencies of the KIEs in these systems. Given the complex nature of p - T studies, we conclude that computational simulations using determined (e.g. X-ray) structures are also needed alongside experimental measurements of reaction rates/KIEs to guide the interpretation of p - T effects. In providing new insight into H-transfer/environmental coupling, combined approaches that unite both atomistic understanding with experimental rate measurements will require careful evaluation on a case-by-case basis. Although individually informative, we conclude that p - T studies do not provide the more generalized insight that has come from studies of the temperature dependence of KIEs.

3.2. Isotope effects and dynamics in enzyme catalysed reactions

A central paradigm in biochemistry is that protein function is defined by structure. However, in solution proteins are inherently dynamic molecules, exhibiting motions on timescales ranging from bond stretches ($\sim 10^3 \text{ cm}^{-1}$; fs) through to slow domain motions and normal mode vibrations ($< 1 \text{ cm}^{-1}$; ms). An important open question in enzymology remains the role of such dynamics, and whether motions/vibrations on time-scales faster than turnover (i.e. k_{cat}) can couple to chemical steps during catalysis (i.e. to the reaction coordinate) (Hay & Scrutton 2012). There has been good progress using NMR approaches in establishing the role of ms–ns dynamics such as loop opening/closing during enzyme turnover (Boehr *et al.* 2006, Henzler-Wildman *et al.* 2007), but direct evidence for the coupling of faster (sub-ns) dynamics to chemistry remains illusive and controversial (Kamerlin & Warshel 2010, Adamczyk *et al.* 2011, Glowacki *et al.* 2012, Hay & Scrutton 2012, Klinman & Kohen 2013, Schwartz 2013) and is inferred largely on the anomalous temperature dependencies of primary kinetic isotope effects (KIEs; e.g. $k_{\text{H}}/k_{\text{D}}$) (Kohen *et al.* 1999, Maglia & Allemann 2003, Hay *et al.* 2007, Heyes *et al.* 2009). The role of fast dynamics remains an important question, because motions on similar timescales to chemistry (ps–fs; specifically, the time required to traverse the transition state) have the potential to profoundly affect the reaction outcome, and thus offer a means to control (enzyme) reactivity (Thomas *et al.* 2008, Hay & Scrutton 2012, Hong & Tantillo 2014). The potential importance of fast motions in H-transfer reactions where quantum mechanical tunneling is a feature of the reaction has been debated intensely (Kamerlin *et al.* 2010, Glowacki *et al.* 2012, Hay & Scrutton 2012, Klinman & Kohen 2013, Schwartz 2013). KIEs and analysis of their temperature dependence are now established as a general approach to investigate quantum mechanical tunneling reactions in enzymes (Basran *et al.* 1999, Kohen *et al.* 1999, Maglia & Allemann 2003, Klinman & Kohen 2013). In the absence of complicating issues (e.g. reaction branching Thibblin & Ahlberg 1989), inflated KIEs (values above the semi-classical limit of ~ 7 at 298 K) are generally taken to be a definitive hallmark of quantum mechanical hydrogen tunneling (Bell 1980). Quantum tunneling is also a feature of many reactions in which intrinsic KIEs are numerically below the maximum value (attributed to the difference in zero point vibrational energies of the C–H and C–D bonds) predicted by semi-classical transition state theory (Pang *et al.* 2008). These findings have been rationalized in the context of simple

Marcus-like (vibronic) models of H-transfer (Bruno & Bialek 1992, Antoniou & Schwartz 1997, Knapp & Klinman 2002, Hay & Scrutton 2008), which have been used widely by the experimental enzymology community to study quantum mechanical tunneling and the inferred importance of dynamics in H-transfer reactions. The limitations of these models have been discussed, and alternative explanations of the temperature dependence of KIEs have been advanced (Nunez *et al.* 2006, Liu & Warshel 2007, Adamczyk *et al.* 2011, Glowacki *et al.* 2012, Roston *et al.* 2012), but semi-quantitatively these simple vibronic models have enabled comparisons to be made of tunneling and inferred dynamics in enzymes, for example, across a reaction series where active site structure and dynamics are altered by site-directed mutagenesis (Meyer *et al.* 2008, Pudney *et al.* 2010) or where studies are made with a single enzyme using multiple substrates (Hothi *et al.* 2008, Pudney *et al.* 2009). Despite their limitations, vibronic models have provided some useful insight into tunneling and the inferred importance of dynamics (Bruno & Bialek 1992, Antoniou & Schwartz 1997, Knapp & Klinman 2002, Hay & Scrutton 2008), especially for estimating the frequencies of inferred compressive dynamics/promoting motions and donor–acceptor distances (Hay *et al.* 2007, Johannissen *et al.* 2007, Meyer *et al.* 2008, Pudney *et al.* 2010, Roston *et al.* 2012). Experimental studies of this type are best interpreted alongside more detailed atomistic simulations of the reaction chemistry where possible, to provide quantitative insight into the reaction free energy barrier, the extent of tunneling, and coupling of the protein environment to the reaction coordinated (Masgrau *et al.* 2006, Pu *et al.* 2006, Pang *et al.* 2008, Luk *et al.* 2013, Ruiz-Pernia *et al.* 2013, Schwartz 2013). More recently, analysis of the temperature dependence of primary KIEs in relation to quantum tunneling and the inferred importance of dynamics have taken on a new direction by employing mass modulated (‘heavy’) enzymes. For many years, investigators have exploited the use of stable isotope-labelled proteins (typically labelled with ^2H , ^{13}C and/or ^{15}N) as an experimental tool, particularly in the NMR and vibrational spectroscopy communities (e.g. ^{13}C and ^{15}N are used as NMR probes, whereas amino acid isotopic labelling is used in FTIR experiments to shift vibrational spectra and to aid in peak assignment). The implicit assumption has generally been that isotopic labelling does not significantly perturb protein function. However, D_2O has been shown to promote rigidification and unfolding of some proteins (Cioni & Strambini 2002), whereas perdeuteration has long been known to significantly reduce the rate of turnover of

alkaline phosphatase (Rokop *et al.* 1969). Recently, Schramm and colleagues showed that isotopically labelled ‘heavy’ purine nucleoside phosphorylase and HIV-1 protease enzymes have measurably slower reaction kinetics (Kipp *et al.* 2011, Silva *et al.* 2011). These data were interpreted in terms of the Born–Oppenheimer approximation, in which increased protein mass (due to labelling) alters bond vibrational frequencies without affecting electrostatic properties of the enzyme (ionisable protons were not labelled). The authors suggested that the lower frequency of (fs) bond vibrations in the ‘heavy enzymes’ may lead to a reduction in conformational sampling and thus chemical barrier crossing; the rate of reaction is proportional to the rate of barrier crossing. Clearly, the ‘heavy enzyme’ methodology can be used as a powerful tool to study enzyme dynamics and others have adopted this approach. We have extended this approach to perturb the temperature dependence of a KIE on the Old Yellow flavoenzyme pentaerythritol tetranitrate reductase (PETNR) catalysed hydride transfer reaction (Pudney *et al.* 2013), although others have measured isotope effects on ‘heavy’ alanine racemase (Toney *et al.* 2013) and dihydrofolate reductase enzymes (Luk *et al.* 2013, Ruiz-Pernia *et al.* 2013). A common finding is that in each case, the catalysed reaction is slower in the ‘heavy’ enzyme suggesting that vibrational coupling of the protein to the reaction coordinate may be a general feature. However, important questions remain. Mass perturbation will affect all vibrations within the protein, so experimental observation of the timescale(s) of any vibrational coupling between protein and chemical coordinate is highly desirable in order to firmly establish the origin of the ‘heavy enzyme’ effect. Further, a computational study of a ‘heavy’ dihydrofolate reductase variant suggests that an increased dynamic coupling to the chemical coordinate is detrimental to dihydrofolate reductase catalysis (Luk *et al.* 2013). It is now timely to also consider whether the dynamic coupling of enzyme motions to the chemical coordinate is generally optimized (e.g. by evolution). ‘Heavy’ enzymes offer a more refined alternative to traditional mutagenesis approaches to study such questions and provide new experimental tools with which to explore the potential importance of dynamics/environmental coupling to the reaction coordinate.

3.3. Pressure–temperature dependence of KIEs

An alternative and complementary experimental approach is to analyse the combined pressure–temperature (p - T) dependence of KIEs with a view to correlating outcomes with T dependence studies of KIEs with conventional and mass-modulated enzymes. However, the usefulness of p - T dependence studies as a probe of environmental coupling/dynamics in enzymatic H-tunneling reactions is uncertain because of the limited subset of reactions that have been studied. Here, we review and extend p - T dependence studies of primary KIEs for H-transfer reactions catalysed by enzyme and simple model systems to investigate their general utility as experimental probes of dynamics. We provide first an overview of the theory that we have developed for analysis of KIEs as a function of pressure and temperature. We then discuss our recent p - T dependence studies with selected flavoprotein and quinoprotein systems, which highlight the utility (and potential problems) of this approach. Finally, we present new p - T dependence studies with the light-activated enzyme protochlorophyllide oxidoreductase (POR) and explore relationships/correlations across multiple datasets (including those from non-enzymatic model chemical studies) to understand how p - T dependence studies can inform on tunneling and/or environmental coupling, and to highlight the strengths and limitations of such an approach. Although a number of vibronic models have been developed to describe H-transfer by vibrationally assisted quantum tunneling (Antoniou & Schwartz 1997, Knapp & Klinman 2002, Hay & Scrutton 2008 and below), the analysis of the temperature and/or pressure dependence of observed rate constants using transition state theory in parallel facilitates comparison with other work; the apparent activation enthalpy, ΔH^\ddagger , and entropy, ΔS^\ddagger (or equivalent; i.e. E_a and A , respectively) are obtained from the Eyring or Arrhenius equations (Eqn 3.1) (Gladstone *et al.* 1941), whereas the apparent activation volume, ΔV^\ddagger , and activation isothermal compressibility, $\Delta\beta^\ddagger$, are obtained from the pressure dependency (Eqn 3.2) (Isaacs *et al.* 1977, Northrop 1999, Hay & Scrutton 2002, Masson & Balny 2005).

$$k_{obs}(T) = k_B T / h \exp(\Delta S^\ddagger / R) \exp(-\Delta H^\ddagger / RT) \\ = A \exp(-E_a / RT) \quad (3.1)$$

$$k_{obs}(p, T) = k_0 \exp(-\Delta V^\ddagger p / RT) \exp(\Delta\beta^\ddagger p^2 / 2RT) \quad (3.2)$$

The temperature and pressure dependencies of KIEs can likewise be fitted to Eqns (3.1) and (3.2) by substituting KIE values for k_{obs} . In this case, the temperature dependence of the KIE is described by the difference in the entropy of activation, $\Delta\Delta S^\ddagger = \Delta S^{\ddagger\text{D}} - \Delta S^{\ddagger\text{H}} \sim R \ln(-A^{\text{H}}/A^{\text{D}})$ and the difference in the enthalpy of activation, $\Delta\Delta H^\ddagger = \Delta H^{\ddagger\text{D}} - \Delta H^{\ddagger\text{H}} \sim \Delta E_{\text{a}}$. Likewise, the pressure dependence of the KIE is described by KIE_0 (the KIE extrapolated to zero pressure), the difference in the activation volume $\Delta\Delta V^\ddagger = \Delta V^{\ddagger\text{H}} - \Delta V^{\ddagger\text{D}}$ and the difference in the activation isothermal compressibility $\Delta\Delta\beta^\ddagger = \Delta\beta^{\ddagger\text{H}} - \Delta\beta^{\ddagger\text{D}}$. A complication arises in that KIE_0 , $(\Delta)\Delta V^\ddagger$ and $(\Delta)\Delta\beta^\ddagger$ may be significantly temperature dependent, so ideally rate constants and KIEs should be measured over a matrix of pressure and temperature values, i.e. a p - T matrix (Hay *et al.* 2007, 2012). Isaacs *et al.* showed that H-transfer reactions with a significant degree of quantum tunneling of the transferred H could exhibit pressure-dependent KIEs (Isaacs *et al.* 1977). Later, Northrop developed a model (Northrop 1999) for the pressure dependence of H-transfer reactions with a small tunneling component (Q), which is based on the Bell correction (Bell 1980):

$$\text{KIE}_{\text{obs}}(p, T) = \text{KIE}_0(Q^{\text{H}}/Q^{\text{D}} - 1)\exp(-\Delta V^{\text{Q}}p/RT) \quad (3.3)$$

Functionally, Eqn (3.3) is similar to Eqn (3.2) if $(\Delta)\Delta\beta^\ddagger$ is fixed to zero, because the observed KIE has an exponential dependence on pressure. Consequently ΔV^{Q} and $\Delta\Delta V^\ddagger$ should be comparable. More recently, we developed a model to account for the p - T dependence of H-tunneling reactions (Eqn 21 in Ref. Hay & Scrutton 2008) based on an approximate vibronic formalism, which can be expressed by:

$$\begin{aligned} \text{KIE}_{\text{obs}}(p, T) &\approx \text{KIE}_0 \exp(-2Ek_{\text{B}}T(\kappa_0 + \Delta\kappa \cdot p)) \exp(E(r_0 - \Delta r \cdot p)^2) \\ E &= (\mu_{\text{h}}\omega_{\text{h}} - \mu_{\text{l}}\omega_{\text{l}})/2\hbar \end{aligned} \quad (3.4)$$

In this case, the observed KIE has a similar pressure response as Eqn (3.2); i.e. the pressure dependence of $\ln(\text{KIE}_{\text{obs}})$ is a quadratic function of pressure. A more general effect of pressure is to perturb pre-existing equilibrium, favouring species with smaller volumes (Northrop 1999, Masson & Balny 2005). Consequently, if multiple conformational states (heterogeneity) are involved in the reaction (as has been proposed by some workers in the field (Nunez *et al.* 2006, Pudney *et al.* 2007,

Glowacki *et al.* 2012, Roston *et al.* 2012), then pressure may perturb rate constants and/or KIEs by perturbing the relative concentration(s) of reactive states (Pudney *et al.* 2009, Hay *et al.* 2012). In this case, the pressure dependence of the KIE may not be well defined, especially for KIEs measured under steady-state turnover conditions in which measured KIEs are an average of those for individual conformational states, weighted to reflect the distribution of these states at a defined pressure (Pudney *et al.* 2009).

3.4. p - T dependence of KIEs in flavoproteins

We initially examined the p - T dependence of the primary KIE on hydride transfer during the reductive half reaction (RHR) of the flavin-containing enzyme morphinone reductase (MR) with the coenzyme NADH (Hay *et al.* 2007, Hay & Scrutton 2008). This reaction involves hydride transfer from the C4 R-hydrogen of NADH to the N5 atom of FMN (Figure 3.1) and can be observed directly using a (variable pressure) stopped-flow instrument. The reaction transients reporting on the chemical step, display a primary and alpha secondary isotope effect and are consistent with transfer by quantum mechanical tunneling (Pudney *et al.* 2006, Pang *et al.* 2008). The temperature dependence of the primary KIE has been described within the context of environmentally coupled (vibronic) Marcus-like models for H-transfer, and the potential importance of fast promoting motions to move the nicotinamide C4 H close to the flavin N5 to optimize H-transfer has been inferred from these data (Hay *et al.* 2007, Pudney *et al.* 2010).

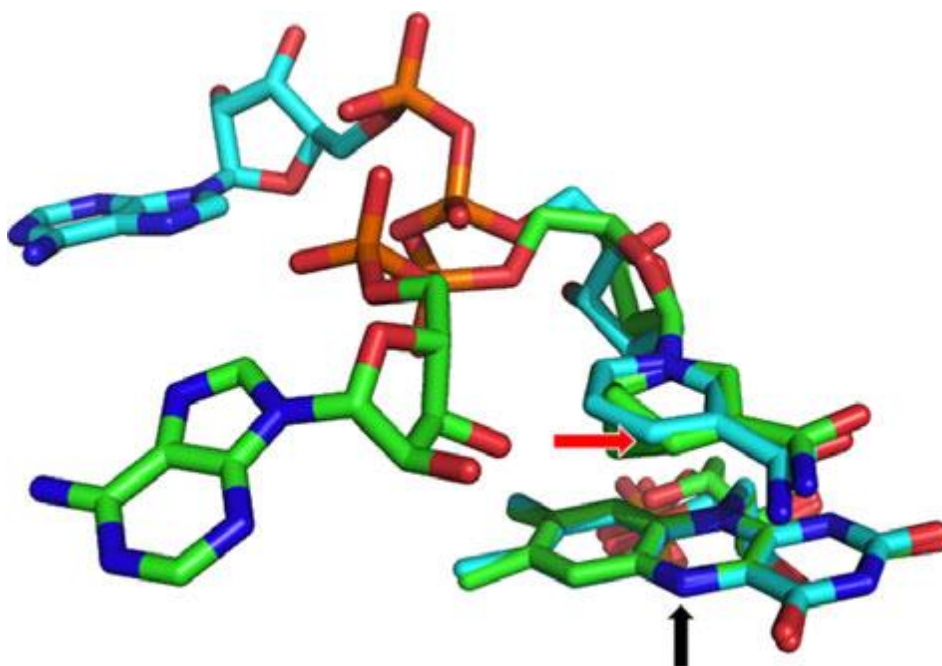


Figure 3.1. Overlay of the FMN and nicotinamide coenzyme within the active sites of NADH₄-bound MR (2R14.pdb, green carbons) and PETNR (3KFT.pdb, teal carbons) (Pudney *et al.* 2007, 2009). The nicotinamide C4 (hydride donor atom) is indicated with a red arrow and the FMN N5 (acceptor) with a black arrow. Hydrostatic pressure appears to reduce the C4–N5 distance due to compression roughly along the vertical axis (Hay *et al.* 2009, Johannissen *et al.* 2011).

More recently, we used mass modulated forms of the flavoenzyme pentaerythritol tetranitrate reductase (PETNR, which is structurally and functionally related to MR) to show that stable isotope labelling of the enzyme perturbs the temperature dependence of the primary KIE. This has been interpreted as establishing a causal relationship between fast motions and enzyme chemistry for hydride transfer from NADH to FMN in this class of enzyme (Pudney *et al.* 2013). In *p-T* studies with MR, both the observed rate constants and primary KIE for hydride transfer from NADH to FMN were found to increase with pressure, whereas $\Delta\Delta H^\ddagger$ was not significantly temperature dependent and the secondary KIE decreased with pressure (Hay *et al.* 2007, 2010). Similar pressure dependencies of the rate and KIE on the RHR of PETNR with NADH and NADPH were observed (Pudney *et al.* 2009). A positive correlation between $\Delta\Delta H^\ddagger$ and $\Delta\Delta\beta^\ddagger$ across these three experiments led us to propose that $\Delta\Delta\beta^\ddagger$ may be an alternative probe of fast dynamics in enzymes (Pudney *et al.* 2009, Hay & Scrutton 2011). Numerical modelling of the *p-T* dependence of the MR primary KIE using an environmentally coupled H-tunneling model has suggested, to a first approximation, that the experimental data are consistent with the donor–acceptor distance oscillating around an equilibrium separation (r_o) (Hay *et al.* 2007, Hay & Scrutton 2008). It is

implied in this analysis that the magnitude of the KIE can increase if the frequency of the oscillation (i.e. the inferred promoting motion) is allowed to increase while the equilibrium separation is simultaneously decreased. This modelling was used to rationalize the observed trend in KIE (and rate constant) for hydride/deuteride transfer as the hydrostatic pressure is increased. As pressure is increased, the inferred effect is to shorten the equilibrium separation between donor and acceptor. This increases the rate of hydride transfer – the transfer of which still involves quantum mechanical tunneling – and leads to both a stiffening of (i.e. increase in oscillator force constant) and a reduction in distance sampling by the inferred promoting motion. Numerical modelling implies that the effect of pressure is to reduce donor–acceptor distance in MR and PETNR. In both enzymes, the nicotinamide moiety of the NAD(P)H coenzyme stacks over the FMN isoalloxazine via a π – π stacking interaction (Figure 3.1) giving rise to a transient long-wavelength charge-transfer species in stopped-flow studies of the reductive half reaction. This charge-transfer species can be stabilized using the coenzyme mimic NAD(P)H₄ – a form of the coenzyme that is unable to transfer hydride from the coenzyme to FMN, but retains its ability to charge transfer with the FMN isoalloxazine ring. Pressure spectroscopy of the ternary complex of MR saturated with NADH₄ has demonstrated a compression of the charge-transfer bond at high pressure (Hay *et al.* 2009), which has been corroborated by molecular dynamics simulations of the MR–NADH complex (Hay *et al.* 2009, Johannissen *et al.* 2011). We have also demonstrated that high pressure leads to a decrease in the observed α -2° KIE on the pre-steady-state hydride transfer from NADH to FMN in MR (Hay *et al.* 2010). This was also rationalized as a reduction in macroscopic reaction barrier width for this reaction, and vibrational analysis by density functional theory of a simple active site model indicated that the decrease in the α -2° KIE with pressure is attributed to a decrease in vibrational coupling between the NADH primary (transferred) and secondary hydrogens in the ‘tunneling ready conformation’ (Hay *et al.* 2010). Numerical models developed for MR (and PETNR) based on the extensive *p-T* analysis of KIEs for MR provide a framework for understanding how modulation of donor–acceptor distances influences the hydride transfer process. Use of these models has been extended to studies with variant forms of MR in which donor–acceptor distances are changed by site-directed mutagenesis in the coenzyme-binding pocket (Pudney *et al.* 2010). Likewise, the effects of using alternative coenzymes (e.g. NADH in place of NADPH, the natural coenzyme for PETNR) to modulate donor–acceptor

distances and the force constant for inferred promoting motions have been discussed (Pudney *et al.* 2010). What is clear is that sub-Angstrom changes in donor–acceptor distance can have a major effect on the rate of hydride transfer, the KIEs obtained and the presumed importance (or otherwise) of promoting motions in facilitating the reaction. Detecting such small perturbations in donor–acceptor distance is experimentally challenging. Recent work, however, shows that ultrafast transient absorption spectroscopy of photoinduced electron transfer rates in NAD(P)H₄-bound MR and PETNR is a sensitive probe of donor–acceptor distance, providing a ‘kinetic ruler’ for probing small perturbations in donor–acceptor distance (Hardman *et al.* 2013).

3.5. p - T dependence of KIEs for aromatic amine dehydrogenase

Our work with flavoprotein systems provided motivation to study the p - T dependence of primary KIEs with the quinoprotein aromatic amine dehydrogenase (AADH). Our studies with MR and PETNR had suggested that pressure might be a useful general probe for both quantum tunneling and compression of the reaction coordinate, and we were keen to investigate the generality of this finding with other systems such as AADH, which is known to catalyse proton transfer by quantum mechanical tunneling (Hay *et al.* 2012). With the substrate tryptamine the KIE for proton/deuterium transfer in the reductive half reaction of AADH is large (~ 55) and variational transition state theory calculations/spectral density analysis from molecular dynamics simulations are consistent with this being a quantum mechanical tunneling reaction, assisted by an inferred promoting vibration (Masgrau *et al.* 2006, Johannissen *et al.* 2007). We have also explored the reaction with alternative substrates (parasubstituted phenylethylamines), mainly because the reaction kinetics are more readily accessed by the stopped-flow method over a temperature range. In these cases, KIEs are smaller (~ 20 – 30 , depending on reaction conditions) and show varying degrees of temperature dependence consistent with the coupling of promoting motions to the reaction coordinate (Hothi *et al.* 2008). The p - T dependence was recently studied with the substrate phenylethylamine, and this highlighted a complex response attributed to a pressure-mediated anisotropic (de)compression of the enzyme (Hay *et al.* 2012). With AADH, increasing pressure was found to decrease the rate of proton transfer, but this is not attributed to significant changes in donor–acceptor distance across the pressure

range. Constant-pressure molecular dynamics simulations have indicated that the average radius of gyration $\langle R_{\text{gyr}} \rangle$ for the AADH–phenylethylamine complex is, as expected, reduced at higher pressures. However, the effect of pressure on the structure of AADH is anisotropic – principal component analysis on the absolute change in atomic coordinates as a function of pressure revealed that the change in the average $\langle R_{\text{gyr}} \rangle$ can be deconvoluted along three vectors, with the majority of the change in $\langle R_{\text{gyr}} \rangle$ occurring in one dimension. Importantly, this vector is not aligned with the reaction coordinate and thus significant alteration (compression or decompression) of the reaction coordinate is not observed in AADH on changing pressure. Our work with AADH has indicated that more complete understanding of pressure effects on KIEs in enzymes is also dependent on gaining atomistic understanding derived from molecular dynamics calculations of known structures, and ultimately through, for example, the use of a computation to generate an ensemble of reactive geometries followed by identification of a rigorous reaction coordinate. Importantly, our work established that a pressure-dependent KIE is not necessarily a definitive hallmark of quantum tunneling. With AADH we observed pressure-independent KIEs even though proton transfer is known to occur, from the temperature dependence of the KIE, by quantum mechanical tunneling. Thus, although semiclassical KIEs are expected to be pressure independent, KIEs for tunneling reactions are variably pressure dependent and in general terms a pressure-independent KIE cannot be used to rule out a tunneling contribution.

3.6. Model chemistry (ascorbate and ferricyanide)

Recently, we analysed the p - T dependence of the KIE on proton-coupled electron transfer (PCET) during ascorbate oxidation by ferricyanide, and demonstrated that this reaction was consistent with vibrationally assisted tunneling of the transferred proton (Kandathil *et al.* 2014). This model chemical system (Figure 3.2) is a potential reference reaction for biochemical transformations catalysed by ascorbate peroxidases and cytochrome b_{561} proteins. Solvent isotope effects have been reported on the first kinetic step (oxidation of ascorbic acid by ferricyanide; k_1) consistent with a PCET reaction. Temperature dependence studies have indicated that: (a) the reaction occurs by quantum mechanical tunneling (Bell 1980); (b) the KIE is temperature dependent, consistent with the promoting motions hypothesis (Karkovic *et al.* 2011, Brala *et al.* 2012); and (c) the temperature dependence is strongly influenced by the solvent

composition (Brala *et al.* 2012). In extending this work, we determined the p - T dependencies of ferricyanide reduction by ascorbate to experimentally evaluate the rate constant for PCET using rapid mixing stopped-flow spectroscopy in H₂O and D₂O-buffered solutions (Kandathil *et al.* 2014). The temperature dependence of the KIE for PCET was found to depend strongly on the presence or absence of tetraethylammonium chloride (TEA) in the reaction buffer, being more pronounced in the presence of TEA. In the absence of TEA, the KIE was marginally temperature dependent; the KIE was, however, found to be significantly pressure dependent, consistent with transfer by quantum tunneling.

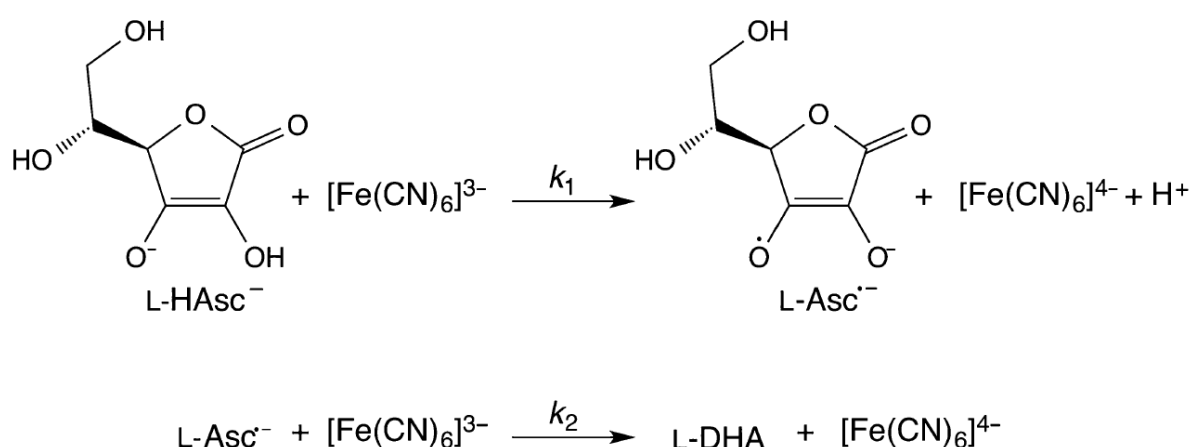


Figure 3.2. Ascorbate (L-Asc-) oxidation by ferricyanide ($[\text{Fe}(\text{CN})_6]^{3-}$) in aqueous solution occurs in two sequential one-electron transfer reactions to produce dehydroascorbic acid (L-DHA).

Of interest was the finding that, in the presence of TEA, the magnitude of the KIE was increased (beyond the maximum expected for semiclassical descriptions of H-transfer), but its pressure dependence was negligible (although maintaining a strong temperature dependence). Like the p - T dependence of the KIE on the AADH reaction (above), the data led us to conclude that, despite previous reports (Isaacs *et al.* 1977, Northrop *et al.* 1999), the absence of a pressure dependence of a KIE on H-transfer is not evidence for a lack of tunneling during the reaction. Instead, we interpreted the combined p - T dependence of the ascorbate KIE such that that: (a) the PCET involves quantum mechanical tunneling of the transferred proton, because the KIE > 7 in the presence of TEA; and (b) the presence of TEA influences vibrational coupling of H-transfer to the environment (i.e. the apparent promoting motion), reflected in changes to the temperature and pressure dependencies of the KIEs. Because the kinetic

properties of the model chemistry are readily modulated by changes in solvent composition, this reaction is suited to exploring in detail the potential role of promoting motions in quantum tunneling in ways not readily achievable with enzyme systems. In many enzyme systems, changes to the temperature and pressure dependence will often require modifications in the immediate protein environment using site-directed mutagenesis, which does not allow one to alter the tunneling characteristics in a relatively straightforward and predictable way. Studies with model systems might, therefore, add significantly to the body of data in the literature and provide tractable systems with which to rigorously test the promoting motions hypotheses often discussed in the enzyme tunneling literature.

3.7. Light-activated POR

In contrast to the thermally activated systems described above, the light-driven chlorophyll biosynthetic enzyme POR provides a unique opportunity to trigger catalysis by using a single pulse of light (Heyes & Hunter 2005, Scrutton *et al.* 2012). POR catalyses the reduction of the C17–C18 double bond of the protochlorophyllide (Pchl_{id}) substrate and has become an important model system for studying the mechanisms of H-transfer reactions (Heyes & Hunter 2005, Scrutton *et al.* 2012). Following illumination, a hydride anion is transferred from the *pro*-S face of NADPH to the C17 position of Pchl_{id} (Heyes *et al.* 2006) and a conserved Tyr residue is proposed to donate a proton to the C18 position (Menon *et al.* 2009). Our previous laser photoexcitation studies have revealed that these two enzymatic H-transfer reactions occur in a sequential mechanism on the microsecond timescale (Heyes *et al.* 2009). By combining studies of the temperature and isotopic dependence, it was shown that both H-transfer reactions proceed by quantum mechanical tunneling and are coupled to promoting motions or vibrations in the enzyme–substrate complex (Heyes *et al.* 2009). Moreover, a breakpoint at -27 °C in the temperature dependence of the hydride transfer rate suggests that motions/vibrations that are important for promoting light-activated hydride tunneling are quenched below -27 °C. We observed no such breakpoint for the proton tunneling reaction, indicating a reliance on different promoting modes for this reaction in the enzyme–substrate complex (Heyes *et al.* 2009). We have now investigated the pressure dependence of both H-transfer steps in POR to examine whether there are any inherent differences in the pressure

dependencies of the proton and hydride transfer reactions. Because catalysis is triggered by photoexcitation of the dark-assembled ternary complex of POR with NADPH and Pchlide, the pressure dependence of the POR–NADPH–Pchlide ternary complex formation was examined first (Figure 3.3). It was found that the K_d for Pchlide increased significantly with increasing pressure (Figure 3.3), likely because of the increased solvation of the active site at higher pressures. Stable ternary complexes were formed at all pressures studied (1 bar to 2 kbar) by using an excess of NADPH/D and POR over Pchlide and by varying the concentration of POR as a function of pressure (Table 3.1).

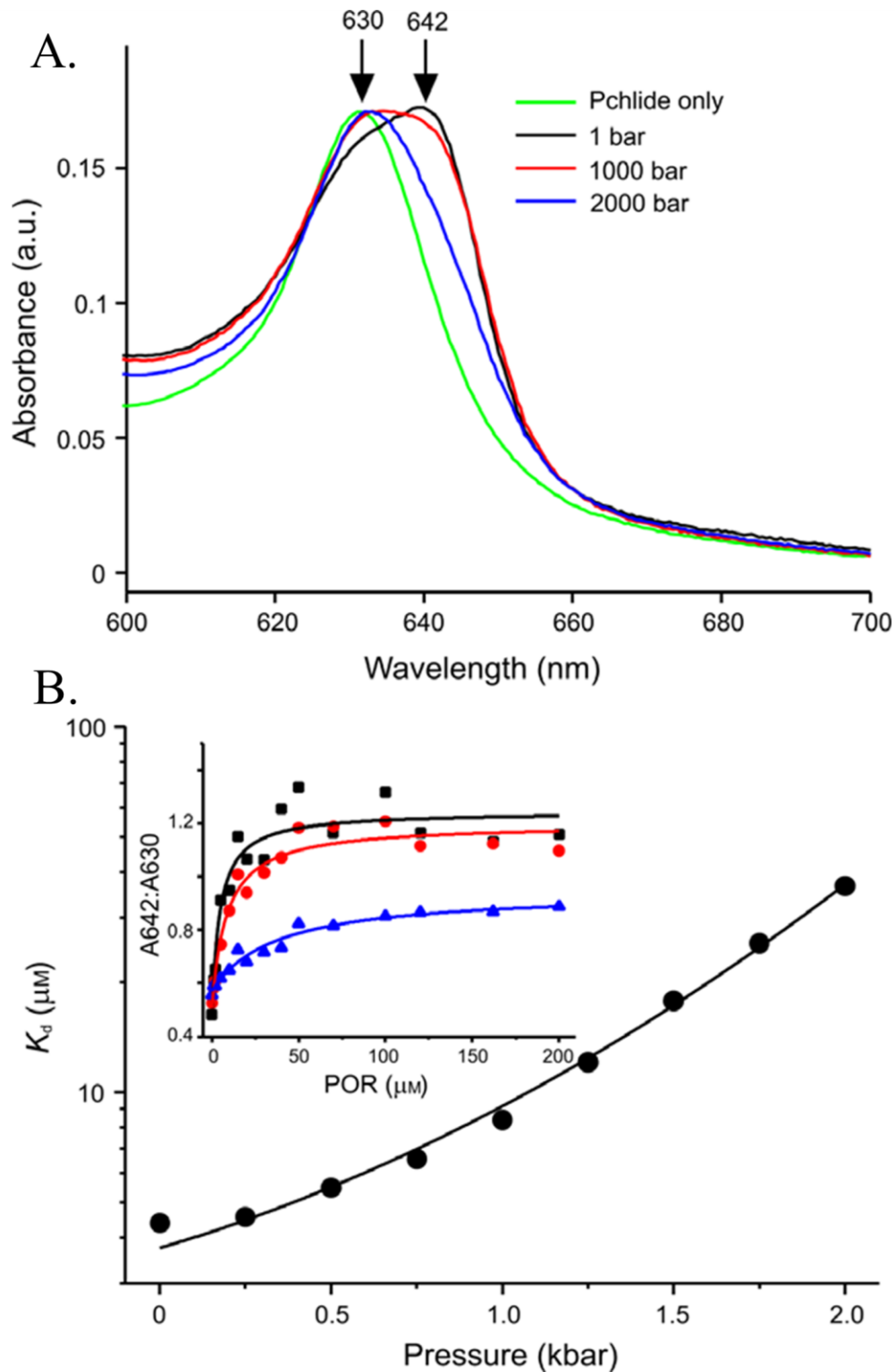


Figure 3.3. Pressure dependence of the ternary enzyme-substrate formation for POR. (A) Absorption spectra of the ternary complex formed from 7 μM Pchl_a, 200 μM NADPH and 100 μM POR measured at 1 bar, 1 kbar and 2 kbar. Spectra were taken at room temperature and are compared with that of Pchl_a measured at 1 bar. The arrows show the peak maxima for Pchl_a and the redshift due to formation of the ternary complex. (B) The pressure dependence of the K_d for Pchl_a. The data were fitted to Eqn (3.5) in the Materials and methods. (Inset) The level of ternary complex formation as a function of POR concentration at 1 bar (black), 1 kbar (red) and 2 kbar (blue). The data were fitted to a hyperbolic function to determine apparent K_d values.

The rate of hydride transfer was measured at a range of pressures between 1 bar and 2 kbar by following the increase in absorbance at 696 nm over 5 μ s in the presence of NADPH and *pro*-S NADP²H upon photoexcitation with a laser pulse at 450 nm (selective transients are shown in Figure 3.4). There is a slight decrease in the hydride transfer rate at higher pressures in the presence of NADPH, whereas the rate for deuteride transfer increases at higher pressure (Figure 3.5 and Table 3.1). The rate of the subsequent proton transfer reaction was measured at a range of pressures between 1 bar and 2 kbar by following the decrease in absorbance at 696 nm over 500 μ s in both protiated and deuterated buffers. There is a more marked decrease in the proton transfer rate at higher pressures compared with hydride transfer, whereas there is a minimal pressure effect on the rate of deuterion transfer (Figure 3.5 and Table 3.1). The data for both the hydride and proton transfer reactions were fitted to Eqn (3.2) to yield pressure-dependent changes in the activation volume and activation isothermal compressibility (Table 3.2). The pressure dependence of the KIEs on the hydride and proton transfers catalysed by POR (Figure 3.5 and Table 3.3) reveal that the isotope effect for both H-transfer reactions decreases significantly at higher pressures. Hence, although there are no clear trends in the pressure dependencies of k_{obs} , the pressure dependence of both KIEs are essentially superimposable, suggesting that there are unlikely to be large differences between the generic pressure response of hydride and proton transfers. If the pressure dependencies of the sequential KIEs on the POR-catalysed reaction are dominated by distance compression rather than changes in vibrational coupling, the KIE data could be interpreted such that the reaction coordinate for both the hydride and proton transfers lay along a similar direction. Further analysis will likely require atomistic structural information (X-ray crystal or NMR structure).

Table 3.1. Tabulated rate constants for the POR-catalysed hydride and proton transfer data shown in Figure 3.1.

Pressure (bar)	[POR] ^a (μ M)	k_{obs} hydride (s^{-1})		k_{obs} proton (s^{-1})	
		H	D	H	D
1	50	2.26 ± 0.21 $\times 10^6$	1.01 ± 0.12 $\times 10^6$	2.39 ± 0.18 $\times 10^4$	1.10 ± 0.05 $\times 10^4$
250	52	2.11 ± 0.18 $\times 10^6$	1.03 ± 0.13 $\times 10^6$	2.31 ± 0.23 $\times 10^4$	0.96 ± 0.08 $\times 10^4$
500	60	2.12 ± 0.17 $\times 10^6$	0.99 ± 0.17 $\times 10^6$	2.11 ± 0.21 $\times 10^4$	0.93 ± 0.07 $\times 10^4$
750	70	2.05 ± 0.12 $\times 10^6$	0.99 ± 0.12 $\times 10^6$	2.10 ± 0.10 $\times 10^4$	0.91 ± 0.14 $\times 10^4$
1000	85	2.01 ± 0.20 $\times 10^6$	1.02 ± 0.06 $\times 10^6$	2.02 ± 0.08 $\times 10^4$	0.90 ± 0.11 $\times 10^4$
1250	110	1.8 ± 0.12 $\times 10^6$	1.11 ± 0.21 $\times 10^6$	1.89 ± 0.09 $\times 10^4$	0.86 ± 0.11 $\times 10^4$
1500	156	1.99 ± 0.25 $\times 10^6$	1.14 ± 0.17 $\times 10^6$	1.71 ± 0.12 $\times 10^4$	0.81 ± 0.09 $\times 10^4$
1750	200	1.85 ± 0.20 $\times 10^6$	1.29 ± 0.26 $\times 10^6$	1.55 ± 0.17 $\times 10^4$	0.83 ± 0.10 $\times 10^4$
2000	260	2.02 ± 0.15 $\times 10^6$	1.56 ± 0.31 $\times 10^6$	1.36 ± 0.26 $\times 10^4$	0.99 ± 0.12 $\times 10^4$

^aThe enzyme concentration used to maintain a saturated ternary complex (see Figure 3.3).

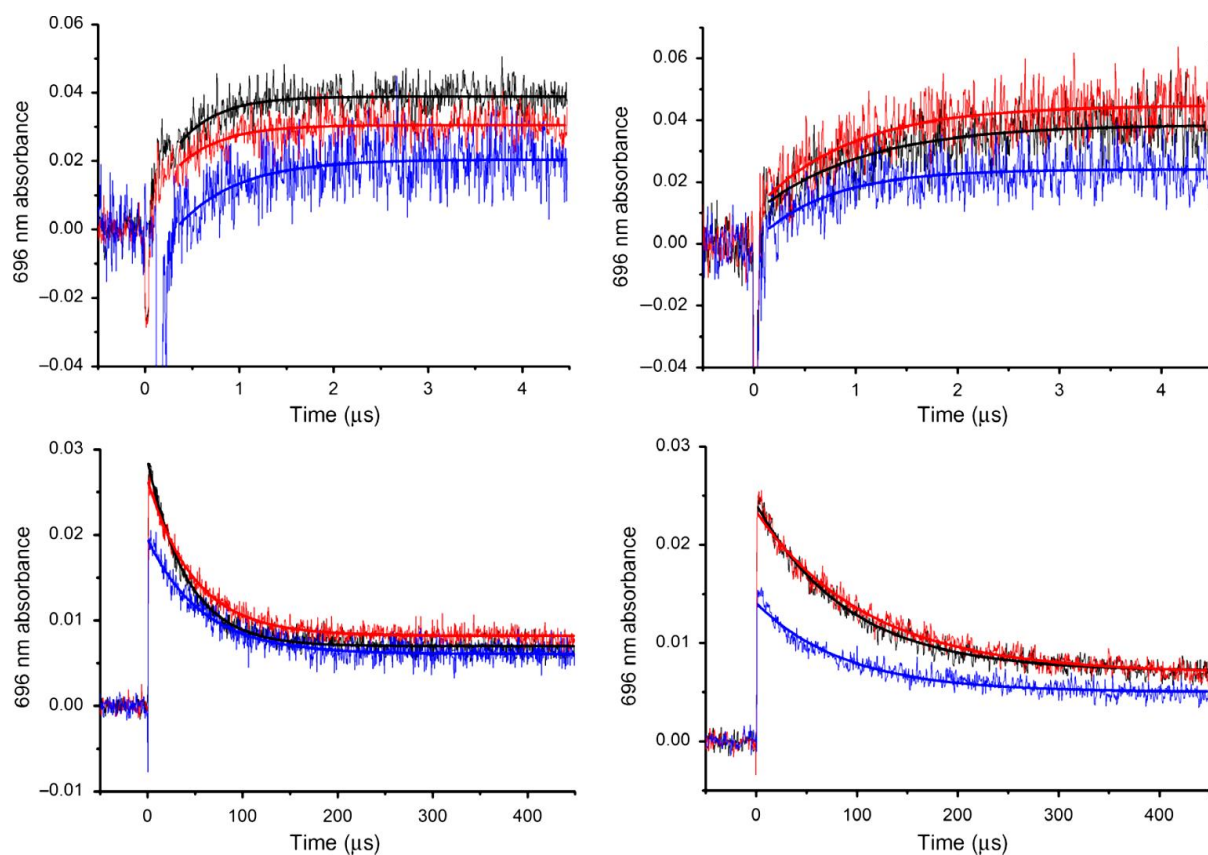


Figure 3.4. Representative POR photolysis transients measuring hydride transfer (upper, left), deuteride transfer (upper, right), proton transfer (lower, left) and deuteron transfer (lower, right) at 1 bar (black), 1 kbar (red) and 2 kbar (blue). Transients are fitted to a single exponential function (solid line), with averaged rate constants given in Table 3.1. Conditions: 50–260 μM POR (Table 3.1), 10 μM Pchlide, 500 μM NADPH, 0.1% 2-mercaptoethanol, 0.1% Triton X-100, 50 mM Tris, 150 mM NaCl, pH 7.5, 298 K. Deuteride transfer was measured using (*S*) - [4- ^2H]-NADPH and deuteron transfer was measured in D_2O buffer, pD 7.5.

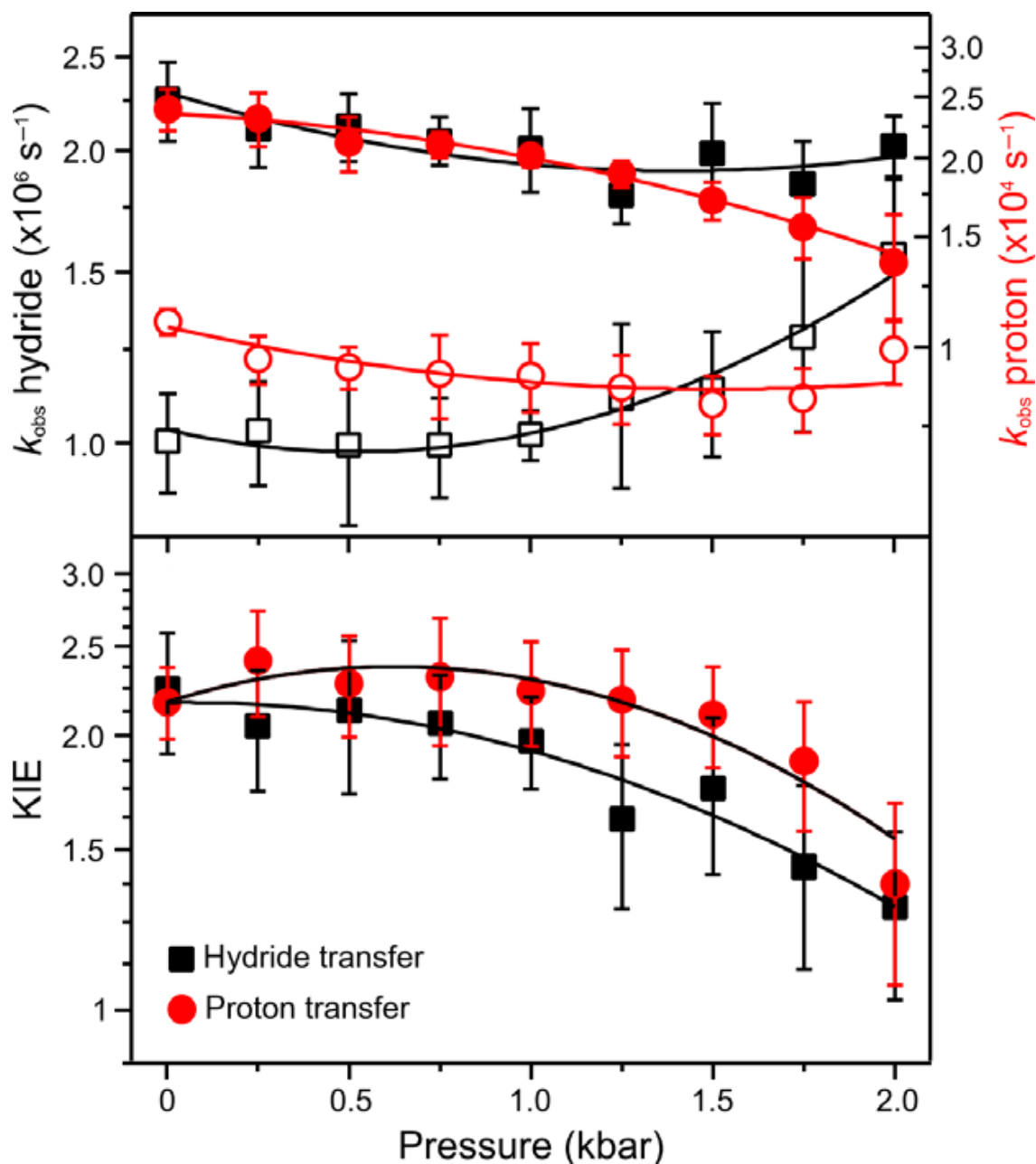


Figure 3.5. (A) Pressure dependencies of the observed rate constants for the sequential hydride and proton transfers catalysed by POR at 25 °C. The rate of hydride transfer from NADPH (black) and proton transfer in H_2O (red) are indicated by filled symbols and the rate of deuteride transfer from *pro-S* NADP^2H (black) and deuteron transfer in D_2O are indicated by open symbols. (B) The pressure dependence of the resulting KIEs. The data have been fitted to Eqn (3.2), with fitting parameters given in Table 3.2 and the KIEs on these parameters given in Table 3.3. The rate constants are listed in Table 3.1.

3.8. Correlating the pressure and temperature of KIEs

As described above, the p – T dependence of a KIE can be largely described by the five parameters: $\Delta\Delta H^\ddagger$, $\Delta\Delta S^\ddagger$, KIE_0 , $\Delta\Delta V^\ddagger$ and $\Delta\Delta\beta^\ddagger$. These parameters are listed in Table 3.3 for the MR, PETNR, AADH, ascorbate and POR experiments described above. We are not aware of other enzyme/biological systems in which both the temperature and pressure dependence of the KIE have been measured, but Table 3.3 should not be taken to be exhaustive. Because the focus of this work is to determine whether pressure offers an alternative probe of the temperature dependence of KIEs, we examined the correlation of $\Delta\Delta S^\ddagger$, KIE_0 , $\Delta\Delta V^\ddagger$ and $\Delta\Delta\beta^\ddagger$ with $\Delta\Delta H^\ddagger$ (Figure 3.6). $\Delta\Delta S^\ddagger$ shows a strong linear correlation with $\Delta\Delta H^\ddagger$, a trend we have previously demonstrated in the context of Arrhenius parameters; $\Delta\Delta S^\ddagger \sim R\ln(-A^H/A^D)$, and we showed that $\ln(A^H/A^D)$ is a linear function of ΔE_a for the KIE on the RHRs of a range of isotopically substituted PETNR enzymes (Pudney *et al.* 2013). There is some correlation between $\Delta\Delta V^\ddagger$ and $\Delta\Delta H^\ddagger$, with more temperature-dependent KIEs exhibiting more negative $\Delta\Delta V^\ddagger$ values (Figure 3.6). However, there is no correlation between $\Delta\Delta\beta^\ddagger$ or KIE_0 and $\Delta\Delta H^\ddagger$. In the context of Eqn (3.4), $\Delta\Delta V^\ddagger$ and $\Delta\Delta\beta^\ddagger$ report on the change with pressure in the vibrational coupling (j) and distance sampling (r), respectively, of the transferred H isotope (Hay & Scrutton 2008). Although this is a simplification, temperature-dependent KIEs have been used as evidence of the vibrational coupling of protein dynamics to the reaction coordinate (Kohen *et al.* 1999, Maglia & Allemann 2003, Hay *et al.* 2007, Heyes *et al.* 2009), so the correlation of $\Delta\Delta V^\ddagger$ with $\Delta\Delta H^\ddagger$ is not unexpected.

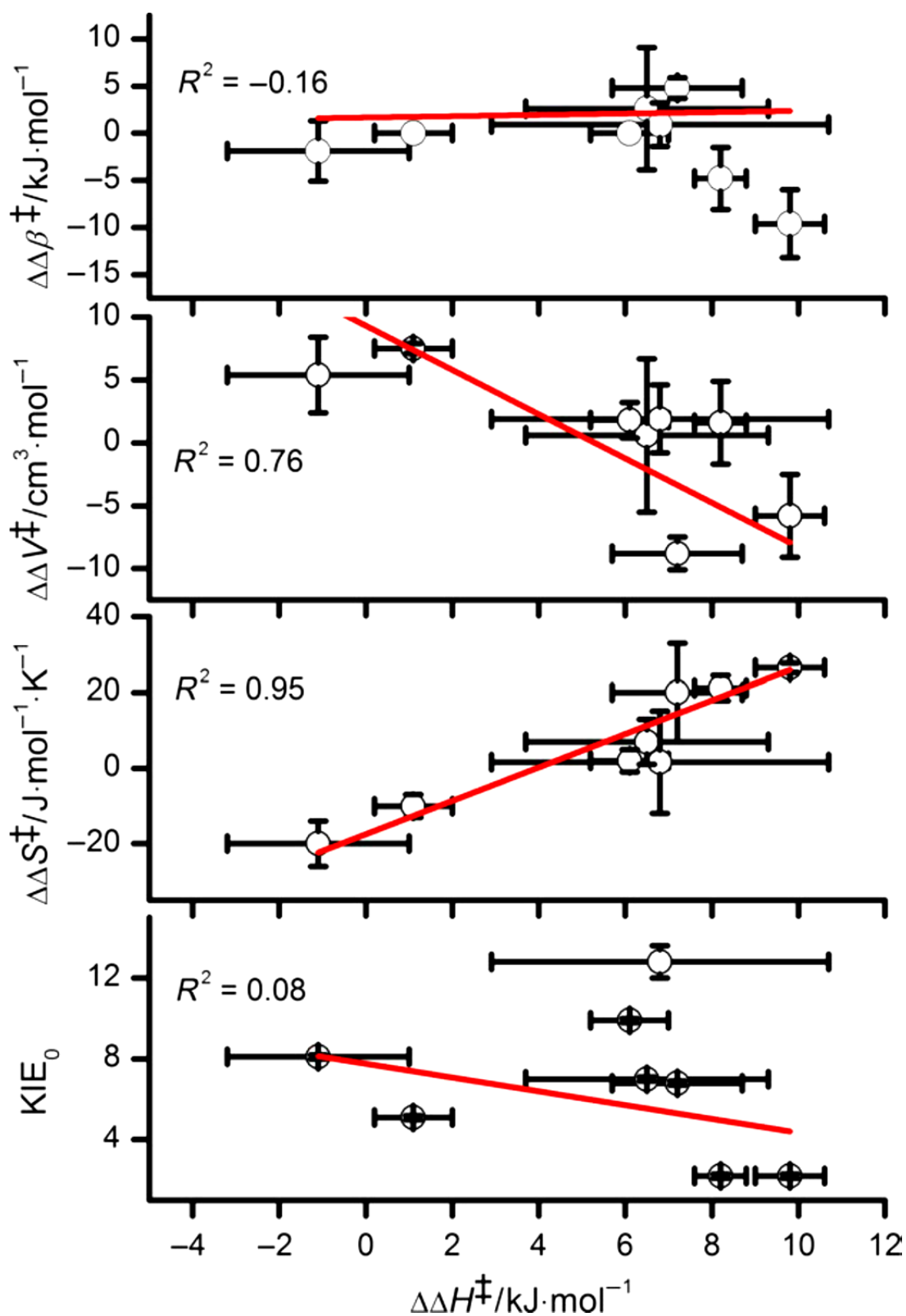


Figure 3.6. Linear correlations of $\Delta\Delta H^\ddagger$ with $\Delta\Delta\beta^\ddagger$, $\Delta\Delta V^\ddagger$, $\Delta\Delta S^\ddagger$ and KIE_0 for the data in Table 3.3. Adjusted R^2 values were determined for the error-weighted linear fits as shown.

3.9. Trends/outlooks/unifying concepts

To date, fast dynamics in enzymes have largely been inferred from the anomalous temperature dependencies of KIEs on H-transfer reactions (Kohen *et al.* 1999, Maglia & Allemann 2003, Hay *et al.* 2007, Heyes *et al.* 2009). However, the atomistic origin of the, sometimes large, temperature dependencies of KIEs remains unresolved, and alternative probes of fast enzyme dynamics are desirable. Hydrostatic pressure offers a fairly convenient and unique method to perturb existing equilibria in chemical systems including enzymes, and we have demonstrated that a range of KIEs on enzyme-catalysed and biochemical reactions are pressure dependent (Table 3.3). However, there is no clear trend between the pressure and temperature dependencies of the KIEs we have examined (Figure 3.6), suggesting that the atomistic origin of these two perturbations are not equivalent. Coupled with this atomistic understanding of pressure responses, studies of the p - T dependence of reaction rates and KIEs provide rich new datasets from which to infer the importance (or otherwise) of dynamics coupled to the reaction coordinate. These datasets should be considered on a case-by-case basis, where they can support/enrich the more generalized conclusions that have emerged from temperature dependence studies of KIEs in relation to enzymatic H-transfer.

Table 3.2. Pressure dependencies of the rate of hydride and proton transfer catalysed by POR.

	Hydride		Proton	
	H	D	H	D
$k_0(\text{s}^{-1})$	(2.30 ± 0.09) $\times 10^6$	(1.03 ± 0.02) $\times 10^6$	(2.35 ± 0.04) $\times 10^4$	(1.08 ± 0.03) $\times 10^4$
$\Delta V^\ddagger(\text{cm}^3 \cdot \text{mol}^{-1})$	6.6 ± 2.2	5.0 ± 1.2	1.7 ± 1.0	7.5 ± 2.3
$\Delta \beta^\ddagger(\text{cm}^3 \cdot \text{mol}^{-1} \cdot \text{kbar}^{-1})$	4.7 ± 2.0	9.5 ± 1.3	-4.7 ± 1.1	4.9 ± 2.5

Table 3.3. Pressure and temperature dependencies of selected 1° KIEs on biological H-transfers. Data were taken from parameters obtained by fitting Eqns (3.1) and (3.2) to experiments performed at 293–298 K. Systems are: MR RHR with NADH (Hay *et al.* 2007, Hay & Scrutton 2008); PETNR RHR with NADH and NADPH (Pudney *et al.* 2009); AADH with phenylethylamine (Hay *et al.* 2012), POR (Heyes *et al.* 2009) and this work; ascorbate oxidation by ferricyanide ± tetraethylammonium chloride (Kandathil *et al.* 2014).

System	KIE ₀	$\Delta\Delta H^\ddagger$ kJ mol ⁻¹	$\Delta\Delta S^\ddagger$ J mol ⁻¹ K ⁻¹	$\Delta\Delta V^\ddagger$ cm ³ mol ⁻¹	$\Delta\Delta\beta^\ddagger$ cm ³ mol ⁻¹ kbar ⁻¹
MR	6.8 ± 0.1	7.2 ± 1.5	20 ± 13	-8.8 ± 1.3	4.8 ± 1.1
PETNR, NADPH	7.0 ± 0.1	6.5 ± 2.8	7 ± 6	0.6 ± 6.1	2.6 ± 6.5
PETNR, NADH	8.1 ± 0.1	-1.1 ± 2.1	-20 ± 6	5.4 ± 3.0	-1.9 ± 3.2
AADH	12.8 ± 0.8	6.8 ± 3.9	1.6 ± 13.5	1.9 ± 2.7	0.9 ± 2.3
POR, hydride	2.2 ± 0.1	8.2 ± 0.6	21.2 ± 3.3	1.6 ± 3.3	-4.8 ± 3.3
POR, proton	2.2 ± 0.1	9.8 ± 0.8	26.5 ± 1.2	-5.8 ± 3.3	-9.6 ± 3.6
Asc, FeCyn	5.1 ± 0.1	1.1 ± 0.9	-10 ± 3	7.5 ± 0.4	0 ^c
Asc, FeCyn, TEA	9.9 ± 0.1	6.1 ± 0.9	2 ± 3	1.8 ± 1.4	0 ^c

^aData fitted with $\Delta\beta$ fixed to 0.

3.10. Materials and methods

Both recombinant POR from *Thermosynechococcus elongates* and Pchl_{ide} were prepared as described previously (Heyes & Hunter 2004). (*S*) - [4-²H] -NADPH was prepared and characterized as previously (Pudney *et al.* 2006). All high-pressure experiments were performed using a high-pressure cell system (ISS Inc., Champaign, IL, USA) with the sample contained in cylindrical cuvette bottles with a 1 cm path length. Absorbance spectra were measured using a Cary 50 spectrometer (Agilent Technologies, Santa Clara, California, USA) with the pressure cell mounted using a custom-made platform. Upon binding to the enzyme, the peak maxima of Pchl_{ide} becomes red-shifted from 630 to 642 nm (Figure 3.1 A.). The K_d for Pchl_{ide} was determined by measuring the ratio of the absorbance peaks at 642 and 630 nm at increasing concentrations of POR and fitted to a hyperbolic function ($\frac{A_{642}}{A_{630}} = \frac{A_{max}*[POR]}{K_d + [POR]}$). Measurements were repeated at a range of pressures from 1 to 2000 bar in 250 bar increments. Samples contained 10 μM Pchl_{ide}, 200 μM NADPH and 0–200 μM POR in 50 mM Tris pH 7.5, 150 mM NaCl, 0.1% 2-mercaptoethanol, 0.1% Triton X-100. The pressure dependence of the K_d for Pchl_{ide} (Figure 3.3) was determined by fitting to Eqn (3.5):

$$K_d(p) = K_{d,0} \exp(-\Delta Vp/RT) \exp(\Delta\beta p^2/2RT) \quad (3.5)$$

where $K_{d,0}$ is the Pchl a K_d at 0 bar ($3.7 \pm 0.4 \mu\text{M}$), ΔV is the activation volume ($-15.9 \pm 3.6 \text{ cm}^3 \cdot \text{mol}^{-1}$) and $\Delta\beta$ is the compressibility ($12.5 \pm 2.5 \text{ cm}^3 \cdot \text{mol}^{-1} \cdot \text{kbar}^{-1}$).

Laser photolysis experiments were performed essentially as described in Heyes *et al.* (2009). Briefly, rate constants for the POR-catalysed hydride and proton transfer were measured using laser photoexcitation of the dark assembled ternary complex (POR–NADPH–Pchl a) at 25 °C. Samples were made up to a total volume of 1300 μL , comprising 50–260 μM POR (increasing concentration at higher pressures), 320 μM NADPH and 15 μM Pchl a in 50 mM Tris pH 7.5, 150 mM NaCl, 0.1% (v/v) 2-mercaptoethanol, 0.1% Triton X-100. Samples were excited at 450 nm using an optical parametric oscillator of a Q-switched Nd:YAG laser (Brilliant B, Quantel) that produces between 6 and 8 ns laser pulses (30 mJ). The detection system is an LKS-60 flash photolysis instrument (Applied Photophysics Ltd., Leatherhead, UK) and is at a right angle to the incident laser beam. Transients were collected at 696 nm and were fitted using a single exponential function to obtain rate constants for the hydride and proton transfer reactions (Figure 3.4). Typically, each data point is an average of two or three separate samples, with two or three shots measured per sample.

Chapter 4

Expression, purification and kinetic characterisation of POR homologues from different evolutionary origins.

Authors:

Robin Hoeven, Derren J. Heyes and Nigel S. Scrutton

Affiliation:

Manchester Institute of Biotechnology, Faculty of Life Sciences, The University of Manchester, Manchester M1 7DN, United Kingdom

Published in:

Manuscript in preparation

4.1. Abstract

Chlorophyll plays an essential role in photosynthetic organisms, and hence, it is important to understand how it is synthesised. One of the key enzymes in the chlorophyll biosynthesis pathway is protochlorophyllide oxidoreductase (POR), which is uniquely dependent on light for catalysis. More specifically, POR is responsible for the reduction of a double bond at the C17-C18 position of the protochlorophyllide (Pchl_{id}) substrate, resulting in the formation of the chlorophyllide (Chl_{id}) product. Upon excitation of the Pchl_{id} substrate the reaction proceeds via a hydride transfer from NADPH to the C17 position followed by a proton transfer from a conserved Tyr residue in the active site to the C18 position. However, it is unclear how such a unique light-activated process has evolved. Therefore, we have overexpressed and purified a number of POR homologues from a wide range of species, spanning the entire evolutionary timescale. The purified enzymes have been characterised in terms of their kinetic and substrate binding properties to obtain estimates for K_m , K_d , K_i , V_{max} and k_{cat} values. In addition, thermodynamic parameters for the two H-transfer steps were acquired for three of the homologues. Consequently, this work provides the important foundations for future studies to elucidate the evolutionary origins of this unique light activated catalytic process.

4.2. Introduction

Only two enzymes are known to require light for catalysis, DNA photolyase and protochlorophyllide oxidoreductase (POR; EC 1.3.1.33) (Lebedev & Timko 1998). This requirement for light makes POR an important regulatory enzyme in the biosynthetic pathway of chlorophyll and the subsequent development of the photosynthetic apparatus (Aubert *et al.* 2000). The reaction catalysed by POR involves the reduction of the C17-C18 double bond of Pchlde to form Chlide, which is a highly endergonic process that requires light energy to proceed. The excited Pchlde molecule is proposed to form an intramolecular charge transfer (ICT) state due to the interaction of a conserved Tyr residue with the propionate group, facilitating the transfer of a hydride from NADPH (*pro-S* face) to the C17 position of Pchlde (Heyes *et al.* 2015). This is immediately followed by a slower proton transfer from a conserved Tyr residue to the negatively charged C18 position of Pchlde, resulting in the formation of the chlorophyllide (Chlide) product (see Figure 4.1; Wilks & Timko 1995, Menon *et al.* 2009, Heyes *et al.* 2009).

In addition to POR, non-angiosperm plants, algae and cyanobacteria contain a light-independent Pchlde reductase, also referred to as dark POR (DPOR), which allows these organisms to produce Chlide in the dark. The DPOR enzyme consists of three separate subunits and uses ATP instead of light to drive the reaction (Fujita & Bauer 2000). As these organisms can produce chlorophyll in the dark the availability of both enzymes maximises the amount of chlorophyll that can be produced (Fujita *et al.* 1992, Suzuki & Bauer 1992, Lidholm & Gustafsson 1991). The existence of DPOR is thought to be why the POR-NADPH-Pchlde ternary complex does not accumulate in dark grown cyanobacteria, with only very low concentrations of POR found in thylakoid and plasma membranes (Rowe & Griffiths 1995, Fujita *et al.* 1998, Heyes *et al.* 2000).

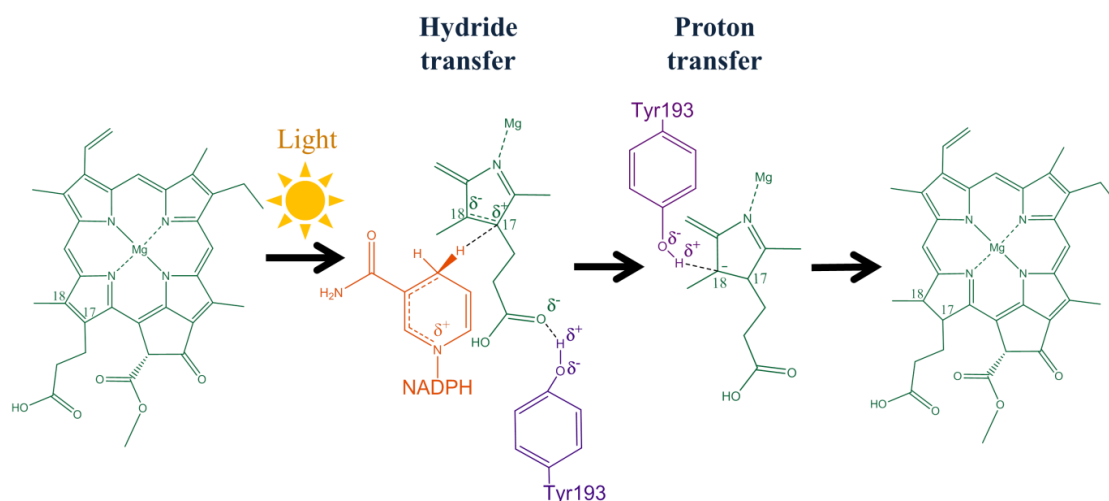


Figure 4.1. Proposed reaction mechanism of POR. Interaction with a conserved Tyr residue (numbering according to *Thermosynechococcus elongatus*) in the active site leads to the formation of a transient intramolecular charge-transfer state of the excited Pchlide molecule, priming the molecule for hydride transfer from NADPH. The ensuing negative charge at the C18 position facilitates proton transfer from a conserved Tyr residue in a subsequent, slower reaction step, forming the Chlide product.

From an evolutionary point of view POR is an attractive model system to understand how catalysis has evolved. The enzyme was introduced into plant cells during the primary symbiosis of an ancestral cyanobacterium and mirrors the transformation from anoxygenic to oxygenic photosynthesis (Burke *et al.* 1993, Fujita 1996, Armstrong 1998). Amongst prokaryotic phototrophs, which also contain the DPOR enzyme, POR is only found in cyanobacteria, suggesting that light-dependent chlorophyll biosynthesis was established prior to eukaryotic photosynthesis (Suzuki & Bauer 1995, Armstrong 1998). Hence, a phylogenetic analysis of POR shows a broad separation into two groups, the ‘ancient’ PORs from a prokaryotic origin, including cyanobacteria and prochlorophytes and the ‘evolved’ PORs from eukaryotes, including algae, liverwort, moss and higher plants (Figure 4.2; Fujita 1996, Heyes *et al.* 2009). Previous studies have shown that the dynamic processes that govern the two H-transfer steps in Pchlide reduction have been differentially optimised during evolution (Heyes *et al.* 2011). In the case of the hydride transfer step, the chemistry is stringently linked to active site structure, and a highly optimised geometry was achieved early in evolution. However, the proton transfer reaction is more variable, and therefore allows for a ‘slower’ optimisation of the protein dynamics to take place.

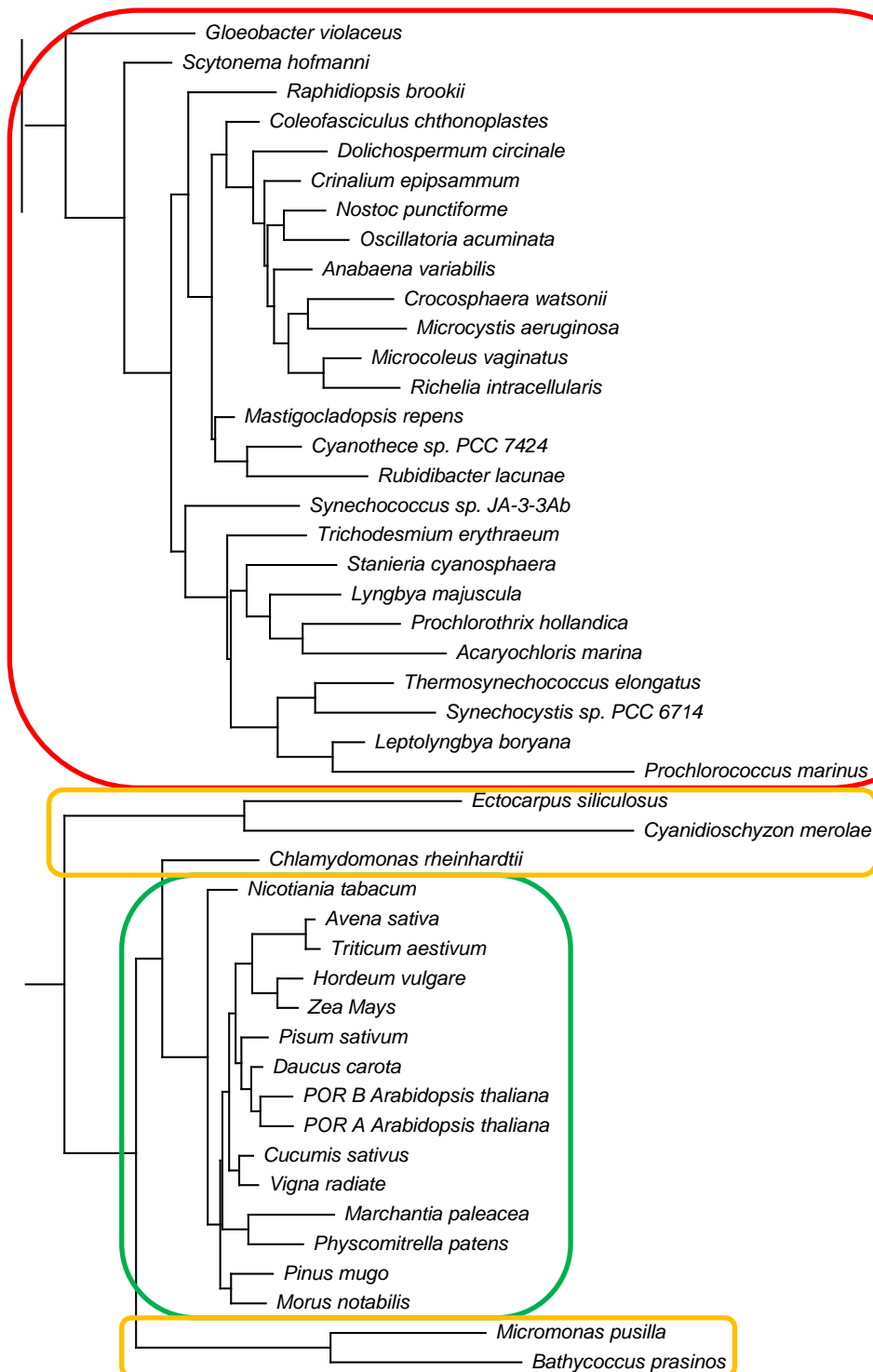


Figure 4.2. Phylogenetic tree of the POR genes. The different groups are marked with boxes, the red box is ‘ancient’ PORs of cyanobacterial and prochlorophyte origin, while the ‘evolved’ PORs include algae (orange) and land plant species (embryophyta; dark green).

In order to provide a more comprehensive study of the evolutionary aspects of POR catalysis a comparative study of a range of different PORs that span the evolutionary timescales has now been carried out. These include ‘ancient’ PORs from cyanobacteria and prochlorophytes (*Nostoc punctiforme*, *Lyngbya majuscula*) and

‘evolved’ PORs from red (*Cyanidioschyzon merolae*) and green algae (*Chlamydomonas reinhardtii*), liverwort (*Marchantia paleacea*), moss (*Physcomitrella patens*), gymnosperm (*Pinus mugo*) and angiosperms (*Daucus carota*, *Nicotiana tabacum*, *Zea mays*). In the current work the expression, purification and kinetic characterisation of these POR homologues are presented and discussed.

4.3. Materials and methods

4.3.1. Construction of expression vector

The POR genes from *Chlamydomonas reinhardtii*, *Cyanidioschyzon merolae*, *Daucus carota*, *Lyngbya majuscula*, *Marchantia paleacea*, *Nicotiana tabacum*, *Nostoc punctiforme*, *Pinus mugo*, *Physcomitrella patens*, and *Zea mays* were synthesised by GenScript (GenScript Inc.) and digested with *Nde*I and *Bam*HI HF restriction enzymes (New England Biolabs Ltd.). The genes were cloned into an *Nde*I and *Bam*HI digested pET9-His vector (derivative of pET9a from Novagen; Heyes *et al.* 2000) and confirmed by sequencing of the plasmid (Eurofins Scientific).

4.3.2. Protein overexpression and purification

The construct were transformed into chemically competent *Escherichia coli* BL21 (DE3) pLysS cells (Agilent Technologies) using the heat-shock method. Transformed cells (pET9-His-POR) were grown in (typically 12) 2 L flasks containing 0.5 L of lysogeny broth (LB) medium and 30 µg/ml of kanamycin and chloramphenicol at 30°C. Upon reaching an optical density (OD) of 0.1 at 600 nm, the growth temperature was lowered to 25°C. Gene expression was induced with 0.1 mM IPTG once an OD of 0.6 was reached, indicative of log phase growth, and the cells were left to grow overnight at 20°C. Finally, harvesting of the cells occurred by centrifugation at 6000 rpm for 10 min in a JLA 8.1000 rotor (Beckman Coulter, Inc.).

The resulting cell pellets of the POR homologues were resuspended in cold binding buffer (500 mM NaCl, 5 mM imidazole, 0.1% Triton X-100, 50 mM MOPS, 100 mM ammonium acetate pH 7) and disrupted by 25 cycles of 20 s pulses of sonication (Bandelin, sonopuls probe VT70T/N494) at 40 % intensity. A centrifugation step at 20 k rpm for 30 min in a JA25:50 rotor (Beckman Coulter Inc.) followed to remove cell debris. Purification of the N-terminally tagged POR proteins was performed by binding to a 5 ml HisTrap FF column (GE Healthcare Life Sciences) pre-equilibrated

with 10 column volumes (cv) of binding buffer using an Äkta protein purification system (GE Healthcare Life Sciences). The column was washed with buffer containing 50 mM and 100 mM imidazole, and the final elution consisted of a gradient from 100 mM to 500 mM imidazole. A second purification step with a blue sepharose 6 fast flow column (GE Healthcare Life Sciences) was performed to remove remaining contaminants. Samples were loaded onto 20 ml column pre-equilibration with blue start buffer (500 mM NaCl, 50 mM MOPS, 100 mM ammonium acetate pH 7), followed by a wash step with 10 cv of blue start buffer. Protein was eluted by a NaCl gradient, from 500 mM to 2.5 M using the BioLogic LP low pressure chromatography system (Bio-Rad laboratories Inc.). The fractions were visualised by SDS-PAGE (12 %; Bio-Rad laboratories Inc.) and the fractions containing the purified POR protein were pooled and concentrated using a Vivaspın 20 (10 kDa MWCO; Sartorius AG). This was followed by buffer exchange into activity buffer (500 mM NaCl, 50 mM MOPS, 100 mM ammonium acetate pH 7) using a CentriPure P100 column (Generon Ltd.) to remove salt. Finally, the protein samples were concentrated to a typical volume of around 4 ml with a Vivaspın 20 (10 kDa MWCO; Sartorius AG), aliquoted in smaller volumes and flash frozen in liquid nitrogen, to be stored at -80°C. Protein concentrations were determined using the Bio-Rad DC assay kit with bovine serum albumin as a standard. A western blot with anti-His-tag antibody was performed on an SDS-PAGE gel. Transfer of the protein to the membrane was carried out by the Trans-Blot[®] Turbo[™] System (Bio-Rad laboratories Inc.), followed by treatment of the membrane with blocking solution and antibodies as described previously (Lindner *et al.* 1997). Visualisation was carried out after treatment of the membrane with luminol and involves the exposure of X-Omat[™] Blue (XB) Film (Eastman Kodak) in a dark room to the membrane.

4.3.3. Substrates and other chemicals

Pchlide was prepared as shown previously (Heyes *et al.* 2003).

All chemicals were obtained from Sigma-Aldrich, except for NADPH (Melford Laboratories Ltd.).

4.3.4. Laser flash photolysis

Laser flash photolysis experiments were performed as outlined previously (Heyes *et al.* 2009). The samples were excited in the Soret band of Pchl_a with a 450 nm pulse from an optical parametric oscillator of a Q-switched Nd:YAG laser (Brilliant B, Quanta). Each data point is the average of at least four measurements. The cuvette used has a 2 mm path length in the pump direction and 1 cm in the probe direction. Samples were 750 µl in volume, containing 50 µM enzyme, 250 µM of NADPH (except *C. reinhardtii*, *C. merolae*, *L. majuscula*, *D. carota*, which had a 2 mM concentration), and 12 µM Pchl_a, in activity buffer (0.5 M NaCl, 50 mM MOPS, 100 mM ammonium acetate, 0.1% Genapol X-080, 0.1% 2-mercaptoethanol). Assembly in the dark prevents turnover and at least 5 min time was given for the ternary complex to form.

4.3.5. Steady-state measurements and binding titrations

UV/vis absorption data were acquired using a Varian Cary 50 UV-Vis spectrophotometer with samples in a 100 µl quartz cuvette (1 cm path length). Illumination of the samples was carried out with a 455 nm LED (Thorlabs, Inc) fitted with a converging lens and held in place to focus the light onto the sample from above. Chl_a formation was followed by measuring the absorbance change at 670 nm, and the initial slope was used to calculate the initial rate of turnover. The concentrations of the substrates and products were calculated using the following extinction coefficients in aqueous solution: NADPH, 6.22 mM⁻¹cm⁻¹ at 340 nm; NADP⁺, 17.8 mM⁻¹cm⁻¹ at 260 nm; Pchl_a, 23.95 mM⁻¹cm⁻¹ at 630 nm and Chl_a, 69.96 mM⁻¹cm⁻¹ at 670 nm. Fluorescence measurements were performed in a Cary Eclipse fluorescence spectrophotometer (Agilent technologies). To reduce dilution effects 3 ml of sample was used in a quartz cuvette with dimensions of 1 cm in length and width.

4.3.6. Phylogeny

The phylogenetic tree was generated using the phylogeny.fr website (Dereeper *et al.* 2008), with a full MUSCLE (Multiple sequence comparison by log-expectation) setting for alignment and one-hundred maximum likelihood bootstrap replicates.

4.4. Results

4.4.1. Vector design

The synthesised genes were successfully cloned into the pET9-His vector, which adds an N-terminal hexahistidine tag, consisting of an extra 20 amino acid residues, to the expressed proteins. The resulting constructs were confirmed to contain the correct insert by restriction digest with *NdeI* and *BamHI* HF restriction enzymes. Furthermore, the vectors were sequenced, which identified the insertion of the correct gene sequences for each homologue.

4.4.2. Expression and purification of His-tagged POR homologues

BL21(DE3) pLysS *E.coli* cells were transformed with each of the separate plasmid clones and grown as described in materials and methods, to overexpress the desired proteins. Presence of the hexahistidine tag allowed the protein to bind the Ni-column and because of POR's affinity for NADPH it can also bind to the blue sepharose column. The resulting SDS-PAGE images and their corresponding Western blots of the purification process are shown in Figures 4.3, 4.4, 4.6, 4.7. The original purification protocol contained a few steps that involved precipitating the protein with high concentrations of ammonium sulphate salt, followed by resuspension in a different buffer *e.g.* blue start buffer (500 mM NaCl, 50 mM MOPS, 100 mM ammonium acetate pH 7; Menon 2009). This procedure rendered all of the POR homologues discussed here unstable, and resuspension was difficult or not possible. Hence, the ammonium sulphate precipitation steps were omitted from the purification protocol. Furthermore, the use of an Äkta protein purification system and an imidazole gradient often resulted in clean enough protein fractions that did not require an additional blue sepharose column purification step. Consequently, less of the POR protein was lost in the wash step and a faster purification protocol reduced the amount of precipitation, resulting in a higher yield.

The purification process for POR homologues from cyanobacteria is shown in figure 4.3. Both homologues (*L. majuscula* and *N. punctiforme*) have good expression levels, but not all of the protein is soluble, as shown by the POR band in the insoluble fraction in lane 4 (Figure 4.3). Both enzymes slowly degrade in solution during the purification process, especially *L. majuscula* POR, which starts to precipitate when concentrating. When this occurred, concentrating was stopped and the formed precipitant was

centrifuged with a benchtop centrifuge (13 000 rpm, 1 min) before the samples were aliquoted and flash frozen in liquid nitrogen to be stored in a -80°C freezer. The average yields after purification and concentrating for *L. majuscula* and *N. punctiforme* are 5 and 20 mg per litre of medium, respectively (Table 4.1). The relatively large difference in yield is mostly due to the precipitation of *L. majuscula* POR.

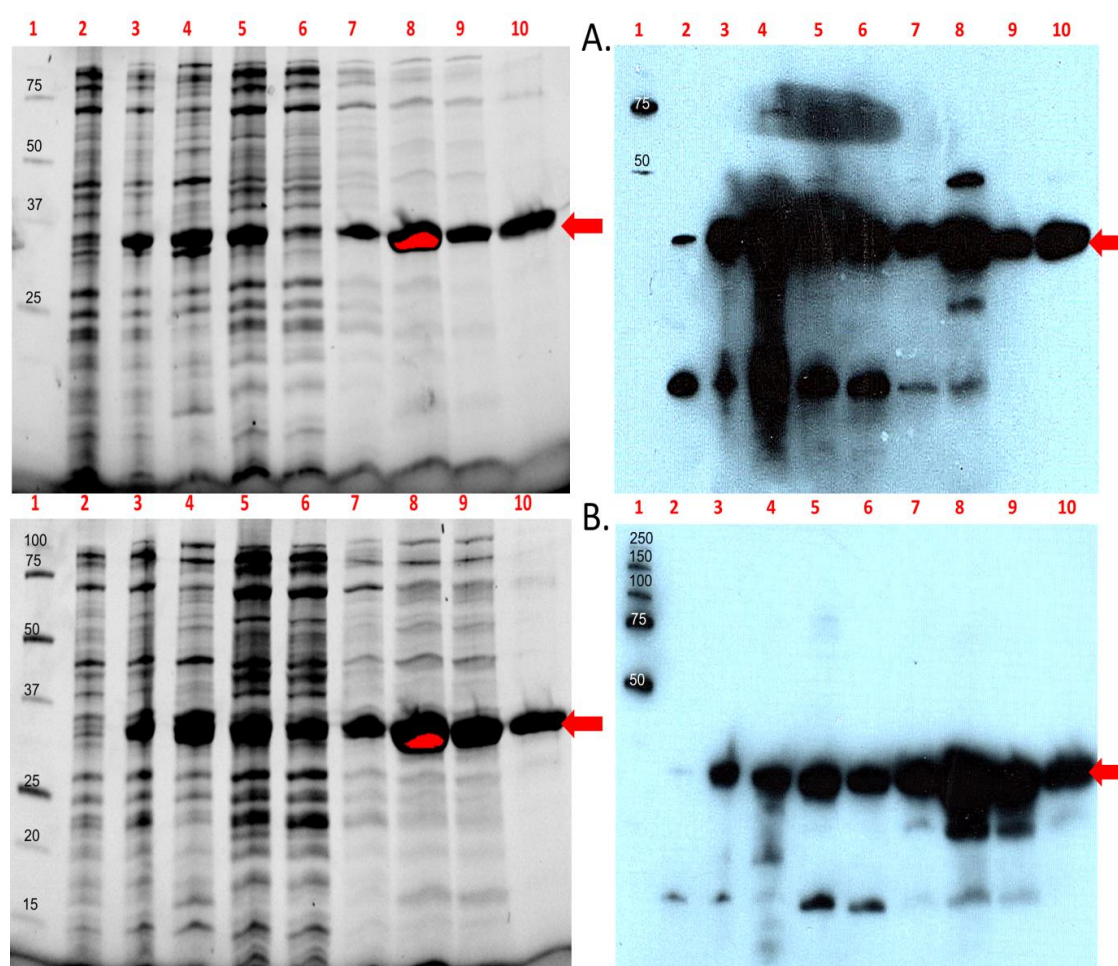


Figure 4.3. Expression and purification of PORs from cyanobacteria. The gels on the left are SDS-PAGE gels, with the corresponding Western-blot on the right hand side, using an anti-His tag antibody. The desired protein is indicated with a red arrow. 1. Precision plus ladder unstained (BioRad) 2. Uninduced cell extract 3. Induced cell extract 4. Insoluble fraction 5. Sonicated cell extract 6. Ni column run-through 7. Ni column wash (20% elution buffer) 8. Ni column elute 9. Blue sepharose run-through 10. Blue sepharose elution. A. SDS-PAGE gel and Western blot for POR from *L. majuscula*. B. SDS-PAGE gel and Western blot for *N. punctiforme*.

The purification process for POR from algae (*C. reinhardtii*, *C. merolae*) is shown in figure 4.4. Expression levels of both enzymes are sufficient, but again not all of the protein is soluble and some loss occurs in the insoluble fraction (lane 4 Figure 4.4). After purification *C. reinhardtii* POR has a good level of yield with an average around 18 mg per litre of medium (Table 4.1), while *C. merolae* POR has a poor average yield of less than 1 mg per litre of medium. The instability of the *C. merolae* protein may be attributed to a misfolding of the enzyme and hence, an expression trial was performed to improve the yield of the protein (Figure 4.5). By using 10 μ M IPTG for induction, rather than 100 μ M, more *C. merolae* POR was expressed, which increased the average yield after purification to about 3 mg per litre medium (Table 4.1). Unfortunately, there were still issues with precipitation during the final concentrating stage. In which case, aggregated protein was removed by centrifugation (13 000 rpm, 1 min) and then the supernatant was flash frozen in liquid nitrogen, prior to storing the protein at -80°C.

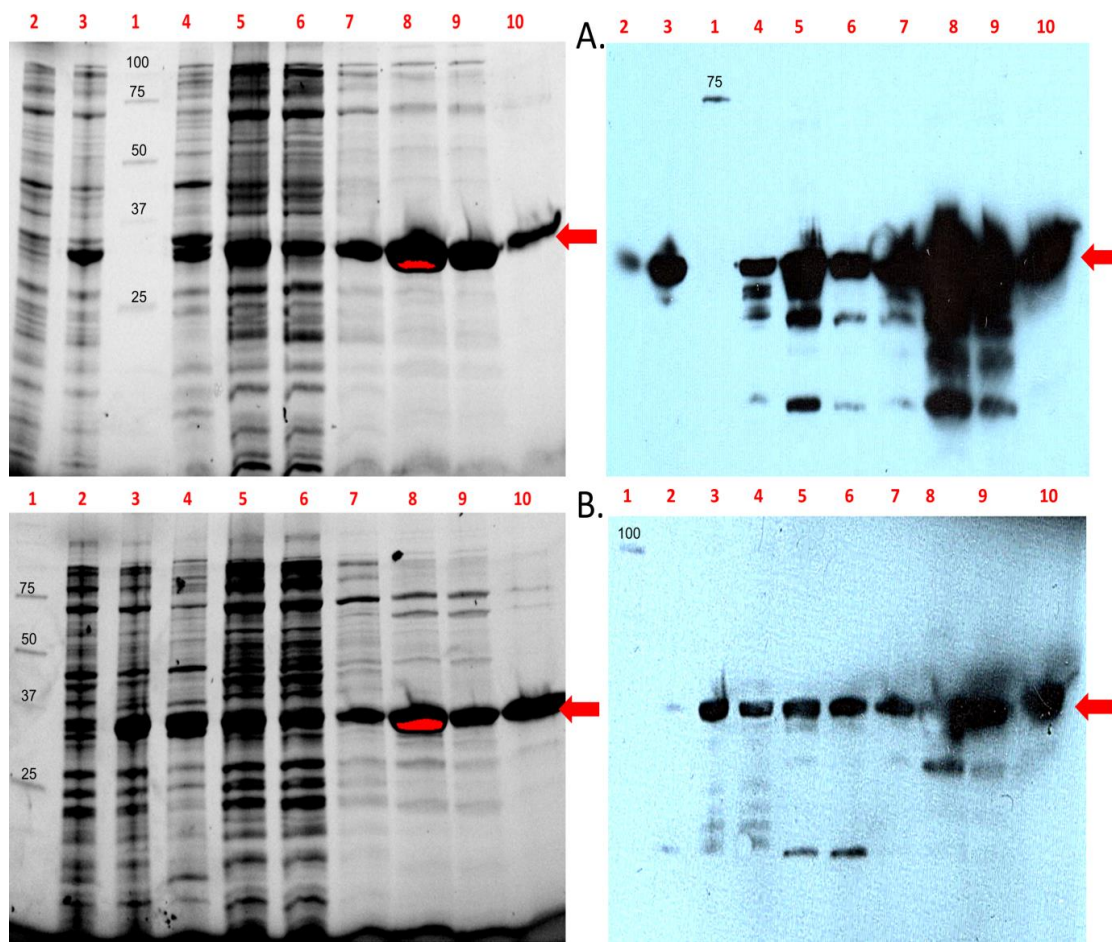


Figure 4.4. Expression and purification of PORs from algae. The gels on the left are SDS-PAGE gels, with the corresponding Western-blot on the right hand side, using an anti-His tag antibody. The desired protein is indicated with a red arrow. 1. Precision plus ladder unstained (BioRad) 2. Uninduced cell extract 3. Induced cell extract 4. Insoluble fraction 5. Sonicated cell extract 6. Ni column run-through 7. Ni column wash (20% elution buffer) 8. Ni column elute 9. Blue sepharose run-through 10. Blue sepharose elution. A. SDS-PAGE gel and Western blot for POR from *C. reinhardtii*. B. SDS-PAGE gel and Western blot for *C. merolae*.

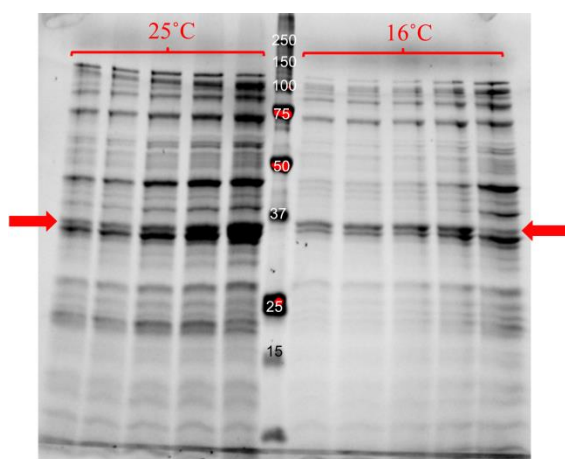


Figure 4.5. Soluble fractions of *C. merolae* from an expression trial using different IPTG concentrations. In the first 5 lanes cells were grown overnight at 25°C and in the 5 lanes on the right side of the Precision plus ladder unstained (Biorad) cells were grown at 16°C overnight. IPTG concentrations were varied for each temperature as follows: (from left to right) 1 mM, 0.5 mM, 0.1 mM, 50 µM, 10 µM. The highest levels of soluble protein were achieved with 10 µM IPTG and with cells grown overnight at 25°C. Red arrows indicate POR protein band a little below the 37 kDa marker. The cells were broken open using a detergent-based BugBuster (Novagen) method to obtain the soluble fraction.

In figure 4.7 the purification process for POR from non-angiosperm land plants, including liverwort (*M. paleacea*), a bryophyte (moss; *P. patens*), and a gymnosperm (*P. mugo*), is shown. All enzymes express well, but a large fraction of the *M. paleacea* and *P. mugo* protein is insoluble (lane 4 Figure 4.7) leading to a particularly low yield after purification of 1 mg per litre of medium in the case of *M. paleacea* (Table 4.1). POR from *P. patens* has a higher average yield after purification of around 8 mg per litre of medium and despite significant loss in the insoluble fraction of *P. mugo* POR it has an average yield after purification of 19 mg per litre of medium (Table 4.1). The relatively low average yield of *M. paleacea* and *P. patens* POR is due to precipitation at the final concentrating stage at which point the precipitant was centrifuged (13 000 rpm, 1 min) and the supernatant flash frozen in liquid nitrogen. *P. patens* POR is more amenable to concentrating and was not found to readily precipitate, leading to a higher yield despite a significant fraction of the protein being insoluble. To improve the *M. paleacea* POR yield a variety of growth conditions were tested to try to increase the amount of soluble protein and/or reduce the precipitation of clean protein fractions. Protein expression was induced with 0 and 0.1 mM IPTG concentrations in the presence and absence of 1 % (w/w) glucose. By adding glucose the promoter of the POR gene on the pET9-His plasmid is repressed until the glucose is consumed by the cells, which strongly suppresses leaky-expression and thereby is thought to reduce

cell-death during the growth phase (Monod *et al.* 1952, Cai *et al.* 2006). However, none of these conditions resulted in any significant improvement in the expression levels of soluble protein (Figure 4.6 A.). Secondly, autoinduction TB medium was used to grow the BL21 (DE3) pLysS cells to regulate the time of induction of POR expression. This resulted in a slight increase in the amount of soluble *M. paleacea* POR, but the overall yield remained low in comparison to other homologues (Figure 4.6 B.).

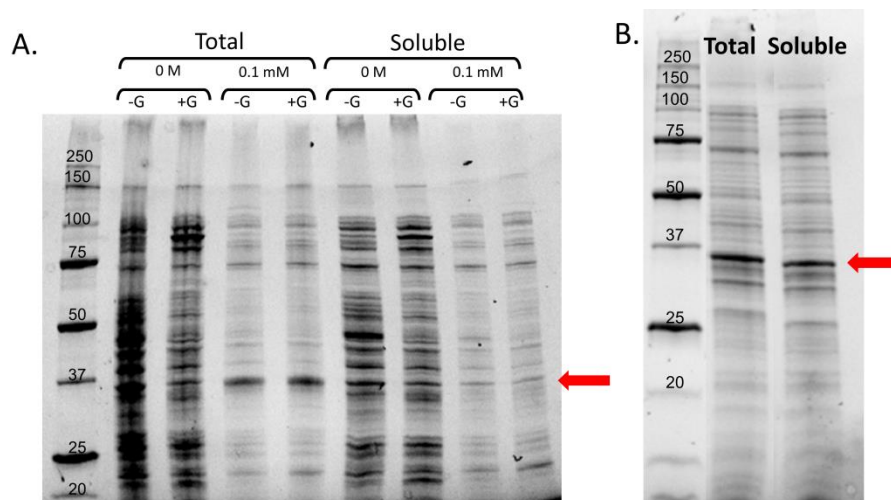


Figure 4.6. Total and soluble fractions of *M. paleacea* POR from an expression trial. A. In the first 4 lanes after the Precision plus ladder unstained (Biorad) the total cell extract is shown for 0 and 0.1 mM IPTG, with or without 1 % glucose. The 4 lanes starting from the right contain the soluble fractions for 0 and 0.1 mM IPTG, with or without 1 % glucose. The cells were grown overnight at 20°C after induction. B. Cells grown in autoinduction medium for 24 hours (after induction) at 20°C contain more soluble protein compared to comparable lanes in panel A. Red arrows indicate the POR protein band a little below the 37 kDa marker. Soluble protein was obtained by breaking open the cells using a detergent-based BugBuster (Novagen) method. A higher level of soluble protein is achieved for autoinduction medium grown for 24 hours after induction.

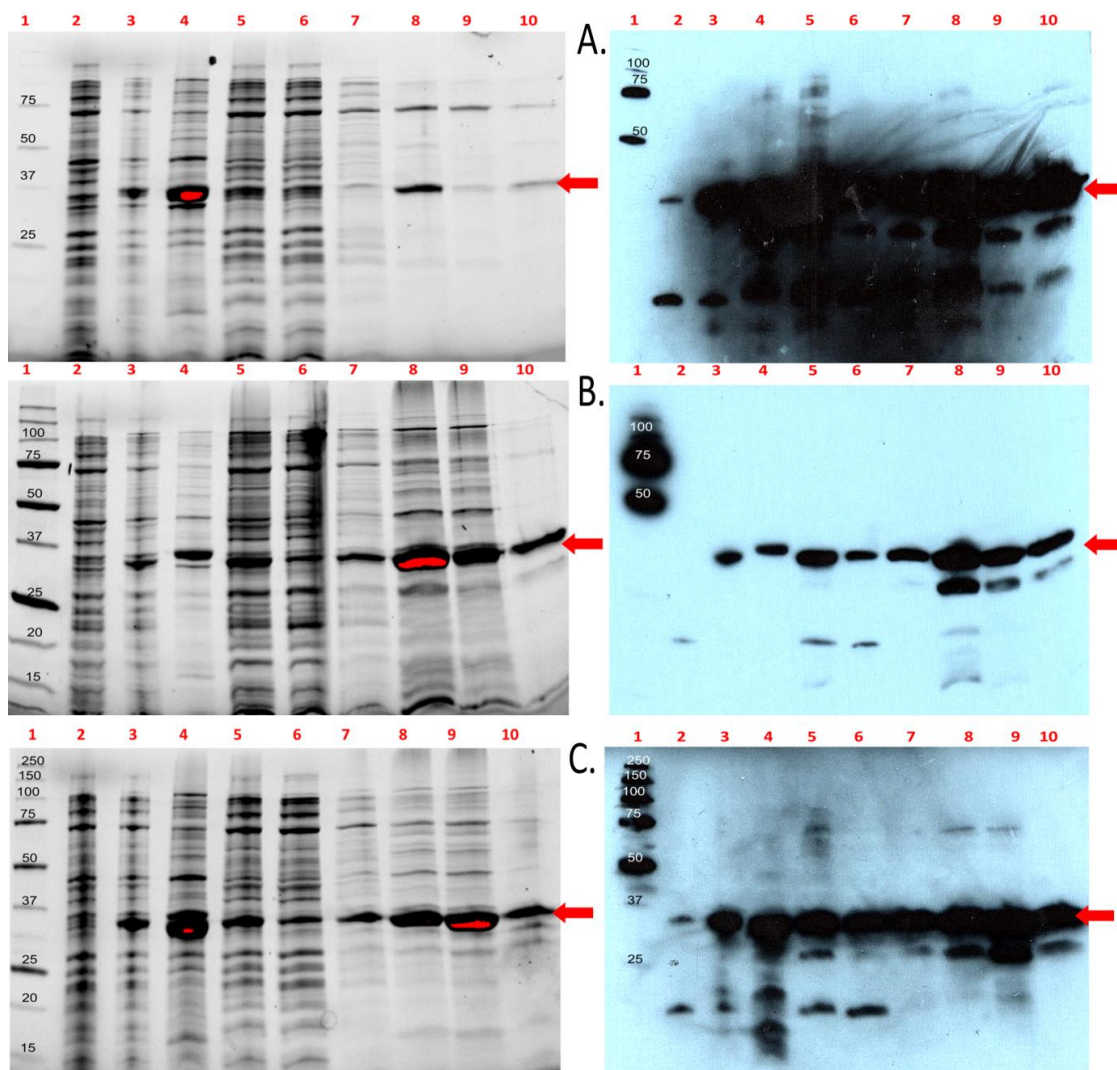


Figure 4.7. Expression and purification of PORs from non-angiosperm land plants. The gels on the left are SDS-PAGE gels, with the corresponding Western-blots on the right hand side using an anti-His tag antibody. The desired protein is indicated with a red arrow. 1. Precision plus ladder unstained (BioRad) 2. Uninduced cell extract 3. Induced cell extract 4. Insoluble fraction 5. Sonicated cell extract 6. Ni column run-through 7. Ni column wash (20% elution buffer) 8. Ni column elute 9. Blue sepharose run-through 10. Blue sepharose elution. A. SDS-PAGE gel and Western blot for POR from *M. paleacea*. B. SDS-PAGE gel and Western blot for *P. patens*. C. SDS-PAGE gel and Western blot for POR from *P. mugo*.

The purification process for PORs from angiosperms is shown in figure 4.8, which includes *D. carota*, *N. tabacum*, and *Z. mays*. All the enzymes have a good level of expression, but for *D. carota* and *N. tabacum* POR a significant amount of this protein is insoluble and is therefore lost (lane 4 Figure 4.8). The average yields of *D. carota*, *N. tabacum*, and *Z. mays* POR after purification are 14, 10 and 18 mg per litre of medium, respectively (Table 4.1). Lower yields for the enzymes from *D. carota* and *N. tabacum* are due to insolubility, as well as precipitation that occurs during the final concentrating step.

The Western-blot analysis detects His-tagged protein and reports on the desired His-tagged POR proteins that have been overexpressed. However, in the case of *N. tabacum* POR very clear additional bands can be observed with a lower molecular weight. Mass spectrometry analysis of these bands confirmed that they were POR from *N. tabacum* (see Figure 4.9). It can be concluded that during the purification process some of the protein degrades into smaller polypeptides (see Figure 4.9 B.). This, together with the observed precipitation, confirms the instability of the enzyme and demands for a short purification protocol to minimise the time for the protein to unfold.

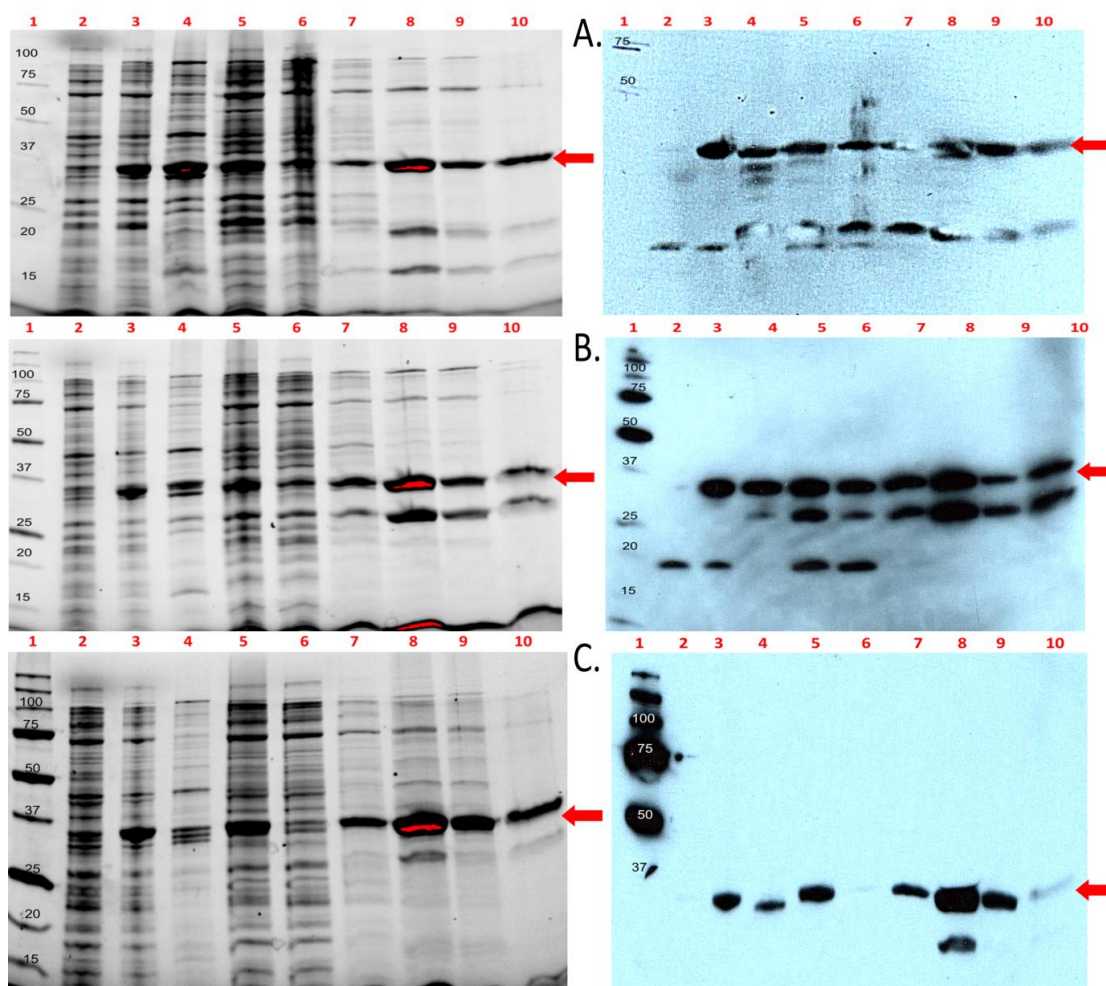


Figure 4.8. Expression and purification of PORs from angiosperms. The gels on the left are SDS-PAGE gels, with the corresponding Western-blot on the right hand side using an anti-His tag antibody. The desired protein is indicated with a red arrow. 1. Precision plus ladder unstained (BioRad) 2. Uninduced cell extract 3. Induced cell extract 4. Insoluble fraction 5. Sonicated cell extract 6. Ni column run-through 7. Ni column wash (20% elution buffer) 8. Ni column elute 9. Blue sepharose run-through 10. Blue sepharose elution. A. SDS-PAGE gel and Western blot for POR from *D.carota*. B. SDS-PAGE gel and Western blot for *N.tabacum*. C. SDS-PAGE gel and Western blot for POR from *Z. mays*.

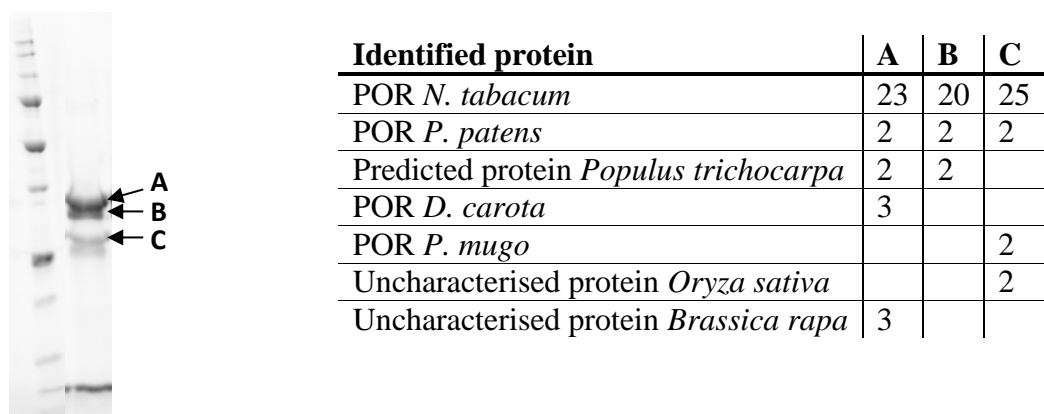


Figure 4.9. Mass spectrometry of indicated bands of *N. tabacum* purification. Bands A, B, and C are shown with an arrow on the SDS-PAGE gel. The numbers for each band in the table represent the number of unique peptides matched to the identified protein. For 2-3 unique peptides, this represents a probable identification, and for 4 or over indicates an almost certain characterisation. All three bands can therefore be identified as POR from *N. tabacum* and it is likely that bands B and C are degradation products.

Table 4.1. The average protein yield after purification for the POR homologues. A summary of the yield for POR from cyanobacteria (red), algae (gold), non-angiosperm land plants (green), and angiosperms (blue).

	Average yield (mg/litre of medium)
<i>L. majuscula</i>	5
<i>N. punctiforme</i>	20
<i>C. reinhardtii</i>	18
<i>C. merolae</i>	1
<i>M. paleacea</i>	3
<i>P. patens</i>	8
<i>P. mugo</i>	19
<i>D. carota</i>	14
<i>N. tabacum</i>	10
<i>Z. mays</i>	18

In summary, all of the POR homologues had a good expression level, but for most of the homologues a significant fraction of the protein was lost due to insolubility and degradation. Furthermore, there were problems with precipitation during the final concentrating step, after which the precipitant was removed by centrifugation and the resulting supernatant was aliquoted and flash frozen in liquid nitrogen to finally be stored at -80°C. A small improvement in the stability of these enzymes can be achieved by addition of 10 % glycerol to the activity buffer. Additionally, the formation of enzyme-substrate complex with NADPH (and Pchl_{ide}) seemed to

provide further stability and hence allowed assays to be carried out with less precipitation issues than during purification.

4.4.3. Kinetic parameters

All of the purified POR enzymes were tested for catalytic activity and were shown to convert Pchlide into Chlide under steady-state conditions upon exposure to light (Figure 4.10). The steady-state kinetic parameters for each POR enzyme were determined by measuring the initial rate of Chlide formation at 670 nm over a range of different substrate concentrations. All of the POR enzymes followed Michaelis-Menten kinetics upon varying the NADPH concentration (Figures 4.11, 4.12, 4.13, 4.14) and the initial rates were fitted to equation 4.1 to obtain V_{\max} and K_m values:

$$v = \frac{d[P]}{dt} = \frac{V_{\max}[S]}{K_m + [S]} \quad 4.1$$

where v is the initial rate of product formation, V_{\max} is the maximum rate at saturating substrate concentration, $[S]$ is the substrate concentration, while K_m is the concentration of substrate at which half the V_{\max} is reached (Michaelis & Menten 1913).

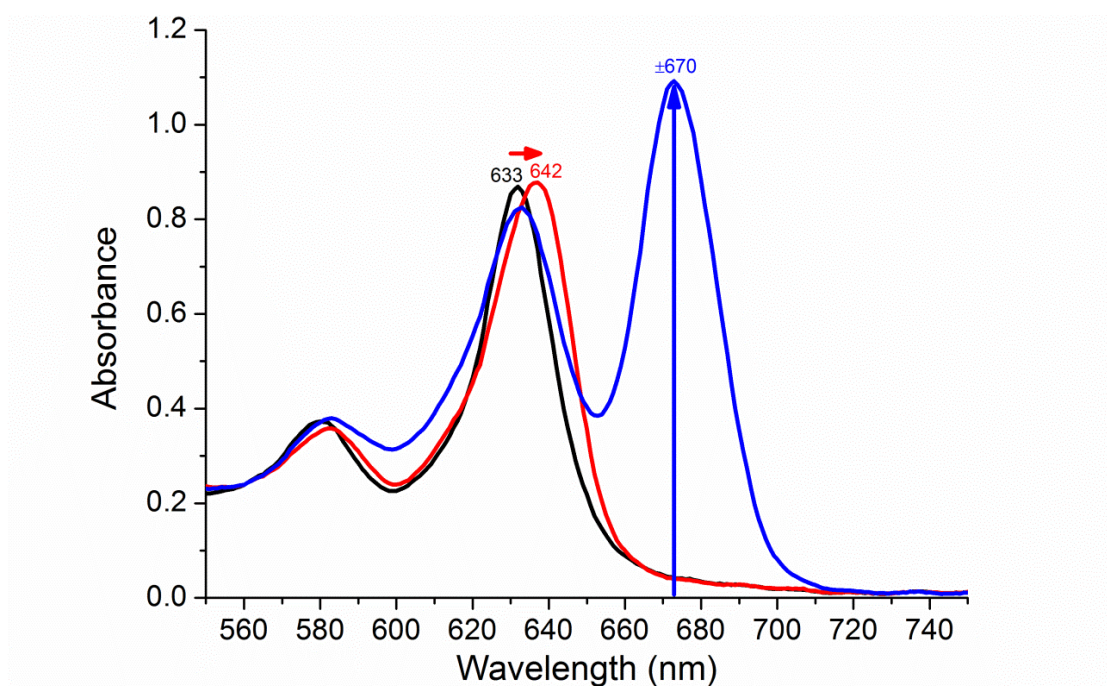


Figure 4.10. Spectral changes associated with POR catalysis. Upon binding of Pchlide to POR (red spectrum) a shift occurs in the Pchlide spectrum (black) of the 633 nm absorption maximum to a maximum around 642 nm (red arrow). Turnover of Pchlide into Chlide results in the formation of an absorbance maximum at approximately 670 nm (blue spectrum and blue arrow).

Figure 4.11 shows the dependence of the rate on NADPH concentration for PORs from cyanobacteria. The V_{\max} for *L. majuscula* POR is approximately three-fold higher and the K_m for NADPH is greater than ten-fold higher compared to the *N. punctiforme* enzyme (Table 4.2). For the algal enzymes (Figure 4.12) the K_m and V_{\max} values for *C. reinhardtii* POR (157 μM , 0.0043 $\mu\text{M/s}$) are very similar to *C. merolae* POR (172 μM , 0.0042 $\mu\text{M/s}$). However, the K_m values for NADPH for both algal PORs are significantly higher than for most of the other POR enzymes (Table 4.2). Similar V_{\max} values of approximately 0.002 $\mu\text{M s}^{-1}$ were obtained for all 3 PORs from non-angiosperm land plants (Figure 4.13). The K_m for NADPH within this group exhibits much greater variability, with low values observed for both *P. patens* (2.21 μM) and *P. mugo* (9.8 μM) PORs, whereas *M. paleacea* POR (138 μM) has a K_m that is more comparable to the algal enzymes. For the PORs from angiosperms (Figure 4.14) the kinetic parameters for the enzyme from *D. carota* POR are significantly different from the other two enzymes with higher V_{\max} and K_m values (Table 4.2).

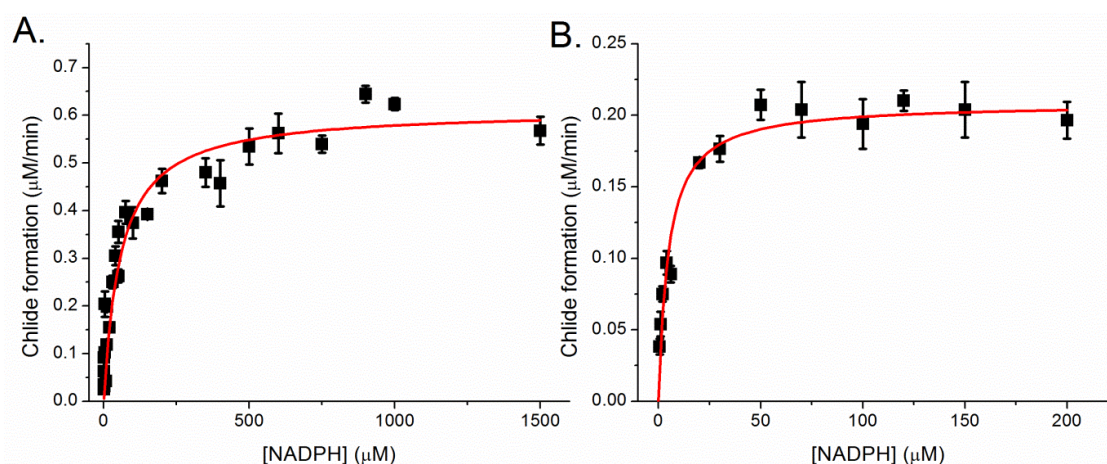


Figure 4.11. The dependence of the initial rate of Chlide formation on the concentration of NADPH for PORs from cyanobacteria. Samples contained 0.1 μM of each POR enzyme, 12 μM Pchlide, 0.1% Triton X-100, 0.1% 2-mercaptoethanol in activity buffer. Initial rates were measured by following the increase in absorbance at 670 nm upon illumination with a 455 nm LED at a fixed distance and a fixed power setting. The data were fitted to equation 4.1 to obtain V_{\max} and K_m for NADPH. Graph A is for POR from *L. majuscula* and graph B is for POR from *N. punctiforme*.

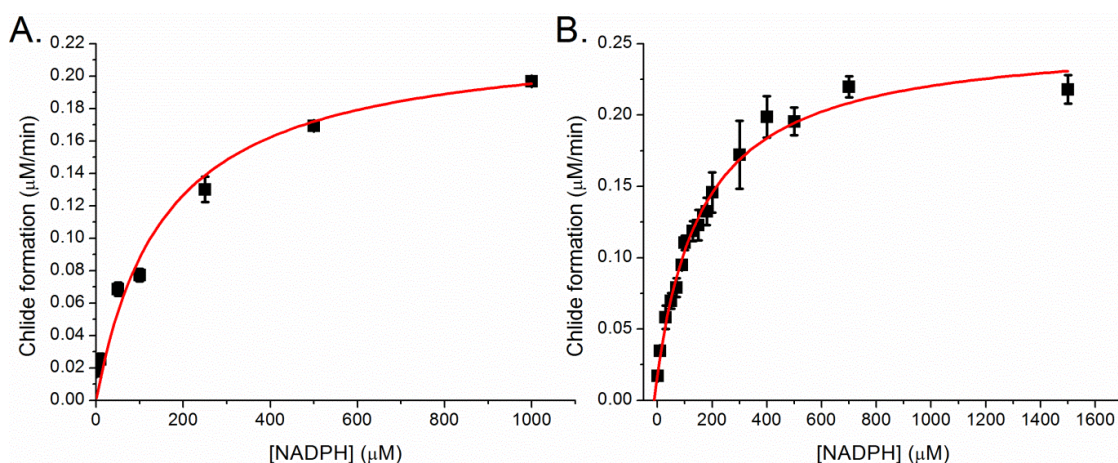


Figure 4.12. The dependence of the initial rate of Chlide formation on the concentration of NADPH for PORs from algae. Samples contained $0.1 \mu\text{M}$ of each POR enzyme, $12 \mu\text{M}$ Pchl_a, 0.1% Triton X-100, 0.1% 2-mercaptoethanol in activity buffer. Initial rates were measured by following the increase in absorbance at 670 nm upon illumination with a 455 nm LED at a fixed distance and a fixed power setting. The data were fitted to equation 4.1 to obtain V_{max} and K_m for NADPH. Graph A is for POR from *C. reinhardtii* and graph B is for POR from *C. merolae*.

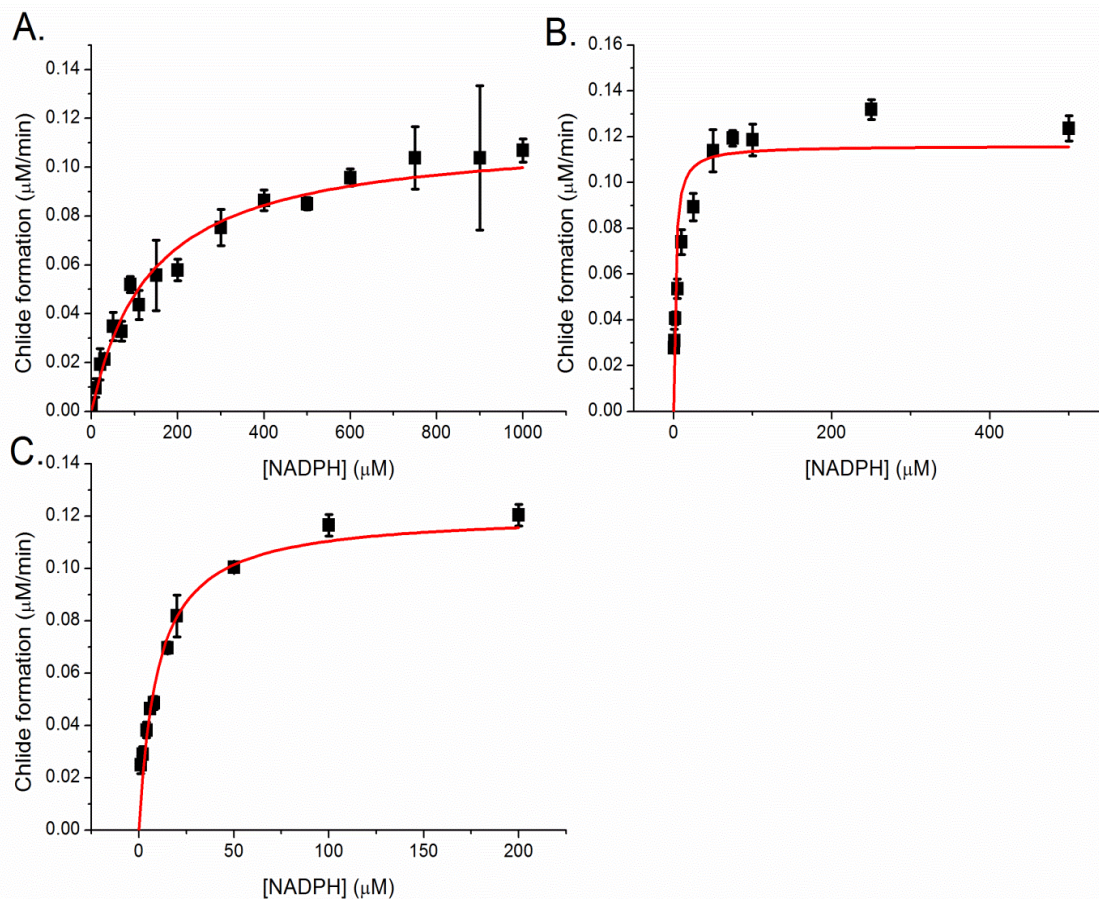


Figure 4.13. The dependence of the initial rate of Chlide formation on the concentration of NADPH for PORs from non-angiosperm land plants. Samples contained $0.1 \mu\text{M}$ of each POR enzyme, $12 \mu\text{M}$ Pchl_a, 0.1% Triton X-100, 0.1% 2-mercaptoethanol in activity buffer. Initial rates were measured by following the increase in absorbance at 670 nm upon illumination with a 455 nm LED at a fixed distance and a fixed power setting. The data were fitted to equation 4.1 to obtain V_{max} and K_m for NADPH. Graph A is for POR from *M. paleacea*, graph B is for POR from *P. patens*, and graph C is for POR from *P. mugo*.

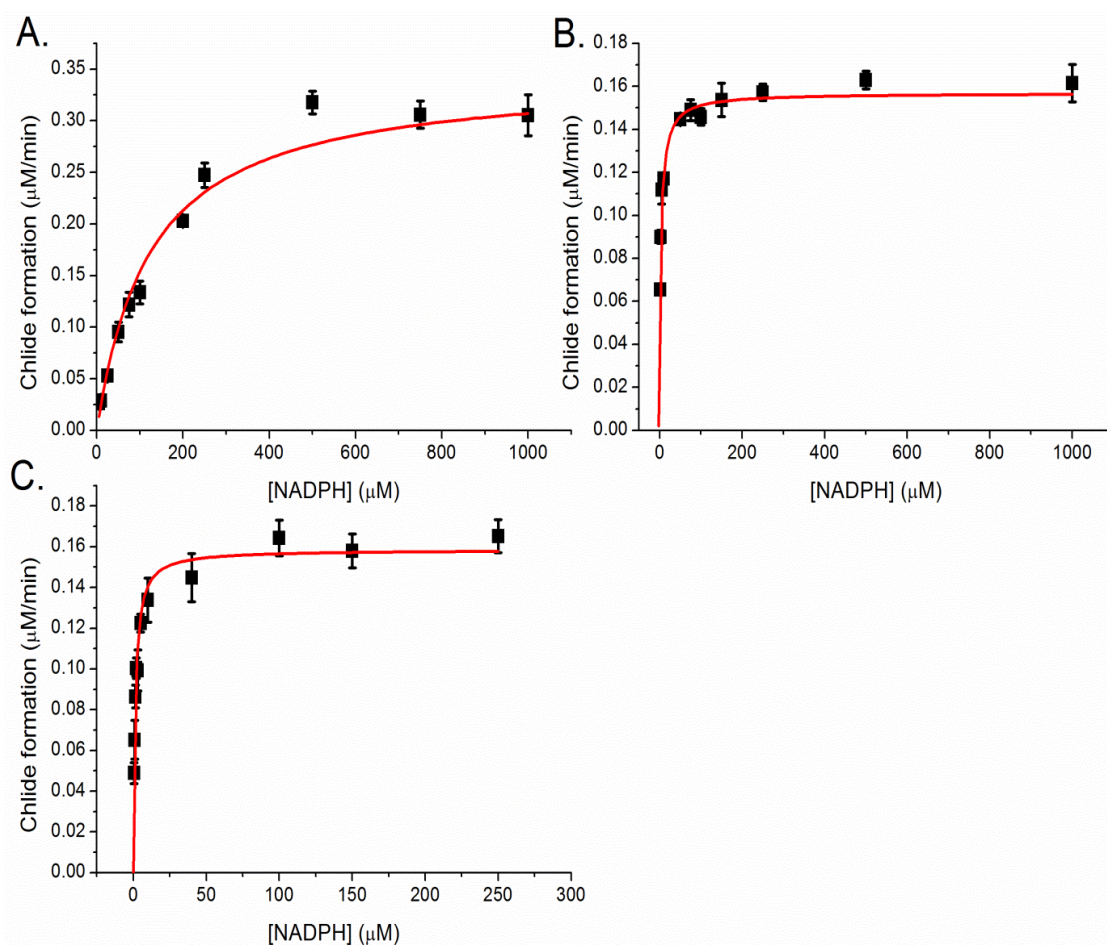


Figure 4.14. The dependence of the initial rate of Chlide formation on the concentration of NADPH for PORs from angiosperms. Samples contained 0.1 μM of each POR enzyme, 12 μM Pchlide, 0.1% Triton X-100, 0.1% 2-mercaptoethanol in activity buffer. Initial rates were measured by following the increase in absorbance at 670 nm upon illumination with a 455 nm LED at a fixed distance and a fixed power setting. The data were fitted to equation 4.1 to obtain V_{max} and K_m for NADPH. Graph A is for POR from *D. carota*, graph B is for POR from *N. tabacum*, and graph C is for POR from *Z. mays*.

Similarly, the initial rate of Chlide formation was also measured at a range of Pchlride concentrations for each of the POR enzymes (Figures 4.15, 4.16, 4.17, 4.18). In contrast to the K_m for NADPH, there is very little variation in the K_m values for Pchlride across all of the POR enzymes, with values ranging from 0.8 μM for *P. patens* POR to 7.8 μM for *L. majuscula* POR. However, it is interesting to note that the dependence of the steady-state rate on Pchlride concentration has evolved a slight substrate inhibition mechanism (see) for PORs from *P. mugo*, *N. tabacum* and *Z. mays* (Figures 4.17 and 4.18). In these cases the data were fitted to equation 4.2 to calculate the inhibition constant (K_i) :

$$v = \frac{V_{max}*[S]}{K_m + \left\{ [S] * \left(1 + \frac{[S]}{K_i} \right) \right\}} \quad 4.2$$

This equation assumes that two substrate units can bind to the enzyme, which leads to a decrease in the rate (v) at higher substrate concentrations. Consequently, K_i values for Pchlride of 7.33 μM , 2.36 μM and 3.22 μM were calculated for *P. mugo*, *N. tabacum* and *Z. mays* PORs, respectively, although there is a relatively large error on the fitting for the enzyme from *N. tabacum*. For the cyanobacterial or algae enzymes it was not possible to determine if substrate inhibition occurs at higher Pchlride concentrations due to experimental limitations. At higher concentrations of Pchlride (>16 μM) inaccuracies in measuring the initial rate occur due to inner-filter effects. Due to the high extinction coefficient of Pchlride in the Soret region most of the 455 nm excitation light is absorbed by sample at the top of the cuvette at higher Pchlride concentrations and the light does not penetrate uniformly throughout the sample (see Figure 4.19). It is important to consider that due to these experimental limitations an underestimation of the K_m can sometimes occur. All of the kinetic parameters obtained from the initial rate data for each of the POR enzymes are summarised in table 4.2.

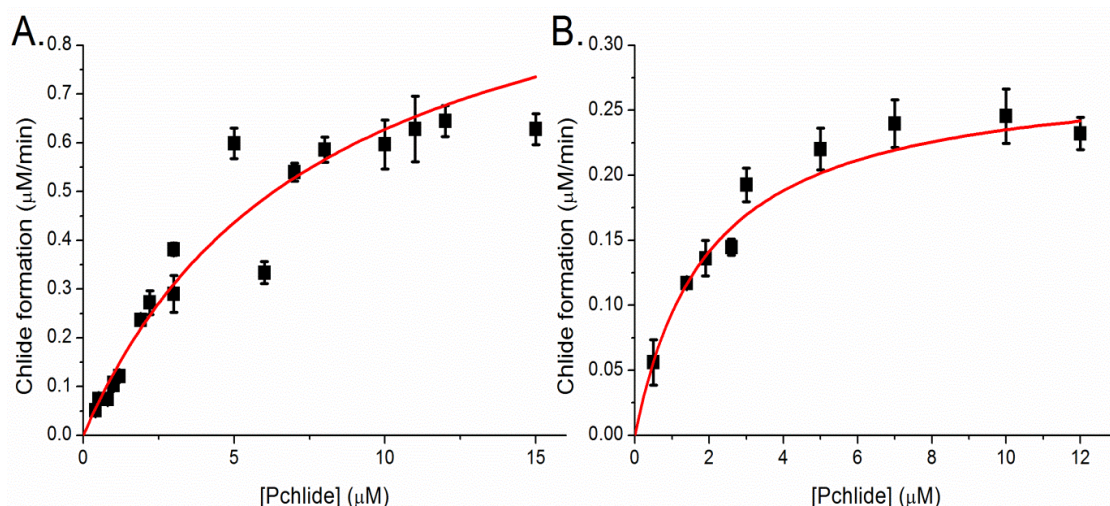


Figure 4.15. The dependence of the initial rate of Chlide formation on the concentration of Pchlide for PORs from cyanobacteria. Samples contained 0.1 μM of each POR enzyme, 0.1% Triton X-100, 0.1% 2-mercaptoethanol in activity buffer with the NADPH concentration ten times the NADPH K_m for the respective protein. Initial rates were measured by following the increase in absorbance at 670 nm upon illumination with a 455 nm LED at a fixed distance and a fixed power setting. The data were fitted to equation 4.1 to obtain the K_m for Pchlide. Graph A is for POR from *L. majuscula*, and graph B is for POR from *N. punctiforme*.

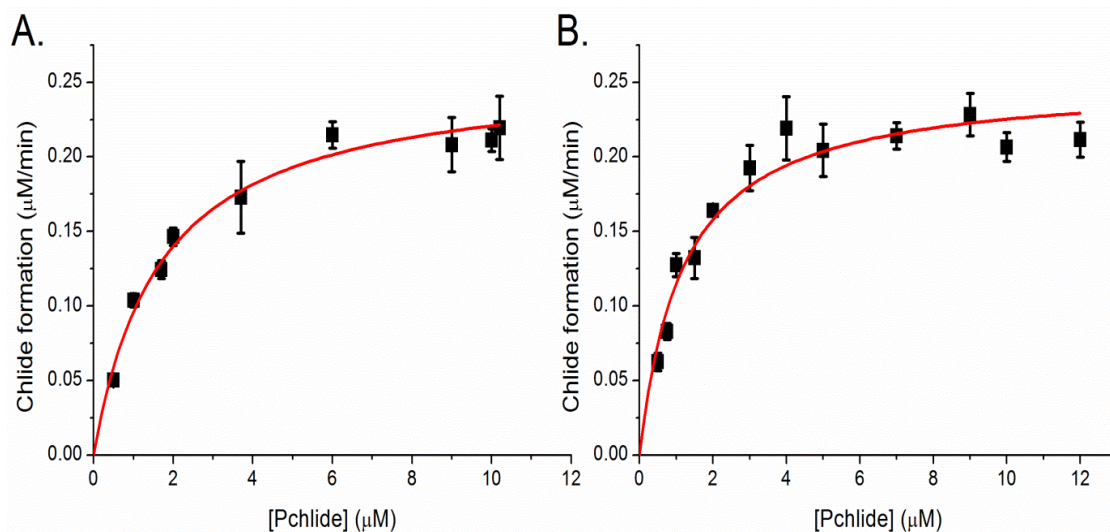


Figure 4.16. The dependence of the initial rate of Chlide formation on the concentration of Pchlide for PORs from algae. Samples contained 0.1 μM of each POR enzyme, 0.1% Triton X-100, 0.1% 2-mercaptoethanol in activity buffer with the NADPH concentration ten times the NADPH K_m for the respective protein. Initial rates were measured by following the increase in absorbance at 670 nm upon illumination with a 455 nm LED at a fixed distance and a fixed power setting. The data were fitted to equation 4.1 to obtain the K_m for Pchlide. Graph A is for POR from *C. reinhardtii*, and graph B is for POR from *C. merolae*.

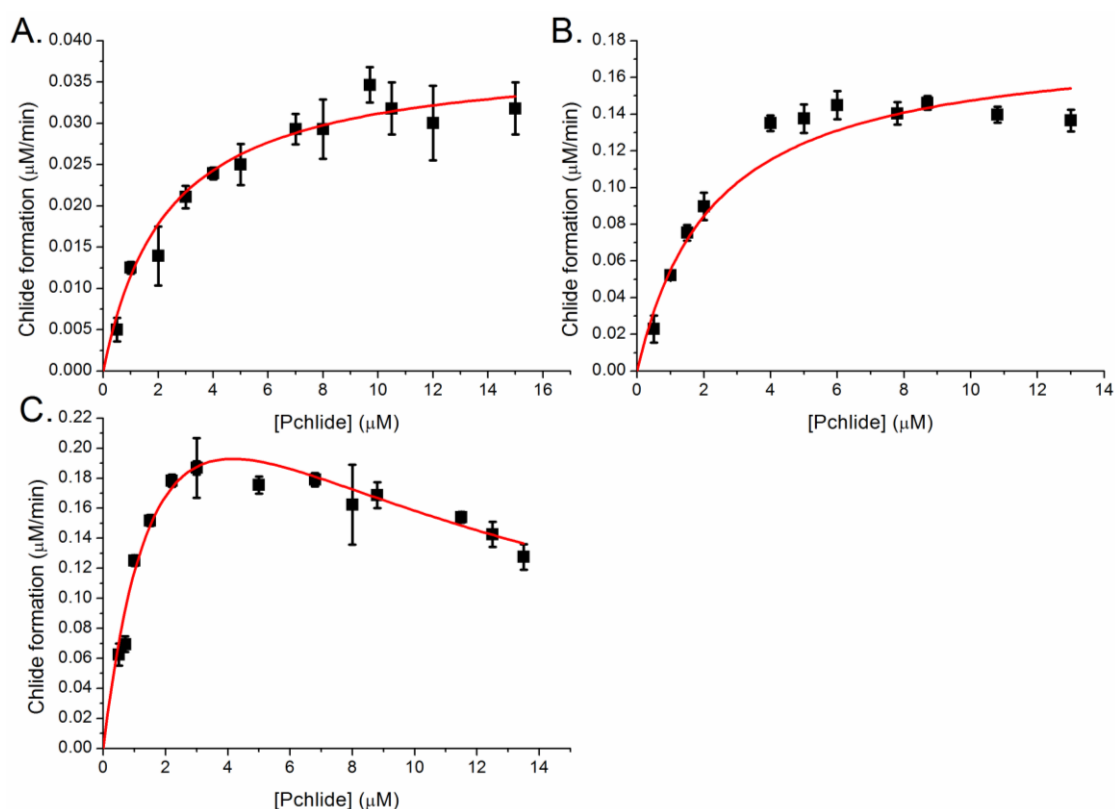


Figure 4.17. The dependence of the initial rate of Chlide formation on the concentration of Pchlide for PORs from non-angiosperm land plants. Samples contained 0.1 μM of each POR enzyme, 0.1% Triton X-100, 0.1% 2-mercaptoethanol in activity buffer with the NADPH concentration ten times the NADPH K_m for the respective protein. Initial rates were measured by following the increase in absorbance at 670 nm upon illumination with a 455 nm LED at a fixed distance and a fixed power setting. The data were fitted to equation 4.1 to obtain the K_m for Pchlide, while graph C (*P. mugo*) was fitted to equation 4.2 to obtain the K_m and K_i for Pchlide. Graph A is for POR from *M. paleacea*, graph B is for POR from *P. patens*, and graph C is for POR from *P. mugo*.

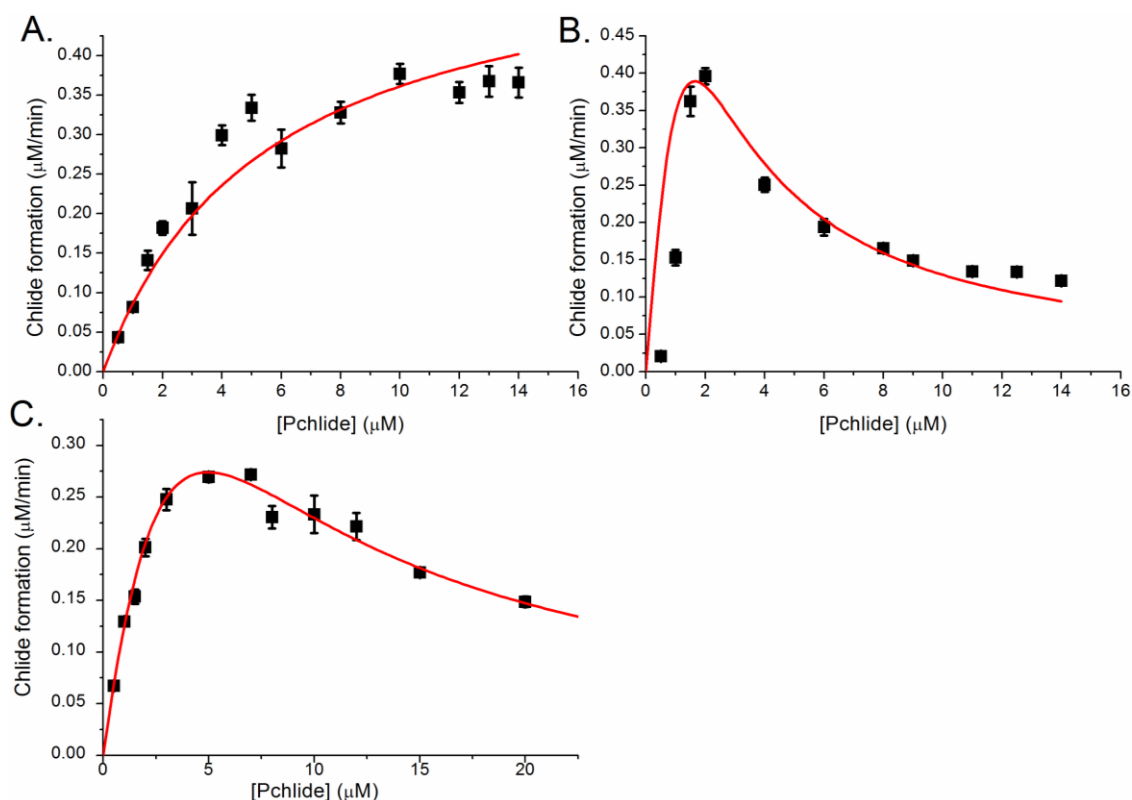


Figure 4.18. The dependence of the initial rate of Chlide formation on the concentration of Pchlide for PORs from angiosperms. Samples contained 0.1 μM of each POR enzyme, 0.1% Triton X-100, 0.1% 2-mercaptoethanol in activity buffer with the NADPH concentration ten times the NADPH K_m for the respective protein. Initial rates were measured by following the increase in absorbance at 670 nm upon illumination with a 455 nm LED at a fixed distance and a fixed power setting. Graphs B and C were fitted to equation 4.2 to obtain the K_m and K_i for Pchlide, while graph A was fitted to equation 4.1 to obtain the K_m for Pchlide. Graph A is for POR from *D. carota*, graph B is for POR from *N. tabacum*, and graph C is for POR from *Z. mays*.

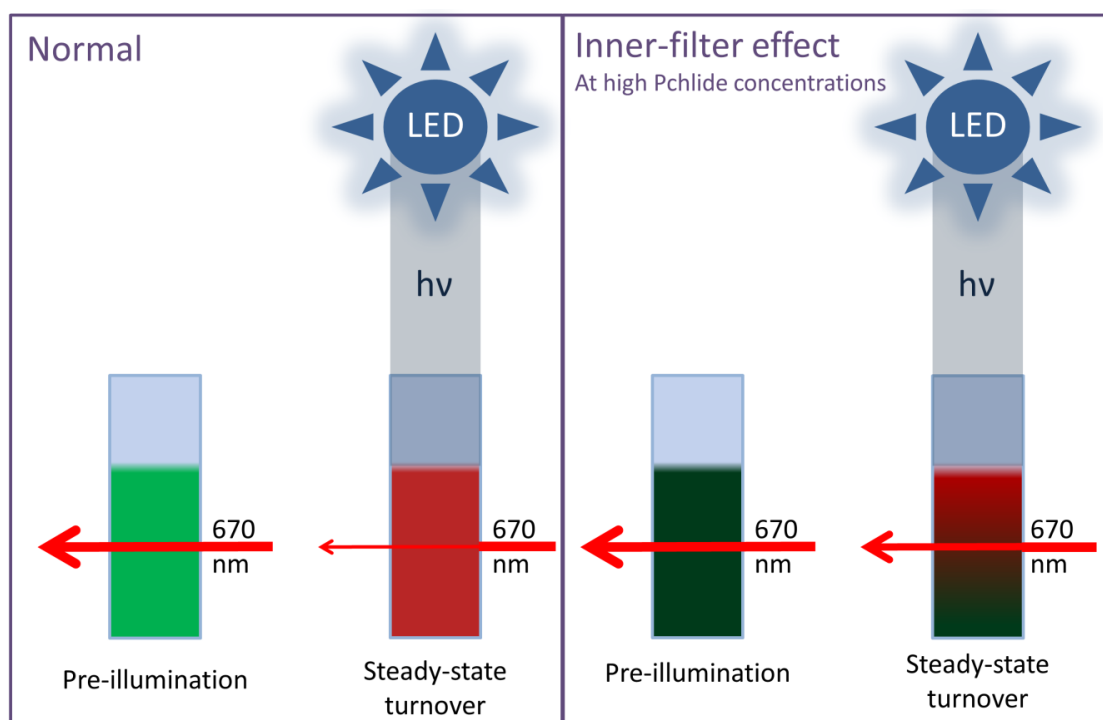


Figure 4.19. Representation of the inner-filter effects observed at high Pchlde concentrations. In the “normal” panel the entire sample is illuminated by the 455 nm light (hv), causing an increased absorbance of 670 nm due to Chlide formation. The inner-filter effect is caused at high Pchlde concentrations ($> 16 \mu\text{M}$) where the top of the sample receives more photons than the bottom. The incident 670 nm light of the spectrophotometer therefore measures a lower change in absorption than would be expected without inner-filter effect.

Table 4.2. Summary of K_m , K_i , V_{\max} and k_{cat} values for each of the POR homologues. Kinetic parameters for POR from cyanobacteria (red), algae (gold), non-angiosperm land plants (green), and angiosperms (blue) are shown.

	NADPH K_m (μM)	Pchlde K_m (μM)	Pchlde K_i (μM)	V_{\max} (μM $\text{min}^{-1} \times 10^{-1}$)	k_{cat} ($\text{s}^{-1} \times 10^{-2}$)
<i>L. majuscula</i>	57.8 ± 13	7.8 ± 1.8		6.12 ± 0.6	10.2 ± 0.9
<i>N. punctiforme</i>	4.8 ± 0.9	2.0 ± 0.3		2.09 ± 0.1	3.5 ± 0.2
<i>C. reinhardtii</i>	157 ± 51	1.7 ± 0.20		2.58 ± 0.13	4.3 ± 0.2
<i>C. merolae</i>	172 ± 17	1.2 ± 0.2		2.52 ± 0.12	4.2 ± 0.2
<i>M. paleacea</i>	138 ± 16	2.3 ± 0.3		1.14 ± 0.04	1.9 ± 0.1
<i>P. patens</i>	2.2 ± 0.5	2.3 ± 0.3		1.16 ± 0.09	1.9 ± 0.2
<i>P. mugo</i>	9.8 ± 0.9	2.4 ± 0.7	7.3 ± 2.2	1.21 ± 0.05	2.0 ± 0.1
<i>D. carota</i>	124 ± 28	5.5 ± 0.7		3.45 ± 0.32	5.8 ± 0.5
<i>N. tabacum</i>	5.9 ± 1.3	4.0 ± 4.0	0.194 ± 0.04	1.03 ± 0.06	1.7 ± 0.1
<i>Z. mays</i>	1.3 ± 0.1	7.7 ± 1.8	3.22 ± 0.82	1.59 ± 0.03	2.6 ± 0.1

4.4.4. NADPH binding constant

In previous studies fluorescence changes have been used to determine the K_d for NADPH binding by measuring Förster resonance energy transfer (FRET) from a conserved tryptophan residue in the active site to NADPH (McFarlane *et al.* 2005, Heyes *et al.* 2008). A similar approach was initially used to measure the binding affinity of NADPH to all of the POR enzymes in the current study. However, a FRET signal could only be observed for two of the POR homologues, *C. merolae* and *N. tabacum*, (Figures 4.20) to determine the binding constant (Figure 4.21). The tryptophans were excited at 280 (*N. tabacum* POR) or 295 nm (*C. merolae* POR), but these wavelengths also excite NADPH directly. This was corrected for by using a NADPH only control (Figure 4.20 B.), which was subtracted from spectra containing enzyme (Figure 4.20 A.) to obtain the FRET signal (Figure 4.20 C.). Finally, the integral of these spectra was taken from 440 to 490 nm and plotted as a function of NADPH concentration (Figure 4.21). K_d values were obtained by fitting the data to a hyperbolic function (Equation 4.3).

$$y = \frac{A_{max}*[S]}{K_d+[S]} \quad 4.3$$

where y is the integral of the fluorescence change from 440 nm to 490 nm, A_{max} is the maximum signal observed, K_d is the binding constant and $[S]$ is the concentration of NADPH.

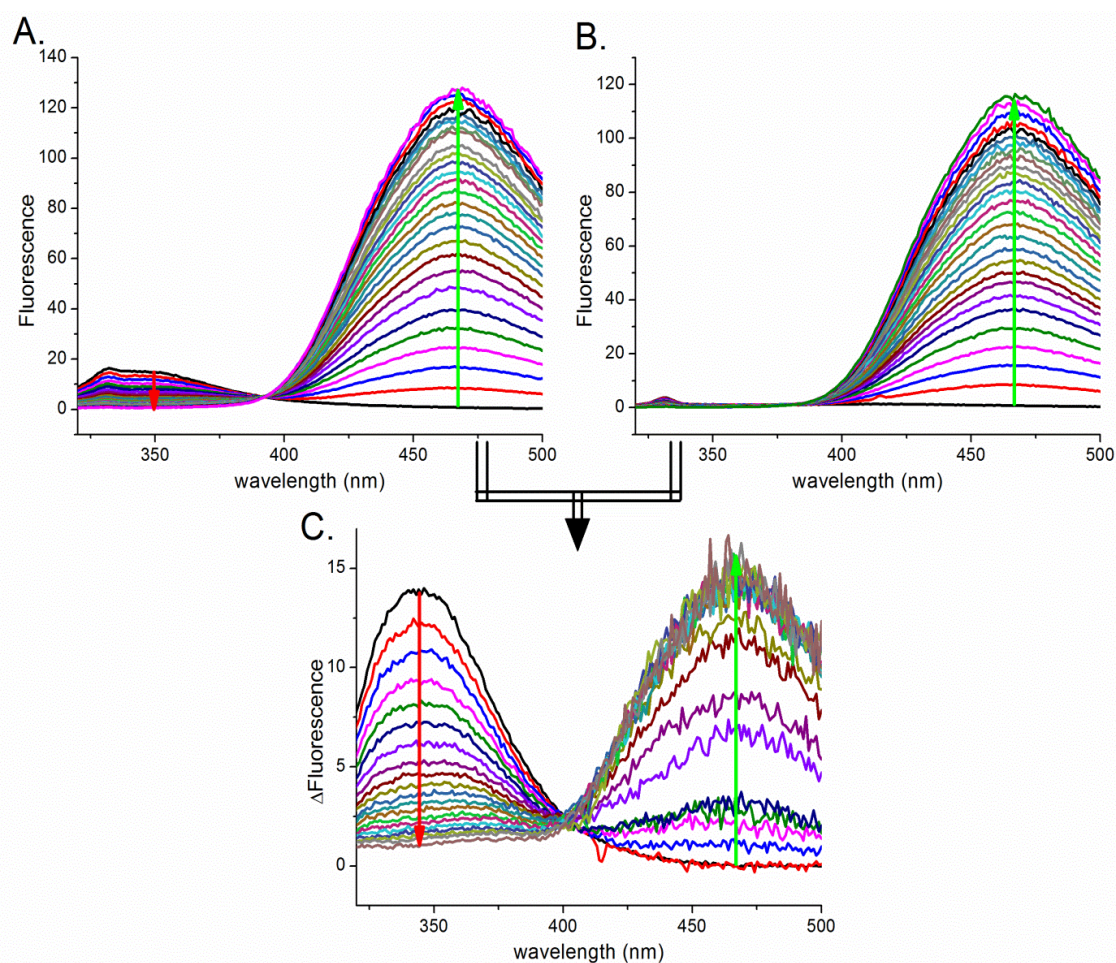


Figure 4.20. Fluorescence spectra associated with NADPH binding for POR from *C. merolae* upon excitation at 295 nm. Samples contained 0.1% 2-mercaptoethanol in activity buffer made up to a 3 ml volume, with NADPH titrated in 1 μ l steps up to a maximum of 1% of the total sample volume (30 μ l). A. Samples contain 0.5 μ M of *C. merolae* POR added to standard conditions. B. Samples contain only buffer. C. Subtraction of the spectra in panel B from those in panel A results in the FRET signal. The peak at approximately 350 nm decreases (red arrow) and the signal at approximately 470 nm increases (green arrow) with more NADPH bound.

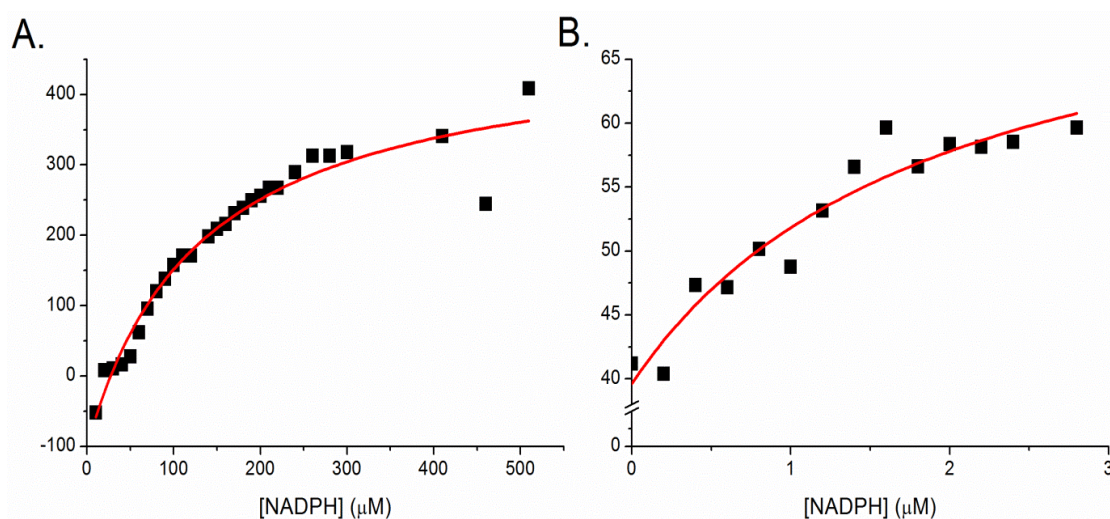


Figure 4.21. Binding titration of NADPH to *C. merolae* and *N. tabacum* POR measured by FRET. Samples containing 0.5 μM *C. merolae* (A) or *N. tabacum* (B) POR in activity buffer (to a total of 3 ml), with 0.1% 2-mercaptoethanol, and were titrated with NADPH (with a stock concentration of ± 30 mM for A. and ± 0.75 mM for B.) titrated in 1 μl steps (10 μM and 0.25 μM steps for A and B, respectively) up to a maximum of 1% of the total sample volume (30 μl). An excitation wavelength of 295 nm was used and the FRET signal was measured using the integral of the 440 to 490 nm emission of the spectra in figure 4.20 C. Equation 4.3 was used to fit the data points to obtain the K_d for NADPH and is shown as a red line.

The remaining eight enzymes did not show a clear FRET signal upon binding NADPH (Figure 4.22). This may be due to the lack of a tryptophan residue in close enough proximity to the bound NADPH or differences in the conformation of the binding pocket. In addition, in some cases with high K_d values, the concentration of NADPH used would be so high that inner filter effects would be a problem at the excitation wavelength used.

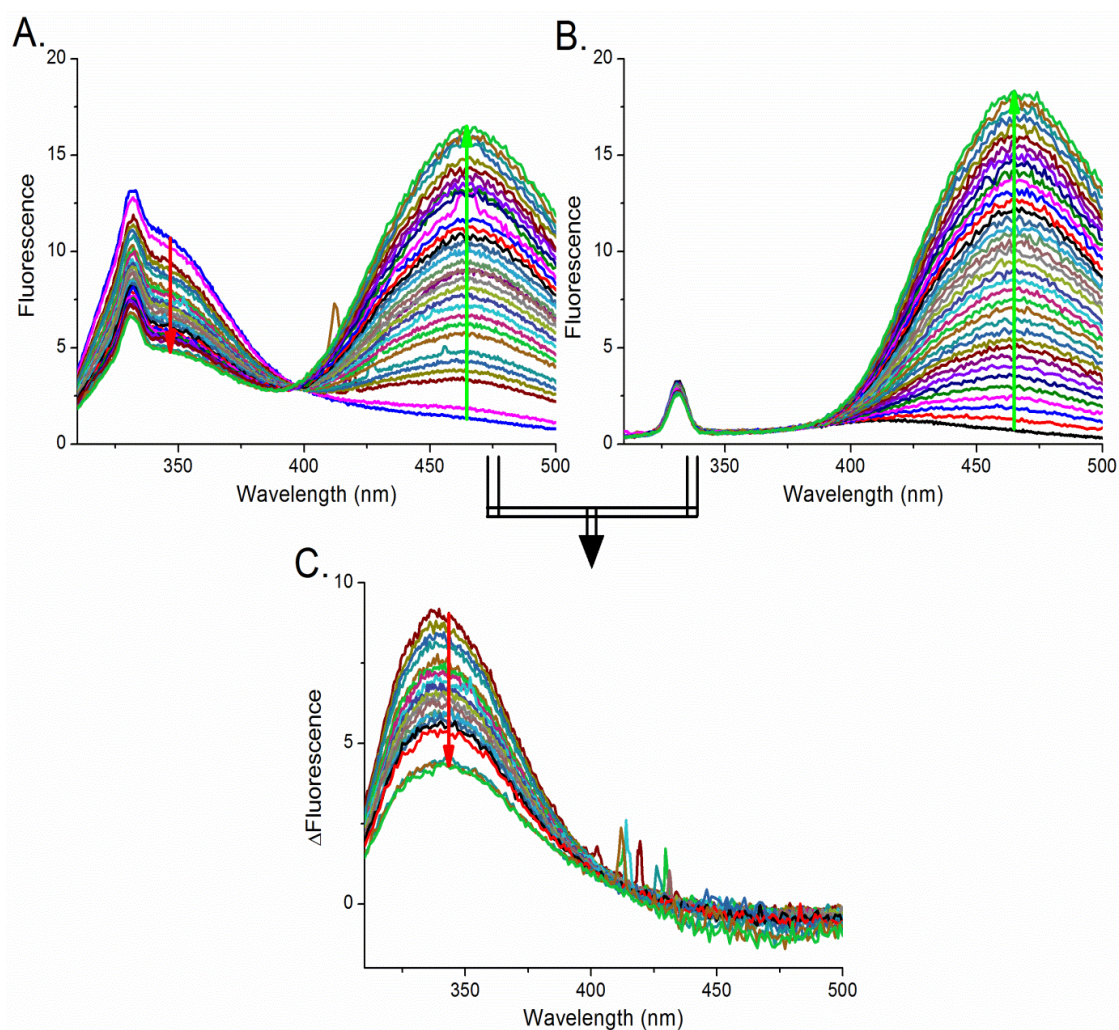


Figure 4.22. Fluorescence spectra associated with NADPH binding for POR from *Z. mays* upon excitation at 295 nm. Samples contained 0.1% 2-mercaptoethanol in activity buffer made up to a 3 ml volume, with NADPH titrated in 1 μ l steps up to a maximum of 1% of the total sample volume (30 μ l). A. Samples contain 0.5 μ M of *Z. mays* POR added to standard conditions. B. Samples contain only buffer. C. Subtraction of the spectra in panel B from those in panel A results in the FRET signal. The peak at approximately 350 nm decreases (red arrow) at higher NADPH concentrations but no increase in the signal at approximately 470 nm was observed.

Consequently, an alternative approach was used to determine the K_d for NADPH that makes use of the shift in the absorbance maximum of Pchl_a from 633 nm to approximately 642 nm upon formation of the ternary complex (POR-NADPH-POR; see Figure 4.10). It is possible to measure this absorbance change by plotting the ratio of absorbance at 642 nm over 633 nm at increasing concentrations of NADPH (see Figures 4.23, 4.24, 4.25, 4.26). The resulting data can be fitted to a tight-binding equation to determine the NADPH K_d value (see Equation 4.4), which takes into account the enzyme concentration used.

$$y = \frac{A_{max}}{2*[E]} * \left\{ ([E] + [S] + K_d) - \sqrt{([E] + [S] + K_d)^2 - 4 * [E] * [S]} \right\} + c \quad 4.4$$

Within the tight-binding or Morrison equation y is the absorbance ratio between 642 nm and 633 nm, A_{max} is the maximum change in absorbance upon binding, $[E]$ and $[S]$ are enzyme and substrate concentration respectively, K_d is the substrate binding constant and c is a constant (Morrison 1969). The equation was used to fit graphs that are assumed to be tight-binding, when the concentration of enzyme and Pchl_a is greater than the concentration of NADPH, or for non-saturating concentrations of NADPH (about 10 times the K_d). All the obtained binding constants for NADPH (Figure 4.23, 4.24, 4.25, 4.26) are summarised in table 4.3 for each POR homologue and divided into the four sub-groups. For the two enzymes (*C. merolae* and *N. tabacum*) where it was possible to use both experimental approaches to measure NADPH binding similar K_d values were obtained in each case (Table 4.3), confirming that the absorbance method is a good alternative to the established fluorescence approach.

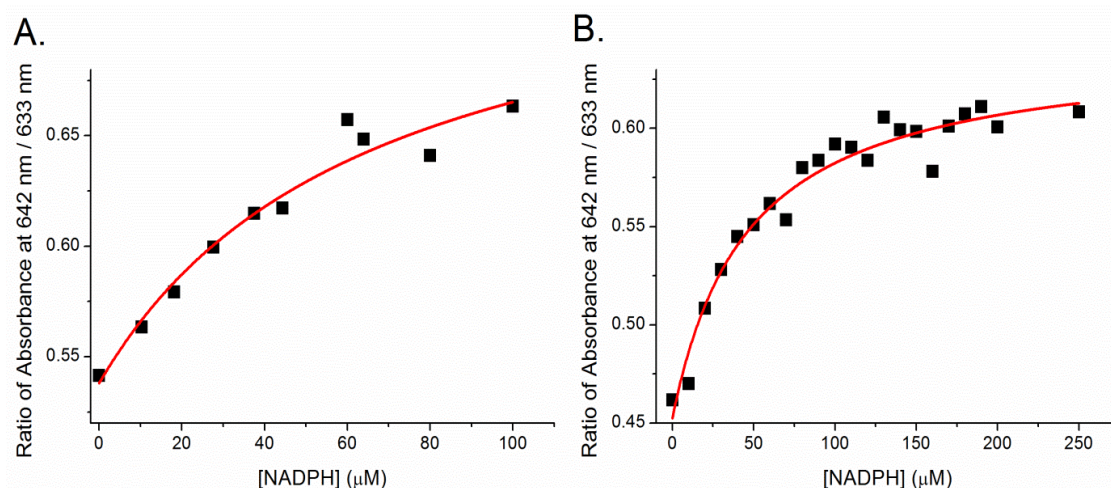


Figure 4.23. The dependence of the POR-Pchl-a-NADPH ternary complex formation on the concentration of NADPH for PORs from cyanobacteria. Samples contained 10 μM of each POR enzyme, 5 μM Pchl-a, 0.1 % Triton X-100, 0.1 % 2-mercaptoethanol in activity buffer. Ternary complex (POR-Pchl-a-NADPH) formation was followed by measuring the increase in the 642 nm over 633 nm absorbance ratio. The data were fitted to equation 4.4 to obtain the K_d for NADPH. Graph A is for POR from *L. majuscula* and graph B is for POR from *N. punctiforme*.

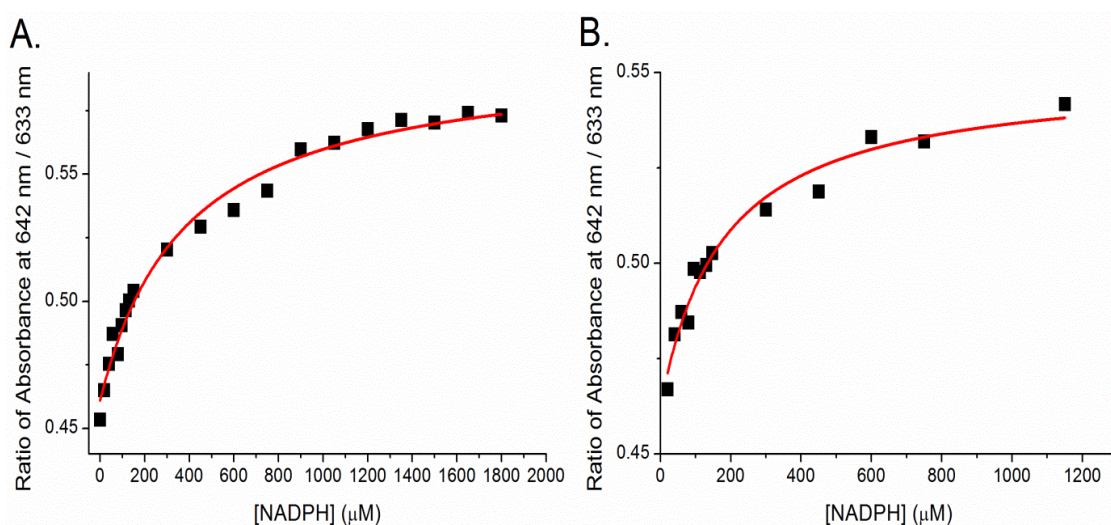


Figure 4.24. The dependence of the POR-Pchl-a-NADPH ternary complex formation on the concentration of NADPH for PORs from algae. Samples contained 10 μM of each POR enzyme, 5 μM Pchl-a, 0.1 % Triton X-100, 0.1 % 2-mercaptoethanol in activity buffer. Ternary complex (POR-Pchl-a-NADPH) formation was followed by measuring the increase in the 642 nm over 633 nm absorbance ratio. The data were fitted to equation 4.4 to obtain the K_d for NADPH. Graph A is for POR from *C. reinhardtii* and graph B is for POR from *C. merolae*.

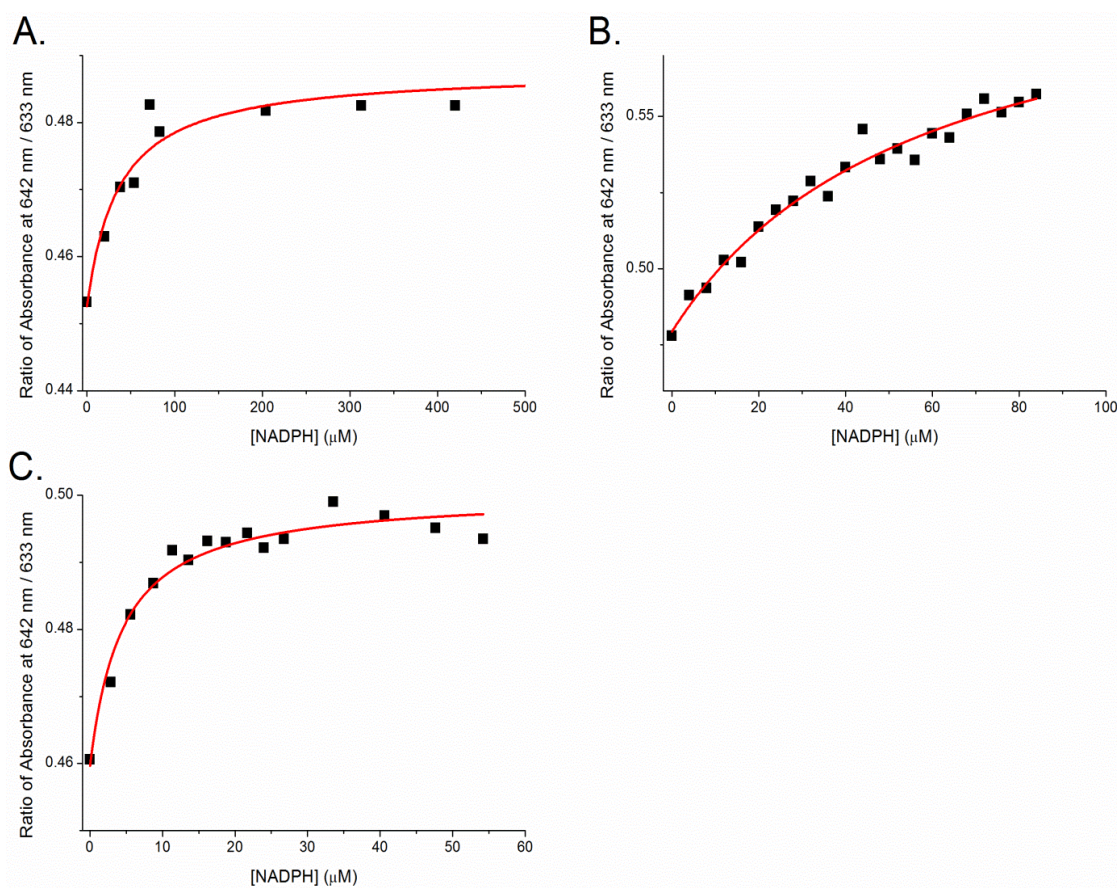


Figure 4.25. The dependence of the POR-Pchl-a-NADPH ternary complex formation on the concentration of NADPH for PORs from non-angiosperm land plants. Samples contained 10 μM of each POR enzyme, 5 μM Pchl-a, 0.1 % Triton X-100, 0.1 % 2-mercaptoethanol in activity buffer. Ternary complex (POR-Pchl-a-NADPH) formation was followed by measuring the increase in the 642 nm over 633 nm absorbance ratio. The data were fitted to equation 4.4 to obtain the K_d for NADPH. Graph A is for POR from *M. paleacea*, graph B is for POR from *P. patens* and graph C is for POR from *P. mugo*.

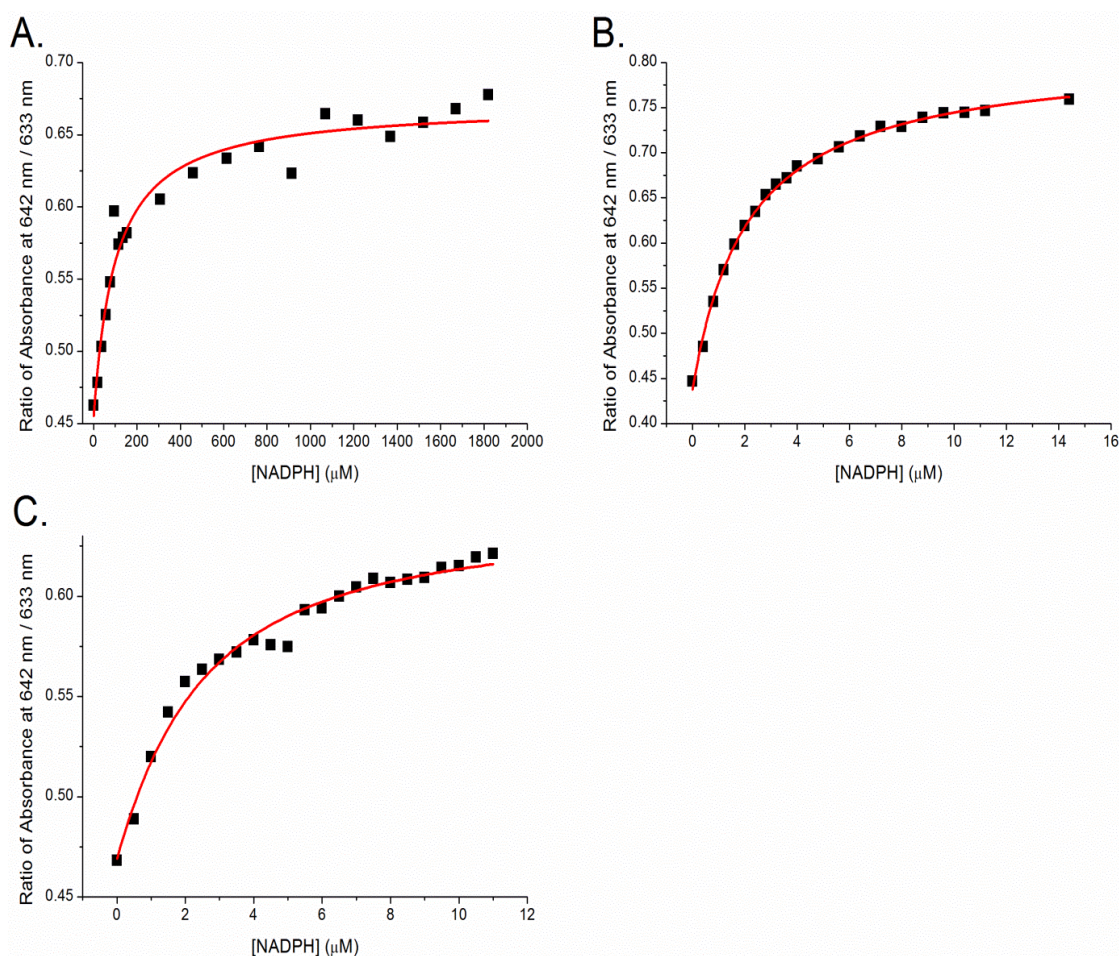


Figure 4.26. The dependence of the POR-Pchlde-NADPH ternary complex formation on the concentration of NADPH for PORs from angiosperms. Samples contained 10 μM of each POR enzyme, 5 μM Pchlde, 0.1 % Triton X-100, 0.1 % 2-mercaptoethanol in activity buffer. Ternary complex (POR-Pchlde-NADPH) formation was followed by measuring the increase in the 642 nm over 633 nm absorbance ratio. The data were fitted to equation 4.4 to obtain the K_d for NADPH. Graph A is for POR from *D. carota*, graph B is for POR from *N. tabacum* and graph C is for POR from *Z. mays*.

Table 4.3. Comparison of K_d values for NADPH binding from fluorescence and absorbance experiments for the different POR enzymes.

NADPH K_d (μ M) fluorescence		NADPH K_d (μ M) Absorbance
<i>L. majuscula</i>		65.6 \pm 29
<i>N. punctiforme</i>		46.3 \pm 9
<i>C. reinhardtii</i>		382 \pm 61
<i>C. merolae</i>	132 \pm 29	176 \pm 47
<i>M. paleacea</i>		36.1 \pm 10
<i>P. patens</i>		57.3 \pm 14
<i>P. mugo</i>		4.46 \pm 0.9
<i>D. carota</i>		103 \pm 20
<i>N. tabacum</i>	1.92 \pm 0.99	2.13 \pm 0.09
<i>Z. mays</i>		1.9 \pm 0.3

4.5. Discussion

In order to provide a more detailed understanding of the evolutionary aspects of POR catalysis ten POR homologues have been selected that span the evolutionary timeframe. The genes for the enzymes from organisms that cover cyanobacteria (*L. majuscula*, *N. punctiforme*), algae (*C. reinhardtii*, *C. merolae*), bryophytes (*P. patens*, *M. paleacea*), gymnosperms (*P. mugo*) and angiosperms (*D. carota*, *N. tabacum*, *Z. mays*) were synthesised and successfully cloned into an expression vector. Heterologous expression in *E. coli* allowed sufficient amounts of catalytically active protein to be extracted and purified *in vitro*. The purity of each enzyme was checked by SDS-PAGE, which also confirmed the correct protein molecular weight of each of the POR homologues. Furthermore, the enzymes were confirmed to contain a His-tag by an anti-His Western blot. In the case of *N. tabacum* POR additional bands were observed that were confirmed by mass-spectrometry to be smaller polypeptide fractions of the POR protein. This suggests that the protein degrades slowly in solution and during the purification process (see Figure 4.8 B. and 4.9).

A steady-state kinetic characterisation was possible for all of the new POR enzymes, allowing the determination of classical enzymology parameters, such as K_m (K_i), K_d , V_{max} , and k_{cat} for both NADPH and Pchlide (where possible; see table 4.2). The K_m for NADPH varies quite significantly across the different POR homologues, although there is no particular pattern in reference to the age of each group. The difference in

K_m for POR from different organisms might be due to different levels of cellular NADPH concentration in each of the organisms.

In addition, we have developed a new method to determine the K_d for NADPH binding that relies on a shift in the absorbance spectrum upon formation of the POR-Pchlide-NADPH ternary complex (Figure 4.10). A comparison of the K_d with the established fluorescence method (McFarlane *et al.* 2005, Heyes *et al.* 2008) for *N. tabacum* and *C. merolae* POR (Table 4.3) confirmed the validity of this technique and provides an alternative approach when FRET is not possible. A comparison of the K_d and K_m values obtained for NADPH in tables 4.2 and 4.3 reveals that they are very similar for the majority of the POR homologues. This suggests that in these cases the binding step, or any conformational changes associated with binding, is rate limiting, which is in agreement with the findings from previous studies (Masuda & Takamiya 2004, Lebedev *et al.* 2001, Heyes *et al.* 2000, Heyes *et al.* 2002). However, the K_d for NADPH for the PORs from *N. punctiforme* and *P. patens* is significantly higher than the K_m , suggesting that one of the subsequent steps in catalysis, such as product release, is rate-limiting at higher NADPH concentrations in these enzymes. Conversely, the K_d for NADPH for the PORs from *M. paleacea* and *N. tabacum* is considerably lower than the K_m , which possibly arises from a POR-Chlide product complex having a higher affinity for NADPH than a POR-Pchlide substrate complex during the catalytic cycle.

In contrast to the K_m for NADPH the K_m for Pchlide shows very little variation amongst the different POR homologues. Interestingly, three of the plant PORs exhibit substrate inhibition for Pchlide, even at relatively low concentrations of Pchlide (<10 μ M). Work by Reed *et al.* (2010) suggests that substrate inhibition can be more than a mere biochemical oddity and has postulated that it can play an important biological role in certain enzymes. As this phenomenon is only observed in plant PORs it is therefore tempting to speculate that substrate inhibition may play a role in prolamellar body formation, which is important for the correct development of chloroplasts and the plant as a whole (Grzyb *et al.* 2013, Cortleven & Schmulling 2015). It is plausible that inhibition of the POR enzyme at higher Pchlide concentrations in higher plants is involved in regulation of prolamellar body formation and/or control chloroplast development. However, in order to move beyond speculation regarding a functional role of substrate inhibition in higher plant PORs will require further investigation through experimental and mathematical methods (Reed *et al.* 2010). As with the K_m

for Pchlide there is also relatively little variation in the k_{cat} values, with the cyanobacterial POR from *L. majuscula* exhibiting the fastest turnover rate at 0.102 s^{-1} . The relatively low k_{cat} values compared to the rate of the H-transfer steps (at least 10^3 s^{-1} ; Heyes *et al.* 2009, 2011) confirm that substrate binding and/or product release steps are rate limiting, in the catalytic cycle. However, it should be noted that the protein samples used were not completely pure, and we do not know how much of the enzyme is catalytically active. Therefore, it is advisable to be cautious in the interpretation and comparison of the V_{max} and k_{cat} values.

In conclusion, we have produced a number of POR enzymes from a wide evolutionary background, ranging from ‘‘ancient’’ cyanobacteria to ‘‘evolved’’ angiosperms. The kinetic parameters have been determined for all of the POR homologues and have provided information about the rate-limiting steps in catalysis. As POR has been proven to be an excellent model system to study the effects of protein motions on catalysis this work provides the basis for more detailed studies on the evolutionary aspects of the catalytic mechanism and any protein dynamics that are required for the reaction chemistry.

Chapter 5

An evolutionary analysis of protein dynamics in the catalytic cycle of the light-driven enzyme protochlorophyllide oxidoreductase (POR).

Authors:

Robin Hoeven, Samantha O. J. Hardman, Nigel S. Scrutton and Derren J. Heyes

Affiliation:

Manchester Institute of Biotechnology, Faculty of Life Sciences, The University of Manchester, Manchester M1 7DN, United Kingdom

Published in:

Manuscript in preparation

5.1. Abstract

The catalytic power of enzymes is highly dependent on protein dynamics but it is currently unclear how motions have evolved to achieve these huge rate enhancements. The light-driven enzyme, protochlorophyllide oxidoreductase (POR) has proven to be an excellent model system to study the link between protein dynamics and catalysis. The catalytic mechanism of POR involves a sequential hydride and proton transfer step, with the first catalytic step requiring light-excitation of the protochlorophyllide (Pchl_{id}) substrate. This obligatory requirement for light provides a unique experimental advantage, compared to thermally-activated enzymes that can only be studied by using rapid mixing strategies, as catalysis can be triggered with a laser pulse and measurements can be made at high solvent viscosities, which is an excellent probe of protein dynamics. Previous measurements on a limited subset of POR enzymes revealed that the protein dynamics required for the two catalytic steps are likely to have evolved along distinct pathways. Here, we have used solvent viscosity measurements to analyse the dynamics coupled to the hydride and proton transfer steps for POR enzymes from a broad evolutionary origin, including cyanobacteria, algae, embryophytes and angiosperms. A significant rate enhancement of both H-transfer steps was observed for all eukaryotic homologues compared to their prokaryotic ancestors, suggesting that optimisation of the active site architecture is likely to have occurred upon endosymbiosis. Moreover, our findings confirm that light-driven hydride transfer is reliant only on localised motion within the active site across all POR enzymes. In contrast, those linked to thermally-activated proton transfer are variable, whereby cyanobacterial PORs require a high level of solvent-coupled protein dynamics to optimise the proton donor-acceptor distance, but evolutionary pressures have acted to remove or minimise such networks in algal and plant PORs. Finally, the excited-state processes involved leading up to hydride transfer were investigated and compared between different evolutionary lineages, which showed the ultrafast excitation steps to be conserved across the lineages.

5.2. Introduction

Enzymes are inherently dynamic molecules but the role of protein dynamics in catalysis remains a key question in providing a detailed mechanistic understanding of how enzymes function (Eisenmesser *et al.* 2002, Henzler-Wildman & Kern 2007, Yahashiri *et al.* 2008, Nagel & Klinman 2010, Bandaria *et al.* 2009, Heyes *et al.* 2009, Pislakov *et al.* 2009, Klinman & Kohen 2013). The importance of conformational changes within the active site and how these local changes are coupled to longer range conformational changes has been hotly debated (Benkovic & Hammes-Schiffer 2003, Kohen *et al.* 1999, Eisenmesser *et al.* 2005, Masgrau *et al.* 2006). Indeed, one of the most challenging questions to address is how the intrinsic motions of enzyme molecules have evolved to achieve catalysis (Yahashiri *et al.* 2008). It is now well established that protein motions are closely linked to the solvent environment and the effects of solvent viscosity on catalysis can provide important information on the dynamics of an enzyme system (Loveridge *et al.* 2011, Hay *et al.* 2008, Heyes *et al.* 2009, Frauenfelder *et al.* 2009, Durin *et al.* 2009). Hence, a detailed, comparative study of the effects of solvent fluctuations on catalysis between enzymes from species that span the evolutionary timescale can provide significant insight into how protein dynamics have been affected by millions of years of evolutionary pressure. However, studies relating solvent perturbation to protein dynamics are often hindered for thermally-activated enzymes due to the limitations of rapid mixing strategies to initiate catalysis. This problem can be overcome by using the light-activated enzyme protochlorophyllide oxidoreductase (POR; EC1.3.1.33), which allows synchronous triggering of catalysis with a laser pulse in a ‘dark-assembled’ enzyme-substrate complex (Heyes & Hunter 2005). POR is also found in a wide range of organisms and is therefore an excellent model system for providing an evolutionary perspective of protein dynamics linked to enzyme catalysis (Yang & Cheng 2004 Heyes *et al.* 2011). POR catalyses the reduction of the C17-C18 double bond of the protochlorophyllide (Pchl_{id}) substrate to form chlorophyllide (Chl_{id}), an essential step in the chlorophyll biosynthesis pathway and subsequent assembly of the photosynthetic apparatus (Heyes & Hunter 2005, Lebedev & Timko 1998). The enzyme-bound Pchl_{id} molecule acts as the photoreceptor in the reaction and upon absorption of light it is proposed to form an intramolecular charge transfer (ICT) state across the C17-C18 double bond, due to excited state interactions with a conserved tyrosine (Tyr193) residue in the enzyme

(Heyes *et al.* 2015). This creates a transient electron-deficient site at the C17 position, which facilitates the nucleophilic attack of a hydride from the *pro-S* face of NADPH on the microsecond timescale (Begley & Young 1989, Heyes *et al.* 2006, Heyes *et al.* 2009). The resulting negative charge at the C18 position allows the subsequent transfer of a proton from the conserved Tyr193 to form the Chlide product (see Figure 5.1; Wilks & Timko 1995, Menon *et al.* 2009). It has been shown that both H-transfer reactions proceed by quantum mechanical tunneling with each step coupled to a different set of fast motions (promoting motions or vibrations) in the enzyme-substrate complex (Heyes *et al.* 2009a, 2009b). Following hydride and proton transfer, a series of ordered product release and coenzyme binding steps are required to complete the catalytic cycle, which are linked to major conformational changes in the enzyme (Heyes *et al.* 2007).

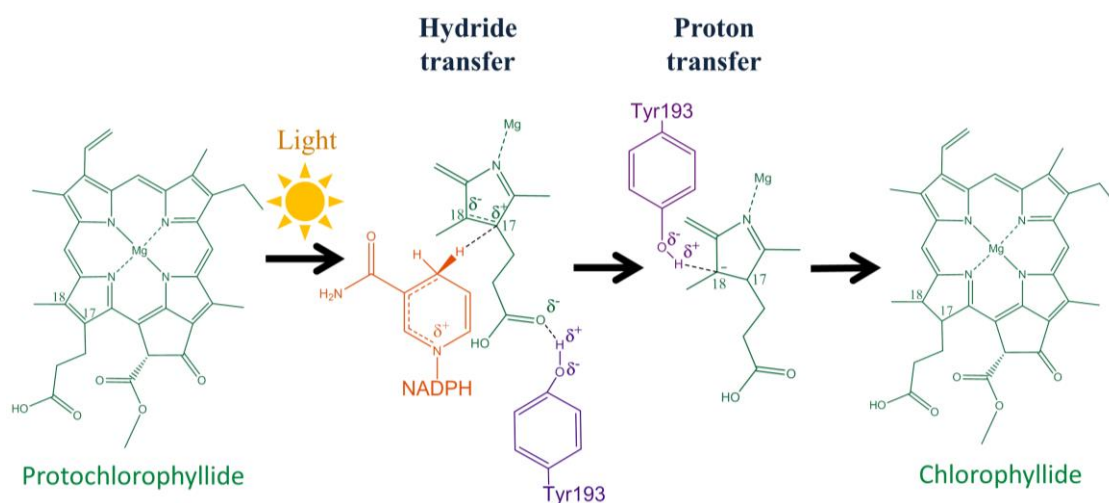


Figure 5.1. The reaction mechanism of protochlorophyllide oxidoreductase (POR). The first step involves the light-activated hydride transfer from NADPH (red) to the C17 position of Pchl, followed by a proton transfer from a conserved Tyr residue (purple) in the active site to the C18 position.

A previous study on POR has shown that it is an attractive model system for studying the evolution of dynamics linked to catalysis (Heyes *et al.* 2011). It is likely that POR arose around 2.4 billion years ago with the rise in atmospheric oxygen levels and was introduced into plant cells during the primary symbiosis of an ancestral cyanobacterium (Reinbothe *et al.* 1996, Hohmann-Marriott & Blankenship 2011, Crowe *et al.* 2013, Suzuki & Bauer 1995, Masuda & Takamiya 2004). Apart from angiosperms, most oxygenic phototrophs still have a light-independent enzyme to reduce Pchl, but amongst prokaryotic phototrophs POR is found only in

cyanobacteria, suggesting that light-dependent chlorophyll biosynthesis was established prior to eukaryotic photosynthesis (Hohmann-Marriott & Blankenship 2011, Yang & Cheng 2004). Based on this evolutionary diversity, it was shown that the protein dynamics coupled to each of H-transfer steps in the reaction may have a distinct evolutionary origin although the study was limited to just 4 POR enzymes (3 cyanobacterial and 1 plant POR; Heyes *et al.* 2011). It was proposed that any motions linked to light-driven hydride transfer are localised to the enzyme active site and are conserved across all POR enzymes due to the difficulty of the chemistry catalysed. However, the dynamics coupled to the proton transfer step vary, where cyanobacterial PORs require complex and solvent-coupled dynamic networks to optimise proton donor-acceptor distances but these networks have been minimised or removed in plant PORs. This twin-track approach to the evolution of protein dynamics has now been investigated in much more detail by expanding the study to include a wide range of new POR enzymes that span the evolutionary timescale, including PORs from cyanobacteria, algae, liverwort, moss, and a number of higher plant species. A full kinetic characterisation and solvent viscosity dependence for the two H-transfer has been undertaken and differences in the dynamic profiles of each enzyme have been correlated to their evolutionary origin.

5.3. Materials and methods

5.3.1. Expression and purification of POR homologues

The POR genes of *Chlamydomonas reinhardtii*, *Cyanidioschyzon merolae*, *Daucus carota*, *Lyngbya majuscula*, *Nicotiana tabacum*, *Nostoc punctiforme*, *Pinus mugo*, *Physcomitrella patens* and *Zea mays* were synthesised by GenScript (GenScript Inc.) and digested with *Nde*I and *Bam*HI HF restriction enzymes (New England Biolabs Ltd.). The genes were cloned into an *Nde*I and *Bam*HI digested pET9-His vector (derivative of pET9a from Novagen; Heyes *et al.* 2000) and confirmed by sequencing of the plasmid (Eurofins Scientific). The full protein sequences encoded by each gene can be found in the Supplementary Data (Figure S5.1).

All POR proteins were overexpressed with an N-terminal His-tag as previously described (Heyes *et al.* 2000). The cell pellets were resuspended in cold binding buffer (500 mM NaCl, 5 mM imidazole, 0.1 % Triton X-100, 50 mM MOPS, 100 mM ammonium acetate pH 7) and disrupted by 25 cycles of 20 s pulses of sonication

(Bandelin, sonopuls probe VT70T/N494) at 40 % intensity. Cell debris was removed by centrifugation at 20 krpm for 30 min in a JA25:50 (Beckman Coulter Inc.) and proteins were purified by binding the His-tagged protein to a 5 ml HisTrap FF column (GE Healthcare Life Sciences) pre-equilibrated with 10 column volumes of binding buffer. The column was washed with buffer containing 50 mM and 100 mM imidazole, followed by a final elution consisting of a gradient from 100 mM to 500 mM imidazole. The fractions were visualised by SDS-PAGE (12 %; Bio-Rad laboratories Inc.) and those containing purified POR protein were pooled and concentrated using a Vivaspın 20 (10 kDa MWCO; Sartorius AG). Finally, the protein underwent buffer exchange into activity buffer (500 mM NaCl, 50 mM MOPS, 100 mM ammonium acetate pH 7) using a CentriPure P100 column (Generon Ltd.) to remove the imidazole. Protein concentrations were determined using the Bio-Rad DC assay kit with bovine serum albumin as a standard. Pchl_{ide} was prepared as described previously (Heyes *et al.* 2003). All chemicals were obtained from Sigma-Aldrich, except for NADPH (Melford Laboratories Ltd.)

5.3.2. Laser flash photolysis

Laser photoexcitation experiments were conducted as outlined previously (Heyes *et al.*, 2009). Each data point was the average of at least four measurements. The cuvette used had a 2 mm pathlength in the pump direction and 1 cm in the probe direction. Samples contained 50 μ M enzyme, 250 μ M NADPH (except *C. reinhardtii*, *C. merolae*, *L. majuscula*, *D. carota* which had a 2 mM concentration due to the reduced affinity for NADPH) and 12 μ M Pchl_{ide} in activity buffer (0.5 M NaCl, 50 mM MOPS, 100 mM ammonium acetate, 0.1 % Genapol X-080, 0.1% 2-mercaptoethanol). Samples for solvent viscosity measurements were prepared using glycerol as the viscosogen by weight and the solution viscosity was calculated as previously described (Hay *et al.* 2008). The observed rate was plotted as a function of solvent viscosity and fitted to Equation 5.1 (Heyes *et al.* 2009, Ansari *et al.* 1992) to explain the protein friction contribution to the system friction.

$$k_{obs} = \frac{k_B T}{h} \left(\frac{1+\sigma}{\eta+\sigma} \right) e^{\frac{-\Delta G}{RT}} \quad 5.1$$

The absolute viscosity is shown as η , and the protein's friction contribution is represented by σ , in centipoise (cP).

5.3.3. *Ultrafast transient pump-probe spectroscopy*

A Ti:sapphire amplifier system (Spectra Physics Solstice Ace) produced 6 mJ of 800 nm pulses at 1 kHz with 100 fs pulse duration. A portion of the output of the amplifier was used to pump a Topas Prime OPA (optical parametric amplifier) with associated NirUVis unit which was used to generate the pump beam centred at 450 nm, with FWHM of ca. 10 nm. A broad band ultrafast pump-probe transient absorbance spectrometer 'Helios' (Ultrafast systems LLC) was used to collect data (at random timepoints) from ~1 ps to 2.6 ns with a time resolution of around 0.2 ps. The probe beam consisted of a white light continuum generated in a sapphire crystal and absorbance changes were monitored between 500 and 750 nm. Data from this setup are referred to as the 'fast' data. A broad band sub-nanosecond pump-probe transient absorbance spectrometer 'Eos' (Ultrafast systems LLC) was used to collect data (at random timepoints) up to either 0.5 or 2 μ s. A 2 kHz white-light continuum fibre laser was used to generate the probe pulses. The delay between pump and probe was controlled electronically. Data from this set-up are referred to as the 'slow' data. For both sets of measurements samples were excited at 450 nm with 0.5 μ J power and a beam diameter of ~ 200 μ m. Samples were flowed at a rate of approximately 30 ml/min through a 0.2 mm pathlength quartz cell (at room temperature) to ensure that a different area of the sample is excited with each pump laser pulse. Samples were prepared in the dark containing 500 μ M POR, 200 μ M Pchl_a and 4 mM NADPH in activity buffer with 10 % glycerol, 0.1 % 2-mercaptoethanol, and 0.5 % Triton X-100.

5.3.4. *Global analysis*

The datasets were analysed globally using the open-source software Glotaran (Snellenburg *et al.* 2012). This procedure reduces the matrix of change in absorbance as a function of time and wavelength, to a model of one or more exponentially decaying time components, as described in the main manuscript, each with a corresponding difference spectrum (species associated difference spectra (SADS)). Errors quoted with the lifetime values are the standard errors calculated during the global analysis. For the analysis, the pre-excitation background was subtracted and both the 'fast' and 'slow' datasets were fitted to a simple sequential model where one

species converts to another, which then persists for the lifetime of the experiment. The 'fast' datasets were the result of one scan of <3 minute duration with data analysed from 1 ps to 2.6 ns. The 'slow' datasets were selected after a collection time such that the ratio of the ground state bleach intensity of Pchl_a:Chl_a was similar in all cases (ca. 4) with data analysed from 5 ns to 500 (or 2000) ns.

5.3.5. Phylogeny

The phylogenetic tree was generated using the phylogeny.fr website (Dereeper *et al.* 2008), with a full MUSCLE setting for alignment and one-hundred maximum likelihood bootstrap replicates.

5.4. Results

5.4.1. Steady-state characterisation of PORs from different evolutionary origins

The phylogeny of POR is widespread among photosynthetic organisms, ranging from prokaryotes, in the form of cyanobacteria, to the most advanced eukaryotes, in the form of higher plants. A phylogenetic analysis of the available gene sequences for POR show broad separation into these two groups (Figure 5.2), although the cyanobacterial group is more diverse than the plant group, indicated by the longer branch lengths. This is in accordance with previous observations, which also showed that adaptation to evolutionary pressures resulted in variable patterns of structural conservation in the different POR enzymes (Nelissen *et al.* 1995, Gupta & Mathews 2010, Heyes *et al.* 2011). Furthermore, during the transition from cyanobacteria to higher plants a third cluster of proteins can be identified from algae. Consequently, to ensure a broad spread of POR enzymes across all evolutionary timescales we have selected PORs from cyanobacteria (*L. majuscula* and *N. punctiforme*), algae (*C. reinhardtii* and *C. merolae*), moss (*P. patens*), a gymnosperm (*P. mugo*) and different higher plant origins (*D. carota*, *N. tabacum* and *Z. mays*) for further analysis. Initially, the catalytic activity of all POR enzymes was measured under steady-state conditions to determine the kinetic parameters for the reaction (Table 4.2). Values for k_{cat} vary from 0.017 s⁻¹ for *N. tabacum* POR to 0.10 s⁻¹ for POR from *L. majuscula*, although these values show no discernible dependence on evolutionary origin. Similarly, there is also a broad spread of values for the K_m for NADPH, ranging from 1.3 μM to approximately 170 μM. However, there is little variability in the K_m values for

Pchl_{ide}, although significantly three of the plant PORs exhibit a considerable degree of substrate inhibition that is not observed for the other POR enzymes (Figure 4.17 and 4.18).

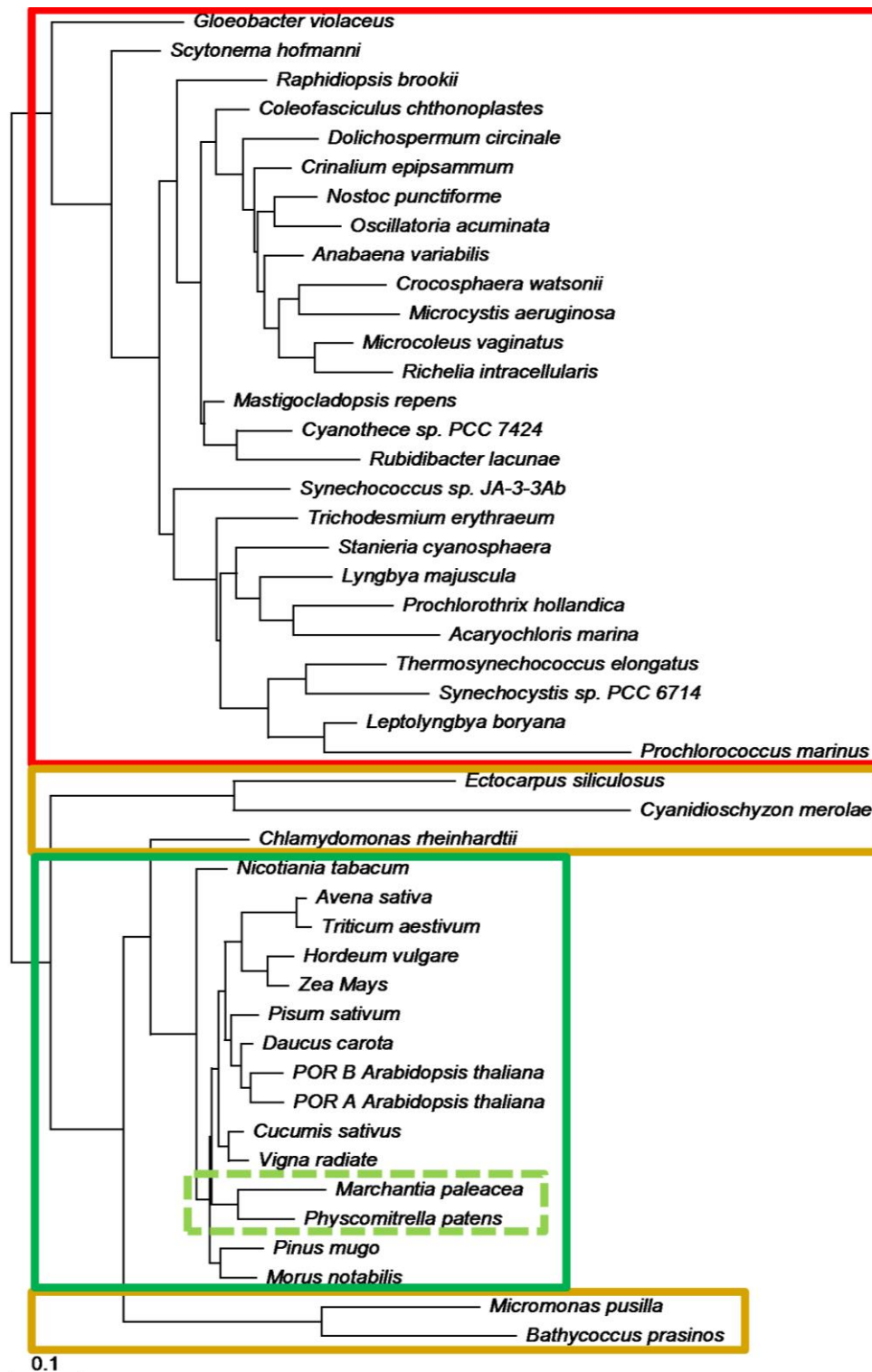


Figure 5.2. Phylogenetic tree of the POR genes. The cyanobacteria and prochlorophytes group (red) is located at the top, while the plants (dark green) are at the bottom, with the branches in between as algae species (gold). The bryophytes (liverwort and moss) are highlighted by the dashed light green box. The scale bar indicates how many amino acids are replacements per site.

5.4.2. *Excited state hydride transfer step*

The catalytic reaction of POR can be triggered by laser photoactivation, allowing the rates of both the hydride and proton transfer steps to be determined by following the absorbance change at 696 nm (Heyes *et al.* 2009, Heyes *et al.* 2002). These measurements have confirmed that the kinetic mechanism of hydride and proton transfer is sequential (*i.e.* hydride precedes proton transfer) for each POR enzyme (Figure S5.2). Interestingly, the rate constants for the initial light-activated hydride transfer differ significantly between cyanobacterial PORs and PORs from a eukaryotic origin, with a much higher rate observed for all eukaryotic PORs (Figure 5.3, table 5.1). Consequently, due to the time resolution of the laser flash photolysis instrumentation (~50 ns) all measurements were performed at 4°C to ensure accurate rates for hydride transfer were obtained. In addition, the amplitude of the absorbance change at 696 nm is a lot higher for the cyanobacterial PORs compared to the enzymes from algae and plants (table 5.1), which is likely to reflect differences in the quantum yield of the reaction. Information on the nature of any protein motions linked to the hydride and proton transfer steps can be gained by measuring the dependence of the reaction rates on solvent viscosity (Ansari *et al.* 1992, Heyes *et al.* 2009, Heyes *et al.* 2011). Hence, the rate of hydride transfer was measured at a high glycerol concentration (60 % or ± 23.7 cP; Chen & Pearlstein 1987) for all of the POR enzymes (Figure S5.3; table 5.1). Importantly, no major differences were observed in the rate of hydride transfer at higher viscosity for any of the POR enzymes, confirming that this step is not influenced by solvent viscosity.

The time-dependent increase in absorbance at 696 nm appears to occur in a biphasic process for the cyanobacterial PORs and hence, these transients were also fitted to a double exponential equation (Figure 5.3). The first exponential rise largely occurs within the dead time of the laser flash instrument and therefore, this value was fixed at 3×10^7 for the purposes of data fitting. Similar rates were obtained for the hydride transfer step using this analysis (Table S5.1) compared to the fitting with a single exponential equation (table 5.1) and again the effects of solvent viscosity were shown to be limited.

Table 5.1. The rates of hydride transfer of the POR homologues at 4°C. The data from approximately 100 ns onwards were fitted to a single exponential equation to obtain the rate constants and amplitudes for the absorbance increase at 696 nm for POR from cyanobacteria (red), algae (gold), bryophyte (green), gymnosperm (purple) and angiosperms (blue). The effects of viscosity on the rate of the hydride transfer step were monitored by repeating measurements in the presence of 60 % glycerol.

	0 % glycerol		60 % glycerol	
	k_{hydride} (s ⁻¹ , x 10 ⁵)	Amplitude (Abs)	k_{hydride} (s ⁻¹ , x 10 ⁵)	Amplitude (Abs)
<i>L. majuscula</i>	11.6 ± 0.1	0.16 ± 0.02	7.7 ± 0.5	0.091 ± 0.024
<i>N. punctiforme</i>	9.4 ± 0.1	0.085 ± 0.017	7.3 ± 0.7	0.082 ± 0.059
<i>T. elongatus</i>	12.6 ± 1.0	0.075 ± 0.022	11.1 ± 1.8	0.073 ± 0.009
<i>C. reinhardtii</i>	41.2 ± 1.5	0.024 ± 0.005	38.3 ± 3.7	0.050 ± 0.011
<i>P. patens</i>	48.1 ± 13	0.043 ± 0.003	54.6 ± 13	0.058 ± 0.016
<i>P. mugo</i>	48.4 ± 5.0	0.028 ± 0.01	48.8 ± 7.5	0.054 ± 0.017
<i>D. carota</i>	39.4 ± 8.6	0.016 ± 0.002	43.6 ± 4.4	0.045 ± 0.014
<i>N. tabacum</i>	48.5 ± 15	0.027 ± 0.002	48.1 ± 5.4	0.030 ± 0.013
<i>Z. mays</i>	30.0 ± 4.6	0.012 ± 0.003	34.4 ± 4.8	0.048 ± 0.008

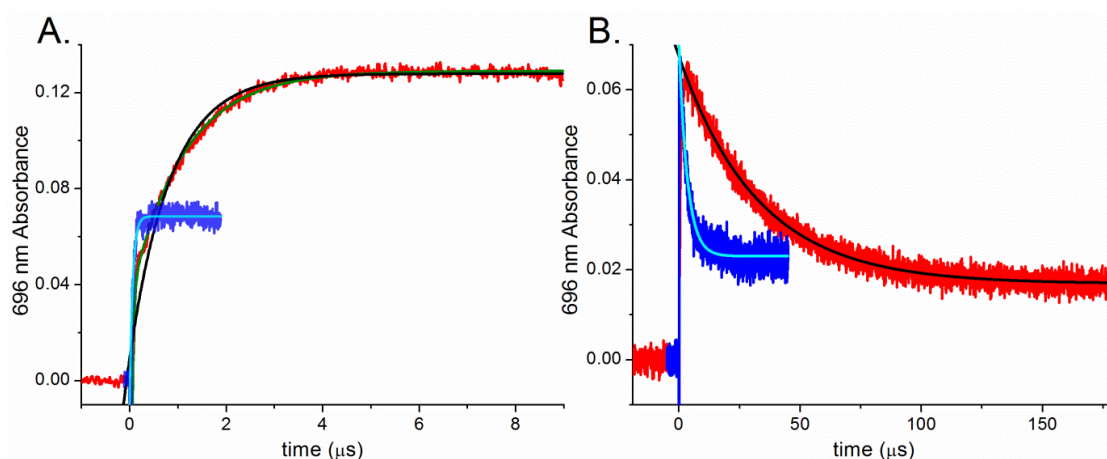


Figure 5.3. Kinetic transients at 696 nm showing rates of hydride and proton transfer for *N. punctiforme* (red) and *N. tabacum* (blue) POR. Samples contained 100 μM of each POR enzyme, 30 μM Pchl_a, 3 mM NADPH, 0.1 % genapol, 0.1 % 2-mercaptoethanol in activity buffer (black). The absorbance changes at 696 nm were measured following laser photoexcitation at 450 nm at 4 (A) and 25°C (B) as described in the *Materials and Methods*. A. The increase in absorbance at 696 nm was fitted to a single exponential (black and cyan) to obtain the rate of hydride transfer. In the case of *N. punctiforme* (cyanobacterium) POR the data were also fitted to a double exponential equation (green) to achieve a better fit. B. The decrease in absorbance was fitted to a single exponential (black and cyan) to obtain the rate of proton transfer.

To explore the origin of the faster rate of hydride transfer the excited state dynamics were investigated by transient pump-probe spectroscopy in the visible region for 5 POR homologues that span the evolutionary timescale. Conventional ultrafast pump-visible absorption-probe measurements over timescales up to ~ 3 ns (‘fast’ datasets) were coupled to those using a transient absorption spectrometer that uses an electronical delay of the probe pulse (‘slow’ datasets) to provide continuous temporal coverage from ps to μs . The time-resolved absorption difference spectra from these measurements were then modelled using global analysis to yield species associated difference spectra (SADS). For clarity only the SADS are shown in the main manuscript, whereas the raw time-resolved data (Figures S5.5) can be found in the supporting information. In all cases, the observed transient spectral changes appear to be fairly similar for all PORs for the ‘fast’ datasets with a ground state bleach (GSB) of Pchl_a at approximately 635 nm and the formation of excited state absorption (ESA) bands on either side of this band (Figure 5.4). The decay of these excited state features can be fitted to a single exponential function for the ‘fast’ datasets to form SADS, 2 on timescales ranging from ~ 350 ps to 1.3 ns. It should be noted that the negative feature at approximately 675 nm is a result of the Chlide product that accumulates during the

course of the measurements and therefore this was minimised by limiting the length of data acquisition to <5 minutes.

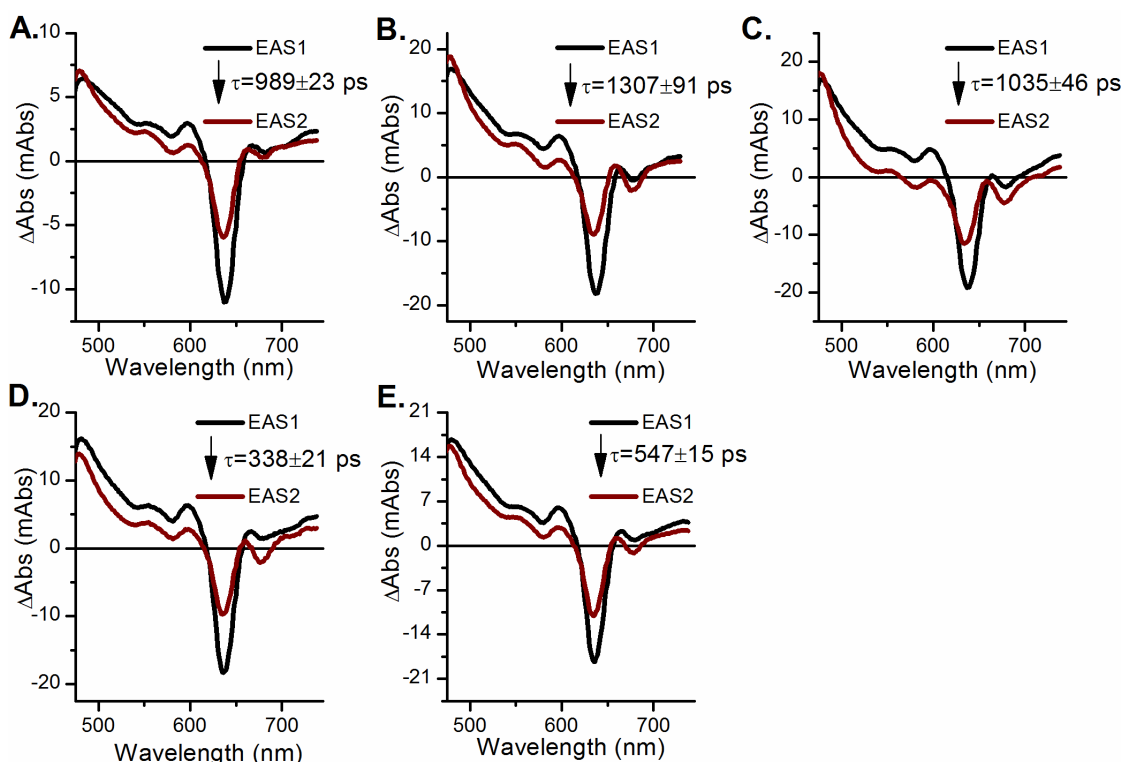


Figure 5.4. Species associated difference spectra (SADS) resulting from a global analysis of time-resolved ‘fast’ absorption data for different POR homologues. SADS are shown for POR from *N. punctiforme* (A), *C. reinhardtii* (B), *P. patens* (C), *D. carota* (D), and *Z. mays* (E) after excitation at 450 nm. The data were fitted to the sequential model as shown within each panel as described in the *Materials and Methods*, and the transition lifetime is shown as τ .

In the ‘slow’ datasets the time-resolved spectral changes from 5 ns to 0.5 μ s (or 2 μ s for the cyanobacterial PORs) were fitted to a single step, sequential model to yield the SADS shown in figure 5.5. The formation of the hydride transfer intermediate, with the characteristic absorbance band at 696 nm, can be observed for all of the POR enzymes. Although previous models have shown that a long-lived triplet state is present on these timescale (Heyes *et al.* 2015), for clarity we have modelled the data based on the assumption that the triplet state is formed within the 5 ns time window of the ‘slow’ data with only minor decay of the species over the 2 μ s timescale. Hence, the spectral features associated with the hydride transfer step will also contain a minor component from the triplet state, although this should be consistent for all of the POR homologues. The resulting lifetimes show clear differences for the formation of hydride transfer intermediate for each of the homologues, in accordance with the rates

of hydride transfer obtained in the laser-flash photolysis experiments (Table 5.1). This confirms that the rate of hydride transfer is approximately 5-10 fold higher for the eukaryotic PORs compared to the cyanobacterial enzymes.

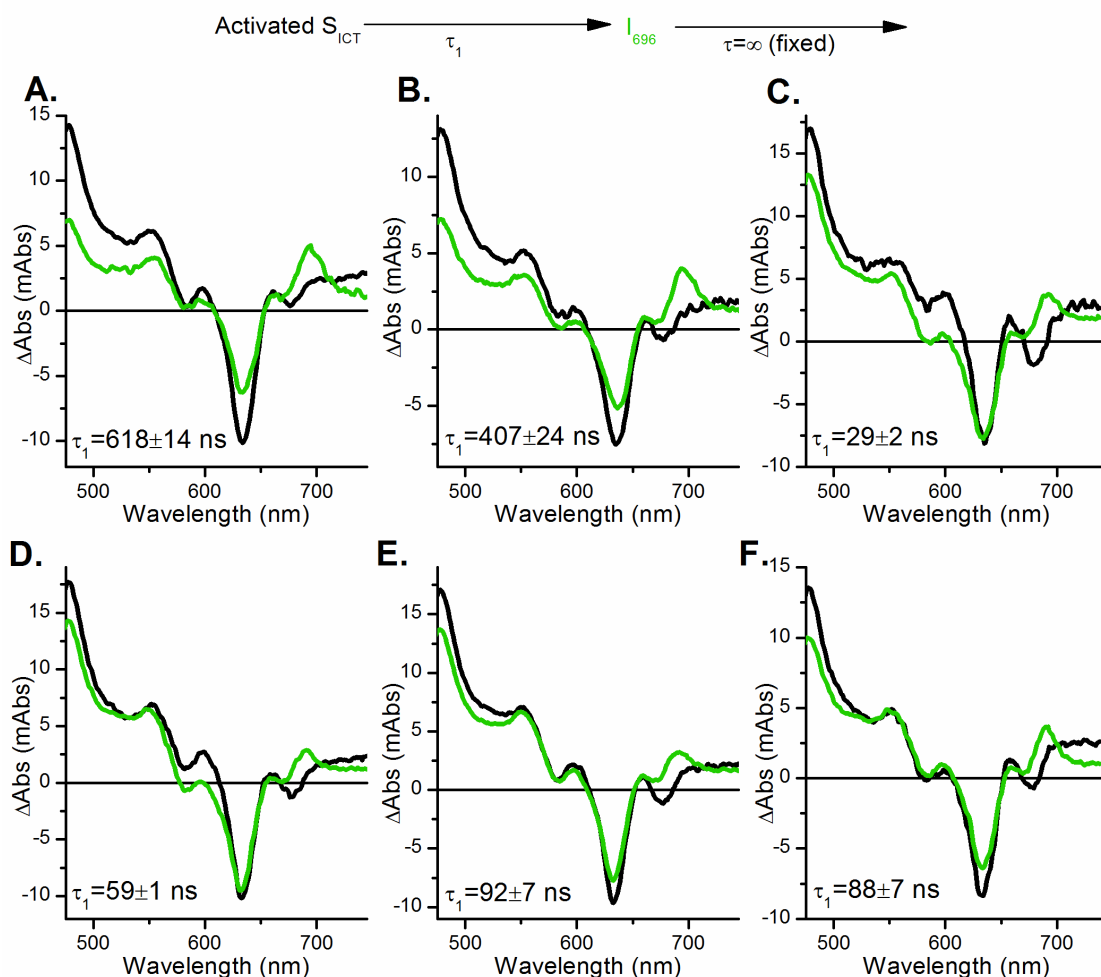


Figure 5.5. Species associated difference spectra (SADS) resulting from a global analysis of time-resolved ‘slow’ absorption data (5 ns to 0.5 μ s or 2 μ s) for different POR homologues. SADS are shown for POR from *N. punctiforme* (A), *C. reinhardtii* (B), *P. patens* (C), *D. carota* (D), *N. tabacum* (E), and *Z. mays* (F) after excitation at 450 nm. The data were fitted to the sequential model above the panel as described in the *Materials and Methods*.

5.4.3. Proton transfer step:

The rate of the thermally-activated proton transfer step was measured by fitting the decrease in absorbance at 696 nm that follows the hydride transfer step to a single exponential equation (figures 5.3 B, S5.5 and Table 5.2). Proton transfer is faster for all eukaryotic PORs compared to the cyanobacterial enzymes (Table 5.2), consistent with a smaller reaction barrier for the reaction. The dependence of solvent viscosity on the rate of proton transfer was investigated to study the extent of solvent control on the internal protein dynamics for this reaction. There were major differences in the viscosity dependence of the proton transfer reaction for each of the POR enzymes, reflecting different dynamical control (Figures 5.5, S5.6 and Table 5.2, S5.2). The effect of viscosity on the observed rate of proton transfer was fitted to equation 5.1 to describe the contribution of the protein friction to the total friction of the system, where a low σ -value indicates a high level of solvent-coupled dynamics required for the reaction (Heyes *et al.* 2009, Ansari *et al.* 1992, Ivkovic-Jensen & Kostic 1997). The rate constant for proton transfer in the cyanobacterial enzymes is very sensitive to changes in the solvent viscosity (~0.2 and 0.5 cP), suggesting that a network of long-range and solvent-slaved protein motions are required for proton transfer. In contrast, the rate constant for proton transfer exhibits only a minimal or no dependence on solvent viscosity for the eukaryotic POR proteins.

Table 5.2. Rates and solvent viscosity-dependence of the proton transfer step for the POR homologues. The rates of proton transfer for POR from cyanobacteria (red), algae (gold), bryophyte (green), gymnosperm (purple) and angiosperms (blue) were measured following laser photoexcitation at 450 nm at 25°C as described in the *Materials and Methods*. The viscosity-dependence of the rate was fitted to equation 5.1 to obtain the protein's friction contribution (σ) and an estimate for the free energy of the reaction (ΔG). A low σ -value indicates a bigger influence of viscosity on the rate.

	Protonation rate (s^{-1} , $\times 10^4$)	σ -value (cP)	ΔG (kJ/mol)
<i>L. majuscula</i>	1.0 ± 0.2	0.47 ± 0.25	47.4 ± 0.2
<i>N. punctiforme</i>	3.1 ± 0.2	0.21 ± 0.14	50.1 ± 0.2
<i>C. reinhardtii</i>	23.5 ± 2.9	71.0 ± 19	42.8 ± 0.1
<i>C. merolae</i>	21.5 ± 1.7	33.3 ± 10	42.6 ± 0.1
<i>P. patens</i>	24.1 ± 1.8	90.5 ± 104	42.2 ± 0.1
<i>P. mugo</i>	22.5 ± 0.1	37.3 ± 22	42.2 ± 0.1
<i>D. carota</i>	22.7 ± 2.3	$>>300$	42.6 ± 0.1
<i>N. tabacum</i>	40.8 ± 3.3	16.3 ± 3.4	40.9 ± 0.1
<i>Z. mays</i>	17.6 ± 0.7	19.4 ± 5.7	42.8 ± 0.1

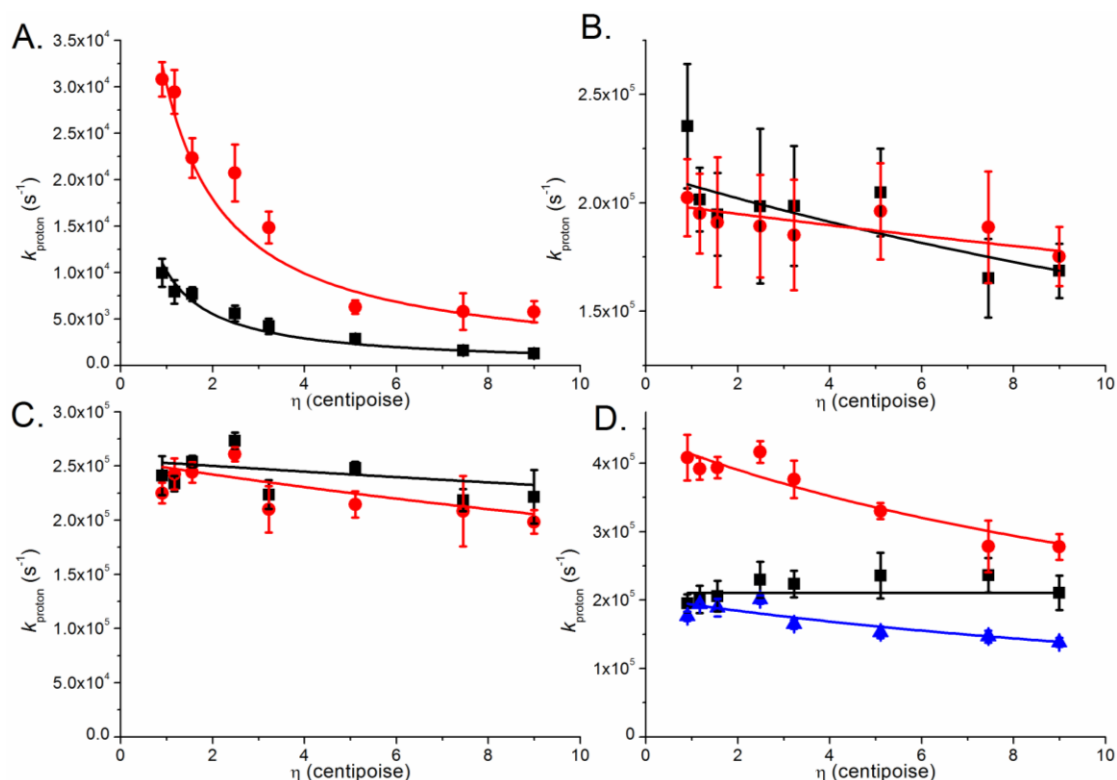


Figure 5.6. Proton transfer rate as a function of solvent viscosity for all POR homologues. The rates of proton transfer were measured at different glycerol concentrations following laser photoexcitation at 450 nm at 25°C as described in the *Materials and Methods*. The data were fitted to equation 5.1 to derive the σ value as an estimate of the level of solvent-coupled protein dynamics. A. Data for the cyanobacterial PORs, including *L. majuscula* (black squares) and *N. punctiforme* (red circles). B. Data for the PORs from algae, including *C. reinhardtii* (black squares) and *C. merolae* (red circles). C. Data for the enzymes from non-flowering land plants, including *P. patens* (black squares) and *P. mugo* (red circles). D. Data for the angiosperm PORs, including *D. carota* (black squares), *N. tabacum* (red circles) and *Z. mays* (blue triangles).

5.4.4. Thermodynamic analysis of the proton transfer step

A thermodynamic analysis of the proton transfer step was performed for three of the POR homologues from different evolutionary origins, one from cyanobacteria (*N. punctiforme*), one from algae (*C. reinhardtii*) and one from angiosperms (*Z. mays*). Laser photoexcitation experiments were repeated at a range of temperatures between 5 °C and 40 °C and the temperature-dependence of the proton transfer rates were analysed in the form of an Eyring plot (Figure 5.6). Activation enthalpies (ΔH^\ddagger) and entropies (ΔS^\ddagger) were estimated from fitting the data to the Eyring equation (equation 5.2):

$$\ln\left(\frac{k}{T}\right) = \frac{-\Delta H^\ddagger}{RT} + \frac{\Delta S^\ddagger}{R} + \ln\left(\frac{k_B}{h}\right) \quad 5.2$$

where k is the rate of the reaction in s^{-1} ; T is temperature; ΔH^\ddagger and ΔS^\ddagger are the standard enthalpy and entropy of the transition state; k_B is the Boltzmann's constant, h is the Planck constant and R is the universal gas constant. A non-linear function was used to fit the curvature in the Eyring plot of *Z. mays* (Figure 5.7 C.) as shown by the dashed line (equation 5.3; Sharma & First 2009). The Gibbs free energy (ΔG^\ddagger) at 298K was calculated with equation 5.4 (Segal 1976, Sharma & First 2009). All of the calculated thermodynamic parameters are shown in table 5.3.

$$\ln\left(\frac{k}{T}\right) = \frac{-\Delta H^\ddagger}{RT} + \frac{\Delta S^\ddagger}{R} + \frac{\Delta C_p}{R} * \left\{-1 + \frac{T_0}{T} + \ln\left(\frac{T_0}{T}\right)\right\} + \ln\left(\frac{k_B}{h}\right) \quad 5.3$$

With k is the rate of proton transfer; R the universal gas constant; h is Planck's constant; k_B the Boltzmann constant; T_0 and T are the reference temperature at 298 K and temperature, respectively; ΔS , ΔH , and ΔC_p are entropy, enthalpy, and heat capacity for the transition state, respectively.

$$\Delta G = \Delta H - T\Delta S \quad 5.4$$

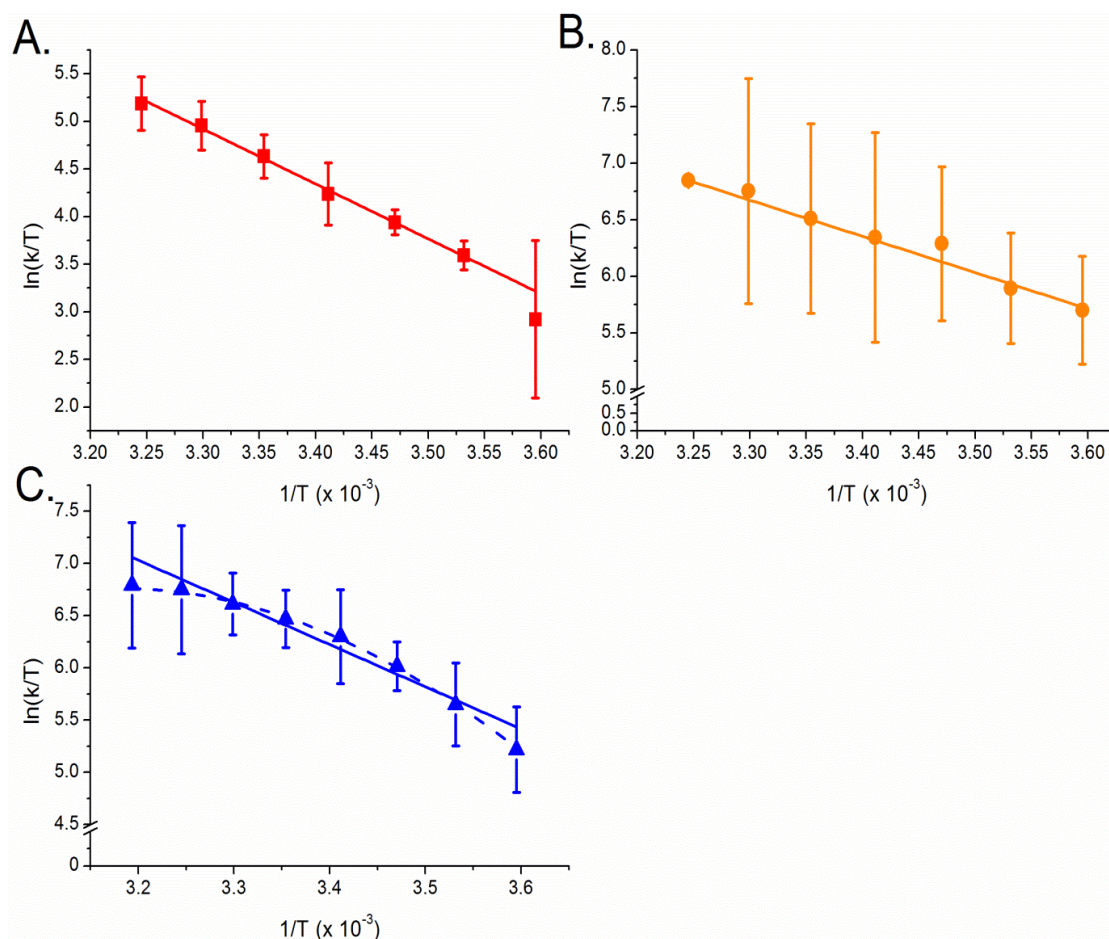


Figure 5.7. Temperature dependence of the rate constants for the proton transfer step for three POR homologues. Eyring plots of $\ln(k_{\text{obs}}/T)$ versus $1/T$ for the proton transfer step are shown for POR from the cyanobacteria *N. punctiforme* (A), the algae *C. reinhardtii* (B) and for the higher plant *Z. mays* (C). Data are shown fitted to the Eyring equation although a more accurate fit of data in graph C is achieved by using equation 5.3 due to the curvature of the Eyring plot. Activation enthalpies, ΔH^\ddagger , and activation entropies, ΔS^\ddagger , are shown in table 5.3. Error bars are calculated from the average of at least 5 kinetic traces.

Table 5.3. The thermodynamic parameters derived from fitting the data in figure 5.6. ΔG^\ddagger was calculated by using equation 5.4 and a temperature of 298 K.

	<i>N. punctiforme</i>	<i>C. reinhardtii</i>	<i>Z. mays</i>
ΔH^\ddagger (kJ/mol)	47.9 ± 1.4	26.6 ± 1.0	33.6 ± 3.4
ΔS^\ddagger (J/mol)	1.57 ± 4.8	-54.3 ± 3.2	-31.6 ± 11
ΔG^\ddagger (kJ/mol)	47.5 ± 1.4	42.8 ± 1.0	43.0 ± 3.4

5.5. Discussion

How enzymes have evolved to optimise the protein dynamics that allow their extraordinary rate enhancements is currently one of the most challenging questions in enzymology (Eisenmesser *et al.* 2002, Henzler-Wildman *et al.* 2007, Yahashiri *et al.*

2008, Nagel & Klinman 2010, Bandaria *et al.* 2009, Heyes *et al.* 2009, Pisliakov *et al.* 2009, Klinman & Kohen 2013). The light-driven enzyme POR is one of the few enzyme systems that allow this problem to be addressed as the catalytic mechanism is well understood and it has an evolutionary history with distinct cyanobacterial and eukaryotic lineages (Yang & Cheng 2004). Previous studies have shown that variable patterns of structural conservation are found among POR enzymes from different evolutionary backgrounds, which has led to the hypothesis that two distinct approaches exist for the evolution of dynamics associated with catalysis (Heyes *et al.* 2011). Based on results on a very limited subset of POR enzymes it was proposed that only localised, conserved protein motions are required for light-driven hydride transfer, whereas the dynamics coupled to the proton transfer step vary depending on evolutionary origin (Heyes *et al.* 2011). However, it is important to note that only 4 different POR enzymes were used in this study and as only one of those was from a eukaryotic, plant origin (*Arabidopsis thaliana*) further validation of this hypothesis is required. Consequently, we have now extended this analysis to include a range of PORs from a broad evolutionary background, including cyanobacteria, algae, bryophytes, gymnosperms and angiosperms. We have measured rates for the two H-transfer steps in the reaction for all of the POR enzymes and have used the solvent viscosity-dependence of the reaction rates to provide further information on the nature of any protein motions linked to the reaction chemistry.

Steady-state measurements on the POR enzymes revealed that some of the plant enzymes show substrate inhibition, even at relatively low Pchl_a concentrations (<10 μ M; see Table 4.2 and Figure 4.17 and 4.18). As no inhibition was observed for the homologues from any of the other organisms, it can be proposed that this phenomenon may play a role in prolamellar body formation. This in turn is known to be important for chloroplast development and consequently for the plant as a whole (Grzyb *et al.* 2013, Cortleven & Schmulling 2015). It is possible that in higher plants prolamellar body formation is regulated by the rate of turnover of POR, which then becomes inhibited at higher concentrations of Pchl_a.

Significantly, there is a considerable increase (approximately 5-10 fold) in the rate of the hydride transfer step for all eukaryotic POR enzymes compared to those from a prokaryotic, cyanobacterial origin, implying a closer positioning of the NADPH and Pchl_a molecules in the active site. This rate of hydride transfer for the plant and algal PORs ($\sim 10^7$ s⁻¹ at 298 K) is significantly faster than any other known hydride transfer

reaction in biology. However, it appears as though the excited state processes that lead to hydride transfer are very similar in all of the POR enzymes, with almost identical spectral changes and only minor differences in the lifetime of a proposed excited state charge transfer state, suggesting that the initial photochemistry has been optimised early in evolution. As this initial step has been shown to involve interactions between the excited state Pchl_a and a conserved Tyr residue it is logical that the active site geometry is optimally configured in all POR enzymes to facilitate this energetically unfavourable light-driven chemistry (Menon *et al.* 2009, Heyes *et al.* 2015). In agreement with previous findings, the rate of hydride transfer for all POR enzymes is independent of solvent viscosity (Heyes *et al.* 2009, 2011). Hence, this implies a lack of large-scale rearrangements for hydride transfer in all POR enzymes and confirms that this reaction chemistry is only controlled by localised protein motions through conservation of protein structure within the enzyme active site (Loveridge *et al.* 2011, Hay *et al.* 2008, Heyes *et al.* 2009, Frauenfelder *et al.* 2009).

The rate of proton transfer was also found to increase significantly for all eukaryotic POR homologues compared to their prokaryotic ancestors. However, in contrast to the hydride transfer step there were major differences in the dependence of the rate of the proton transfer reaction on solvent viscosity for each of the POR enzymes, which can be correlated with variability in the degree of solvent control on the protein dynamics required for this step. In agreement with previous measurements, all of the cyanobacterial enzymes showed a high degree of viscosity-dependence, which suggests that they require significant protein reorganisation to ensure that an optimum proton donor-acceptor distance is achieved (Heyes *et al.* 2011). Conversely, in the eukaryotic POR enzymes there is only a minimal dependence on solvent viscosity for the rate of proton transfer, implying that there is little, or no, role for large-scale, solvent-coupled protein dynamics during this stage of catalysis. It is likely that the faster proton transfers observed for all of the eukaryotic POR enzymes require only localised motions and suggests that optimisation of the active site architecture is likely to have occurred upon endosymbiosis for this step. Previous measurements have shown that evolutionary pressures have resulted in a much higher level of overall structural conservation among the eukaryotic PORs compared to the cyanobacterial enzymes (Heyes *et al.* 2011). This conservation of protein structure is likely to have reduced or removed the dependence on complex dynamical networks and coupling to solvent dynamics for the proton transfer step. Consequently, as the dynamic ‘reach’

from the active site is minimised in the eukaryotic enzymes, it can be concluded that evolution has ensured that the active site chemistry is less susceptible to the possible negative effects of distal mutations in the protein. In terms of the thermodynamic data for this step the algal and plant PORs have lower ΔH^\ddagger , ΔS^\ddagger , and ΔG^\ddagger values than the cyanobacterial POR, suggesting a low energy barrier for proton transfer in those enzymes. However, the curvature observed in the Eyring plot of *Z. mays* (Figure 5.6 C.) may be caused by a temperature-dependent change in enthalpy or alternatively, may be due to the presence of a number of different enzyme conformations (Sharma & First 2009).

In conclusion, we have now carried out a comprehensive evolutionary analysis of the dynamics required for catalysis in the light-activated POR enzyme. By extending our studies to include many new POR enzymes from a broad evolutionary spread we have been able to provide further evidence that the dynamics coupled to each step in the reaction has a distinct evolutionary origin. Protein dynamics coupled to the light-driven hydride transfer are conserved across all POR enzymes and are likely to be localised to the enzyme active site. This is suggestive of a strong evolutionary pressure to maintain an optimised reaction geometry in the active site due to the high stringency of this catalytic step. In contrast, the dynamical control of proton transfer is more variable, although it is likely that evolution has acted to optimise the reaction chemistry by employing only localised active site dynamics. It is likely that evolutionary pressures to localise the dynamics protects the enzyme from any deleterious, distal mutations in the protein and is more efficient than the long-range, complex networks of protein dynamics observed in the prokaryotic enzymes.

Supplementary information - Chapter 5

An evolutionary analysis of protein dynamics in the catalytic cycle of the light-driven enzyme protochlorophyllide oxidoreductase (POR).

Authors:

Robin Hoeven, Samantha O. J. Hardman, Nigel S. Scrutton and Derren J. Heyes

Affiliation:

Manchester Institute of Biotechnology, Faculty of Life Sciences, The University of Manchester, Manchester M1 7DN, United Kingdom

```

Lyngbya_majuscula -----
Nostoc_punctiforme -----
Thermosynechococcus_elongatus -----
Nicotiana_tabacum MALQAASLLPSAFSIHKEGKSCATLKDSSLFGVALSYNQKSKFIPPAAWN 50
Pinus_mugo -----
Daucus_carota MALQAASFLPSSFINKEGKANVSLKETSLSFGVTFSDSLRTDFSSLRTR- 49
Physcomitrella_patens -----
Marchantia_paleacea -----
Zea_Mays -----ASFLGVRLAADGLKLDTTALG----- 21
Chlamydomonas_rheinhardtii -----
Cyanidioschyzon_merolae -----

```

```

Lyngbya_majuscula -----MENDHKSTVIIITGASSGVG 19
Nostoc_punctiforme -----MVQDRKSTVVIITGASSGVG 19
Thermosynechococcus_elongatus -----MSDQPRPTVIIITGASSGVG 19
Nicotiana_tabacum KELTKKIAAVPIRAQIAATT-PAVNQSTSEQKTLRKGNVITGASSGLG 99
Pinus_mugo -----SKKTDKGNVITGASSGLG 20
Daucus_carota RGCRQISQGTGAIQSQAVATT-PSVNRATGEGKTLRKGSVIIITGASSGLG 98
Physcomitrella_patens -----SSKKTDTKSTVIIITGASSGLG 21
Marchantia_paleacea -----SSKKTATKSTCIIITGASSGLG 21
Zea_Mays LRTVVRVSSADIRAQTAAVSSPSVTPASPSGKTLRKGTAVITGASSGLG 71
Chlamydomonas_rheinhardtii -----ATQQKQTALIIITGASSGLG 18
Cyanidioschyzon_merolae -----GPKQSQIAVITGASSGVG 18

```

```

Lyngbya_majuscula LEAARALATTGWHVVMACRNLDKAEKAAQEVGIPKD-SYNTALYIDLASF 68
Nostoc_punctiforme LYAAKALAE-RGWYVVMACRDVAKAQLAAQSVGIPHQGSYTIMHIDLSSL 68
Thermosynechococcus_elongatus LYATKALANR-GWHVIMACRNLKAEQAANKLQIPPE-AYTILHLDLSSL 67
Nicotiana_tabacum LATAKAIGETGEWHVIMACRDFLKAERAAKSVGIPKE-NYTMHLDLSSL 148
Pinus_mugo LATAKALGESGKWHIIMACRDFLKAERMAKSVGIPKE-NYSVMHLDLSSL 69
Daucus_carota LATAKALAE-TGKWHVIMACRDFLKAERAAKSVGIPKE-NYTMHLDLSSL 147
Physcomitrella_patens LATAKVLADSGEWHVIMACRDFLKAERAAKSVGIPKE-NYTMHCDLSSL 70
Marchantia_paleacea LATAKALADTGEWHVIMACRDFLKAERAAKSVGIPKD-SYTVIHCDLASF 70
Zea_Mays LATAKALAE-TGKWHVIMACRDFLKAERAAKSVGIPKD-SFTVHLDLSSL 120
Chlamydomonas_rheinhardtii LNAAKALAA-TGEWHVIMACRDFLKAERAAKSVGIPKD-SYTVIHCDLSSL 67
Cyanidioschyzon_merolae LYAARALVNRGNWHVIMACRDIIDRAERAADSVNLPKD-AYTVLHCDLADF 67

```

```

Lyngbya_majuscula ASVRQFVNAFRATGRT--LDALVCNAAIYLPLSKEPLNPEGYELSVATN 116
Nostoc_punctiforme DSVRFVKNFRASGHS--LDALVCNAAIYMPILKEPLRSPEGYELTVTTN 116
Thermosynechococcus_elongatus ASVRGFVESFRALNRP--LRALVCNAAVYYPPLKEPIYSVDGYEITVATN 115
Nicotiana_tabacum ESVRFVDTFRRSGRP--LDALVCNAAVYLPTAKEPTFTADGFELSVGTN 196
Pinus_mugo ESVRFADNFRSGRP--LDVLVCNAAIYLPTAKLPTYTAEGFELSVGTN 117
Daucus_carota DSVRFVETFRSERP--LDVLVCNAAVYFPTAKEPTYTADGFELSVGTN 195
Physcomitrella_patens NSVKQFVDNFRSGRP--LDVLVCNAAVYLPTAKEPRYTADGFELSVGTN 118
Marchantia_paleacea DSVRAFVDNFRTERQ--LDVLVCNAAVYFPTDKEPKFSAEGFELSVGTN 118
Zea_Mays DSVRFVRNVRLKMP--IDVVVCNAAVYQPTAKEPSYTADGFEMSVGVN 168
Chlamydomonas_rheinhardtii ESVRFVQNFKASGR--LDALVCNAAVYLPTAKEPRFTADGFELSVGTN 115
Cyanidioschyzon_merolae ASVLKFEVRELSSVARVDHLALICNAAIWHPRDKKPRFTVDGIEETMQVC 117

```

Lyngbya_majuscula HLGHFLLCNLMLEDLNKSSSS--QPRLVIVGTVTANPKELGGKIPIAPPD 165
Nostoc_punctiforme HLGHFLLCNLMLEDLKSSS--EPRLVILGTVTHNPDELGGKIPP--RPD 162
Thermosynechococcus_elongatus HLGHFLLINLLEDLNKS PES-DKRLVILGTVTANRKELGGKIPIAPPD 164
Nicotiana_tabacum HLGHFLLSRLLDDDLKSDYP-QKRLIIVGSITGNTNTLAGNVPP--KAN 243
Pinus_mugo HLGHFLLARLELDDLKSSDFN-SKRVIIVGSITGNTNTLAGNVPP--KAN 164
Daucus_carota HLGHFLLSRLLDDDLNKSDYP-SKRLIIVGSITGNTNTLAGNVPP--KAN 242
Physcomitrella_patens HLGHFLLANLLMEDIQHKENNNRSRVIIIVGSITGNTNTVAGNVPP--KAN 166
Marchantia_paleacea HMGHFLLARLLMEDIQAKDS-LKRMIIVGSITGNSNTVAGNVPP--KAN 165
Zea_Mays HLGHFLLARLELDDLKSDYP-QKRLIIVGSITGNTNTLAGNVPP--KAN 215
Chlamydomonas_rheinhardtii HLGHFLLTNLLDDDLKNAPNK-QPRCIIVGSITGNTNTLAGNVPP--KAN 162
Cyanidioschyzon_merolae HLSHLLLCRELLPKLIKISRG---RIVFLTQTHTSPNSLP GKIPP--QAR 161

.:: * . : : : * : : : * . : : *:*

Lyngbya_majuscula LGDLKGFEFGFKPPI--MINGKAFKSGKAYKDSL CNMLTMRELHHRYH 213
Nostoc_punctiforme LGDLQGFAEGFKEPIS--MIDGKKFEPVKAYKDSVCNVLTMRHLQRHY 210
Thermosynechococcus_elongatus LGNLEGFEKEGFKKPIA--MINGKFFKSGKAYKDSL CNMLTARELHRRFH 212
Nicotiana_tabacum LGDLRGLSGGLNSLNCSPMIDGGEFDGAKAYKDSVCNM LTMQE FHRHF 213
Pinus_mugo LGDLRLAGGLNGVNI SPMDGGEFDGAKAYKDSVCNM LTMQE FHRHY 214
Daucus_carota LGDLRGLAGGLNGMNSSAMIDGA EFDGAKAYKDSVCNM LTMQE FHRHY 292
Physcomitrella_patens LGDLRLAGGLDGVR SSVIMIDGGEFDGAKAYKDSVCNM LTMQE MHRFH 216
Marchantia_paleacea LHGLRGLAGGLNGVNSSSMIDGGEFDGAKAYKDSVCNM FTMQE FHRHY 216
Zea_Mays LGDLRLAGGLNGVSSVMIDGGEFDGAKAYKDSVCNM LTMQE FHRHY 265
Chlamydomonas_rheinhardtii LGDLSGLAAGVPAAN--PMMDGGEFN GAKAYKDSKVACMM TVRMHQRFH 210
Cyanidioschyzon_merolae LGDLSGLAAGLGPQTG-MVDSGFPEPTKAY DAKAANVLTKALSDRYG 210

.* : * . : : * . *** : . : * : : *

Lyngbya_majuscula DSTGIVFSSLYPGCAETALFRNHYSLFQ-KLFPLFQKNIT KGYVSQELA 262
Nostoc_punctiforme ESTGIVFNSLYPGCAETPLFRNHYP LFQ-KIFPLFQKYIT KGYVSQELA 259
Thermosynechococcus_elongatus ESTGIVFNSLYPGCADT PLFRHHFP LFQ-KLFPLFQKKITGGYVSQELA 261
Nicotiana_tabacum EETGIAFASLYPGCIATGLFRNHIP LF-ALFPPFQKYIT KGYVSEAEA 342
Pinus_mugo EETGITFASLYPGCIATTGLFREHIPLFR-LLFPPFQKYIT KGVFVEEEA 263
Daucus_carota EETGITFASLYPGCIATTGLFREHIP LF-RLFPPFQKYIT KGYVSEAES 341
Physcomitrella_patens EKTGVTFASLYPGCIATTGLFREHYSLF-RLFPPFQKYIT KGYVSEES 265
Marchantia_paleacea AETGITFSSLYPGCIAETGLFRNHVTLFR-RLFPPFQKYIT KGYVSEEEA 264
Zea_Mays EETGVTFASLYPGCIATTGLFREHIPLFR-LLFPPFQKYIT KGYVSEEEA 314
Chlamydomonas_rheinhardtii DATGITFASLYPGCIAETGLFREHVPLFK-RLFPPFQKYIT KGYVSEEEA 259
Cyanidioschyzon_merolae RD-GVTSVAIFPGCVADSNLFREKRGWFRHVFFPILQ KYIT RQYVP NDEA 259

*.: : : **.* : : **.* : * . : **.* ** * : . : :

Lyngbya_majuscula GDRLATVVADPNYNKSGVYW SWGNRQKEGRKSFVQVESNEAMD DS KAKRL 312
Nostoc_punctiforme GERVA AVADPEYNQSGVYW SWGNRQKEDGKSFVQKVSP QARD DD DKGDRL 309
Thermosynechococcus_elongatus GERVAVVADPEFRQSGVHWSWGNRQKEGRKAFVQELS AEAS DEQKARRL 311
Nicotiana_tabacum GKRLAQVVRDP SLKSGVYWSWNNTSS----SFENQLS KEASDAEKAKKL 388
Pinus_mugo GKRLAQV VSNPSLT KSGVYWSWNNSG----SFENQLSEEASD PEKAKKL 309
Daucus_carota GKRLAQV VSEPSLT KSGVYWSWNKDSA----SFENQLSEEASD VEKARKV 387
Physcomitrella_patens GRRLAQV VSDPSMNKSGVYWSWNQSG----SFENELS QEASDAEKAKKL 311
Marchantia_paleacea KRMAQV VSDPKLSKSGVYWSWNKD SG----SFENELS EEASDAEKAKKL 310
Zea_Mays GKRLAQV VSDPSLT KSGVYWSWNKNSA----SFENQLSEEASD ADKAKKL 360
Chlamydomonas_rheinhardtii GRRLAAVIS DPKL NKSGAYWSWSSTTG----SFDNQV SEEVADDS KASKL 305
Cyanidioschyzon_merolae GRRVA EVATQGQFS DSGSYQWRGKYTEGREKTPKQVIEPTYE IDKADQL 309

* **.* : . . ** : : * : : **.* : : . : *. : :

Lyngbya_majuscula WELSEKLVGLR----- 323
Nostoc_punctiforme WQLSAKLVGLA----- 320
Thermosynechococcus_elongatus WELSEKLVGLA----- 322
Nicotiana_tabacum WEVSEKLVGLA----- 399
Pinus_mugo WEISEKLVGLA----- 320
Daucus_carota WEVSEKLVGLA----- 398
Physcomitrella_patens WEVSEKLVGLA----- 322
Marchantia_paleacea WELSERLSGLV----- 321
Zea_Mays WEISEKLVGLA----- 371
Chlamydomonas_rheinhardtii WDISA KLVGLSA----- 317
Cyanidioschyzon_merolae YELSLDLIDQALRRR GLKSTILAPV 334

*** * *

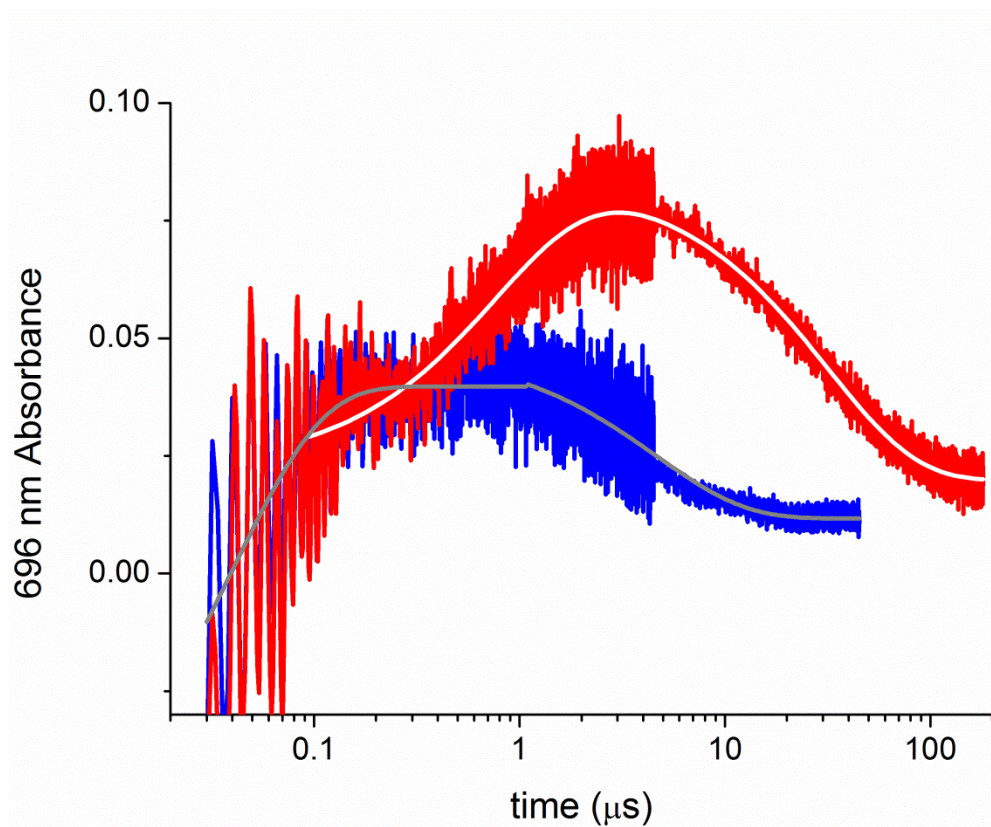


Figure S5.2. Representative transients showing the absorbance changes at 696 nm for the hydride and proton transfer steps on a log scale. The data in red are for the ‘slow’ cyanobacterial POR from *N. punctiforme*, while the data in blue are from a ‘fast’ reaction for the ‘evolved’ higher plant enzyme from *P. mugo*. Formation of an intermediate (hydride transfer) with an absorbance maximum at 696 nm is followed by proton transfer (decay in absorbance at 696 nm) to form the Chlide product.

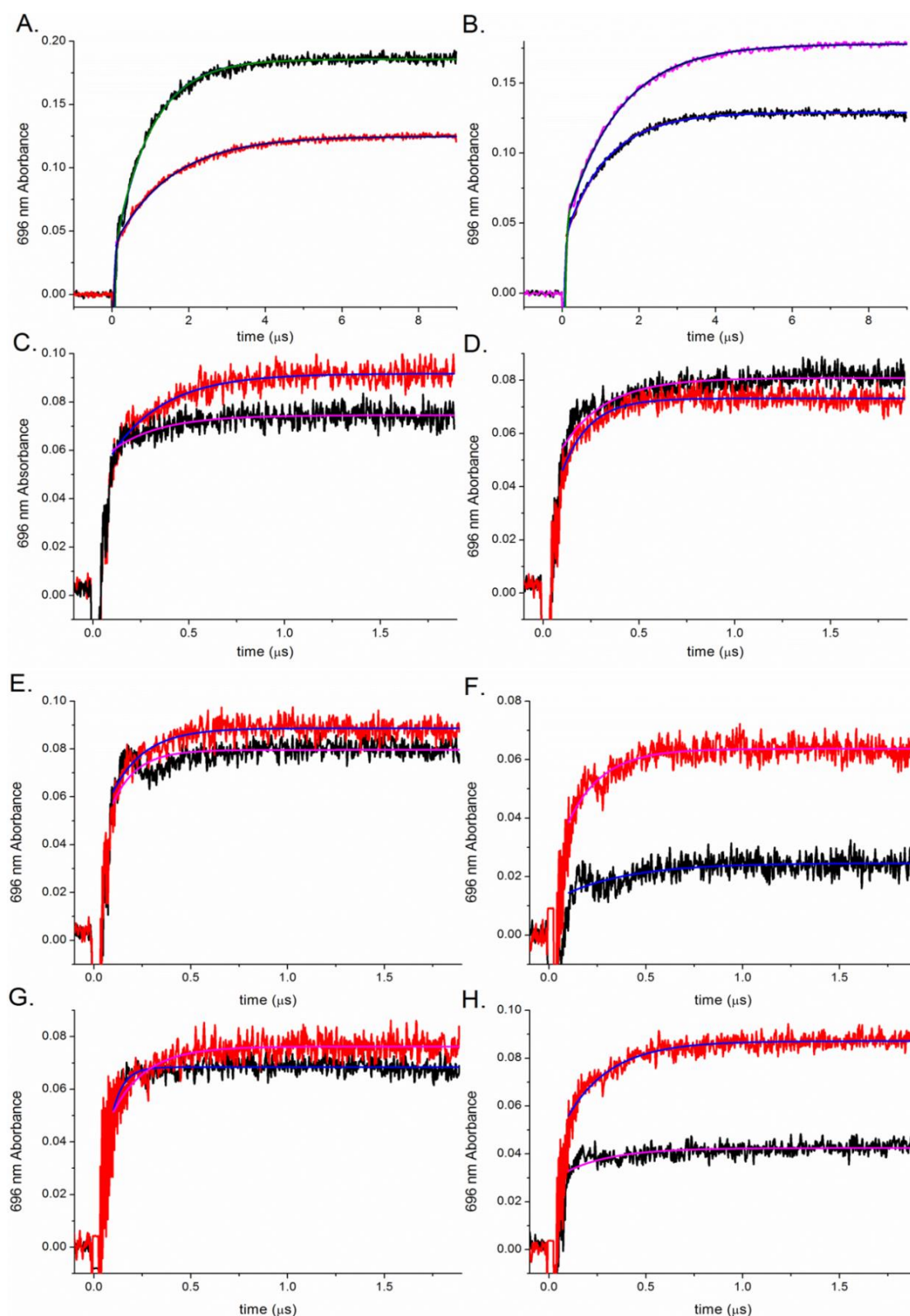


Figure S5.3. Transients for hydride transfer for all POR homologues at 4°C. Samples contained 100 μM of each POR enzyme, 30 μM Pchl_a, 3 mM NADPH, 0.1 % Genapol and 0.1 % 2-mercaptoethanol in activity buffer with 0 % glycerol (black) and with 60 % glycerol (red). Fitting of the data was done to both a single (blue and cyan) and a double (green and purple) exponential equation for POR from *L. majuscula* (A) and *N. punctiforme* (B). POR from *C. reinhardtii* (C), *P. patens* (D), *P. mugo* (E), *D. carota* (F), *N. tabacum* (G) and *Z. mays* (H) were fitted to a single exponential equation from approximately 100 ns onwards.

Table S5.1. The rates of hydride transfer for the cyanobacterial POR homologues at 4°C obtained by fitting to a double exponential equation. The data were fitted to a double exponential equation, where the first rate constant (k_1) was fixed at $3 \times 10^7 \text{ s}^{-1}$ and the calculated rate constants for hydride transfer (k_2) and their respective amplitudes are shown.

	0 % glycerol		60 % glycerol	
	k_{hydride} (s^{-1} , $\times 10^5$)	Amplitude (Abs)	k_{hydride} (s^{-1} , $\times 10^5$)	Amplitude (Abs)
<i>L. majuscula</i>	11.1 ± 0.4	$0.149 \pm 0.013 \times 10^{-1}$	7.6 ± 0.4	0.089 ± 0.023
<i>N. punctiforme</i>	9.1 ± 0.9	0.083 ± 0.017	7.1 ± 0.7	0.081 ± 0.058
<i>T. elongatus</i>	9.9 ± 0.3	0.072 ± 0.023	9.0 ± 0.5	0.069 ± 0.009

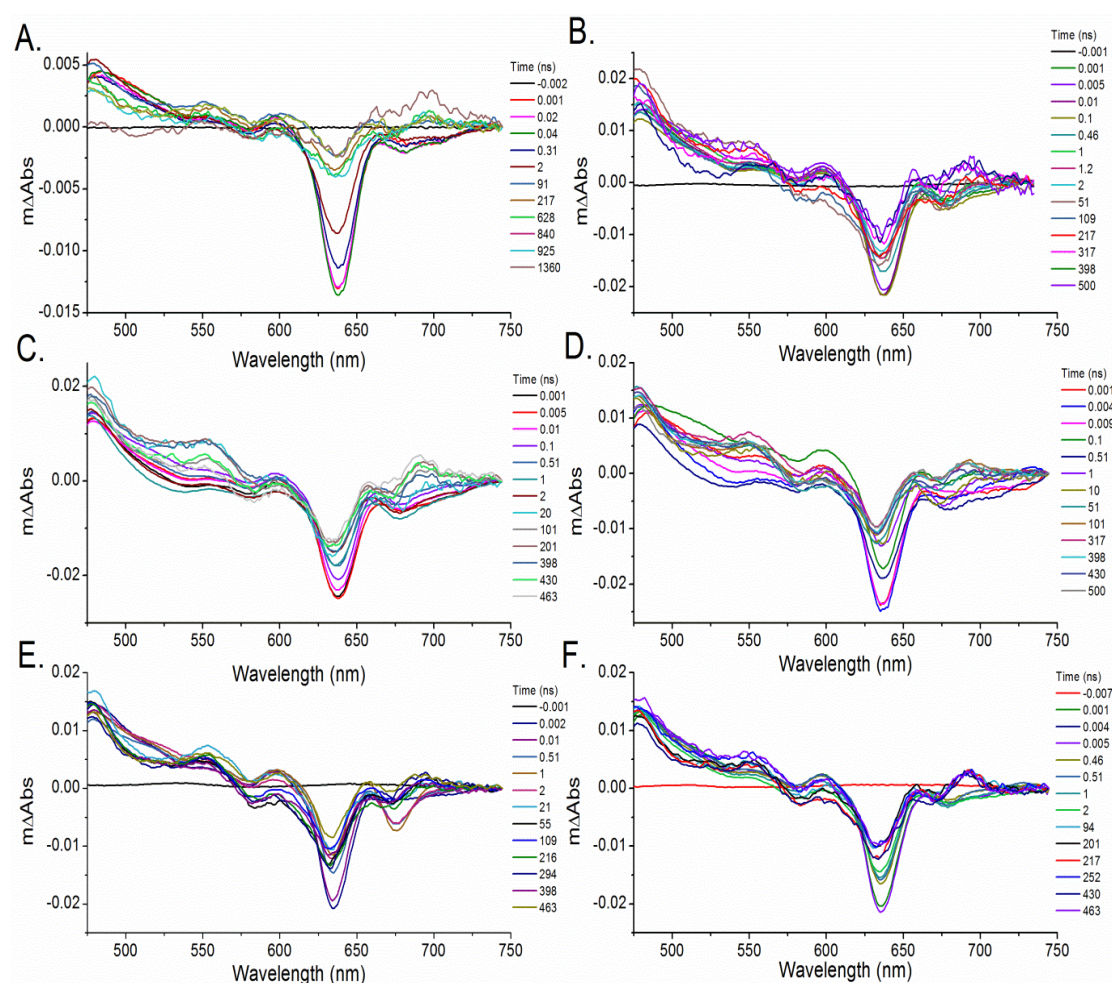


Figure S5.4. Time-resolved spectroscopy data for three representative POR homologues after photoexcitation with a laser pulse centred at ~450 nm. Time-resolved difference spectra were recorded between 1 ps and 2 μs (A) or 0.5 μs (B, C, D, E, and F) as described in *Materials and methods* for POR from *N. punctiforme* (A), *C. reinhardtii* (B), *P. patens* (C), *D. carota* (D), *N. tabacum* (E), and *Z. mays* (F).

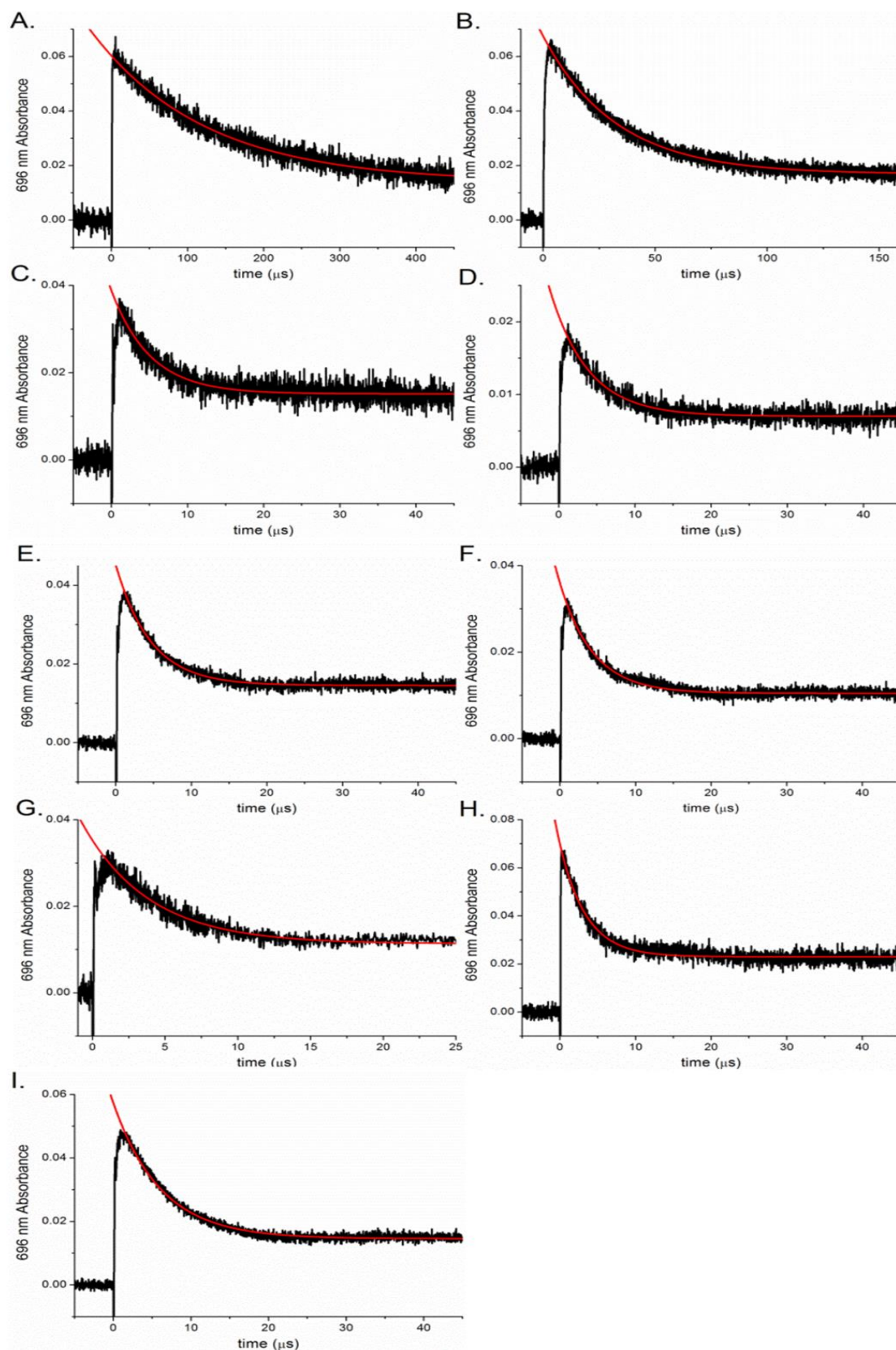


Figure S5.5. Transients for proton transfer for all POR homologues at 25°C. Samples contained 100 μM of each POR enzyme, 30 μM Pchlide, 3 mM NADPH, 0.1 % Triton X-100 and 0.1 % 2-mercaptoethanol in activity buffer. The red lines are the single exponential fits used to calculate the rates of proton transfer (table 5.2) for POR from *L. majuscula* (A), *N. punctiforme* (B), *C. reinhardtii* (C), *C. merolae* (D), *P. patens* (E), *P. mugo* (F), *D. carota* (G), *N. tabacum* (H) and *Z. mays* (I).

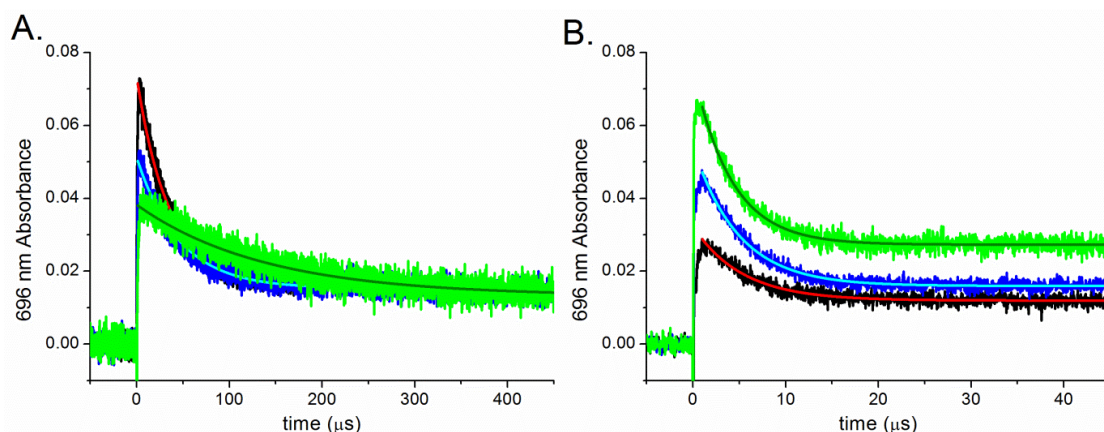


Figure S5.6. Comparison of the proton transfer transients for a viscosity-dependent and viscosity-independent POR homologue. Samples contained 50 μM of each POR enzyme, 15 μM Pchl a , NADPH is 10x NADPH K_m for respective protein, 0.1 % Triton X-100, 0.1 % 2-mercaptoethanol in activity buffer with added glycerol to make up a solvent viscosity of 0.9 cP (black), 1.42 cP (blue), and 3.98 cP (green). A. Rate of proton transfer for *N. punctiforme* decreases with increase in solvent-viscosity. B. Rate of proton transfer for *D. carota* remains similar at all solvent-viscosities.

Table S5.2. Rates of proton transfer at different solvent viscosities for all POR homologues. The data were fitted to a single exponential equation and the resulting rate constants at each of the solvent-viscosities are shown for POR from cyanobacteria (red), algae (gold), bryophyte (green), gymnosperm (purple) and angiosperms (blue). k_{proton} is the protonation rate constant.

η (cP)	<i>L. majuscula</i> k_{proton} (s^{-1} , $\times 10^3$)	<i>N. punctiforme</i> k_{proton} (s^{-1} , $\times 10^4$)	<i>C. reinhardtii</i> k_{proton} (s^{-1} , $\times 10^5$)	<i>C. merolae</i> k_{proton} (s^{-1} , $\times 10^5$)
0.90	9.97 ± 1.5	3.08	2.35 ± 0.3	2.02 ± 0.2
1.17	8.10 ± 1.2	2.94	2.01 ± 0.3	1.95 ± 0.2
1.56	7.41 ± 0.7	2.23	1.95 ± 0.2	1.91 ± 0.3
2.49	5.76 ± 0.1	2.07	1.98 ± 0.4	1.89 ± 0.2
3.22	4.72 ± 0.3	1.48	1.99 ± 0.3	1.85 ± 0.3
5.11	2.75 ± 0.2	0.63	2.05 ± 0.2	1.96 ± 0.2
7.45	1.59 ± 0.04	0.57	1.65 ± 0.2	1.89 ± 0.3
9.0	1.22 ± 0.1	0.57	1.65 ± 0.1	1.75 ± 0.1

η (cP)	<i>P. patens</i> k_{proton} (s^{-1} , $\times 10^5$)	<i>P. mugo</i> k_{proton} (s^{-1} , $\times 10^5$)	<i>D. carota</i> k_{proton} (s^{-1} , $\times 10^5$)	<i>N. tabacum</i> k_{proton} (s^{-1} , $\times 10^5$)	<i>Z. mays</i> k_{proton} (s^{-1} , $\times 10^5$)
0.9	2.41 ± 0.2	2.25 ± 0.1	1.95 ± 0.1	4.08 ± 0.3	1.76 ± 0.1
1.17	2.34 ± 0.1	2.43 ± 0.1	2.01 ± 0.2	3.92 ± 0.2	1.94 ± 0.04
1.56	2.54 ± 0.1	2.44 ± 0.1	2.06 ± 0.2	3.93 ± 0.2	1.89 ± 0.1
2.49	2.73 ± 0.1	2.61 ± 0.1	2.30 ± 0.3	4.16 ± 0.2	2.01 ± 0.1
3.22	2.24 ± 0.1	2.10 ± 0.2	2.24 ± 0.2	3.76 ± 0.3	1.65 ± 0.1
5.11	2.48 ± 0.1	2.15 ± 0.1	2.36 ± 0.3	3.30 ± 0.1	1.53 ± 0.1
7.45	2.19 ± 0.1	2.08 ± 0.3	2.36 ± 0.3	3.78 ± 0.4	1.47 ± 0.1
9.0	2.22 ± 0.2	1.98 ± 0.1	2.11 ± 0.3	3.78 ± 0.2	1.38 ± 0.1

Chapter 6

Discussion

6.1. Discussion

Within this thesis we set out to study the dynamics that are linked to catalysis in the unique light-activated enzyme, protochlorophyllide oxidoreductase (POR) through a variety of methods. The enzyme from *Thermosynechococcus elongatus* has been extensively studied previously (McFarlane *et al.* 2005, Heyes *et al.* 2009a, 2009b, 2011) and hence, was considered a good starting point to investigate the effects of pressure on the rate of the two H-transfer steps in the reaction. The effects of hydrostatic pressure have been suggested to be a possible probe of dynamics coupled to H-transfer reactions (Northrop 2006, Hay & Scrutton 2008). To infer how enzyme dynamics are affected by pressure in POR the influence of pressure on the KIE of both the hydride and proton transfer reactions was measured. A comparison of these pressure-effects with those carried out on other enzymes does not identify a uniform mode of action for pressure on the enzyme dynamics along the reaction coordinate (Hay *et al.* 2007, Johannissen *et al.* 2011, Pudney, McGrory, *et al.* 2009, Pudney *et al.* 2013). Consequently, a case by case interpretation of the data is advised, which ideally requires complementary structural and computational modelling techniques to pinpoint a more accurate model for the effects of pressure on the protein motions required for catalysis. The current lack of structural data for POR therefore prevents an in-depth interpretation of the data.

In Heyes *et al.* (2011) it was proposed that POR underwent a twin-track evolution of the protein dynamics involved in the hydride and proton transfer steps. We have confirmed this to be the case by studying POR homologues from a much wider evolutionary spread than in the original study (Heyes *et al.* 2011). We started by expression and purification of these enzymes, which required a few optimisation steps to achieve an acceptable amount of protein. Interestingly, one of the species of algae, *Cyanidioschyzon merolae*, is known to grow in high sulphur, acidic, hot spring environments (45°C, pH 1.5; Matsuzaki *et al.* 2004) and hence, in the future it may be possible to improve the yield of this enzyme by performing the purification steps in a buffer with a low pH. Furthermore, it has been shown that it possess a highly robust photosystem II that is adapted to a low pH, which might mean that a low buffer pH during purification increases the stability (no precipitation) and therefore the yield of this homologue (Krupnik *et al.* 2013, Nilsson *et al.* 2014).

Analysis of classical enzymological parameters for these homologues has identified a few interesting features that could be interesting to investigate in further research. Firstly, the K_m for NADPH can vary greatly between the different PORs, which we hypothesised, could be a reflection on the cellular NADPH concentrations in each of the organisms. Secondly, discrepancies between the K_d and K_m for NADPH were found for a few homologues, which can be suggestive of steps other than substrate binding becoming rate-limiting in the catalytic cycle. In order to work out the exact mechanism for these enzymes it will be necessary to measure the binding parameters and rate constants for all substrate binding and product release steps in the reaction (Heyes & Hunter 2004, Heyes *et al.* 2007, 2008). Thirdly, the dependence of the steady-state rate showed a Pchl_a substrate inhibition pattern for POR homologues from higher plants. We suggested that this could be part of a regulatory role in etioplast formation, with a consequent role in chloroplast development. This regulatory role could be investigated by replacing the POR gene in these higher plants with an algae homologue similar to (Masuda *et al.* 2009).

Most intriguing is the discovery of a faster hydride transfer rate in POR enzymes from eukaryotic organisms. We used visible ultrafast transient absorption and global analysis to compare the prokaryotic and eukaryotic PORs, but no major differences in the excited state processes were discovered other than the faster rate. Future experiments could involve transient absorption measurements in the infrared region to test the model developed in Heyes *et al.* (2015) for POR from *T. elongatus*. These measurements could potentially provide further insight into the role of excited state interactions that lead to the faster rates of hydride transfer in these enzymes.

In addition, a difference in the amplitude of the hydride transfer step was observed between eukaryotic and prokaryotic homologues, which is likely to be caused by a lower quantum yield in the eukaryotic PORs. An in-depth comparison of the quantum yield between these two groups of enzymes would provide more conclusive evidence for this finding. It can be speculated that the presence of other pigments and complexes can function as light-harvesting antennae in algal and plant PORs that are capable of transferring this energy to Pchl_a (Reinbothe *et al.* 2010, 2003, Buhr *et al.* 2008). This could then lead to a lower quantum yield for the POR-NADPH-Pchl_a ternary complex in these organisms.

Finally, in conclusion, it is clear that detailed structural data in the form of crystallographic X-ray diffraction or NMR data would significantly enhance our

understanding of the dynamic interactions that are important for catalysis in POR. Further crystallisation trials with the POR homologues discussed in this thesis may be a potential route for obtaining a crystal structure. Importantly, a crystal structure of POR would open up the exciting possibility of studying the structures of the intermediate states that are formed during catalysis and identifying the regions of the protein and the residues that play a dynamic role in the catalytic mechanism.

References

Chapter 1 – Introduction

- Alhambra, C., Corchado, J.C., Sánchez, M.L., Gao, J. & Truhlar, D.G., 2000. Quantum Dynamics of Hydride Transfer in Enzyme Catalysis. *J. Am. Chem. Soc.*, 122(8), pp.8197–8203.
- Angiolillo, P.J., Lin, V.S.Y., Vanderkooi, J.M. & Therien, M.J., 1995. EPR spectroscopy and photophysics of the lowest photoactivated triplet state of a series of highly conjugated (porphinato) Zn arrays. *J. Am. Chem. Soc.*, 117(50), pp.12514–12527.
- Antoniou, D., Caratzoulas, S., Kalyanaraman, C., Mincer, J.S. & Schwartz, S.D., 2002. Barrier passage and protein dynamics in enzymatically catalyzed reactions. *Eur. J. Biochem.*, 269(13), pp.3103–3112.
- Antoniou, D. & Schwartz, S.D., 2011. Protein dynamics and enzymatic chemical barrier passage. *J. Phys. Chem. B*, 115(51), pp.15147–15158.
- Armstrong, G.A., 1998. Greening in the dark: Light-independent chlorophyll biosynthesis from anoxygenic photosynthetic bacteria to gymnosperms. *J. Photochem. Photobiol. B Biol.*, 43(2), pp.87–100.
- Armstrong, G.A., Runge, S., Frick, G., Sperling, U. & Apel, K., 1995. Identification of NADPH:Protochlorophyllide Oxidoreductases A and B: A Branched Pathway for Light-Dependent Chlorophyll Biosynthesis in *Arabidopsis thaliana*. *Plant Physiol.*, 108, pp.1505–1517.
- Aubert, C., Vos, M.H., Mathis, P., Eker, A. P. & Brettel, K., 2000. Intraprotein radical transfer during photoactivation of DNA photolyase. *Nature*, 405(6786), pp.586–590.
- Baker, M.E., 1994. Protochlorophyllide reductase is homologous to human carbonyl reductase and pig 20 beta-hydroxysteroid dehydrogenase. *Biochem. J.*, 300(Pt 2), pp.605–607.
- Bandaria, J.N., Cheatum, C.M. & Kohen, A., 2009. Examination of enzymatic H-tunneling through kinetics and dynamics. *J. Am. Chem. Soc.*, 131(29), pp.10151–10155.
- Basran, J., Sutcliffe, M.J. & Scrutton, N.S., 1999. Enzymatic H-transfer requires vibration-driven extreme tunneling. *Biochemistry*, 38(10), pp.3218–3222.
- Bauer, C.E., Bollivar, D.W. & Suzuki, J.Y., 1993. Genetic analyses of photopigment biosynthesis in eubacteria: A guiding light for algae and plants. *J. Bacteriol.*, 175(13), pp.3919–3925.

- Begley, T.P. & Young, H., 1989. Protochlorophyllide Reductase. 1. Determination of the Regiochemistry and the Stereochemistry of the Reduction of Protochlorophyllide to Chlorophyllide. *J. Am. Chem. Soc.*, 111(18), pp.3095–3096.
- Bell, R.P., 1980. The application of tunnel corrections in chemical kinetics. In *The tunnel effect in chemistry*. London: Chapman and Hall, pp. 51–140.
- Belyaeva, O.B., Timofeev, K.N. & Litvin, F.F., 1988. The primary reactions in the protochlorophyll(ide) photoreduction as investigated by optical and ESR spectroscopy. *Photosynth. Res.*, 15(3), pp.247–256.
- Benkovic, S.J. & Hammes-Schiffer, S., 2003. A perspective on enzyme catalysis. *Science*, 301(5637), pp.1196–1202.
- Benyajati, C., Place, A. R., Powers, D. a & Sofer, W., 1981. Alcohol dehydrogenase gene of *Drosophila melanogaster*: relationship of intervening sequences to functional domains in the protein. *Proc. Natl. Acad. Sci. U. S. A.*, 78(5), pp.2717–2721.
- Birve, S.J., Selstam, E. & Johansson, L.B., 1996. Secondary structure of NADPH: protochlorophyllide oxidoreductase examined by circular dichroism and prediction methods. *Biochem. J.*, 317 (Pt 2, pp.549–555.
- Blankenship, R.E., 2001. Molecular evidence for the evolution of photosynthesis. *Trends Plant Sci.*, 6(1), pp.4–6.
- Boehr, D.D., Dyson, H.J. & Wright, P.E., 2006. An NMR perspective on enzyme dynamics. *Chem. Rev.*, 106(8), pp.3055–3079.
- Bruno, W.J. & Bialek, W., 1992. Vibrationally enhanced tunneling as a mechanism for enzymatic hydrogen transfer. *Biophys. J.*, 63(3), pp.689–699.
- Buhr, F., El Bakkouri, M., Valdez, O., Pollmann, S., Lebedev, N., Reinbothe, S. & Reinbothe, C., 2008. Photoprotective role of NADPH:protochlorophyllide oxidoreductase A. *Proc. Natl. Acad. Sci. U. S. A.*, 105(34), pp.12629–12634.
- Burke, D.H., Hearst, J.E. & Sidow, A., 1993. Early evolution of photosynthesis: clues from nitrogenase and chlorophyll iron proteins. *Proc. Natl. Acad. Sci. U. S. A.*, 90(15), pp.7134–7138.
- Cameron, C.E. & Benkovic, S.J., 1997. Evidence for a functional role of the dynamics of glycine-121 of *Escherichia coli* dihydrofolate reductase obtained from kinetic analysis of a site-directed mutant. *Biochemistry*, 36(50), pp.15792–15800.
- Cha, Y., Murray, C.J. & Klinman, J.P., 1989. Hydrogen tunneling in enzyme reactions. *Science*, 243, pp.1325–1330.
- Choquet, Y., Rahire, M., Girard-Bascou, J., Erickson, J. & Rochaix, J.D., 1992. A chloroplast gene is required for the light-independent accumulation of chlorophyll in *Chlamydomonas reinhardtii*. *EMBO J.*, 11(5), pp.1697–1704.

- Colindres-Rojas, M., Wolf, M.M.N., Grob, R., Seidel, S., Dietzek, B., Schmitt, M., Popp, J., Hermann, G. & Diller, R., 2011. Excited-state dynamics of protochlorophyllide revealed by subpicosecond infrared spectroscopy. *Biophys. J.*, 100(1), pp.260–267.
- Cui, Q. & Karplus, M., 2002. Quantum mechanics/molecular mechanics studies of triosephosphate isomerase-catalyzed reactions: Effect of geometry and tunneling on proton-transfer rate constants. *J. Am. Chem. Soc.*, 124(12), pp.3093–3124.
- Dahlin, C., Aronsson, H., Wilks, H.M., Lebedev, N., Sundqvist, C. & Timko, M.P., 1999. The role of protein surface charge in catalytic activity and chloroplast membrane association of the pea NADPH: Protochlorophyllide oxidoreductase (POR) as revealed by alanine scanning mutagenesis. *Plant Mol. Biol.*, 39(2), pp.309–323.
- Davarifar, A., Antoniou, D. & Schwartz, S.D., 2011. The promoting vibration in human heart lactate dehydrogenase is a preferred vibrational channel. *J. Phys. Chem. B*, 115(51), pp.15439–15444.
- Devault, D., 1980. Quantum mechanical tunneling in biological systems. *Q. Rev. Biophys.*, 13(4), pp.387–564.
- Dietzek, B., Kiefer, W., Hermann, G., Popp, J. & Schmitt, M., 2006. Solvent effects on the excited-state processes of protochlorophyllide: A femtosecond time-resolved absorption study. *J. Phys. Chem. B*, 110(9), pp.4399–4406.
- Dietzek, B., Maksimenka, R., Siebert, T., Birckner, E., Kiefer, W., Popp, J., Hermann, G. & Schmitt, M., 2004. Excited-state processes in protochlorophyllide a – a femtosecond time-resolved absorption study. *Chem. Phys. Lett.*, 397(1-3), pp.110–115.
- Dietzek, B., Tschierlei, S., Hanf, R., Seidel, S., Yartsev, A., Schmitt, M., Hermann, G. & Popp, J., 2010. Dynamics of charge separation in the excited-state chemistry of protochlorophyllide. *Chem. Phys. Lett.*, 492(1-3), pp.157–163.
- Dietzek, B., Tschierlei, S., Hermann, G., Yartsev, A., Pascher, T., Sundström, V., Schmitt, M. & Popp, J., 2009. Protochlorophyllide a: A Comprehensive Photophysical Picture. *ChemPhysChem*, 10(1), pp.144–150.
- Dufresne, A. *et al.*, 2003. Genome sequence of the cyanobacterium *Prochlorococcus marinus* SS120, a nearly minimal oxyphototrophic genome. *Proc. Natl. Acad. Sci. U. S. A.*, 100(17), pp.10020–10025.
- Durin, G., Delaunay, A., Darnault, C., Heyes, D.J., Royant, A., Vernede, X., Hunter, C.N., Weik, M. & Bourgeois, D., 2009. Simultaneous measurements of solvent dynamics and functional kinetics in a light-activated enzyme. *Biophys. J.*, 96(5), pp.1902–1910.
- Dutta, S., Li, Y.L., Rock, W., Houtman, J.C.D., Kohen, A. & Cheatum, C.M., 2012. 3-Picolyl Azide Adenine Dinucleotide As a Probe of Femtosecond To Picosecond Enzyme Dynamics. *J. Phys. Chem. B*, 116(1), pp.542–548.

- Fierke, C. A., Johnson, K. A. & Benkovic, S.J., 1987. Construction and evaluation of the kinetic scheme associated with dihydrofolate reductase from *Escherichia coli*. *Biochemistry*, 26(13), pp.4085–4092.
- Fisher, E., 1894. The influence of configuration on enzyme activity. (Translated from German). *Dtsch Chem Ges*, 27, pp.2984–2993.
- Franck, F., Sperling, U., Frick, G., Pochert, B., van Cleve, B., Apel, K. & Armstrong, G.A., 2000. Regulation of etioplast pigment-protein complexes, inner membrane architecture, and protochlorophyllide a chemical heterogeneity by light-dependent NADPH: Protochlorophyllide oxidoreductases A and B. *Plant Physiol.*, 124, pp.1678–1696.
- Fraser, J.S., Clarkson, M.W., Degnan, S.C., Erion, R., Kern, D. & Alber, T., 2009. Hidden alternative structures of proline isomerase essential for catalysis. *Nature*, 462(7273), pp.669–673.
- Fujita, Y., 1996. Protochlorophyllide reduction: a key step in the greening of plants. *Plant Cell Physiol.*, 37(4), pp.411–421.
- Fujita, Y. & Bauer, C.E., 2000. Reconstitution of light-independent protochlorophyllide reductase from purified Bchl and BchN-BchB subunits: In vitro confirmation of nitrogenase-like features of a bacteriochlorophyll biosynthesis enzyme. *J. Biol. Chem.*, 275(31), pp.23583–23588.
- Fujita, Y., Takagi, H. & Hase, T., 1998. Cloning of the gene encoding a protochlorophyllide reductase: the physiological significance of the co-existence of light-dependent and -independent protochlorophyllide reduction systems in the cyanobacterium *Plectonema boryanum*. *Plant Cell Physiol.*, 39(2), pp.177–185.
- Fujita, Y., Takahashi, Y., Chuganji, M. & Matsubara, H., 1992. The *nifH*-Like (*frxC*) Gene Is Involved in the Biosynthesis of Chlorophyll in the Filamentous Cyanobacterium *Plectonema boryanum*. *Plant Cell Physiol.*, 33(1), pp.81–92.
- Glasstone, S., Laidler, K.J. & Eyring, H., 1941. *The Theory of Rate Processes*, New York: McGraw-Hil.
- Gray, H.B. & Winkler, J.R., 1996. Electron transfer in proteins. *Annu. Rev. Biochem.*, 65, pp.537–561.
- Griffiths, W.T., 1980. Substrate-specificity studies on protochlorophyllide reductase in barley (*Hordeum vulgare*) etioplast membranes. *Biochem. J.*, 186(1), pp.267–278.
- Grzyb, J.M., Solymosi, K., Strzałka, K. & Mysliwa-Kurdziel, B., 2013. Visualization and characterization of prolamellar bodies with atomic force microscopy. *J. Plant Physiol.*, 170(14), pp.1217–1227.
- Hammes, G.G., 2002. Multiple conformational changes in enzyme catalysis. *Biochemistry*, 41(26), pp.8221–8228.

- Hammes-Schiffer, S., 2006. Hydrogen tunneling and protein motion in enzyme reactions. *Acc. Chem. Res.*, 39(2), pp.93–100.
- Hammes-Schiffer, S., 2002. Impact of enzyme motion on activity. *Biochemistry*, 41(45), pp.13335–13343.
- Hammes-Schiffer, S., 2004. Quantum-classical simulation methods for hydrogen transfer in enzymes: A case study of dihydrofolate reductase. *Curr. Opin. Struct. Biol.*, 14(2), pp.192–201.
- Hammes-Schiffer, S. & Soudackov, A. V., 2008. Proton-coupled electron transfer in solution, proteins, and electrochemistry. *J. Phys. Chem. B*, 112(45), pp.14108–14123.
- Hanf, R., Fey, S., Dietzek, B., Schmitt, M., Reinbothe, C., Reinbothe, S., Hermann, G. & Popp, J., 2011. Protein-induced excited-state dynamics of protochlorophyllide. *J. Phys. Chem. A*, 115(27), pp.7873–7881.
- Hay, S., Johannissen, L.O., Hothi, P., Sutcli, M.J. & Scrutton, N.S., 2012. Pressure Effects on Enzyme-Catalyzed Quantum Tunneling Events Arise from Protein-Specific Structural and Dynamic Changes. *J. Am. Chem. Soc.*, 134, pp.9749–9754.
- Hay, S., Pudney, C.R., Sutcliffe, M.J. & Scrutton, N.S., 2008. Are environmentally coupled enzymatic hydrogen tunneling reactions influenced by changes in solution viscosity? *Angew. Chemie Int. Ed.*, 47(3), pp.537–540.
- Hay, S. & Scrutton, N.S., 2012. Good vibrations in enzyme-catalysed reactions. *Nat. Chem.*, 4(3), pp.161–168.
- Hay, S. & Scrutton, N.S., 2008. Incorporation of hydrostatic pressure into models of hydrogen tunneling highlights a role for pressure-modulated promoting vibrations. *Biochemistry*, 47(37), pp.9880–9887.
- Hay, S., Sutcliffe, M.J. & Scrutton, N.S., 2007. Promoting motions in enzyme catalysis probed by pressure studies of kinetic isotope effects. *Proc. Natl. Acad. Sci. U. S. A.*, 104(2), pp.507–512.
- Helfrich, M., Schoch, S., Scha, W. & Ryberg, M., 1996. Absolute Configuration of Protochlorophyllide a and Substrate. *J. Am. Chem. Soc.*, 118, pp.2606–2611.
- Henneke, M. & Wedding, R.T., 1975. NAD-Phenol Complex Formation, the Inhibition of Malate Dehydrogenase by Phenols, and the Influence of Phenol Substituents on Inhibitory Effectiveness. *Arch. Biochem. Biophys.*, 168, pp.443–449.
- Henzler-Wildman, K. A., Lei, M., Thai, V., Kerns, S.J., Karplus, M. & Kern, D., 2007. A hierarchy of timescales in protein dynamics is linked to enzyme catalysis. *Nature*, 450(7171), pp.913–916.
- Henzler-Wildman, K. A. & Kern, D., 2007. Dynamic personalities of proteins. *Nature*, 450(7172), pp.964–972.

- Heyes, D.J., Hardman, S.J.O., Hedison, T.M., Hoeven, R., Greetham, G.M., Towrie, M. & Scrutton, N.S., 2015. Excited-State Charge Separation in the Photochemical Mechanism of the Light-Driven Enzyme Protochlorophyllide Oxidoreductase. *Angew. Chemie Int. Ed.*, 54(5), pp.1512–1515.
- Heyes, D.J., Hardman, S.J.O., Mansell, D., Gardiner, J.M. & Scrutton, N.S., 2012. Mechanistic Reappraisal of Early Stage Photochemistry in the Light-Driven Enzyme Protochlorophyllide Oxidoreductase. *PLoS One*, 7(9).
- Heyes, D.J., Heathcote, P., Rigby, S.E.J., Palacios, M. a., Van Grondelle, R. & Hunter, C.N., 2006. The first catalytic step of the light-driven enzyme protochlorophyllide oxidoreductase proceeds via a charge transfer complex. *J. Biol. Chem.*, 281(37), pp.26847–26853.
- Heyes, D.J. & Hunter, C.N., 2009. Biosynthesis of Chlorophyll and Bacteriochlorophyll. In *Tetrapyrroles*. Molecular Biology Intelligence Unit, pp. 235–249.
- Heyes, D.J. & Hunter, C.N., 2004. Identification and characterization of the product release steps within the catalytic cycle of protochlorophyllide oxidoreductase. *Biochemistry*, 43(25), pp.8265–8271.
- Heyes, D.J. & Hunter, C.N., 2005. Making light work of enzyme catalysis: Protochlorophyllide oxidoreductase. *Trends Biochem. Sci.*, 30(11), pp.642–649.
- Heyes, D.J. & Hunter, C.N., 2002. Site-directed mutagenesis of Tyr-189 and Lys-193 in NADPH: protochlorophyllide oxidoreductase from *Synechocystis*. *Biochem. Soc. Trans.*, 30(4), pp.601–604.
- Heyes, D.J., Hunter, C.N., van Stokkum, I.H.M., van Grondelle, R., Groot, M.L., Grondelle, R. Van & Groot, M.L., 2002. Ultrafast enzymatic reaction dynamics in. *Nat. Struct. Biol.*, 10(6), pp.388–389.
- Heyes, D.J., Levy, C., Sakuma, M., Robertson, D.L. & Scrutton, N.S., 2011. A twin-track approach has optimized proton and hydride transfer by dynamically coupled tunneling during the evolution of protochlorophyllide oxidoreductase. *J. Biol. Chem.*, 286(13), pp.11849–11854.
- Heyes, D.J., Levy, C., Sakuma, M., Robertson, D.L. & Scrutton, N.S., 2011. A twin-track approach has optimized proton and hydride transfer by dynamically coupled tunneling during the evolution of protochlorophyllide oxidoreductase. *J. Biol. Chem.*, 286(13), pp.11849–11854.
- Heyes, D.J., Menon, B.R.K., Sakuma, M. & Scrutton, N.S., 2008. Conformational Events during Ternary Enzyme - Substrate Complex Formation Are Rate Limiting in the Catalytic Cycle of the Light-Driven Enzyme. *Biochemistry*, 47, pp.10991–10998.
- Heyes, D.J., Ruban, A. V, Wilks, H.M. & Hunter, C.N., 2002. Enzymology below 200 K: the kinetics and thermodynamics of the photochemistry catalyzed by

protochlorophyllide oxidoreductase. *Proc. Natl. Acad. Sci. U. S. A.*, 99(17), pp.11145–50.

Heyes, D.J., Ruban, A. V. & Hunter, C.N., 2003. Protochlorophyllide oxidoreductase: “Dark” reactions of a light-driven enzyme. *Biochemistry*, 42(2), pp.523–528.

Heyes, D.J., Sakuma, M. & Scrutton, N.S., 2007. Laser excitation studies of the product release steps in the catalytic cycle of the light-driven enzyme, protochlorophyllide oxidoreductase. *J. Biol. Chem.*, 282(44), pp.32015–32020.

Heyes, D.J., Sakuma, M. & Scrutton, N.S., 2009. Solvent-Slaved Protein Motions Accompany Proton but Not Hydride Tunneling in Light-Activated Protochlorophyllide Oxidoreductase. *Angew. Chemie Int. Ed.*, 121(21), pp.3908–3911.

Heyes, D.J., Sakuma, M., de Visser, S.P. & Scrutton, N.S., 2009. Nuclear quantum tunneling in the light-activated enzyme protochlorophyllide oxidoreductase. *J. Biol. Chem.*, 284(6), pp.3762–3767.

Heyes, D.J. & Scrutton, N.S., 2009. Conformational changes in the catalytic cycle of protochlorophyllide oxidoreductase: what lessons can be learnt from dihydrofolate reductase? *Biochem. Soc. Trans.*, 37(Pt 2), pp.354–357.

Hilvert, D., 2000. Critical analysis of antibody catalysis. *Annu. Rev. Biochem.*, 69, pp.751–93.

Holtorf, H., Reinbothe, S., Reinbothe, C., Berezina, B. & Apel, K., 1995. Two routes of chlorophyllide synthesis that are differentially regulated by light in barley (*Hordeum vulgare* L.). *Proc. Natl. Acad. Sci. U. S. A.*, 92(8), pp.3254–3258.

Hong, Y.J. & Tantillo, D.J., 2014. Biosynthetic consequences of multiple sequential post-transition-state bifurcations. *Nat. Chem.*, 6(2), pp.104–111.

Johannissen, L.O., Hay, S., Scrutton, N.S. & Sutcliffe, M.J., 2007. Proton tunneling in aromatic amine dehydrogenase is driven by a short-range sub-picosecond promoting vibration: Consistency of simulation and theory with experiment. *J. Phys. Chem. B*, 111(10), pp.2631–2638.

Johannissen, L.O., Scrutton, N.S. & Sutcliffe, M.J., 2011. How does pressure affect barrier compression and isotope effects in an enzymatic hydrogen tunneling reaction? *Angew. Chemie Int. Ed.*, 50(9), pp.2129–2132.

Jonsson, T., Glickman, M.H., Sun, S. & Klinman, J.P., 1996. Experimental evidence for extensive tunneling of hydrogen in the lipoygenase reaction: Implications for enzyme catalysis. *J. Am. Chem. Soc.*, 118(42), pp.10319–10320.

Kallberg, Y., Oppermann, U., Jörnvall, H. & Persson, B., 2002. Short-chain dehydrogenases/reductases (SDRs). Coenzyme-based functional assignments in completed genomes. *Eur. J. Biochem.*, 269(18), pp.4409–4417.

- Kaneko, T. *et al.*, 1996. Sequence analysis of the genome of the unicellular cyanobacterium *Synechocystis* sp. strain PCC6803. II. Sequence determination of the entire genome and assignment of potential protein-coding regions. *DNA Res.*, 3(3), pp.109–136.
- Kipp, D.R., Silva, R.G. & Schramm, V.L., 2011. Mass-dependent bond vibrational dynamics influence catalysis by HIV-1 protease. *J. Am. Chem. Soc.*, 133(48), pp.19358–19361.
- Klement, H., Helfrich, M., Oster, U., Schoch, S. & Rüdiger, W., 1999. Pigment-free NADPH:protochlorophyllide oxidoreductase from *Avena sativa* L. Purification and substrate specificity. *Eur. J. Biochem.*, 265(3), pp.862–874.
- Klinman, J.P., 2010. A new model for the origin of kinetic hydrogen isotope effects. *J. Phys. Org. Chem.*, 23(7), pp.606–612.
- Klinman, J.P. & Kohen, A., 2013. Hydrogen tunneling links protein dynamics to enzyme catalysis. *Annu. Rev. Biochem.*, 82, pp.471–496.
- Knapp, M.J. & Klinman, J.P., 2002. Environmentally coupled hydrogen tunneling: Linking catalysis to dynamics. *Eur. J. Biochem.*, 269(13), pp.3113–3121.
- Knapp, M.J., Rickert, K. & Klinman, J.P., 2002. Temperature-dependent isotope effects in soybean Lipoxygenase-1: Correlating hydrogen tunneling with protein dynamics. *J. Am. Chem. Soc.*, 124(15), pp.3865–3874.
- Kohchi, T., Umesono, K., Ogura, Y., Komine, Y., Nakahigashi, K., Komano, T., Yamada, Y., Ozeki, H. & Ohyama, K., 1988. A nicked group II intron and tainsplicing in liverwort, *Marchantia polymorpha*, chloroplasts. *Nucleic acid Res.*, 16(21), pp.10025–10036.
- Kohen, A., Cannio, R., Bartolucci, S. & Klinman, J.P., 1999. Enzyme dynamics and hydrogen tunneling in a thermophilic alcohol dehydrogenase. *Nature*, 399(6735), pp.496–499.
- Kohen, A. & Klinman, J.P., 1998. Enzyme catalysis: Beyond classical paradigms. *Acc Chem Res*, 31(7), pp.397–404.
- Kohen, A. & Klinman, J.P., 2000. Protein flexibility correlates with degree of hydrogen tunneling in thermophilic and mesophilic alcohol dehydrogenases. *J. Am. Chem. Soc.*, 122(43), pp.10738–10739.
- Koshland, D.E., 1958. Application of a Theory of Enzyme Specificity to Protein Synthesis. *Proc. Natl. Acad. Sci. U. S. A.*, 44, pp.98–104.
- Koshland, D.E., 1994. The Key–Lock Theory and the Induced Fit Theory. *Angew. Chemie Int. Ed. English*, 33, pp.2375–2378.
- Kuznetsov, A. M. & Ulstrup, J., 1999. Proton and hydrogen atom tunneling in hydrolytic and redox enzyme catalysis. *Can. J. Chem.*, 77(5-6), pp.1085–1096.

- Lebedev, N. & Timko, M.P., 1999. Protochlorophyllide oxidoreductase B-catalyzed protochlorophyllide photoreduction in vitro: insight into the mechanism of chlorophyll formation in light-adapted plants. *Proc. Natl. Acad. Sci. U. S. A.*, 96(17), pp.9954–9959.
- Lebedev, N. & Timko, M.P., 1998. Protochlorophyllide photoreduction. *Photosynth. Res.*, 58(1), pp.5–23.
- Lidholm, J. & Gustafsson, P., 1991. Homologues of the green algal *gidA* gene and the liverwort *frxC* gene are present on the chloroplast genomes of conifers. *Plant Mol. Biol.*, 17, pp.787–798.
- Lienhard, G.E., 1973. Enzymatic catalysis and transition-state theory. *Science*, 180(82), pp.149–154.
- Lightstone, F.C. & Bruice, T.C., 1996. Ground state conformations and entropic and enthalpic factors in the efficiency of intramolecular and enzymatic reactions .1. Cyclic anhydride formation by substituted glutarates, succinate, and 3,6-endoxo- Δ^4 -tetrahydrophthalate monophenyl esters. *J. Am. Chem. Soc.*, 118(11), pp.2595–2605.
- Maglia, G. & Allemann, R.K., 2003. Evidence for Environmentally Coupled Hydrogen Tunneling during Dihydrofolate Reductase Catalysis. *J. Am. Chem. Soc.*, 125(44), pp.13372–13373.
- Marcus, R. A. & Sutin, N., 1985. Electron transfers in chemistry and biology. *Biochim. Biophys. Acta - Rev. Bioenerg.*, 811(3), pp.265–322.
- Masson, P. & Balny, C., 2005. Linear and non-linear pressure dependence of enzyme catalytic parameters. *Biochim. Biophys. Acta - Gen. Subj.*, 1724(3), pp.440–450.
- Masuda, T., Fusada, N., Shiraishi, T., Kuroda, H., Awai, K., Shimada, H., Ohta, H. & Takamiya, K.I., 2002. Identification of two differentially regulated isoforms of protochlorophyllide oxidoreductase (POR) from tobacco revealed a wide variety of light- and development-dependent regulations of POR gene expression among angiosperms. *Photosynth. Res.*, 74(2), pp.165–172.
- Masuda, T. & Takamiya, K.-I., 2004. Novel Insights into the Enzymology, Regulation and Physiological Functions of Light-dependent Protochlorophyllide Oxidoreductase in Angiosperms. *Photosynth. Res.*, 81(1), pp.1–29.
- McFarlane, M.J., Hunter, C.N. & Heyes, D.J., 2005. Kinetic characterisation of the light-driven protochlorophyllide oxidoreductase (POR) from *Thermosynechococcus elongatus*. *Photochem. Photobiol. Sci.*, 4(12), pp.1055–1059.
- Melander, L. & Saunders, W.H., 1987. *Reaction rates of isotopic molecules* 4th ed. Krieger, ed., New York: Wiley-Interscience.
- Menon, B.R.K., Davison, P.A., Hunter, C.N., Scrutton, N.S. & Heyes, D.J., 2010. Mutagenesis alters the catalytic mechanism of the light-driven enzyme protochlorophyllide oxidoreductase. *J. Biol. Chem.*, 285(3), pp.2113–2119.

- Menon, B.R.K., Waltho, J.P., Scrutton, N.S. & Heyes, D.J., 2009. Cryogenic and laser photoexcitation studies identify multiple roles for active site residues in the light-driven enzyme protochlorophyllide oxidoreductase. *J. Biol. Chem.*, 284(27), pp.18160–18166.
- Miller, D. & Agard, D., 1999. Enzyme specificity under dynamic control: A normal mode analysis of a -Lytic Protease. *J Mol. Biol*, 286(1), pp.267–278.
- Moser, C.C., Page, C.C. & Dutton, P.L., 2006. Darwin at the molecular scale: selection and variance in electron tunneling proteins including cytochrome c oxidase. *Philos. Trans. R. Soc. Lond. B. Biol. Sci.*, 361(1472), pp.1295–1305.
- Muraki, N., Nomata, J., Ebata, K., Mizoguchi, T., Shiba, T., Tamiaki, H., Kurisu, G. & Fujita, Y., 2010. X-ray crystal structure of the light-independent protochlorophyllide reductase. *Nature*, 465(7294), pp.110–114.
- Nagel, Z.D. & Klinman, J.P., 2006. Tunneling and dynamics in enzymatic hydride transfer. *Chem. Rev.*, 106(8), pp.3095–3118.
- Nagel, Z.D. & Klinman, J.P., 2010. Update 1 of: Tunneling and Dynamics in Enzymatic Hydride Transfer. *Chem. Rev.*, 110, pp.41–67.
- Nagel, Z.D., Meadows, C.W., Dong, M., Bahnson, B.J. & Klinman, J.P., 2012. Active site hydrophobic residues impact hydrogen tunneling differently in a thermophilic alcohol dehydrogenase at optimal versus nonoptimal temperatures. *Biochemistry*, 51(20), pp.4147–4156.
- Nakamura, Y. *et al.*, 2003. Complete Genome Structure of *Gloeobacter violaceus* PCC 7421, a Cyanobacterium that Lacks Thylakoids. *DNA Res.*, 10(4), pp.137–145.
- Nomata, J., Kondo, T., Mizoguchi, T., Tamiaki, H., Itoh, S. & Fujita, Y., 2014. Dark-operative protochlorophyllide oxidoreductase generates substrate radicals by an iron-sulphur cluster in bacteriochlorophyll biosynthesis. *Sci. Rep.*, 4, pp.1–7.
- Northrop, D.B., 1999. Effects of high pressure on isotope effects and hydrogen tunneling. *J. Am. Chem. Soc.*, 121(14), pp.3521–3524.
- Northrop, D.B., 2006. Unusual origins of isotope effects in enzyme-catalysed reactions. *Philos. Trans. R. Soc. Lond. B. Biol. Sci.*, 361(1472), pp.1341–1349.
- Ohyama, K., Fukuzawa, H., Kohchi, T., Shirai, H., Sano, T., Sano, S., Umesono, K., Shiki, Y., Takeuchi, M., Chang, Z., Aota, S., Inokuchi, H. & Ozeki, H., 1986. Chloroplast gene organization deduced from complete sequence of liverwort *Marchantia polymorpha* chloroplast DNA. *Nature*, 322, pp.572–574.
- Okamura, M.Y., Paddock, M.L., Graige, M.S. & Feher, G., 2000. Proton and electron transfer in bacterial reaction centers. *Biochim. Biophys. Acta*, 1458(1), pp.148–163.

Olsson, M.H.M., Siegbahn, P.E.M. & Warshel, A., 2004. Simulations of the large kinetic isotope effect and the temperature dependence of the hydrogen atom transfer in lipoxygenase. *J. Am. Chem. Soc.*, 126(9), pp.2820–2828.

Oosawa, N., Masuda, T., Awai, K., Fusada, N., Shimada, H., Ohta, H. & Takamiya, K.I., 2000. Identification and light-induced expression of a novel gene of NADPH-protochlorophyllide oxidoreductase isoform in *Arabidopsis thaliana*. *FEBS Lett.*, 474(2-3), pp.133–136.

Paddock, M.L., Feher, G. & Okamura, M.Y., 2003. Proton transfer pathways and mechanism in bacterial reaction centers. *FEBS Lett.*, 555(1), pp.45–50.

Parker, V.D., Zhao, Y., Lu, Y. & Zheng, G., 1998. Application of non-steady-state kinetics to resolve the kinetics of proton-transfer reactions between methylarene radical cations and pyridine bases. *J. Am. Chem. Soc.*, 120(49), pp.12720–12727.

Pauling, L., 1948. Chemical achievement and hope for the future. *Am Sci.*, 36, pp.51–8.

Pudney, C.R., Guerriero, A., Baxter, N.J., Johannissen, L.O., Waltho, J.P., Hay, S. & Scrutton, N.S., 2013. Fast protein motions are coupled to enzyme H-transfer reactions. *J. Am. Chem. Soc.*, 135(7), pp.2512–2517.

Pudney, C.R., Hay, S., Levy, C., Pang, J., Sutcliffe, M.J., Leys, D. & Scrutton, N.S., 2009. Evidence to support the hypothesis that promoting vibrations enhance the rate of an enzyme catalyzed H-tunneling reaction. *J. Am. Chem. Soc.*, 131(47), pp.17072–17073.

Pudney, C.R., Johannissen, L.O., Sutcliffe, M.J., Hay, S. & Scrutton, N.S., 2010. Direct analysis of donor-acceptor distance and relationship to isotope effects and the force constant for barrier compression in enzymatic H-tunneling reactions. *J. Am. Chem. Soc.*, 132(32), pp.11329–11335.

Pudney, C.R., McGrory, T., Lafite, P., Pang, J., Hay, S., Leys, D., Sutcliffe, M.J. & Scrutton, N.S., 2009. Parallel pathways and free-energy landscapes for enzymatic hydride transfer probed by hydrostatic pressure. *ChemBioChem*, 10(8), pp.1379–1384.

Raskin, V.I. & Schwartz, A., 2002. The charge-transfer complex between protochlorophyllide and NADPH: An intermediate in protochlorophyllide photoreduction. *Photosynth. Res.*, 74(2), pp.181–186.

Reed, R. A., Purrello, R., Prendergast, K. & Spiro, T.G., 1991. Resonance Raman characterization of the radical anion and triplet states of zinc tetraphenylporphine. *J. Phys. Chem.*, 95(24), pp.9720–9727.

Reinbothe, C., Buhr, F., Pollmann, S. & Reinbothe, S., 2003. In vitro reconstitution of light-harvesting POR-protochlorophyllide complex with protochlorophyllides a and b. *J. Biol. Chem.*, 278(2), pp.807–815.

Reinbothe, S., Reinbothe, C., Apel, K. & Lebedev, N., 1996. Evolution of chlorophyll biosynthesis--the challenge to survive photooxidation. *Cell*, 86(5), pp.703–5.

Richard, M., Tremblay, C. & Bellemare, G., 1994. Chloroplastic genomes of *Ginkgo biloba* and *Chlamydomonas moewusii* contain a *chlB* gene encoding one subunit of a light-independent protochlorophyllide reductase. *Curr Genet.* 513, pp.159–165.

Rod, T.H., Radkiewicz, J.L. & Brooks, C.L., 2003. Correlated motion and the effect of distal mutations in dihydrofolate reductase. *Proc. Natl. Acad. Sci. U. S. A.*, 100(12), pp.6980–6985.

Rodríguez, I. & González-Velasco, J., 1990. Self-sensitized photopolymerization of pyrrole. *J. Chem. Soc. Chem. Commun.*, 104(5), pp.387–388.

Roston, D., Cheatum, C.M. & Kohen, A., 2012. Hydrogen Donor – Acceptor Fluctuations from Kinetic Isotope Effects: A Phenomenological Model. *Biochemistry*, 51, pp.6860–6870.

Rüdiger, W., Böhm, S., Helfrich, M., Schulz, S. & Schoch, S., 2005. Enzymes of the last steps of chlorophyll biosynthesis: Modification of the substrate structure helps to understand the topology of the active centers. *Biochemistry*, 44(32), pp.10864–10872.

Ruiz-Pernia, J.J., Luk, L.Y.P., García-Meseguer, R., Martí, S., Loveridge, E.J., Tuñón, I., Moliner, V. & Allemann, R.K., 2013. Increased dynamic effects in a catalytically compromised variant of *Escherichia coli* dihydrofolate reductase. *J. Am. Chem. Soc.*, 135(49), pp.18689–18696.

Ryberg, M. & Sundqvist, C., 1982. Characterization of prolamellar bodies and prothylakoids fractionated from wheat etioplasts. *Physiol. Plant.*, 56(2), pp.125–132.

Saen-Oon, S., Quaytman-Machleder, S., Schramm, V.L. & Schwartz, S.D., 2008. Atomic detail of chemical transformation at the transition state of an enzymatic reaction. *Proc. Natl. Acad. Sci. U. S. A.*, 105(43), pp.16543–16548.

Schnell, J.R., Dyson, H.J. & Wright, P.E., 2004. Structure, dynamics, and catalytic function of dihydrofolate reductase. *Annu. Rev. Biophys. Biomol. Struct.*, 33, pp.119–140.

Schoefs, B. & Franck, F., 2003. Protochlorophyllide Reduction: Mechanisms and Evolution. *Am. Soc. Photobiol.*, 78(6), pp.543–557.

Scrutton, N.S., Basran, J. & Sutcliffe, M.J., 1999. New insights into enzyme catalysis. Ground state tunneling driven by protein dynamics. *Eur. J. Biochem.*, 264(3), pp.666–671.

Scrutton, N.S., Louise Groot, M. & Heyes, D.J., 2012. Excited state dynamics and catalytic mechanism of the light-driven enzyme protochlorophyllide oxidoreductase. *Phys. Chem. Chem. Phys.*, 14(25), p.8818.

- Sen, A. & Kohen, A., 2010. Enzymatic tunneling and kinetic isotope effects: Chemistry at the crossroads. *J. Phys. Org. Chem.*, 23(7), pp.613–619.
- Shediac, R., Gray, M.H.B., Tetsuo Uyeda, H., Johnson, R.C., Hupp, J.T., Angiolillo, P.J. & Therien, M.J., 2000. Singlet and triplet excited states of emissive, conjugated bis(porphyrin) compounds probed by optical and EPR spectroscopic methods. *J. Am. Chem. Soc.*, 122(29), pp.7017–7033.
- Shui, J., Saunders, E., Needleman, R., Nappi, M., Cooper, J., Hall, L., Kehoe, D. & Stowe-Evans, E., 2009. Light-dependent and light-independent protochlorophyllide oxidoreductases in the chromatically adapting cyanobacterium *Fremyella diplosiphon* UTEX 481. *Plant Cell Physiol.*, 50(8), pp.1507–1521.
- Silva, R.G., Murkin, A. S. & Schramm, V.L., 2011. Femtosecond dynamics coupled to chemical barrier crossing in a Born-Oppenheimer enzyme. *Proc. Natl. Acad. Sci.*, 108(46), pp.18661–18665.
- Skinner, J.S. & Timko, M.P., 1998. Loblolly pine (*Pinus taeda* L.) contains multiple expressed genes encoding light-dependent NADPH:protochlorophyllide oxidoreductase (POR). *Plant Cell Physiol.*, 39(8), pp.795–806.
- Sperling, U., van Cleve, B., Frick, G., Apel, K. & Armstrong, G.A., 1997. Overexpression of light-dependent PORA and PORB in plants depleted of endogenous POR by far-red light enhances seedling survival in white light and protects against photooxidative damage. *Plant J.*, 12, pp.649–658.
- Spikes, J.D. & Bommer, J.C., 1991. Chlorophyll and related pigments as photosensitizers in biology and medicine. In H. Scheer, ed. *Chlorophylls*. Boca Raton, FL: CRC Press.
- Stojković, V., Perissinotti, L.L., Lee, J., Benkovic, S.J. & Kohen, A., 2010. The effect of active-site isoleucine to alanine mutation on the DHFR catalyzed hydride-transfer. *The Royal Society of Chemistry*, 46(47), pp.8974–8976.
- Sundqvist, C. & Dahlin, C., 1997. With chlorophyll pigments from prolamellar bodies to light-harvesting complexes. *Physiol. Plant.*, 100(4), pp.748–759.
- Sutcliffe, M.J., Masgrau, L., Roujeinikova, A., Johannissen, L.O., Hothi, P., Basran, J., Ranaghan, K.E., Mulholland, A.J., Leys, D. & Scrutton, N.S., 2006. Hydrogen tunneling in enzyme-catalysed H-transfer reactions: flavoprotein and quinoprotein systems. *Philos. Trans. R. Soc. Lond. B. Biol. Sci.*, 361(1472), pp.1375–1386.
- Sutcliffe, M.J. & Scrutton, N.S., 2002. A new conceptual framework for enzyme catalysis: Hydrogen tunneling coupled to enzyme dynamics in flavoprotein and quinoprotein enzymes. *Eur. J. Biochem.*, 269(13), pp.3096–3102.
- Sutcliffe, M.J. & Scrutton, N.S., 2000. Enzymology takes a quantum leap forward. *Philos. Trans. R. Soc. Lond. A*, 358(1766), pp.367–386.

- Suzuki, J.Y. & Bauer, C.E., 1995. A prokaryotic origin for light-dependent chlorophyll biosynthesis of plants. *Proc. Natl. Acad. Sci. U. S. A.*, 92(9), pp.3749–3753.
- Suzuki, J.Y. & Bauer, C.E., 1992. Light-Independent Chlorophyll Biosynthesis : Involvement of the Chloroplast Gene *chlL* (*frxC*). *Plant Cell*, 4 (August), pp.929–940.
- Sytina, O. A., Heyes, D.J., Hunter, C.N., Alexandre, M.T., van Stokkum, I.H.M., van Grondelle, R. & Groot, M.L., 2008. Conformational changes in an ultrafast light-driven enzyme determine catalytic activity. *Nature*, 456(7224), pp.1001–1004.
- Sytina, O. A., Novoderezhkin, V.I., Van Grondelle, R. & Groot, M.L., 2011. Modeling of multi-exciton transient absorption spectra of protochlorophyllide aggregates in aqueous solution. *J. Phys. Chem. A*, 115(43), pp.11944–11951.
- Sytina, O. A., van Stokkum, I.H.M., Heyes, D.J., Hunter, C.N. & Groot, M.L., 2012. Spectroscopic characterization of the first ultrafast catalytic intermediate in protochlorophyllide oxidoreductase. *Phys. Chem. Chem. Phys.*, 14(2), p.616.
- Sytina, O. A., Stokkum, I. van & Heyes, D., 2010. Protochlorophyllide excited-state dynamics in organic solvents studied by time-resolved visible and mid-infrared spectroscopy. *J. Phys. Chem.*, (C), pp.4335–4344.
- Tanaka, R. & Tanaka, A., 2007. Tetrapyrrole biosynthesis in higher plants. *Annu. Rev. Plant Biol.*, 58, pp.321–346.
- Thomas, J.B., Waas, J.R., Harmata, M. & Singleton, D. A., 2008. Control Elements in Dynamically Determined Selectivity on a Bifurcating Surface. *J. Am. Chem. Soc.*, 130(44), pp.14544–14555.
- Townley, H.E., Griffiths, W.T. & Nugent, J.P., 1998. A reappraisal of the mechanism of the photoenzyme protochlorophyllide reductase based on studies with the heterologously expressed protein. *FEBS Lett.*, 422(1), pp.19–22.
- Townley, H.E., Sessions, R.B., Clarke, A.R., Dafforn, T.R. & Trevor Griffiths, W., 2001. Protochlorophyllide oxidoreductase: A homology model examined by site-directed mutagenesis. *Proteins Struct. Funct. Genet.*, 44(3), pp.329–335.
- De Vault, D. & Chance, B., 1966. Studies of photosynthesis using a pulsed laser. *Biophys. J.*, 6, pp.825–847.
- Virgin, H.I., 1963. The physiology of chlorophyll formation in relation to structural changes in chloroplasts. *Photochem. Photobiol.*, 2, pp.83–91.
- Von Wettstein, D., Gough, S. & Kannangara, C.G., 1995. Chlorophyll Biosynthesis. *Plant Cell*, 7(7), pp.1039–1057.
- Wilks, H.M. & Timko, M.P., 1995. A light-dependent complementation system for analysis of NADPH:protochlorophyllide oxidoreductase: identification and

mutagenesis of two conserved residues that are essential for enzyme activity. *Proc. Natl. Acad. Sci. U. S. A.*, 92(3), pp.724–8.

Wolfenden, R., 2006. Degrees of difficulty of water-consuming reactions in the absence of enzymes. *Chem. Rev.*, 106(8), pp.3379–3396.

Yahashiri, A., Howell, E.E. & Kohen, A., 2008. Tuning of the H-transfer coordinate in primitive versus well-evolved enzymes. *ChemPhysChem*, 9(7), pp.980–982.

Yang, J. & Cheng, Q., 2004. Origin and evolution of the Light-Dependent Protochlorophyllide Oxidoreductase (LPOR) genes. *Plant Biol.*, 6(5), pp.537–544.

Yuan, M., Zhang, D.W., Zhang, Z.W., Chen, Y.E., Yuan, S., Guo, Y.R. & Lin, H.H., 2012. Assembly of NADPH: Protochlorophyllide oxidoreductase complex is needed for effective greening of barley seedlings. *J. Plant Physiol.*, 169(13), pp.1311–1316.

Zhao, G.-J. & Han, K.-L., 2008. Site-specific solvation of the photoexcited protochlorophyllide a in methanol: formation of the hydrogen-bonded intermediate state induced by hydrogen-bond strengthening. *Biophys. J.*, 94(1), pp.38–46.

Zhong, L.B., Wiktorsson, B., Ryberg, M. & Sundqvist, C., 1996. The Shibata shift; effects of in vitro conditions on the spectral blue-shift of chlorophyllide in irradiated isolated prolamellar bodies. *J. Photochem. Photobiol. B Biol.*, 36(3), pp.263–270.

Chapter 2 – Experimental set-up

Ansari, A., Jones, C.M., Henry, E.R., Hofrichter, J. & Eaton, W.A., 1992. The role of solvent viscosity in the dynamics of protein conformational changes. *Science*, 256(5065), pp.1796–1798.

Brouers, M. & Michel-Wolwertz, M.R., 1983. Estimation of protochlorophyll(ide) contents in plant extracts; re-evaluation of the molar absorption coefficient of protochlorophyll(ide). *Photosynth. Res.*, 4(3), pp.265–270.

Cameron, C.E. & Benkovic, S.J., 1997. Evidence for a functional role of the dynamics of glycine-121 of *Escherichia coli* dihydrofolate reductase obtained from kinetic analysis of a site-directed mutant. *Biochemistry*, 36(50), pp.15792–15800.

Dereeper, A., Guignon, V., Blanc, G., Audic, S., Buffet, S., Chevenet, F., Dufayard, J.-F., Guindon, S., Lefort, V., Lescot, M., Claverie, J.-M. & Gascuel, O., 2008. Phylogeny.fr: robust phylogenetic analysis for the non-specialist. *Nucleic acid Res.*, 36, pp.W465–W469.

Griffiths, W.T., 1975. Characterization of the terminal stages of chlorophyll (ide) synthesis in etioplast membrane preparations. *Biochem. J.*, 152(3), pp.623–635.

Hay, S., Pudney, C.R., Sutcliffe, M.J. & Scrutton, N.S., 2008. Are environmentally coupled enzymatic hydrogen tunneling reactions influenced by changes in solution viscosity? *Angew. Chemie Int. Ed.*, 47(3), pp.537–540.

Heyes, D.J., Sakuma, M. & Scrutton, N.S., 2009. Solvent-Slaved Protein Motions Accompany Proton but Not Hydride Tunneling in Light-Activated Protochlorophyllide Oxidoreductase. *Angew. Chemie Int. Ed.*, 121, pp.3908–3911.

Heyes, D.J., Sakuma, M., de Visser, S.P. & Scrutton, N.S., 2009. Nuclear quantum tunneling in the light-activated enzyme protochlorophyllide oxidoreductase. *J. Biol. Chem.*, 284(6), pp.3762–3767.

Klement, H., Helfrich, M., Oster, U., Schoch, S. & Rüdiger, W., 1999. Pigment-free NADPH:protochlorophyllide oxidoreductase from *Avena sativa* L. Purification and substrate specificity. *Eur. J. Biochem.*, 265(3), pp.862–874.

Martin, G.E., Timko, M.P. & Wilks, H.M., 1997. Purification and kinetic analysis of pea (*Pisum sativum* L.) NADPH:protochlorophyllide oxidoreductase expressed as a fusion with maltose-binding protein in *Escherichia coli*. *Biochem. J.*, 325 (Pt 1, pp.139–145.

Snellenburg, J.J., Laptenok, S.P., Seger, R., Mullen, K.M. & Stokkum, I.H.M., 2012. Glotaran: A Java-Based Graphical User Interface for the R Package TIMP. *J. Stat. Softw.*, 49(3), pp.1–22.

Yang, Z. & Bauer, C.E., 1990. *Rhodobacter capsulatus* Genes Involved in Early Steps of the Bacteriochlorophyll biosynthetic pathway. *J. Bacteriol.*, 172(9), pp.5001–5010.

Chapter 3 - Does the pressure dependence of kinetic isotope effects report usefully on dynamics in enzyme H-transfer reactions?

Adamczyk, A.J., Cao, J., Kamerlin, S.C.L. & Warshel, A. (2011) Catalysis by dihydrofolate reductase and other enzymes arises from electrostatic preorganization, not conformational motions. *Proc. Natl. Acad. Sci. U. S. A.* 108, 14115–14120.

Antoniou, D. & Schwartz, S.D. (1997) Large kinetic isotope effects in enzymatic proton transfer and the role of substrate oscillations. *Proc. Natl. Acad. Sci. U. S. A.* 94, 12360–12365.

Basran, J., Sutcliffe, M.J. & Scrutton, N.S. (1999) Enzymatic H-transfer requires vibration-driven extreme tunneling. *Biochemistry* 38, 3218–3222.

Bell, R. (1980) *The Tunnel Effect in Chemistry*. Chapman and Hall, London.

Boehr, D.D., McElheny, D., Dyson, H.J. & Wright, P.E. (2006) The dynamic energy landscape of dihydrofolate reductase catalysis. *Science* 313, 1638–1642.

Brala, C.J., Karkovic, A., Sajenko, I., Pilepic, V. & Ursic, S. (2012) Sizeable increase of kinetic isotope effects and tunneling in coupled electron-proton transfers in presence of the quaternary ions. PCET processes and hydrogen tunneling as a “probe” for structuring and dynamical phenomena in water solution. *Z. Phys. Chem.* 226, 29–46.

Bruno, W.J. & Bialek, W. (1992) Vibrationally enhanced tunneling as a mechanism for enzymatic hydrogen transfer. *Biophys. J.* 63, 689–699.

Cioni, P. & Strambini, G.B. (2002) Effect of heavy water on protein flexibility. *Biophys. J.* 82, 3246–3253.

Gladstone, S., Laidler, K.J. & Eyring, H. (1941) *The Theory of Rate Processes*. McGraw-Hill, New York.

Glowacki, D.R., Harvey, J.N. & Mulholland, A.J. (2012) Taking Ockham’s razor to enzyme dynamics and catalysis. *Nat. Chem.* 4, 169–176.

Hardman, S.J., Pudney, C.R., Hay, S. & Scrutton, N.S. (2013) Excited state dynamics can be used to probe donor-acceptor distances for H-tunneling reactions catalyzed by flavoproteins. *Biophys. J.* 105, 2549–2558.

Hay, S., Sutcliffe, M.J. & Scrutton, N.S. (2007) Promoting motions in enzyme catalysis probed by pressure studies of kinetic isotope effects. *Proc. Natl. Acad. Sci. U. S. A.* 104, 507–512.

Hay, S. & Scrutton, N.S. (2008) Incorporation of hydrostatic pressure into models of hydrogen tunneling highlights a role for pressure-modulated promoting vibrations. *Biochemistry* 47, 9880–9887.

Hay, S., Pudney, C.R., McGrory, T.A., Pang, J.Y., Sutcliffe, M.J. & Scrutton, N.S. (2009) Barrier compression enhances an enzymatic hydrogen-transfer reaction. *Angew. Chem. Int. Ed.* 48, 1452–1454.

Hay, S., Pudney, C.R., Sutcliffe, M.J. & Scrutton, N.S. (2010) Probing active site geometry using high pressure and secondary isotope effects in an enzyme catalysed ‘deep’ H-tunneling reaction. *J. Phys. Org. Chem.* 23, 696–701.

Hay, S. & Scrutton, N.S. (2011) Examining the importance of dynamics, barrier compression and hydrogen tunneling in enzyme catalysed reactions. *Procedia Chem.* 3, 306–315.

Hay, S., Johannissen, L.O., Hothi, P., Sutcliffe, M.J. & Scrutton, N.S. (2012) Pressure effects on enzyme catalyzed quantum tunneling events arise from protein specific structural and dynamic changes. *J. Am. Chem. Soc.* 134, 9749–9754.

Hay, S. & Scrutton, N.S. (2012) Good vibrations in enzyme catalysed reactions. *Nat. Chem.* 4, 161–168.

Henzler-Wildman, K.A., Thai, V., Lei, M., Ott, M., Wolf-Watz, M., Fenn, T., Pozharski, E., Wilson, M.A., Petsko, G.A., Karplus, M. *et al.* (2007) Intrinsic motions along an enzymatic reaction trajectory. *Nature* 450, 838–844.

Heyes, D.J. & Hunter, C.N. (2004) Identification and characterization of the product release steps within the catalytic cycle of protochlorophyllide oxidoreductase. *Biochemistry* 43, 8265–8271.

Heyes, D.J. & Hunter, C.N. (2005) Making light work of enzyme catalysis: protochlorophyllide oxidoreductase. *Trends Biochem. Sci.* 30, 642–649.

Heyes, D.J., Heathcote, P., Rigby, S.E., Palacios, M.A., van Grondelle R & Hunter CN (2006) The first catalytic step of the light-driven enzyme protochlorophyllide oxidoreductase proceeds via a charge transfer complex. *J. Biol. Chem.* 281, 26847–26853.

Heyes, D.J., Sakuma, M., de Visser, S.P. & Scrutton, N.S. (2009) Nuclear quantum tunneling in the light-activated enzyme protochlorophyllide oxidoreductase. *J. Biol. Chem.* 284, 3762–3767.

Hong, Y.J. & Tantillo, D.J. (2014) Biosynthetic consequences of multiple sequential post-transition-state bifurcations. *Nat. Chem.* 6, 104–111.

Hothi, P., Hay, S., Roujeinikova, A., Sutcliffe, M.J., Lee, M., Leys, D., Cullis, P.M. & Scrutton, N.S. (2008) Driving force analysis of proton tunneling across a reactivity series for an enzyme-substrate complex. *ChemBioChem* 9, 2839–2845.

Isaacs, N.S., Javaid, K. & Rannala, E. (1977) Pressure effects on proton tunneling. *Nature* 268, 372.

Johannissen, L.O., Hay, S., Scrutton, N.S. & Sutcliffe, M.J. (2007) Proton tunneling in aromatic amine dehydrogenase is driven by a short-range subpicosecond promoting vibration: consistency of simulation and theory with experiment. *J. Phys. Chem. B* 111, 2631–2638.

Johannissen, L.O., Scrutton, N.S. & Sutcliffe, M.J. (2011) How does pressure affect barrier compression and isotope effects in an enzymatic hydrogen tunneling reaction? *Angew. Chem. Int. Ed.* 50, 2129–2132.

Kamerlin, S.C., Mavri, J. & Warshel, A. (2010) Examining the case for the effect of barrier compression on tunneling, vibrationally enhanced catalysis, catalytic entropy and related issues. *FEBS Lett.* 584, 2759–2766.

Kamerlin, S.C.L. & Warshel, A. (2010) An analysis of all the relevant facts and arguments indicates that enzyme catalysis does not involve large contributions from nuclear tunneling. *J. Phys. Org. Chem.* 23, 677–684.

Kandathil, S.M., Driscoll, M.D., Dunn, R.V., Scrutton, N.S. & Hay, S. (2014) Proton tunneling and promoting vibrations during the oxidation of ascorbate by ferricyanide? *Phys. Chem. Chem. Phys.* 16, 2256–2259.

Karkovic, A., Brala, C.J., Pilepic, V. & Ursic, S. (2011) Solvent-induced hydrogen tunneling in ascorbate proton-coupled electron transfers. *Tetrahedron Lett.* 52, 1757–1761.

Kipp, D.R., Silva, R.G. & Schramm, V.L. (2011) Mass-dependent bond vibrational dynamics influence catalysis by HIV-1 protease. *J. Am. Chem. Soc.* 133, 19358–19361.

Klinman, J.P. & Kohen, A. (2013) Hydrogen tunneling links protein dynamics to enzyme catalysis. *Annu. Rev. Biochem.* 82, 471–496.

Knapp, M.J. & Klinman, J.P. (2002) Environmentally coupled hydrogen tunneling. Linking catalysis to dynamics. *Eur. J. Biochem.* 269, 3113–3121.

Kohen, A., Cannio, R., Bartolucci, S. & Klinman, J.P. (1999) Enzyme dynamics and hydrogen tunneling in a thermophilic alcohol dehydrogenase. *Nature* 399, 496–499.

Liu, H. & Warshel, A. (2007) Origin of the temperature dependence of isotope effects in enzymatic reactions: the case of dihydrofolate reductase. *J. Phys. Chem. B* 111, 7852–7861.

Luk, L.Y., Javier Ruiz-Pernia, J., Dawson, W.M., Roca, M., Loveridge, E.J., Glowacki, D.R., Harvey, J.N., Mulholland, A.J., Tunon, I., Moliner, V. *et al.* (2013) Unraveling the role of protein dynamics in dihydrofolate reductase catalysis. *Proc. Natl. Acad. Sci. U. S. A.* 110, 16344–16349.

- Maglia, G. & Allemann, R.K. (2003) Evidence for environmentally coupled hydrogen tunneling during dihydrofolate reductase catalysis. *J. Am. Chem. Soc.* 125, 13372–13373.
- Masgrau, L., Roujeinikova, A., Johannissen, L.O., Hothi, P., Basran, J., Ranaghan, K.E., Mulholland, A.J., Sutcliffe, M.J., Scrutton, N.S. & Leys, D. (2006) Atomic description of an enzyme reaction dominated by proton tunneling. *Science* 312, 237–241.
- Masson, P. & Balny, C. (2005) Linear and non-linear pressure dependence of enzyme catalytic parameters. *Biochem. Biophys. Acta.* 1724, 440–450.
- Menon, B.R., Waltho, J.P., Scrutton, N.S. & Heyes, D.J. (2009) Cryogenic and laser photoexcitation studies identify multiple roles for active site residues in the light-driven enzyme protochlorophyllide oxidoreductase. *J. Biol. Chem.* 284, 18160–18166.
- Meyer, M.P., Tomchick, D.R. & Klinman, J.P. (2008) Enzyme structure and dynamics affect hydrogen tunneling: the impact of a remote side chain (i553) in soybean lipoxygenase-1. *Proc. Natl. Acad. Sci. U. S. A.* 105, 1146–1151.
- Northrop, D.B. (1999) Effects of high pressure on isotope effects and hydrogen tunneling. *J. Am. Chem. Soc.* 121, 3521–3524.
- Nunez, S., Tresadern, G., Hillier, I.H. & Burton, N.A. (2006) An analysis of reaction pathways for proton tunneling in methylamine dehydrogenase. *Philos. Trans. R. Soc. Lond. B Biol. Sci.* 361, 1387–1398.
- Pang, J., Hay, S., Scrutton, N.S. & Sutcliffe, M.J. (2008) Deep tunneling dominates the biologically important hydride transfer reaction from NADH to FMN in morphinone reductase. *J. Am. Chem. Soc.* 130, 7092–7097.
- Pu, J., Gao, J. & Truhlar, D.G. (2006) Multidimensional tunneling, recrossing, and the transmission coefficient for enzymatic reactions. *Chem. Rev.* 106, 3140–3169.
- Pudney, C.R., Hay, S., Sutcliffe, M.J. & Scrutton, N.S. (2006) Alpha-secondary isotope effects as probes of “tunneling-ready” configurations in enzymatic H-tunneling: insight from environmentally coupled tunneling models. *J. Am. Chem. Soc.* 128, 14053–14058.
- Pudney, C.R., Hay, S., Pang, J.Y., Costello, C., Leys, D., Sutcliffe, M.J. & Scrutton, N.S. (2007) Mutagenesis of morphinone reductase induces multiple reactive configurations and identifies potential ambiguity in kinetic analysis of enzyme tunneling mechanisms. *J. Am. Chem. Soc.* 129, 13949–13956.
- Pudney, C.R., Hay, S., Levy, C., Pang, J.Y., Sutcliffe, M.J., Leys, D. & Scrutton, N.S. (2009) Evidence to support the hypothesis that promoting vibrations enhance the rate of an enzyme catalyzed H-tunneling reaction. *J. Am. Chem. Soc.* 131, 17072–17073.

- Pudney, C.R., McGrory, T., Lafite, P., Pang, J.Y., Hay, S., Leys, D., Sutcliffe, M.J. & Scrutton, N.S. (2009) Parallel pathways and free-energy landscapes for enzymatic hydride transfer probed by hydrostatic pressure. *ChemBioChem* 10, 1379–1384.
- Pudney, C.R., Johannissen, L.O., Sutcliffe, M.J., Hay, S. & Scrutton, N.S. (2010) Direct analysis of donor acceptor distance and relationship to isotope effects and the force constant for barrier compression in enzymatic H-tunneling reactions. *J. Am. Chem. Soc.* 132, 11329–11335.
- Pudney, C.R., Guerriero, A., Baxter, N.J., Johannissen, L.O., Waltho, J.P., Hay, S. & Scrutton, N.S. (2013) Fast protein motions are coupled to enzyme H-transfer reactions. *J. Am. Chem. Soc.* 135, 2512–2517.
- Rokop, S., Gajda, L., Parmerter, S., Crespi, H.L. & Katz, J.J. (1969) Purification and characterization of fully deuterated enzymes. *Biochem. Biophys. Acta.* 191, 707–715.
- Roston, D., Cheatum, C.M. & Kohen, A. (2012) Hydrogen donor-acceptor fluctuations from kinetic isotope effects: a phenomenological model. *Biochemistry* 51, 6860–6870.
- Ruiz-Pernia, J.J., Luk, L.Y., Garcia-Meseguer, R., Marti, S., Loveridge, E.J., Tunon, I., Moliner, V. & Allemann, R.K. (2013) Increased dynamic effects in a catalytically compromised variant of *Escherichia coli* dihydrofolate reductase. *J. Am. Chem. Soc.* 135, 18689–18696.
- Schwartz, S.D. (2013) Protein dynamics and the enzymatic reaction coordinate. *Top. Curr. Chem.* 337, 189–208.
- Scrutton, N.S., Groot, M.L. & Heyes, D.J. (2012) Excited state dynamics and catalytic mechanism of the light-driven enzyme protochlorophyllide oxidoreductase. *Phys. Chem. Chem. Phys.* 14, 8818–8824.
- Silva, R.G., Murkin, A.S. & Schramm, V.L. (2011) Femtosecond dynamics coupled to chemical barrier crossing in a Born-Oppenheimer enzyme. *Proc. Natl. Acad. Sci. U. S. A.* 108, 18661–18665.
- Thibblin, A. & Ahlberg, P. (1989) Reaction branching and extreme kinetic isotope effects in the study of reaction mechanisms. *Chem Soc Rev* 18, 209–224.
- Thomas, J.B., Waas, J.R., Harmata, M. & Singleton, D.A. (2008) Control elements in dynamically determined selectivity on a bifurcating surface. *J. Am. Chem. Soc.* 130, 14544–14555.
- Toney, M.D., Castro, J.N. & Addington, T.A. (2013) Heavy enzyme kinetic isotope effects on proton transfer in alanine racemase. *J. Am. Chem. Soc.* 135, 2509–2511.

Chapter 4 - Expression, purification and kinetic characterisation of POR homologues from different evolutionary origins.

Armstrong, G.A., 1998. Greening in the dark: Light-independent chlorophyll biosynthesis from anoxygenic photosynthetic bacteria to gymnosperms. *J. Photochem. Photobiol. B Biol.*, 43(2), pp.87–100.

Aubert, C., Vos, M.H., Mathis, P., Eker, A. P. & Brettel, K., 2000. Intraprotein radical transfer during photoactivation of DNA photolyase. *Nature*, 405(6786), pp.586–590.

Burke, D.H., Hearst, J.E. & Sidow, A., 1993. Early evolution of photosynthesis: clues from nitrogenase and chlorophyll iron proteins. *Proc. Natl. Acad. Sci. U. S. A.*, 90(15), pp.7134–7138.

Cai, L., Friedman, N. & Sunny Xie, X., 2006. Stochastic protein expression in individual cells at the single molecule level. *Nature*, 440, pp.358–362.

Cortleven, A. & Schmulling, T., 2015. Regulation of chloroplast development and function by cytokinin. *J. Exp. Bot.*, 66, 4999–5013.

Dereeper, A., Guignon, V., Blanc, G., Audic, S., Buffet, S., Chevenet, F., Dufayard, J.-F., Guindon, S., Lefort, V., Lescot, M., Claverie, J.-M. & Gascuel, O., 2008. Phylogeny.fr: robust phylogenetic analysis for the non-specialist. *Nucleic acid Res.*, 36, pp.W465–W469.

Fujita, Y., 1996. Protochlorophyllide reduction: a key step in the greening of plants. *Plant Cell Physiol.*, 37(4), pp.411–421.

Fujita, Y. & Bauer, C.E., 2000. Reconstitution of light-independent protochlorophyllide reductase from purified Bchl and BchN-BchB subunits: In vitro confirmation of nitrogenase-like features of a bacteriochlorophyll biosynthesis enzyme. *J. Biol. Chem.*, 275(31), pp.23583–23588.

Fujita, Y., Takagi, H. & Hase, T., 1998. Cloning of the gene encoding a protochlorophyllide reductase: the physiological significance of the co-existence of light-dependent and -independent protochlorophyllide reduction systems in the cyanobacterium *Plectonema boryanum*. *Plant Cell Physiol.*, 39(2), pp.177–185.

Fujita, Y., Takahashi, Y., Chuganji, M. & Matsubara, H., 1992. The *nifH*-Like (*frxC*) Gene Is Involved in the Biosynthesis of Chlorophyll in the Filamentous Cyanobacterium *Plectonema boryanum*. *Plant Cell Physiol.*, 33(1), pp.81–92.

Grzyb, J.M., Solymosi, K., Strzałka, K. & Mysliwa-Kurdziel, B., 2013. Visualization and characterization of prolamellar bodies with atomic force microscopy. *J. Plant Physiol.*, 170(14), pp.1217–1227.

Heyes, D.J., Hardman, S.J.O., Hedison, T.M., Hoeven, R., Greetham, G.M., Towrie, M. & Scrutton, N.S., 2015. Excited-State Charge Separation in the Photochemical Mechanism of the Light-Driven Enzyme Protochlorophyllide Oxidoreductase. *Angew. Chemie Int. Ed.*, 54(5), pp.1512–1515.

Heyes, D.J., Levy, C., Sakuma, M., Robertson, D.L. & Scrutton, N.S., 2011. A twin-track approach has optimized proton and hydride transfer by dynamically coupled tunneling during the evolution of protochlorophyllide oxidoreductase. *J. Biol. Chem.*, 286(13), pp.11849–11854.

Heyes, D.J., Martin, G.E.M., Reid, R.J., Hunter, C.N. & Wilks, H.M., 2000. NADPH : protochlorophyllide oxidoreductase from *Synechocystis*: overexpression, purification and preliminary characterisation. 483, pp.47–51.

Heyes, D.J., Martin, G.E.M., Reid, R.J., Hunter, C.N. & Wilks, H.M., 2000. NADPH:protochlorophyllide oxidoreductase from *Synechocystis*: Overexpression, purification and preliminary characterisation. *Fed. Eur. Biochem. Soc. Lett.*, 483(1), pp.47–51.

Heyes, D.J., Menon, B.R.K., Sakuma, M. & Scrutton, N.S., 2008. Conformational Events during Ternary Enzyme - Substrate Complex Formation Are Rate Limiting in the Catalytic Cycle of the Light-Driven Enzyme. *Biochemistry*, 47, pp.10991–10998.

Heyes, D.J., Ruban, A. V, Wilks, H.M. & Hunter, C.N., 2002. Enzymology below 200 K: the kinetics and thermodynamics of the photochemistry catalyzed by protochlorophyllide oxidoreductase. *Proc. Natl. Acad. Sci. U. S. A.*, 99(17), pp.11145–50.

Heyes, D.J., Ruban, A. V. & Hunter, C.N., 2003. Protochlorophyllide oxidoreductase: “Dark” reactions of a light-driven enzyme. *Biochemistry*, 42(2), pp.523–528.

Heyes, D.J., Sakuma, M., de Visser, S.P. & Scrutton, N.S., 2009. Nuclear quantum tunneling in the light-activated enzyme protochlorophyllide oxidoreductase. *J. Biol. Chem.*, 284(6), pp.3762–3767.

Lebedev, N., Karginova, O., McIvor, W. & Timko, M.P., 2001. Tyr275 and Lys279 stabilize NADPH within the catalytic site of NADPH:protochlorophyllide oxidoreductase and are involved in the formation of the enzyme photoactive state. *Biochemistry*, 40(42), pp.12562–12574.

Lebedev, N. & Timko, M.P., 1998. Protochlorophyllide photoreduction. *Photosynth. Res.*, 58(1), pp.5–23.

Lidholm, J. & Gustafsson, P., 1991. Homologues of the green algal *gidA* gene and the liverwort *frxC* gene are present on the chloroplast genomes of conifers. *Plant Mol. Biol.*, 17, pp.787–798.

Lindner, P., Bauer, K., Krebber, A., Nieba, L., Kremmer, E., Krebber, C., Honegger, A., Klinger, B., Mocikat, R. & Plückthun, A., 1997. Specific detection of His-tagged

proteins with recombinant anti-His tag scFv-phosphatase or scFv-phage fusions. *Biotechniques*, 22(1), pp.140–149.

Masuda, T. & Takamiya, K.I., 2004. Novel insights into the enzymology, regulation and physiological functions of light-dependent protochlorophyllide oxidoreductase in angiosperms. *Photosynth. Res.*, 81(1), pp.1–29.

McFarlane, M.J., Hunter, C.N. & Heyes, D.J., 2005. Kinetic characterisation of the light-driven protochlorophyllide oxidoreductase (POR) from *Thermosynechococcus elongatus*. *Photochem. Photobiol. Sci.*, 4(12), pp.1055–1059.

Menon, B.R.K., 2009. *Kinetic and mechanistic studies of the light activated enzyme Protochlorophyllide oxidoreductase (POR) by protein engineering*. University of Manchester.

Menon, B.R.K., Waltho, J.P., Scrutton, N.S. & Heyes, D.J., 2009. Cryogenic and laser photoexcitation studies identify multiple roles for active site residues in the light-driven enzyme protochlorophyllide oxidoreductase. *J. Biol. Chem.*, 284(27), pp.18160–18166.

Michaelis, L. & Menten, M.L., 1913. Die Kinetik der Invertinwirkung (Translated from German). *Biochem. Z.*, 49, pp.333–369

Monod, J., Pappenheimer, A.M.J. & Cohen-Bazire, G., 1952. The kinetics of the biosynthesis of β -galactosidase in *Escherichia coli* as a function of growth. *Biochim. Biophys. Acta*, 9, pp.648–660.

Morrison, J.F., 1969. Kinetics of the reversible inhibition of enzyme-catalysed reactions by tight-binding inhibitors. *Biochim. Biophys. Acta*, 185, pp.269–286.

Reed, M.C., Lieb, A. & Nijhout, H.F., 2010. The biological significance of substrate inhibition: A mechanism with diverse functions. *BioEssays*, 32(5), pp.422–429.

Rowe, J.D. & Griffiths, W.T., 1995. Protochlorophyllide reductase in photosynthetic prokaryotes and its role in chlorophyll synthesis. *Biochem. J.*, 311 (Pt 2), pp.417–424.

Suzuki, J.Y. & Bauer, C.E., 1995. A prokaryotic origin for light-dependent chlorophyll biosynthesis of plants. *Proc. Natl. Acad. Sci. U. S. A.*, 92(9), pp.3749–3753.

Suzuki, J.Y. & Bauer, C.E., 1992. Light-Independent Chlorophyll Biosynthesis : Involvement of the Chloroplast Gene *chlL* (frxC). *Plant Cell*, 4, pp.929–940.

Wilks, H.M. & Timko, M.P., 1995. A light-dependent complementation system for analysis of NADPH:protochlorophyllide oxidoreductase: identification and mutagenesis of two conserved residues that are essential for enzyme activity. *Proc. Natl. Acad. Sci. U. S. A.*, 92(3), pp.724–8.

Chapter 5 - An evolutionary analysis of protein dynamics in the catalytic cycle of the light-driven enzyme protochlorophyllide oxidoreductase (POR).

Ansari, A., Jones, C.M., Henry, E.R., Hofrichter, J. & Eaton, W.A., 1992. The role of solvent viscosity in the dynamics of protein conformational changes. *Science*, 256(5065), pp.1796–1798.

Bandaria, J.N., Cheatum, C.M. & Kohen, A., 2009. Examination of enzymatic H-tunneling through kinetics and dynamics. *J. Am. Chem. Soc.*, 131(29), pp.10151–10155.

Begley, T.P. & Young, H., 1989. Protochlorophyllide Reductase. 1. Determination of the Regiochemistry and the Stereochemistry of the Reduction of Protochlorophyllide to Chlorophyllide. *J. Am. Chem. Soc.*, 111(18), pp.3095–3096.

Benkovic, S.J. & Hammes-Schiffer, S., 2003. A perspective on enzyme catalysis. *Science*, 301(5637), pp.1196–1202.

Chen, Y. & Pearlstein, A.J., 1987. Viscosity-Temperature Correlation for Glycerol-Water solutions. *Ind. Eng. Chem. Res.*, 26(8), pp.1670–1672.

Cortleven, A. & Schmulling, T., 2015. Regulation of chloroplast development and function by cytokinin. *J. Exp. Bot.*, 66, 4999–5013.

Crowe, S.A., Døssing, L.N., Beukes, N.J., Bau, M., Kruger, S.J., Frei, R. & Canfield, D.E., 2013. Atmospheric oxygenation three billion years ago. *Nature*, 501(7468), pp.535–8.

Dereeper, A., Guignon, V., Blanc, G., Audic, S., Buffet, S., Chevenet, F., Dufayard, J.-F., Guindon, S., Lefort, V., Lescot, M., Claverie, J.-M. & Gascuel, O., 2008. Phylogeny.fr: robust phylogenetic analysis for the non-specialist. *Nucleic acids Res.*, 36, pp.W465–W469.

Durin, G., Delaunay, A., Darnault, C., Heyes, D.J., Royant, A., Vernede, X., Hunter, C.N., Weik, M. & Bourgeois, D., 2009. Simultaneous measurements of solvent dynamics and functional kinetics in a light-activated enzyme. *Biophys. J.*, 96(5), pp.1902–1910.

Eisenmesser, E.Z., Bosco, Daryl, A., Akke, M. & Kern, D., 2002. Enzyme dynamics during catalysis. *Science*, 295, pp.1520–1523.

Eisenmesser, E.Z., Millet, O., Labeikovsky, W., Korzhnev, D.M., Wolf-Watz, M., Bosco, D. a, Skalicky, J.J., Kay, L.E. & Kern, D., 2005. Intrinsic dynamics of an enzyme underlies catalysis. *Nature*, 438(7064), pp.117–121.

- Frauenfelder, H., Chen, G., Berendzen, J., Fenimore, P.W., Jansson, H., McMahon, B.H., Stroer, I.R., Swenson, J. & Young, R.D., 2009. A unified model of protein dynamics. *Proc. Natl. Acad. Sci.*, 106(13), pp.5129–5134.
- Goujon, M., McWilliam, H., Li, W., Valentin, F., Silvano, S., Paern, J. & Lopez, R., 2010. A new bioinformatics analysis tools framework at EMBL-EBI. *Nucleic acids Res.*, 38, pp.W695–W699.
- Grzyb, J.M., Solymosi, K., Strzałka, K. & Mysliwa-Kurdziel, B., 2013. Visualization and characterization of prolamellar bodies with atomic force microscopy. *J. Plant Physiol.*, 170(14), pp.1217–1227.
- Gupta, R.S. & Mathews, D.W., 2010. Signature proteins for the major clades of Cyanobacteria. *BMC Evol. Biol.*, 10, p.24.
- Hay, S., Pudney, C.R., Sutcliffe, M.J. & Scrutton, N.S., 2008. Are environmentally coupled enzymatic hydrogen tunneling reactions influenced by changes in solution viscosity? *Angew. Chemie Int. Ed.*, 47(3), pp.537–540.
- Henzler-Wildman, K. A., Lei, M., Thai, V., Kerns, S.J., Karplus, M. & Kern, D., 2007. A hierarchy of timescales in protein dynamics is linked to enzyme catalysis. *Nature*, 450(7171), pp.913–916.
- Henzler-Wildman, K. & Kern, D., 2007. Dynamic personalities of proteins. *Nature*, 450(7172), pp.964–972.
- Heyes, D.J., Hardman, S.J.O., Hedison, T.M., Hoeven, R., Greetham, G.M., Towrie, M. & Scrutton, N.S., 2015. Excited-State Charge Separation in the Photochemical Mechanism of the Light-Driven Enzyme Protochlorophyllide Oxidoreductase. *Angew. Chemie Int. Ed.*, 54(5), pp.1512–1515.
- Heyes, D.J., Heathcote, P., Rigby, S.E.J., Palacios, M. A., Van Grondelle, R. & Hunter, C.N., 2006. The first catalytic step of the light-driven enzyme protochlorophyllide oxidoreductase proceeds via a charge transfer complex. *J. Biol. Chem.*, 281(37), pp.26847–26853.
- Heyes, D.J. & Hunter, C.N., 2005. Making light work of enzyme catalysis: Protochlorophyllide oxidoreductase. *Trends Biochem. Sci.*, 30(11), pp.642–649.
- Heyes, D.J., Levy, C., Sakuma, M., Robertson, D.L. & Scrutton, N.S., 2011. A twin-track approach has optimised proton and hydride transfer by dynamically-coupled tunneling during the evolution of protochlorophyllide oxidoreductase. *J. Biol. Chem.*, 286(13), pp.11849–11854.
- Heyes, D.J., Martin, G.E.M., Reid, R.J., Hunter, C.N. & Wilks, H.M., 2000. NADPH:protochlorophyllide oxidoreductase from *Synechocystis*: Overexpression, purification and preliminary characterisation. *Fed. Eur. Biochem. Soc. Lett.*, 483(1), pp.47–51.

Heyes, D.J., Ruban, A. V, Wilks, H.M. & Hunter, C.N., 2002. Enzymology below 200 K: the kinetics and thermodynamics of the photochemistry catalyzed by protochlorophyllide oxidoreductase. *Proc. Natl. Acad. Sci. U. S. A.*, 99(17), pp.11145–50.

Heyes, D.J., Ruban, A. V. & Hunter, C.N., 2003. Protochlorophyllide oxidoreductase: “Dark” reactions of a light-driven enzyme. *Biochemistry*, 42(2), pp.523–528.

Heyes, D.J., Sakuma, M. & Scrutton, N.S., 2007. Laser excitation studies of the product release steps in the catalytic cycle of the light-driven enzyme, protochlorophyllide oxidoreductase. *J. Biol. Chem.*, 282(44), pp.32015–32020.

Heyes, D.J., Sakuma, M. & Scrutton, N.S., 2009. Solvent-Slaved Protein Motions Accompany Proton but Not Hydride Tunneling in Light-Activated Protochlorophyllide Oxidoreductase. *Angew. Chemie Int. Ed.*, 121, pp.3908–3911.

Heyes, D.J., Sakuma, M., de Visser, S.P. & Scrutton, N.S., 2009. Nuclear quantum tunneling in the light-activated enzyme protochlorophyllide oxidoreductase. *J. Biol. Chem.*, 284(6), pp.3762–3767.

Hohmann-Marriott, M.F. & Blankenship, R.E., 2011. Evolution of photosynthesis. *Annu. Rev. Plant Biol.*, 62, pp.515–548.

Ivkovic-Jensen, M. & Kostic, N.M., 1997. Effects of Viscosity and Temperature on the Kinetics of the Electron-Transfer reaction between the triplet state of Zinc Cytochrome c and Cupriplastocyanin. *Biochemistry*, 36, pp.8135–8144.

Klinman, J.P. & Kohen, A., 2013. Hydrogen tunneling links protein dynamics to enzyme catalysis. *Annu. Rev. Biochem.*, 82, pp.471–496.

Kohen, A., Cannio, R., Bartolucci, S. & Klinman, J.P., 1999. Enzyme dynamics and hydrogen tunneling in a thermophilic alcohol dehydrogenase. *Nature*, 399(6735), pp.496–499.

Larkin, M.A., Blackshields, G., Brown, N.P., Chenna, R., McGettigan, P.A., McWilliam, H., Valentin, F., Wallace, I.M., Wilm, A., Lopez, R., Thompson, J.D., Gibson, T.J. & Higgins, D.G., 2007. Clustal W and Clustal X version 2.0. *Bioinformatics*, 23(21), pp.2947–2948.

Lebedev, N. & Timko, M.P., 1998. Protochlorophyllide photoreduction. *Photosynth. Res.*, 58(1), pp.5–23.

Loveridge, E.J., Tey, L.H., Behiry, E.M., Dawson, W.M., Evans, R.M., Whittaker, S.B.M., Günther, U.L., Williams, C., Crump, M.P. & Allemann, R.K., 2011. The role of large-scale motions in catalysis by dihydrofolate reductase. *J. Am. Chem. Soc.*, 133(50), pp.20561–20570.

Masgrau, L., Roujeinikova, A., Johannissen, L.O., Hothi, P., Basran, J., Ranaghan, K.E., Mulholland, A.J., Sutcliffe, M.J., Scrutton, N.S. & Leys, D., 2006. Atomic

description of an enzyme reaction dominated by proton tunneling. *Science*, 312(5771), pp.237–241.

Menon, B.R.K., Waltho, J.P., Scrutton, N.S. & Heyes, D.J., 2009. Cryogenic and laser photoexcitation studies identify multiple roles for active site residues in the light-driven enzyme protochlorophyllide oxidoreductase. *J. Biol. Chem.*, 284(27), pp.18160–18166.

Nagel, Z.D. & Klinman, J.P., 2010. Update 1 of: Tunneling and Dynamics in Enzymatic Hydride Transfer. *Chem. Rev.*, 110, pp.41–67.

Pisliakov, A. V, Cao, J., Kamerlin, S.C.L. & Warshel, A., 2009. Enzyme millisecond conformational dynamics do not catalyze the chemical step. *Proc. Natl. Acad. Sci. U. S. A.*, 106(41), pp.17359–17364.

Reinbothe, S., Reinbothe, C., Apel, K. & Lebedev, N., 1996. Evolution of chlorophyll biosynthesis - The challenge to survive photooxidation. *Cell*, 86(5), pp.703–705.

Segal, I.H., 1976. *Biochemical calculations*, 2nd Ed., New York: John Wiley and Sons, Inc.

Sharma, G. & First, E. A., 2009. Thermodynamic analysis reveals a temperature-dependent change in the catalytic mechanism of *Bacillus stearothermophilus* tyrosyl-tRNA synthetase. *J. Biol. Chem.*, 284(7), pp.4179–4190.

Snellenburg, J.J., Laptinok, S.P., Seger, R., Mullen, K.M. & Stokkun, I.H.M., 2012. Glotaran: A Java-Based Graphical User Interface for the R Package TIMP. *J. Stat. Softw.*, 49(3), pp.1–22.

Wilks, H.M. & Timko, M.P., 1995. A light-dependent complementation system for analysis of NADPH:protochlorophyllide oxidoreductase: identification and mutagenesis of two conserved residues that are essential for enzyme activity. *Proc. Natl. Acad. Sci. U. S. A.*, 92(3), pp.724–8.

Yahashiri, A., Howell, E.E. & Kohen, A., 2008. Tuning of the H-transfer coordinate in primitive versus well-evolved enzymes. *ChemPhysChem*, 9(7), pp.980–982.

Yang, J. & Cheng, Q., 2004. Origin and evolution of the Light-Dependent Protochlorophyllide Oxidoreductase (LPOR) genes. *Plant Biol.*, 6(5), pp.537–544.